

Western Australian School of Mines

Department of Mining Engineering and Surveying

Corrosion of Rock Reinforcement in Underground Excavations

Rhett Colin Hassell

**This thesis is presented for the Degree of
Doctor of Philosophy
of Curtin University of Technology**

February 2008

DECLARATION

To the best of my knowledge and belief this thesis contains no material previously published by any other person except where due acknowledgement has been made.

This thesis contains no material which has been accepted for the award of any other degree or diploma in any university.

Signed:

Date:

ABSTRACT

The effect of corrosion on the performance of rock support and reinforcement in Australian underground mines has not been widely researched and is generally not well understood. This is despite the number of safety concerns and operational difficulties created by corrosion in reducing the capacity and life expectancy of ground support. This thesis aims to investigate corrosion and relate how the environmental conditions in Australian underground hard rock mines impact on the service life of rock support and primarily rock reinforcement.

Environmental characterisation of underground environments was completed at a number of mine sites located across Australia. This provided an improved understanding of the environmental conditions in Australian underground hard rock mines. Long-term testing on the impact of corrosion on the load bearing capacity of reinforcement and support under controlled experimental conditions was conducted in simulated underground environments. Rock reinforcement elements were examined *in-situ* by means of overcoring of the installed reinforcement and surrounding rock mass. Laboratory testing of the core determined changes in load transfer properties due to corrosion damage. These investigations provided an excellent understanding of the corrosion processes and mechanisms at work. Corrosion rates for a range of underground environments were established through the direct exposure and evaluation of metallic coupons in underground *in-situ* and simulated environments.

It was found that the study of corrosion is challenging due to the time required to gather meaningful data. In particular, the wide range of materials that comprise ground support systems means that it is impossible to examine all the possible combinations of variables and their potential influence on the observed levels of corrosion and measured corrosion rates. Despite these challenges, the systematic investigation has resulted in new corrosivity classifications for both groundwater and atmospheric driven corrosion processes for various reinforcement and support systems used in the Australian underground mining industry. Previous corrosivity classifications were not found applicable. Furthermore, these new corrosivity classifications are simpler than previous classifications and corrosion rates may be predicted from readily obtained measurements of ground water dissolved oxygen and atmospheric relative humidity. Different types of reinforcement and surface support systems have been rated with respect to their corrosion resistance and estimates have been made for the expected service life for various rates of corrosion.

ACKNOWLEDGEMENTS

Many people have contributed to the completion of this thesis. Foremost, has been my supervisor Professor Ernesto Villaescusa whose enthusiasm for research combined with his attention to particulars provided for motivation and focus throughout the project. Dr Alan Thompson, associate supervisor, whose input never failed to amaze with its significance. Thank you to you both for your guidance and support.

The financial support of the following sponsoring companies and institutes is gratefully acknowledged: Mineral and Energy Research Institute of Western Australia (MERIWA), BHP Billiton, Goldfields Australia, Barrick Gold, Xstrata, Strata Control Systems, 360 Drilling, Cooperative Research Centre for Mining Technology and Equipment (CRC Mining) and the Western Australian School of Mines (WASM). Scholarships from the Australian Postgraduate Award Scheme and MERIWA have been greatly appreciated.

My sincerest appreciation also goes to:

- The numerous site based personnel who provided for much during the site visits from information, insight, corroded ground support specimens, water samples or just a lift underground.
- Mr Brett Scott and Mr Lance Fraser for their many hours spent helping with the technical issues that arose with the corrosion chambers and the overcoring rig.
- Staff members of the Department of Mining Engineering and WASM administration for their help throughout the project, in particular Dr Jianping Li and Mr Chris Windsor.

Finally to my family and beautiful partner Michelle, whose love, support and understanding was greatly appreciated.

TABLE OF CONTENTS

DECLARATION	I
ABSTRACT	II
ACKNOWLEDGEMENTS.....	III
TABLE OF CONTENTS.....	IV
LIST OF FIGURES.....	VII
LIST OF TABLES	XIV
 CHAPTER 1	
INTRODUCTION	1
1.1 OUTLINE OF INVESTIGATIONS INTO CORROSION OF SUPPORT AND REINFORCEMENT IN AUSTRALIAN UNDERGROUND MINES.....	4
 CHAPTER 2	
CORROSION FUNDAMENTALS AND GROUND SUPPORT USED IN AUSTRALIAN UNDERGROUND MINES	7
2.1 INTRODUCTION.....	7
2.2 MECHANICS OF CORROSION	7
2.3 THE UNDERGROUND MINING ENVIRONMENT	13
2.4 PROTECTION OF STEEL FROM CORROSION.....	20
2.5 ROCK SUPPORT AND REINFORCEMENT PRINCIPLES	23
2.6 INVESTIGATED ROCK SUPPORT AND REINFORCEMENT USED IN AUSTRALIAN UNDERGROUND MINES	27
2.7 DISCUSSION AND CONCLUSIONS	39
 CHAPTER 3	
ENVIRONMENTAL CONDITIONS IN AUSTRALIAN METALLIFEROUS UNDERGROUND MINES.....	40
3.1 INTRODUCTION.....	40
3.2 CORROSION ASSESSMENT SYSTEM FOR UNDERGROUND MINES	40
3.3 ENVIRONMENTAL CONDITIONS AT SELECTED AUSTRALIAN MINES	47
3.4 ATMOSPHERIC CONDITIONS IN AUSTRALIAN METALLIFEROUS UNDERGROUND MINES	78
3.5 GROUNDWATER CONDITIONS IN AUSTRALIAN METALLIFEROUS UNDERGROUND MINES.....	80
3.6 DISCUSSION AND CONCLUSIONS	88

CHAPTER 4

REINFORCEMENT AND SUPPORT TESTING USING A SIMULATED UNDERGROUND

ENVIRONMENT	90
4.1 INTRODUCTION.....	90
4.2 DEVELOPMENT OF THE SIMULATED UNDERGROUND ENVIRONMENT.....	90
4.3 TESTING OF CEMENT GROUTED CABLE STRAND AND REBAR REINFORCEMENT ELEMENTS	96
4.4 TESTING OF THE SWELLEX BOLT	126
4.5 TESTING OF CABLE BOLT BARREL AND WEDGE ANCHORS.....	131
4.6 DISCUSSION AND CONCLUSIONS	144

CHAPTER 5

OVERCORING OF ROCK REINFORCEMENT IN UNDERGROUND MINES.....146

5.1 INTRODUCTION.....	146
5.2 DEVELOPMENT OF THE WASM OVERCORING RIG.....	147
5.3 LABORATORY TESTING OF OVERCORED SAMPLES	150
5.4 OVERCORING AT KUNDANA MINE	154
5.5 OVERCORING AT ARGO MINE	166
5.6 OVERCORING AT LEVIATHAN MINE	183
5.7 OVERCORING AT OTHER MINES	192
5.8 DISCUSSION AND CONCLUSIONS	198

CHAPTER 6

CALCULATION OF CORROSION RATES BY DIRECT TESTING OF COUPONS200

6.1 INTRODUCTION.....	200
6.2 AIM OF TESTING	201
6.3 METHODOLOGY	202
6.4 RESULTS FROM THE CORROSION CHAMBERS	205
6.5 RESULTS FROM TESTING IN UNDERGROUND MINES	207
6.6 DISCUSSION AND CONCLUSIONS	211

CHAPTER 7

CORROSIVITY CLASSIFICATIONS FOR AUSTRALIAN UNDERGROUND MINES.....213

7.1 INTRODUCTION.....	213
7.2 GROUNDWATER CORROSIVITY CLASSIFICATION.....	213
7.3 ATMOSPHERIC CORROSIVITY CLASSIFICATION	228

CHAPTER 8

CORROSION OF ROCK SUPPORT AND REINFORCEMENT.....234

8.1	INTRODUCTION.....	234
8.2	CORROSION PROTECTION METHODS	234
8.3	ROCK REINFORCEMENT SYSTEMS	236
8.4	ROCK SUPPORT SYSTEMS.....	246

CHAPTER 9

CONCLUSIONS.....248

9.1	LIMITATIONS AND RECOMMENDATIONS FOR FUTURE WORK.....	250
-----	--	-----

REFERENCES252

APPENDIX A CORROSION ASSESSMENT DATA SHEET.....	260
APPENDIX B EMPIRICAL CALCULATIONS TO DETERMINE INTERNAL SWELLEX CORROSION	264
APPENDIX C GALVANISED FRICTION ROCK STABILISER CORROSION DAMAGE CLASSIFICATION	268
APPENDIX D GROUNDWATER CORROSIVITY CLASSIFICATIONS	271
APPENDIX E ATMOSPHERIC CORROSION CLASSIFICATIONS	276

LIST OF FIGURES

Figure 2.1	Schematic representation of the electrochemical iron corrosion process (Roberge 2000).	10
Figure 2.2	Schematic representation of uniform corrosion, pitting corrosion and stress corrosion cracking.	12
Figure 2.3	The influence of temperature and relative humidity on atmospheric corrosion (Roberge 2000).	14
Figure 2.4	Effect of oxygen concentration on the corrosion of low-carbon steel from (Uhlig & Revie 1985).	16
Figure 2.5	The effect of temperature on the corrosion rate of steel.	17
Figure 2.6	Effect of NaCl concentration on the corrosion rate of iron in aerated room-temperature solutions from (Uhlig & Revie 1985).	18
Figure 2.7	The effect of pH on the corrosion rate (CISA 1994).	19
Figure 2.8	Load transfer and embedment length concepts (Villaescusa & Wright 1997).	24
Figure 2.9	Categories of reinforcing element load transfer types: (a) DMFC, (b) CMC and (c) CFC (Windsor & Thompson 1993).	26
Figure 2.10	The components of a friction rock stabiliser (Hoek, Kaiser & Bawden 1995).	28
Figure 2.11	The components of the Swellex bolt (Hoek, Kaiser & Bawden 1995).	30
Figure 2.12	A basic cable bolt assembly (Thompson 2004b).	31
Figure 2.13	Schematic representation of a yielding cable bolt (Thompson 2004b).	32
Figure 2.14	The components of a CT bolt.	35
Figure 2.15	The components of the Hollow Groutable Bolt (HGB) (Hoek, Kaiser & Bawden 1995).	35
Figure 2.16	The components of a resin grouted rock bolt using threaded bar (Hoek, Kaiser & Bawden 1995).	36
Figure 2.17	Grouted dowel using reinforcement bar inserted into a grout-filled hole (Hoek, Kaiser & Bawden 1995).	37
Figure 3.1	Hygrometer (left) and portable TPS 90-FMLV field lab (right) used to collect environmental information.	42
Figure 3.2	Using a Pearpoint borehole camera to inspect the internal surface of a Friction Rock Stabiliser.	43
Figure 3.3	Diagrammatic representation of groundwater recharge into hard rock aquifers: (i) Evaporation, leading to saline and dense groundwater; (ii) Downward flow of dense groundwater; (iii) Back-flow of saline groundwaters leading to higher salinity at depth (D J Gray 2001).	45
Figure 3.4	Stronger discontinuity connectivity allows the groundwater to interact with more reinforcement and support.	46
Figure 3.5	Location of assessed underground mines.	47
Figure 3.6	External and internal view of FRS from the S/P3 South Decline, approximately 6 months age.	50
Figure 3.7	External and internal view of FRS of 2 years age, some steel corrosion is evident.	50
Figure 3.8	Internal pictures of a FRS after two months (left) and four months (right) installation in a shear associated with high groundwater flow.	54
Figure 3.9	Internal picture a jumbolt after two (left) and four months (right) installation in a shear associated with high groundwater flow.	54

Figure 3.10	External (left) and internal (right) view of corrosion damage to a galvanised FRS that has been affected by earlier groundwater flow.	58
Figure 3.11	No corrosion of the plate (left), but strong corrosion of the FRS reinforcement (rights) at 2.1m depth.....	58
Figure 3.12	Failure of a 15 mm diameter point anchored bolt after 15 years of installation due to atmospheric corrosion.	62
Figure 3.13	Damage to a CT bolt by mechanised equipment has broken off the plate and nut revealing the element and plastic sheath with no evidence of cement grouting.	65
Figure 3.14	Highly corroded FRS (left) and non-corroded FRS (right) of same age (2 years) installed within one meter of each other.....	66
Figure 3.15	Rehabilitation of corroded reinforcement elements. Original reinforcement was installed over 10 years prior.	69
Figure 3.16	Condition of support after undergoing corrosion attack from only atmospheric variables after eight (left) and three (right) years.	69
Figure 3.17	Corrosion damage to 15 year old surface fixtures at Level 1 platform.	73
Figure 3.18	Minor surface corrosion of black friction bolt at Level 3 access approximately five years age. ..	73
Figure 3.19	Corrosion damage to galvanised FRS in the hanging wall development (left) and ore drive (right).	74
Figure 3.20	Severely corroded FRS at Olympic Dam Mine; the area is damp but groundwater flow is minor.	76
Figure 3.21	Rehabilitation of corroded reinforcement at Olympic Dam Mine.	77
Figure 3.22	Location map of Yilgarn Craton, separated into four regions based on TDS content, with rainfall (mm) in isohyets (D J Gray 2001).....	82
Figure 3.23	The calculated dissolved oxygen concentration compared to the actual measured concentration.	85
Figure 3.24	Relationship between the TDS and chloride ion concentrations.	87
Figure 3.25	A weak correlation between the TDS and sulphate ion concentrations.	88
Figure 4.1	CLIPSAM multi-port instrumentation unit (left), heat lamp (top right) and humidifier unit (bottom right).	92
Figure 4.2	Monitoring of temperature in the corrosion chambers.	94
Figure 4.3	Monitoring of humidity in the corrosion chambers.....	94
Figure 4.4	Cracking of the grout column due to joint dilation.	97
Figure 4.5	Cracking within a resin grouted column, these cracks present a path for the surrounding environment to interact with the reinforcement.	98
Figure 4.6	Plain (top) and compact (bottom) cable bolt strands.....	99
Figure 4.7	20 mm diameter thread bar.	99
Figure 4.8	The split pipe testing system.	102

Figure 4.9	The testing set up showing the Avery machine in the background and the PC and analogue data collector to the left. A closer view of the split pipe is shown on the right.	103
Figure 4.10	A typical WASM corrosion chamber (left) and water flow through simulated geological discontinuity (right).....	104
Figure 4.11	Typical failure of the strand elements with plain strand (left) and bulbed strand (right).	105
Figure 4.12	Stages of corrosion damage of strand elements.	106
Figure 4.13	Typical load-displacement plot of single plain strand with methocel additive (0.5 m embedment length).	107
Figure 4.14	Typical load-displacement plot of single plain strand with MCI additive (0.5 m embedment length).....	109
Figure 4.15	Typical load-displacement plot of single bulbed strand with methocel additive (0.5 m embedment length).	111
Figure 4.16	Typical load-displacement plot of single bulbed strand with MCI additive (0.5 m embedment length).	111
Figure 4.17	Typical load-displacement plot of compact strand with MCI additive (0.5 m embedment length).	112
Figure 4.18	Good quality grout was observed for all horizontally placed samples inspected.	113
Figure 4.19	Migration of corrosion along the bolt axis was not observed.....	114
Figure 4.20	Typical load-displacement plot of black thread bar with methocel additive (0.5 m embedment length).	115
Figure 4.21	Typical load-displacement plot of black thread bar with MCI additive (0.5 m embedment length).	115
Figure 4.22	Typical load-displacement plot of galvanised thread bar with methocel additive (0.5 m embedment length).....	116
Figure 4.23	Typical load-displacement plot of CT bolt element with methocel additive (0.5 m embedment length).	116
Figure 4.24	Corrosion of the thread bar elements of same age.	117
Figure 4.25	Load-displacement plot of black thread bar element with MCI additive that experienced slippage at low loads.	118
Figure 4.26	A cut section of a black thread bar with MCI additive sample that pulled through the top 0.5 m embedment length.	118
Figure 4.27	Sufficient opening of crack width to allow for corrosion did not take place until after the 181 day test.	120
Figure 4.28	Variations in time of failure due to water flow being concentrated in one area (left) or spread around the circumference of strand (right).....	121
Figure 4.29	Comparison of results between plain and bulbed strand (0.5m embedment length).	122
Figure 4.30	Comparison of all strand results between the non-inhibitor and inhibitor grout mixes (0.5m embedment length).....	123
Figure 4.31	Summary of strand results by corrosion chamber (0.5m embedment length).	124

Figure 4.32	The expected service life of cable strand in the corrosion chamber environments.	125
Figure 4.33	Longitudinal and cross sectional view of Swellex bolt during installation (Villaescusa, Thompson & Windsor 2006).	127
Figure 4.34	Internal condition of the Swellex bolt after 97 days.....	129
Figure 4.35	Anchors with strand receded compared with original position in a WA mine (Thompson 2004b).	131
Figure 4.36	Flat end anchor and hemispherical ended anchor.	133
Figure 4.37	Schematic representation of split pipe testing system.	134
Figure 4.38	Laboratory testing of the barrel and wedge anchors.	135
Figure 4.39	Hemispherical barrel and three-part wedge anchor with compact strand before and after placement in corrosion chambers.....	136
Figure 4.40	Typical load-displacement plot for hemispherical barrel and three part wedge anchor, after 10 months in corrosion chamber.	137
Figure 4.41	Internal condition of failed barrel and three part wedge anchor. Note the corrosion on the barrel surface and the shearing of the wedge teeth.....	137
Figure 4.42	Internal condition of barrel and three-part wedge anchor that did not fail after 297 days in corrosion chamber.....	138
Figure 4.43	Hemispherical barrel and three-part wedge with compact strand, bitumen coating, before and after placement in corrosion chamber.	139
Figure 4.44	Typical load displacement plot for galvanised hemispherical barrel and three-part wedge after 91 days in corrosion chamber.	140
Figure 4.45	Internal condition of galvanised barrel and wedge after testing.....	140
Figure 4.46	Typical load-displacement responses for barrels and two part wedge following 297 days of exposure in a corrosion chamber.....	141
Figure 4.47	Total wedge movement of anchors after 297 days in the corrosion chamber.	143
Figure 5.1	Overcoring trials of the prototype overcoring rig.	147
Figure 5.2	Overcoring drill rig.	148
Figure 5.3	Full recovery from overcoring friction rock stabiliser collars in very poor rock mass.	149
Figure 5.4	Samples being prepared for testing.....	151
Figure 5.5	Testing of overcored samples to determine relative load transfer.....	152
Figure 5.6	Two reinforcement elements following push (left) and pull (right) testing from 300 mm embedment length.	152
Figure 5.7	Measurement of maximum pit depth along bolt axis.	153
Figure 5.8	Friction bolt is prepared for tensile strength testing (left), and tensile testing of friction bolt (right).	153
Figure 5.9	Schematic diagram of the Strzelecki Decline with overcore locations marked by grey arrows..	155
Figure 5.10	Slippage of the FRS at the element/rock interface.....	157
Figure 5.11	Load displacement plot of galvanised 47 mm diameter friction bolts (250-300 mm embedment lengths).....	158

Figure 5.12	Load displacement plot of galvanised 47 mm diameter friction bolts (400-500 mm embedment lengths).....	159
Figure 5.13	Relationship between the peak frictional strength and the embedment length for galvanised 47 mm diameter friction bolts.	159
Figure 5.14	Normalised results of pull tests.	161
Figure 5.15	Failure of friction bolt during tensile testing within pitted region.	161
Figure 5.16	Maximum penetration rates due to pitting along bolt axis for severely, highly and moderately corroded bolts.....	163
Figure 5.17	Open joints (left) have allowed groundwater to flow and interact with the steel element. The same section (right) but with the rock removed displaying severe pitting.	164
Figure 5.18	Relationship between maximum tensile strength and maximum pit depth.	165
Figure 5.19	Overcoring conditions at the N1 Access Drive (top left), N3 Access Drive (top right) and N12 Access Drive (below centre).	167
Figure 5.20	Graph of the average discontinuity spacing showing the differences between the rock mass in the walls and the backs.	169
Figure 5.21	Summary of load-displacement results for all pull tests from the N1 Access Drive (300 mm embedment length).....	171
Figure 5.22	Summary of load-displacement results from pull tests for the N3 Access Drive (300 mm embedment length).....	172
Figure 5.23	Good grouting of sample N1-3A (top) and poorer grouting of sample N3-9B (bottom).	172
Figure 5.24	Load-displacement results from pull tests of N12 Access Drive 6A and 6B (300 mm embedment length).	173
Figure 5.25	Combination of pull test capacities for all FRS tests (300 mm embedment length).	174
Figure 5.26	Frictional capacity per metre of embedment length of collar (A) and toe (B) samples normalised from pull tests of 300 mm embedment length.....	175
Figure 5.27	Overcored friction bolts with grout removed. Grout protected the element with galvanising still present. Voids in the grout have allowed some corrosion to occur.	179
Figure 5.28	Comparison between the discontinuity spacing and the peak frictional load from pull testing. .	180
Figure 5.29	Schematic representation of the friction bolt dimensions before (left) and after (right) installation.	181
Figure 5.30	Calculated hole diameter compared to the tested peak frictional load.	182
Figure 5.31	Maximum tensile strength and the rate of penetration due to pitting corrosion.	177
Figure 5.32	Grouted HGB displaying thin steel wall and internal grout.	184
Figure 5.33	Severe corrosion of a HGB face plates due to flooding of mine workings.	185
Figure 5.34	Overcored HGB samples from the Leviathan Mine.	186
Figure 5.35	Poor grouting leading to low load transfers for sample HGB 4-C.	187
Figure 5.36	Encapsulation quality for plain cable sample 1-A (left) and sample 2-A (right).	187
Figure 5.37	Combination of relative push test capacities for all HGB tests (embedment length 300 mm)....	188
Figure 5.38	Peak and residual load for relative push test of HGB along bolt axis.	189

Figure 5.39	Light surface corrosion in fully grouted areas (top) with isolated areas of stronger surface corrosion where grout encapsulation was not as good (bottom).	190
Figure 5.40	Minor corrosion of bolt even when open joint intersect exposed element.	191
Figure 5.41	Corrosion protection due to migration of grout preventing groundwater interaction with bolt. .	191
Figure 5.42	Severe corrosion of friction bolt and deposition of solids.	192
Figure 5.43	Recovered 47 mm galvanised friction rock stabiliser.	193
Figure 5.44	Load-displacement plot of a galvanised 47 mm diameter friction rock stabiliser (300 mm embedment length).....	194
Figure 5.45	Cement grout migration interlocking a broken rock mass.	195
Figure 5.46	Extremely corroded friction rock stabilisers recovered from Olympic Dam Mine.	196
Figure 5.47	Load-displacement plot of galvanised friction rock stabiliser from Olympic Dam operations (300 mm embedment length).	197
Figure 5.48	Overcored CT bolt with cement grout on the inside of the tube (top) but not outside (bottom).	197
Figure 5.49	Poor encapsulation of a resin bolt from Olympic Dam Mine.	198
Figure 6.1	Coupon following sand blasting (left) and fitted with identification tag (right).	203
Figure 6.2	Placement of corrosion coupons in an underground environment.	203
Figure 6.3	Corrosion coupons collected from Enterprise Mine after 213 days in an atmospheric environment (left) and from Cannington Mine after 354 days in a groundwater affected environment (right).	204
Figure 6.4	Corrosion rates for each WASM chamber over time.	207
Figure 6.5	Corrosion rates from coupons for each location at the Argo Mine.	208
Figure 6.6	Corrosion rates from coupons at each location at Cannington Mine.....	209
Figure 6.7	Corrosion rates from coupons for each location at Enterprise Mine.	210
Figure 7.1	Comparison between the calculated LSI rating and the corrosion chamber corrosion rates.	217
Figure 7.2	Comparison between the calculated DIN rating and the corrosion chamber corrosion rates.	217
Figure 7.3	Comparison between the calculated Li & Lindblad (1999) rating and the corrosion chamber corrosion rates.	219
Figure 7.4	Relationship between the corrosion chamber corrosion rates and the temperature of the groundwater.	221
Figure 7.5	Relationship between the corrosion chamber corrosion rates and the TDS of the groundwater.	221
Figure 7.6	Relationship between the corrosion chamber corrosion rates and the dissolved oxygen content of the groundwater.....	222
Figure 7.7	Comparison of the coupon tests results for the corrosion chambers over time.	223
Figure 7.8	Corrosion coupon test data from the field and chambers grouped by water velocity.	225
Figure 7.9	Corrosivity classification for groundwater affected, Australian hard rock environments.	226
Figure 7.10	Relationship between corrosion rates and W_{dry} rating.....	230
Figure 7.11	Relationship between the corrosion rate and temperature from a) Roberge (2000) and b) from the site coupon rates and measured temperature.	232
Figure 7.12	Relationship between coupon corrosion rates and relative humidity from a) Roberge (2000) and b) from the site coupon rates and measured humidity.....	232

Figure 8.1	The estimated time taken for a 20% reduction in steel thickness of a 47 mm diameter, nominal 3 mm thickness FRS corresponding to a 50% decrease in pull out strength.	238
Figure 8.2	Service life estimates for cable strand in strong groundwater flow environments.	241
Figure 8.3	Estimated service life to yield failure for 20 mm thread bar due to corrosion at various working stresses (percentage of yield strength).	244
Figure 8.4	Estimated service life to ultimate failure for 20 mm thread bar due to corrosion at various working stresses (percentage of yield strength).	244
Figure 8.5	Estimated service life to yield failure for 25 mm thread bar due to corrosion at various working stresses (percentage of yield strength).	245
Figure 8.6	Estimated service life to ultimate failure for 25 mm thread bar due to corrosion at various working stresses (percentage of yield strength).	245

LIST OF TABLES

Table 2.1	Chemical composition and mechanical properties of HA350 grade steel for friction rock stabilisers.....	28
Table 3.1	Atmospheric variables at Argo Mine	48
Table 3.2	Groundwater variables tested <i>in situ</i> at Argo Mine.....	49
Table 3.3	Groundwater assay of dissolved ions from Argo Mine.....	49
Table 3.4	Atmospheric variables at Cannington Mine.....	52
Table 3.5	Groundwater variables tested <i>in situ</i> at Cannington Mine.	52
Table 3.6	Groundwater assay of dissolved ions from Cannington Mine.	53
Table 3.7	Atmospheric variables at Darlot Mine.	55
Table 3.8	Groundwater variables from aquifer one tested <i>in situ</i> at Darlot Mine	56
Table 3.9	Groundwater assay of dissolved ions from aquifer one at Darlot Mine.....	56
Table 3.10	Groundwater variables from aquifer two tested <i>in situ</i> at Darlot Mine.....	56
Table 3.11	Groundwater assay of dissolved ions from aquifer two at Darlot Mine.....	57
Table 3.12	Results of mesh pull tests at Darlot Mine.	59
Table 3.13	Groundwater variables tested <i>in situ</i> at Enterprise Mine.....	60
Table 3.14	Groundwater assay of dissolved ion at Enterprise Mine.	61
Table 3.15	Atmospheric variables at Enterprise Mine.	61
Table 3.16	Atmospheric variables at Kanowna Belle Mine.....	63
Table 3.17	Groundwater variables from aquifer one tested <i>in situ</i> at Kanowna Belle Mine.....	64
Table 3.18	Groundwater assay of dissolved ions from aquifer one at Kanowna Belle Mine.....	64
Table 3.19	Groundwater variables from aquifer two tested <i>in situ</i> at Kanowna Belle Mine.	64
Table 3.20	Groundwater assay of dissolved ions from aquifer two at Kanowna Belle Mine.	64
Table 3.21	Atmospheric variables at Kundana Mine.	67
Table 3.22	Groundwater variables tested <i>in-situ</i> at Kundana Mine.	68
Table 3.23	Groundwater assay of dissolved ions from Kundana Mine.....	68
Table 3.24	Atmospheric variables at Leinster Nickel Operations.....	71
Table 3.25	Groundwater variables measured <i>in situ</i> at Leinster Nickel Operations from the sub level cave.	72
Table 3.26	Groundwater assay of dissolved ions at Leinster Nickel Operations from the sub-level cave.....	72
Table 3.27	Groundwater variables measured <i>in situ</i> at Leinster Nickel Operations from the return air way.....	72
Table 3.28	Testing of weld mesh samples collected from Leinster Nickel Operations.	74
Table 3.29	Atmospheric variables at Olympic Dam Mine.....	75
Table 3.30	Groundwater variables tested <i>in situ</i> at Olympic Dam Mine.	76
Table 3.31	Groundwater assay of dissolved ions from 44 Cyan 19 at Olympic Dam Mine.	76
Table 3.32	Groundwater variables measured <i>in situ</i> and assayed for other Australian underground mines.....	78
Table 3.33	Atmospheric measurements at selected Australian underground mine sites.....	79
Table 3.34	Average <i>in situ</i> groundwater measurements at Australian underground mines.	81
Table 3.35	Average groundwater analysis assays from Australian underground mines.	87
Table 4.1	Atmospheric conditions in each corrosion chamber.	93

Table 4.2	Average groundwater measurements for each corrosion chamber.....	95
Table 4.3	Variations in groundwater properties.....	96
Table 4.4	Summary of standard reinforcement elements tested.....	101
Table 4.5	Laboratory results of corrosion and failure loads for single plain strand elements.....	108
Table 4.6	Laboratory results of corrosion and failure loads for single bulbed strand elements.....	110
Table 4.7	Laboratory results of corrosion and failure loads for compact strand elements.....	112
Table 4.8	Uniaxial compressive strength tests of the grout samples.....	119
Table 4.9	Actual service life of cable strand in the (accelerated) corrosion chamber environments.....	120
Table 4.10	Changes in the chemistry of the residual water.....	129
Table 4.11	Calculations of the depth of corrosion for the three scenarios.....	130
Table 4.12	Tested combinations of barrel and wedge anchors.....	134
Table 4.13	Summary of test results.....	136
Table 5.1	Recovery of overcored elements from Kundana Mine.....	156
Table 5.2	Corrosion classification for galvanised friction bolts.....	156
Table 5.3	Summary of test results from the Kundana Mine overcoring.....	157
Table 5.4	Normalised results for pull test data from Kundana Mine.....	160
Table 5.5	Maximum penetration rates for overcored elements at 0.5m intervals along the bolt axis.....	163
Table 5.6	Chemical analysis of corrosion products.....	165
Table 5.7	Recovery of overcored elements from Argo Mine.....	168
Table 5.8	Summary of test results from the Argo Mine overcoring.....	170
Table 5.9	Normalised results for the peak load and residual load.....	175
Table 5.10	Pitting rate of overcored elements along bolt axis.....	177
Table 5.11	Loss of galvanising along bolt axis.....	178
Table 5.12	Analysis of groundwater taken from a perched stope.....	184
Table 5.13	Recovery of overcored elements from Leviathan Mine.....	186
Table 5.14	Summary of pull and push testing results.....	187
Table 5.15	Summary of relative push tests capacities for HGB tests.....	189
Table 6.1	Chemical composition and mechanical properties of HA300 grade steel.....	202
Table 6.2	Groundwater conditions in the corrosion chambers for the duration of the coupon testing.....	206
Table 6.3	Rates of corrosion for coupons in the corrosion chambers.....	206
Table 6.4	Rates of corrosion in selected environments at Argo Mine.....	208
Table 6.5	Rates of corrosion in selected environment at Cannington Mine.....	209
Table 6.6	Rates of corrosion in selected environments at Enterprise Mine.....	210
Table 6.7	Rates of corrosion in selected environments at Olympic Dam Mine.....	211
Table 7.1	LSI ratings for studied Australian underground mine groundwaters.....	215
Table 7.2	DIN 50929 corrosion classification ratings for Australian underground mine groundwaters.....	216
Table 7.3	Li and Lindblad (1999) corrosion classification ratings for Australian underground mine groundwaters.....	218
Table 7.4	Range of maximum expected corrosion rates for HA300 grade steel in groundwater affected, Australian hard rock environments.....	227

Table 7.5	Descriptions of groundwater flow conditions (Bieniawski 1989).....	227
Table 7.6	Li and Lindblad (1999) dry rock ratings for various underground environments.	230
Table 7.7	Corrosivity classification for underground, hard rock, metalliferous atmospheric environments.	233
Table 8.1	Relative longevity of reinforcement systems subjected to similar corrosive environments.....	236
Table 8.2	Estimated time taken for a 20% reduction in steel thickness of a 47mm diameter, 3mm thickness FRS corresponding to a 50% decrease in pull out strength.....	238
Table 8.3	Service life estimates for cable strand in strong groundwater flow environments.....	241
Table 8.4	Relative longevity of support systems subjected to similar corrosive environments.	246
Table 8.5	Qualitative assessment for longevity of black plates in a range of corrosive environments.	247

CHAPTER 1 INTRODUCTION

The effect of corrosion on the performance of rock support and reinforcement in Australian underground mines has not been widely researched and is generally not well understood. Corrosion reduces the capacity and life expectancy of ground support creating a number of safety concerns and operational difficulties in underground mining. It is the purpose of this thesis to present a corrosivity classification for the various Australian underground hard rock mining environments, relating how the environment impacts on the service life of rock support and reinforcement and ultimately providing guidelines for the design of ground support in various underground environments.

No systematic field study on this subject has ever been undertaken in metalliferous, hard rock mines in Australia despite the need for a comprehensive study to achieve a more complete understanding being recognised since 1995 (Ranasooriya, Richardson & Yap 1995). Corrosion has been found to be in part responsible for 29% of all rock bolt failures and 25% of all cable bolt failures during rock falls within the Australian mining industry (Potvin et al. 2001).

In the past two decades, some 45% of fatal accidents and 24% of lost time injuries in Western Australian underground mines have been due to rock falls (Harvey 1999). Fatalities due to rock falls were more than three times more numerous than the next most common cause (Department of Industry and Resources 1997).

The economic impact of rock falls associated with the rehabilitation of mine development can run into the tens of millions of dollars as entire sections of ground support are replaced due to the uncertainty of their condition. Scheduling and productivity conflicts arise due to the loss of personnel and equipment involved in the rehabilitation and the restricted mine access.

The purpose of rock support and reinforcement is to maintain excavations safe and open for their intended lifespan. Failure to achieve this outcome impacts on the safety of personnel and equipment and can also significantly influence the economics of a mining operation.

Legislative requirements such as the Western Australian Mines Safety and Inspection Regulations 1995 (Department of Industry and Resources 2002) that form part of the Mines Safety and Inspection Act 1994 ensure that “appropriate measures are taken to ensure the proper design, installation and quality control of rock support and reinforcement”. Supplementary guidelines further elaborate that “rock reinforcement and support should be matched to the ground conditions; anything less could not be said to be sound geotechnical engineering practice. Corrosion is an important factor that needs to be considered in the design and selection of the rock support and reinforcement” (Department of Industry and Resources 1997).

Current geotechnical engineering design methods for underground mining have only a minor amount of information regarding corrosion and its effects. While the literature on corrosion is exhaustive those publications that relate specifically to the unique underground mining environment are limited. Much of the civil engineering guidelines and research, the closest engineering field to geotechnical engineering, are impractical to employ due to the large disparities in excavation life, design risk and subsequent costs between the two disciplines. Design methods for underground mining need to take into account the economics of a mining operation, thus employing safe, yet practical guidelines.

The types of support and reinforcement required in a particular location are dependent upon several factors that include the strength of the rock mass, the geometry of the excavation, the stresses present in the rock, the blasting practices, and the weathering and corrosion processes applicable at the site (Villaescusa 1999a; Windsor & Thompson 1993). All these factors impact on the capacity of a ground support scheme; however,

Sundholm (1987) suggests that corrosion is one of the major factors determining which reinforcement type can be used as permanent support.

The initial step in developing a design criterion is to have a good understanding of the corrosion potential of the environment in which the reinforcement and support is being installed. The underground mining environment is unique in that it is situated hundreds of metres below the surface and the engineering material, the rock mass, is highly variable even on a mine scale. Authors that have attempted with varying degrees of success to classify the underground mining environment in terms of its corrosivity have been Rawat (1976) for the Jharia coal fields in India, Higginson and White (1983) in South African Gold Mines, Li and Lindblad (1999) who proposed a corrosivity classification for the underground environment based on work in central Europe and Robinson and Tyler (1999) for the Mt Isa Mines in Australia.

These classifications along with other internationally recognised classifications for surface environments (e.g. DIN 50929-3 1985) were found to be inadequate when applied to Australian underground mining environments. This defined a need to develop a more representative classification based on measured and observed parameters that provide an assessment of the corrosivity and corresponding rates of corrosion within the Australian context.

An understanding of the environment in which the support and reinforcement system is being installed in is only one part of the research. How the system reacts to that environment, specifically the effect corrosion has on its ability to operate as designed is a major focus of the research. The mechanisms of corrosion attack, the modes of failure and the estimated service life will be examined for the different underground environments.

A wide selection of support and reinforcement systems is commercially available for use in the mining industry. Some include corrosion protection measures such as zinc galvanising, plastic sheathing and application of chemical inhibitors; others require the

application of cement or resin grouts. The ability to investigate all current systems in use is not realistic, and only the most common types of support and reinforcement and corrosion protection methods are included in this study. These include friction rock stabilisers, cable bolts, cement grouted elements, resin grouted elements, weld mesh and bolt plates.

Regardless of the system used, the impact corrosion has over time on the element's ability to maintain design requirements in a range of environmental conditions is not well understood. The final outcomes of this report are new classifications that categorise the underground environment based on measured environmental properties and provide an estimated rate of corrosion. This will be used in determining rock support and reinforcement serviceability design guidelines that provide an approximate service life for a range of reinforcement elements and support systems. The subsequent transfer of this knowledge to the mining industry will deliver a significant improvement in operational safety and cost saving.

1.1 Outline of investigations into corrosion of support and reinforcement in Australian underground mines

The organisational structure of the report is provided in the following paragraphs; it defines the links between the conducted research and the stated aims. Chapter 2 presents an overview of the important corrosion principles that apply to the underground environment and a description of the investigated rock support and reinforcement systems. The chapter also reviews existing literature regarding the effect of corrosion on ground support. The significant gaps in knowledge on the environmental conditions of underground mines and the effect corrosion has on support and reinforcement are discussed.

Based on the review conducted in Chapter 2 it was considered necessary to have an improved understanding of the underground environment and especially the main causes

of reinforcement corrosion. This would assist in defining the scope of the future experiments. Comprehensive and systematic data collection was carried out at eight underground mine sites across Australia collecting data on environmental variables and levels of visible corrosion damage to surface support and reinforcement elements. Chapter 3 discusses the results of this survey at each mine site and produces a summary of environmental conditions that can be considered a suitable cross-section of Australian metalliferous underground mines.

Chapters 4 and 5 discuss the development and results from the two principal research methods that investigate the effect of corrosion upon the surface support and reinforcement elements. The first research method was developed to overcome the difficulty and cost associated with ensuring adequate experimental controls for extended time periods (years) in the constantly changing nature of a working underground mine, in which the local environmental conditions are continually modified. This was achieved by simulating the underground environment by the use of purpose built corrosion chambers. Chapter 4 describes the requirements and subsequent development of the corrosion chambers. The methodology and results for a range of experiments conducted within these chambers are presented.

In addition, an overwhelming need to examine the bolts *in-situ* to complement the simulated results led to the development of a purpose built drill rig capable of overcoring reinforcement elements within a production mining environment. Overcoring programs were conducted at five underground mine sites, collecting data from a range of reinforcement elements of various ages and installed conditions. The recovered rock and reinforcement element core provides an accurate sample of the rock bolt system/rock mass interface allowing detailed analysis. The samples were examined and tested in the laboratory to gain a full insight into how corrosion was affecting the reinforcement. This work is presented in Chapter 5.

Chapter 6 describes the calculation of corrosion rates by direct testing of coupons. This method provides representative corrosion rates for a range of environments, helping to

define the main influences on the corrosivity. Chapter 7 reviews published classifications and investigates the relationship between the environmental parameters and measured corrosion rates discussed in Chapter 6. The outcome is the proposal of two new corrosivity classifications for groundwater affected and atmospheric environments in Australian underground hard rock mines.

The detrimental effect corrosion causes on the service life of rock reinforcement and support is discussed in Chapter 8. This chapter draws on data and analysis from the environmental survey, corrosion chamber experiments, overcoring of the reinforcement elements and the corrosivity classifications to provide estimated service lives for friction rock stabilisers, cable bolts and solid steel bar elements. Modes of failure and the benefit of corrosion protection methods are discussed.

Conclusions to the research and analysis conducted are presented in Chapter 9. Also discussed are limitations with the data and the subsequent analysis. Recommendations for further investigations into the corrosion of rock reinforcement and support are given.

CHAPTER 2 CORROSION FUNDAMENTALS AND GROUND SUPPORT USED IN AUSTRALIAN UNDERGROUND MINES

2.1 Introduction

As stated in Chapter 1 the effect of corrosion on the performance of rock support and reinforcement in Australian underground mines has not been widely researched. There is, however, extensive knowledge on general corrosion principles and to a lesser extent on the engineering application of rock support and reinforcement. This chapter provides a review and summary for those corrosion and ground support principles that are important in order to understand the corrosion of rock reinforcement in underground mines.

Section 2.2 provides an overview of iron corrosion principles and the forms of corrosion that may occur on support and reinforcement. A description of the underground mining environment with emphasis on the environmental factors that control the corrosivity is examined in Section 2.3. Section 2.4 discusses common corrosion protection methods. Rock support and reinforcement theory is discussed in Section 2.5 with Section 2.6 describing the main ground support types being investigated including previous related research.

2.2 Mechanics of corrosion

Corrosion is the destructive result of a chemical reaction between a metal or metal alloy and its environment (D A Jones 1996). The basic cause is the inherent instability of metals in their refined forms (CISA 1994). The large amounts of energy needed to extract metals from their minerals are emitted during the electrochemical reactions that produce corrosion. Corrosion returns the metal to its combined state in chemical

compounds that are similar to or even identical to the minerals from which the metals were extracted.

The electrochemical corrosion process that occurs in metals at ambient temperatures involves the transfer of electronic charge in aqueous solutions and can be described as an electrochemical cell. There are four basic components of the cell:

- An anode
- A cathode
- An electrically conducting solution
- An electrically conducting path (i.e. connection) between the anode and the cathode.

For corrosion to take place a common electrolyte must cover both electrodes. The two electrodes (anode and cathode) must be in electrical contact, generally through direct physical contact. There needs to be a sufficient difference in potential between the two electrodes to cause the current to flow and a sustained cathodic reaction must occur (CISA 1994).

2.2.1 Iron corrosion

Iron and various grades of steel are the main components used in support and reinforcement elements in underground mines. The mechanisms for the corrosion of iron are integral to understanding how different environments will change the rate and type of corrosion. A description of how each component of the electrochemical cell operates in the corrosion of iron is shown diagrammatically in Figure 2.1.

The anode is the site where the metal is corroded; the electrolyte solution is the corrosive mechanism with the cathode forming the other electrode. The cathode is not consumed or destroyed by the reaction taking place. The anode and the cathode can be part of the same metal surface or two metals in contact with each other; neither is permanently placed and can move locations on the metal surface.

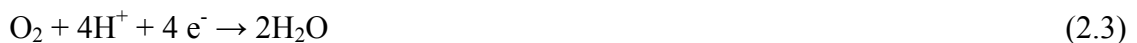
At the anode the metal in its elemental form is converted into a metal cation and dissolved into the electrolyte. The anodic or oxidation reaction for iron (Fe) is:



The released atoms must be utilised at some other point for the electrochemical reaction to occur. The cathodic or reduction reaction takes place at the cathode and is often much slower than the anodic reaction and controls the corrosion rate (cathodic control). The chemical reaction that occurs is dependent on the characteristics of the electrolyte. Within neutral and acid solutions exposed to ambient air the reduction of dissolved oxygen is observed (D A Jones 1996) by their respective reactions:



And in acid solutions

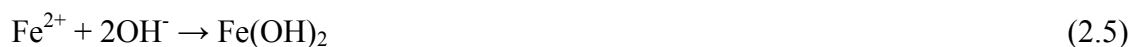


In the absence of all other reduction reactions water will be reduced by



For most mining applications the electrolyte solutions (mine groundwater) is near neutral and the cathodic reaction 2.2 would be expected to occur and is shown schematically in Figure 2.1. Localised environmental conditions may occur however, and other reactions such as, 2.3 or 2.4 may take place.

In the most common case involving a neutral solution, the soluble ferrous ions (Fe^{2+}) formed at the anode will meet with the hydroxide ions (OH^-) formed at the cathode at regions away from the electrolytic action to form ferrous oxide:



The ferrous oxide forms the diffusion-barrier layer next to the iron surface through which the dissolved oxygen must diffuse. Oxygen supply generally becomes limited by the diffusion capacity of the increasing thickness of the corrosion products limiting the rate of corrosion. The colour of ferrous oxide is white when pure but is normally green to greenish black due to incipient oxidation by air. On the outer surface of the oxide film access to the dissolved oxygen converts the ferrous oxide to ferric hydroxide by the following reaction:



Ferric hydroxide is orange to red-brown in colour and is the major constituent of ordinary rust. It exists as either magnetic or nonmagnetic Fe_2O_3 (hematite). Rust films normally consist of three layers of iron oxides in different states of oxidation (Roberge 2000).

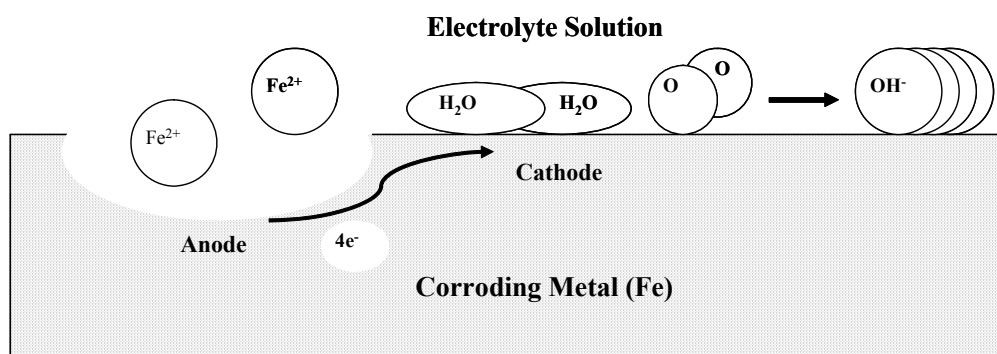


Figure 2.1 Schematic representation of the electrochemical iron corrosion process (Roberge 2000).

2.2.2 Passivity

In many metals, including iron and zinc, the corrosion rate decreases due to the formation of thin, protective, hydrated oxide, corrosion-product surface film that acts as a barrier to the anodic reactions. Most commercially available corrosion resistant alloys

depend on passive films for their corrosion resistance, with chromium a key alloying element. The passive film forms by direct electrochemical reactions generally as an oxide, but there is no visible evidence of the film on the surface of the metal. As the passive film is extremely thin and fragile, its breakdown can result in unpredictable localised forms of corrosion (D A Jones 1996).

2.2.3 Electrode potentials

The potential difference or driving force between the anode and cathode controls the electron flow and consequently has an impact on the corrosion rate. Standard electrode potentials of different electrochemical reactions have been measured and are commonly found in many reference texts. For a given electrochemical cell, the less reactive or noble reaction will be the cathode, while the more reactive reaction will be the anode.

Most steel corrosion occurs on a single metal surface with the cathodic reaction the reduction of oxygen in water as described in reaction 2.2. The potentials generated by this reaction are:

O^2/OH^- +0.401 volts cathode

Fe^{2+}/Fe -0.441 volts anode

The potential difference of 0.842 volts indicates that steel corrosion will occur in aerated waters. This indicates only a potential for the reaction to occur; factors such as the prevalent environmental conditions will determine the rate at which corrosion takes place.

A common coupling of metals is the sacrificial zinc (Zn) coating over steel (Fe). The potentials generated are:

Fe^{2+}/Fe -0.441 volts cathode

Zn^{2+}/Zn -0.763 volts anode

The potential difference of 0.322 volt between the coupled metals means that zinc will preferentially corrode for steel. The use of zinc as a corrosion protection method is discussed later in this section.

2.2.4 Forms of corrosion on support and reinforcement in the underground environment

The nature of the corrosion process will depend upon the interaction between a material and its environment. There are various forms of corrosion; however, only three types have been identified to be relevant to this research. These are uniform corrosion, pitting corrosion and stress corrosion cracking, all shown schematically in Figure 2.2. Other corrosion types such as galvanic and crevice corrosion may be present but are not considered a significant influence.

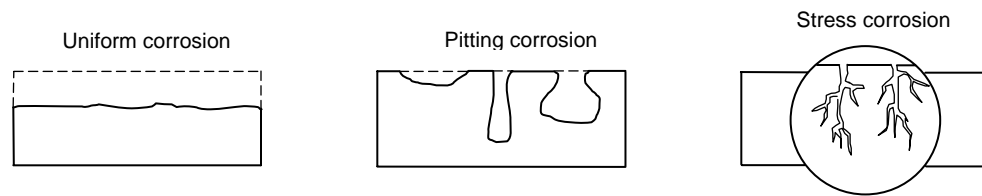


Figure 2.2 Schematic representation of uniform corrosion, pitting corrosion and stress corrosion cracking

Uniform corrosion occurs when the anodic and cathodic areas on the metal surface change position continuously, resulting in a regular removal of metal from the surface. For this to occur the corrosive environment must have access to all parts of the metal surface, and the metal itself must be metallurgically and compositionally uniform. These requirements are not always prevalent and some degree of non-uniformity is tolerated within the definition of uniform corrosion (D A Jones 1996). This corrosion form is relatively predictable and is often incorporated into design.

Pitting corrosion is the highly selective attack of metals at defects in the passive oxide layer that results in relatively rapid penetration at small discrete areas. The corrosion attack is in the form of pits, which can be shallow, deep or undercut and are usually covered by the corrosion products making identification difficult. Pitting usually occurs in solutions containing chlorides, and becomes autocatalytic as the anodic reaction becomes localised within the pit and cations are liberated into the pit solution creating a charge imbalance. As a result, anions such as chloride ions diffuse from the bulk

electrolyte solution to the pit to equalise the charge. This has the combined effect of further simulating corrosion by forming soluble corrosion products (CISA 1994) as well as acidification. Pitting is considered to be more dangerous than uniform corrosion as it is difficult to detect, predict and design against (Roberge 2000).

Stress corrosion cracking (SCC) is used to describe service failures in materials that occur by slow environmentally induced crack propagation (Jones & Ricker 1990). The cracking is induced from the combined influences of tensile stress and a corrosive environment and crack propagation proceeds slowly until it reaches its critical length and rapid fracturing occurs. The required tensile stresses may be in the form of directly applied or residual stresses. Usually, most of the surface remains undamaged, with fine cracks penetrating into the material and thus is very difficult to detect and damage is not easily predicted. SCC is not commonly thought to occur in the hard rock metalliferous mines investigated in this project. However, some evidence of stress corrosion cracking and corrosion fatigue was observed in failed rock bolts from the Big Bell gold mine (Collins 2002). Reinforcement failure by this corrosion form has been investigated in a number of Australian coal mines by Hebblewhite et al. (2004) in environmental conditions that are not found in hard rock mines. The report concluded that by changing the steel grade of the reinforcement elements to a higher fracture toughness the problem may be eliminated.

2.3 The underground mining environment

The environment a material is placed in, along with the material properties ultimately controls the types and rates of corrosion. Environmental conditions in underground mines are never homogenous and are constantly changing; only approximations can be made for classifying the environment and such approximations must be constantly reviewed. There are three main environmental influences that affect the installed ground support in terms of corrosion. These are the atmosphere, the groundwater, and the rock mass.

2.3.1 Atmospheric variables

Atmospheric corrosion is the corrosion of materials exposed to air and its pollutants and has been reported to account for more failures in terms of cost than any other factor (Roberge 2000). Humidity is essential for atmospheric corrosion as it (along with the temperature) controls the condensation of water (electrolyte) onto the metal surface (see Figure 2.3). The commencement of condensation is referred to as the critical humidity. The length of time conditions are favourable for the formation of a surface layer of moisture is referred to as the time of wetness (TOW). This is a function of the relative humidity and temperature. Below the freezing point of water the corrosion rate is negligible, but with increases in temperature the rate of corrosion increases, although the TOW is generally reduced.

For iron, the critical humidity appears to be about 60%; at this level, rust slowly begins to form. At 75 to 80% relative humidity, there is a sharp increase in corrosion rate that is speculated to occur because of the capillary condensation of moisture within the rust corrosion product layer. At 90% relative humidity, there is another increase in the corrosion rate corresponding to the vapour pressure of ferrous sulphate. The critical relative humidity for zinc appears to be between 50 and 70%.

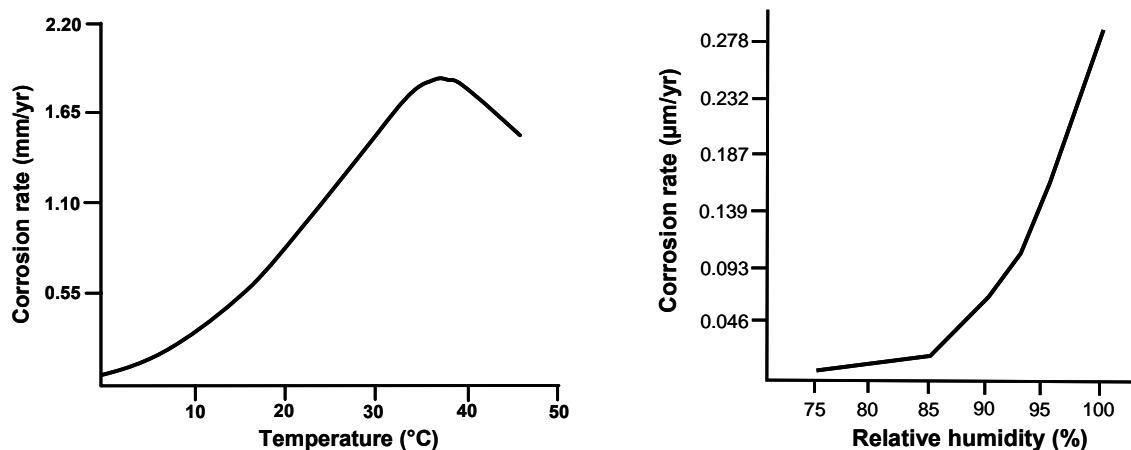


Figure 2.3 The influence of temperature and relative humidity on atmospheric corrosion (Roberge 2000).

The thin film electrolytes are often invisible to the naked eye and tend to form on metallic surfaces after the critical humidity is reached. The critical humidity is generally accepted to be approximately 60% relative humidity for an atmosphere with no pollutants. Corrosion of uncontaminated surfaces, however, is often relatively low in unpolluted atmospheres

The level of contaminants often controls the rate of atmospheric corrosion by enhancing the electrolytic properties and stability of water films condensing. Pollutants such as sulphur dioxide (SO₂) mix with the electrolyte producing sulphuric acid which renders the corrosion product films non-protective (D A Jones 1996). Sulphur dioxide along with other pollutants such as atmospheric chlorides, nitrogen compounds and dust particles can also reduce the relative humidity necessary to cause water condensation by absorbing water from the atmosphere. In atmospheres containing 0.01% SO₂, the corrosion rate of carbon steel is as much as six times higher than those with no pollutants (Kaesche 1985). The process of blasting and the use of diesel equipment in underground mines are the major sources of contaminants in underground mines. These can be further concentrated due to restricted ventilation systems.

2.3.2 Groundwater variables

Groundwater flowing from the rock mass is present in nearly all underground mines. The affected elements are not generally submerged but are located at the water/atmosphere interface that is analogous to marine splash zones. Marine splash zones generally have a higher corrosion rate than areas where the metal is continuously submerged (Bardel 2004). The corrosivity of the waters, either fresh or saline, is not controlled by one variable, but includes a number of parameters that are interrelated.

Dissolved oxygen is required for corrosion to occur in neutral and alkaline waters. Any factors affecting the level of dissolved oxygen will proportionally affect the corrosion of steel (D A Jones 1996). The rate of corrosion of iron and steel in aerated waters at a constant temperature and salinity is a direct linear function of the dissolved oxygen concentration, as shown in Figure 2.4. The solubility of dissolved oxygen decreases with

increasing temperature and salinity. However, the effects of dissolved oxygen on the corrosion rate are often stronger than those of temperature and salinity.

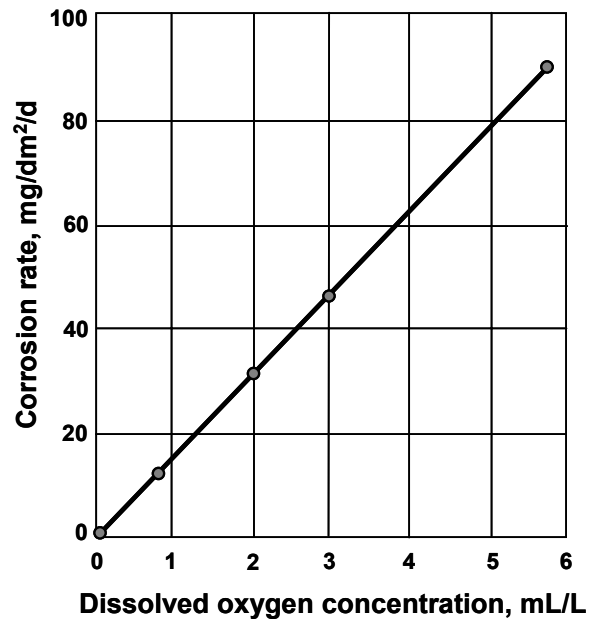


Figure 2.4 Effect of oxygen concentration on the corrosion of low-carbon steel from (Uhlig & Revie 1985).

When all other factors are held constant, an increase in temperature increases the corrosivity of waters. If the dissolved oxygen concentration is held constant, the corrosion rate of low-carbon steel in seawater will approximately double for each 30 °C increase in temperature (see Figure 2.5) (Heidersbach 1990), up to a peak of approximately 80°C above which dissolved oxygen is lost from the system as the boiling point of water is reached.

The concentrations of major ions influence the conductivity of the water, with chlorides influencing the breakdowns of passive films. The total salinity is generally referred to as the Total Dissolved Solids (TDS) and expressed as parts per million (ppm) with individual concentration of anions and cations described in milligrams per litre (mg/L). The high conductivity of saline waters means that large areas of exposed cathode surface are available to support the relatively small anodic areas at which pitting corrosion takes

place. Additionally chloride and sulphate ions play a significant role in the penetration and breakdown of any protective film that might have formed on the metal surface. The higher the salinity of the water, the more readily the chloride ions succeed in penetrating the passive film and initiating localised corrosion (Heidersbach 1990).

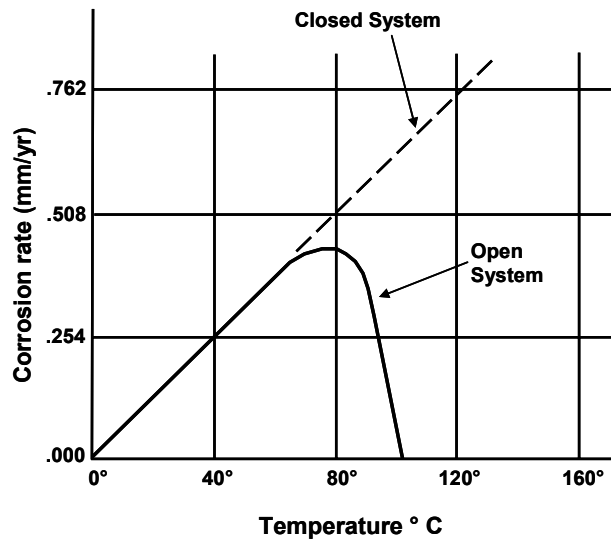


Figure 2.5 The effect of temperature on the corrosion rate of steel.

The effect of increasing the halite (NaCl) concentration on the relative corrosion rate of iron is shown in Figure 2.6. The maximum corrosion rate occurs near 35,000 ppm, the approximate salinity of seawater. Further increases in salinity reduce the rate of corrosion due to a decrease in the level of dissolved oxygen. For metals that corrode uniformly, variations in corrosion rate due to salinity are small compared to those caused by changes in oxygen concentration and temperature (Heidersbach 1990).

Waters that contain dissolved calcium and magnesium cations may precipitate a layer of water-insoluble, carbonate salt on a metal surface known as scaling. This film commonly slows or prevents corrosion by providing a barrier between the metal and the electrolyte. The tendency for calcium carbonate to form and provide corrosion resistance in fresh water is measured by the saturation index. Its effect in reducing corrosion in saline waters is impeded as the deposits formed are more porous and less effective as a protective coating. There exists a critical value for chloride concentration; approximately

25 ppm, above which the carbonate protective scale is ineffective (Sastri, Hoey & Revie 1994).

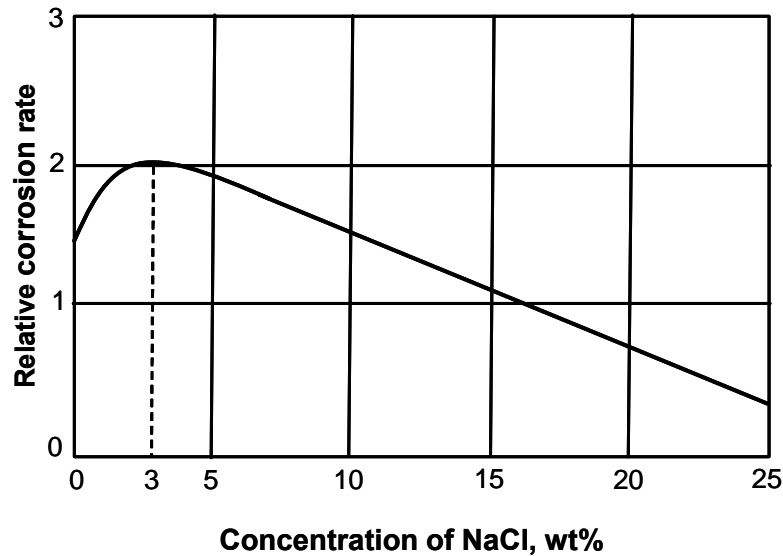


Figure 2.6 Effect of NaCl concentration on the corrosion rate of iron in aerated room-temperature solutions from (Uhlig & Revie 1985).

The control the pH value exerts on the corrosivity of a system depends to a large degree on the solubility of the corrosion product (usually the oxide) formed on the metal surface. Under normal conditions, the corrosion rate of steel is independent of pH values between 4 and 10 as shown in Figure 2.7. Below a pH of 4 the oxide is soluble and corrosion increases, due the availability of H^+ ions. At pH above 10, corrosion rate is low, due to the formation of a passive ferric oxide film.

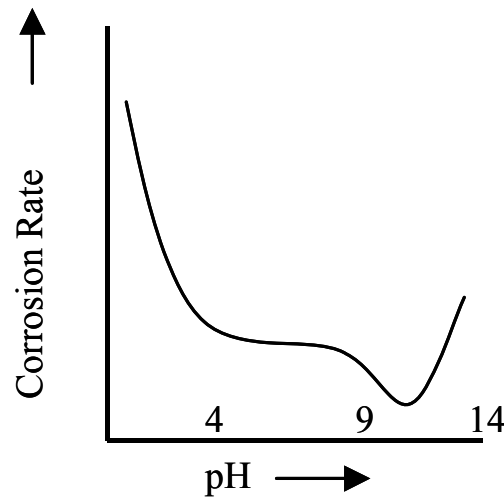


Figure 2.7 The effect of pH on the corrosion rate (CISA 1994).

Micro-organisms within waters can influence corrosion in a variety of ways, from the creation of differential aeration cells, to the excretion of corrosive species, to direct involvement in the electrochemical process termed microbiologically influenced corrosion (MIC) (CISA 1994). While there has been no indication of MIC in hard rock groundwaters, Hebblewhite et al. (2004) noted in coal mines bacteria associated with corrosion, specifically in pyritic clay bands.

The velocity of the water past a material surface can damage any protective layer allowing a high rate of corrosion to continue. The extent of the erosion damage will be determined by the hardness of the material, the tenacity and wear resistance of the surface layer, the turbulence close to the surface, and the presence of abrasive particles in the fluid (CISA 1994). High rates of flow also bring a greater quantity of dissolved oxygen in contact with the metal surface thus further influencing the corrosion rate.

2.3.3 Rock mass variables

The rock mass is the material that the support and reinforcement is installed in and indirectly influences the corrosive potential of a mine environment. Rock mass structures are primarily important as they provide a conduit for ground and fill water flow. Major geological structures such as faults and shears allow the flow of

groundwater into the mine from surrounding aquifers. The extent of the area affected by the water is increased by the presence of interconnected, dilated geological structures (joints), which allow the groundwater to travel and dissipate at significant distances from the source. Opening of joints can occur during the initial excavation or subsequently at a later date due to blasting or stress changes.

The mineralogy associated with the different rock masses is not expected to influence the corrosion potential of an environment. The majority of minerals are generally inert and do not enhance the corrosion process in any major way. An exception is for sulphide minerals. These reactive minerals oxidise, producing localised acidic conditions when exposed to air and water. The oxidation reaction may also create an electrochemical corrosion cell with the rock reinforcement, further accelerating corrosion. Such occurrences will only occur in specific areas where the sulphide content of the rock mass is high.

2.4 Protection of steel from corrosion

The protection of steel from corrosion is often essential for most support and reinforcement applications. The chief factors that determine whether steel needs to be protected include: the overall economics, environmental conditions, degree of protection needed for the projected life of the part, consequences of unexpected service failure, and importance of appearance. The final outcome should be the most effective and economic method of achieving that protection. The protection of steels is achieved through two methods; the first is to separate the metal from the environment, the second to reduce the reactivity of the environment (Bryson 1990).

The separation of the metal from the environment can be achieved with metallic, organic or inorganic coatings and film-forming inhibitors. Organic coatings such as paint, powder coatings, rubber linings and epoxy resins act primarily as a physical barrier between the substrate and the corrosive environment. Inorganic coatings include enamel,

ceramics and cement. The use of cement and resin grouted reinforcement elements is common in underground mining applications. Cement and resin grouts provide a physical barrier to the local environment. In addition cement grout inhibits corrosion by providing an alkaline environment through which any electrolyte has to pass and allows for passivation of the steel.

The major factors that cause steel embedded in cementitious systems to corrode are the influences of carbonation and chloride infiltration (Slater 1990). When a concrete structure is exposed to water containing salts, chloride ions from these will slowly penetrate into the concrete, mostly through the pores in the hydrated cement paste. The chloride ions will eventually reach the steel and then accumulate to beyond a certain concentration level, at which the protective film is destroyed and the steel begins to corrode (Corrosion Doctors 2006).

Carbonation occurs when carbonic acid comes into contact with the cement from atmospheric carbon dioxide. The rate of carbonation in concrete is directly dependent on the water/cement ratio (w/c) of the concrete; the higher the ratio the greater is the depth of carbonation in the concrete. In concrete of reasonable quality, that is properly consolidated and has no cracking, the expected rate of carbonation is very low (Virmani & Clemena 1998).

Coatings of metallic zinc are generally regarded as the most economical means of protecting against corrosion and are common for the protection of support and reinforcement. For most reinforcement elements zinc is usually applied by hot dip galvanising to a thickness of approximately 85 microns (600 g/m^2) and should conform to Australian Standard 4680 (1999). For coatings on steel wire Australian Standard 4534 (2006) is followed with a range of possible coating masses between 80 to 725 g/m^2 . For weld mesh a coating mass of 80 g/m^2 is generally used.

Zinc provides a three-fold protection. It operates initially by providing a tough and adherent coating, which seals the underlying metal from contact with a corrosive

environment. If the coating is breached so that the steel is exposed, the zinc corrodes preferentially. Zinc corrosion products then form a barrier on the exposed steel protecting the steel and preventing the need for zinc to continue to corrode sacrificially. The corrosion rate of zinc is generally much less than steel in most environments. Exceptions are for waters with a pH less than 4 and greater than 12.5, and when the temperature is greater than 60 °C, when zinc then becomes more noble than steel and induces pitting in the steel.

Problems may arise with the use of zinc coatings in cement grout as gas bubbles may occur at the cement/zinc interface due to the formation of hydrogen gas when the grout is still wet. The gas bubbles result in a weak, spongy interface with a higher permeability. This can be avoided by the addition of chromium trioxide to the cement (Windsor 2004). Other metallic coatings include cadmium, chromium, nickel and aluminium; however, these are not commonly used for the protection of ground support products due to the increased costs.

The reactivity of an environment can be reduced through cathodic or anodic protection. Cathodic protection is widely used to protect structures buried in soil or immersed in seawaters and is achieved by electrochemically connecting a sacrificial anode or by using an impressed current that is connected to the structure being protected. Environmental conditions in underground mines do not facilitate this style of protection as the material is not wholly immersed in an electrolyte. Anodic protection has a limited use for the mining industry (CISA 1994) and the chemical treatment of groundwaters is not viable. For these reasons cathodic, anodic or chemical treatment of the environment is not feasible for the protection of ground support and reinforcement.

Corrosion inhibitors are chemical compounds that when added to a corrosive environment in small concentrations, reduces the aggressive nature of the environment by a reaction at the metal/solution interface (CISA 1994). There are three major types of inhibitors; passivation inhibitors that prevent the anodic corrosion reaction, precipitation inhibitors that block the cathodic reaction by deposition at the cathode and absorption

inhibitors that provide a chemisorbed layer of organic molecules that protect the metal by physically blocking the surface to oxygen. These may provide some benefit in reducing corrosion damage of support and reinforcement.

In addition to the active forms of corrosion prevention described, design and material selection are as important to the overall corrosion performance. This is generally the domain of manufacturers with the end users, being the mining companies, having limited input.

2.5 Rock support and reinforcement principles

The purpose of rock support and reinforcement is to maintain excavations safe and open for their intended life spans; for mining applications this ranges from months to tens of years. There are a wide range of commercially available support and reinforcement products; however, it is important to clearly distinguish the difference between support and reinforcement. Windsor and Thompson (1993) characterise support as to include all methods which essentially provide surface restraint to the rock mass by installation of structural elements on the excavation boundary. Reinforcement is considered to include methods which modify the interior behaviour of the rock mass by installation of structural elements within the rock mass. The term ground support however, describes both support and reinforcement installed in the rock mass.

Primary ground support is applied during or immediately after excavation to ensure safe working conditions. It may provide part, or may form the whole, of the ground support regime. Any additional support or reinforcement applied at a later stage is termed secondary. Support or reinforcement may also be classified as being either active or passive. Active ground support imposes a predetermined load to the rock surface generally through the form of tensioned reinforcement. Passive ground support is not installed with an applied loading, but develops its loads as the rock mass deforms (Brady & Brown 1993).

Support methods work by providing a reactive force at the excavation face and respond to inward movement of the surrounding rock. The more complex behaviour of a reinforcing system is explained through the load transfer concept. The concept shown schematically in Figure 2.8 can be used to understand the stabilising action of all the reinforcing devices and their effect on excavation stability. The concept can be explained by three individual components (Windsor & Thompson 1993):

1. Rock movement at the excavation boundary, which causes load transfer from the unstable rock, wedge or slab to the reinforcing element.
2. Transfer of load via the reinforcing element from the unstable surface region to a stable interior region within the rock mass.
3. Transfer of the reinforcing element load to the rock mass in the stable zone.

A supported rock block may fall due to failure of any of the three separate components of load transfer due to insufficient steel capacity (rupture of the reinforcing element) or inadequate load transfer (slippage). The critical embedment length is the minimum length of reinforcement that is needed to mobilise the full capacity or strength of the bolt.

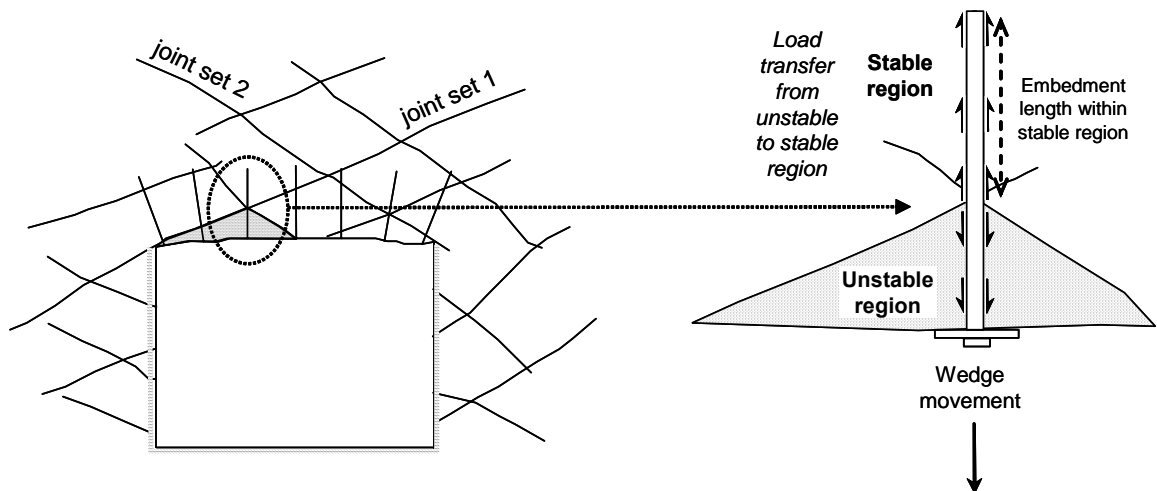


Figure 2.8 Load transfer and embedment length concepts (Villaescusa & Wright 1997).

The load transfer mechanisms for all reinforcing elements and the rock mass can be placed within three categories as developed by Windsor and Thompson (1993). The categories shown in Figure 2.9 are continuously frictionally coupled (CFC), continuously mechanically coupled (CMC) and discrete mechanically and frictionally coupled (DMFC). The effect corrosion will have on the load transfer mechanisms will be different for each category.

Continuous frictionally coupled (CFC) elements are installed in direct contact with the rock mass. Load transfer results from frictional forces between the reinforcement element and the borehole wall (Windsor & Thompson 1993). This is achieved by either the installation of an oversized element into an undersized borehole e.g. Split Set (R L Davis 1979) or by the expansion of an undersized section into an oversized borehole e.g. Swellex.

Continuous mechanically coupled elements (CMC) rely on a fixing agent, generally cement or resin grout, which fills the annulus between the element and the borehole wall for the entire borehole length. The major function of the grout is to provide a mechanism for load transfer between the rock and the reinforcing element. The reinforcing element is manufactured in a variety of cross-sectional shapes to produce a geometrical interference between the element and the grout creating a mechanical key. When the geometrical interference extends over the length of the element, it is coupled continuously to the rock mass by way of the grout (Windsor & Thompson 1993).

A discrete mechanically and frictionally coupled element (DMFC) transfers the load at two discrete points, the borehole collar and the anchor point, with the remaining element length being decoupled from the rock mass. The anchor point, which is located at some depth in the borehole, is either mechanically (grouted anchor) or frictionally (expansion shell) coupled to the rock mass over a relatively short interval usually limited to less than 500 mm. This anchor must be strong enough to mobilise the full capacity of the element.

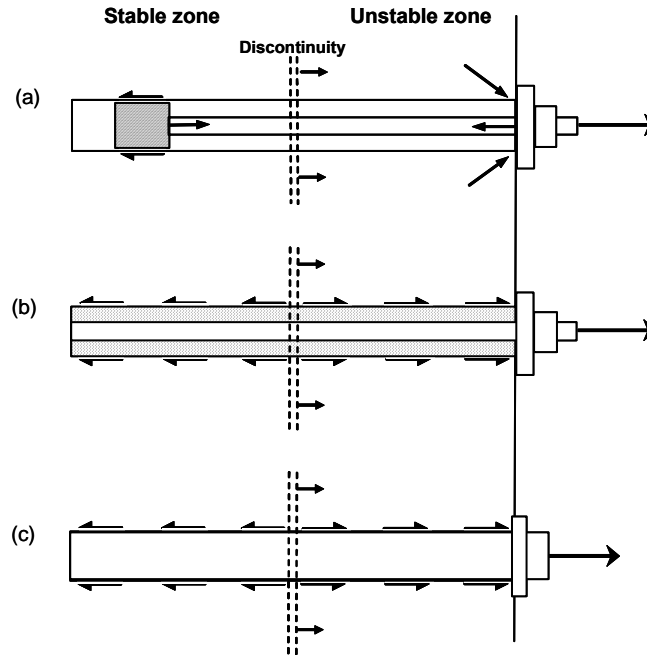


Figure 2.9 Categories of reinforcing element load transfer types: (a) DMFC, (b) CMC and (c) CFC (Windsor & Thompson 1993).

2.6 Investigated rock support and reinforcement used in Australian underground mines

Despite the extensive variety of commercially available reinforcement elements and their widespread use; estimated at 500,000,000 units annually in civil and mining industries worldwide (Windsor & Thompson 1993), all types can be categorised as either CFC, CMC or DMFC. The effect of corrosion on the load transfer capacity for each category will be somewhat similar despite different commercial names and slight variations in design. The following support and reinforcement devices described are certainly not inclusive to all that is available, but constitute the main ground support observed in Australian underground mines.

2.6.1 *Friction rock stabilisers*

The friction rock stabilisers, also known by their commercial names Split Set (R L Davis 1979), Strata Bolt (Strata Control Systems 2006) and Friction Bolt (DSI 2006b), consist of a hollow round tube with a slot along the entire length. When driven into a drilled hole of smaller diameter the friction between the steel tube and the rock provides support as shown in Figure 2.10. They rely on the load transfer resulting from friction between the reinforcement element and the borehole wall. The initial strength per metre of embedment length is limited by the radial prestress set up during installation. This is a function of the friction rock stabiliser diameter, the borehole diameter and any geometrical irregularities occurring in the borehole wall.

Thin-walled, 34 – 47 mm diameter galvanised friction rock stabilisers are extensively used as reinforcement for long life excavations. The reinforcement elements generally have a nominal wall thickness of 3 mm and are mechanically installed using jumbos. They are manufactured using a HA350 grade steel to Australian Standards 1594 (AS 1594 2002) with chemical composition and mechanical properties shown in Table 2.1.

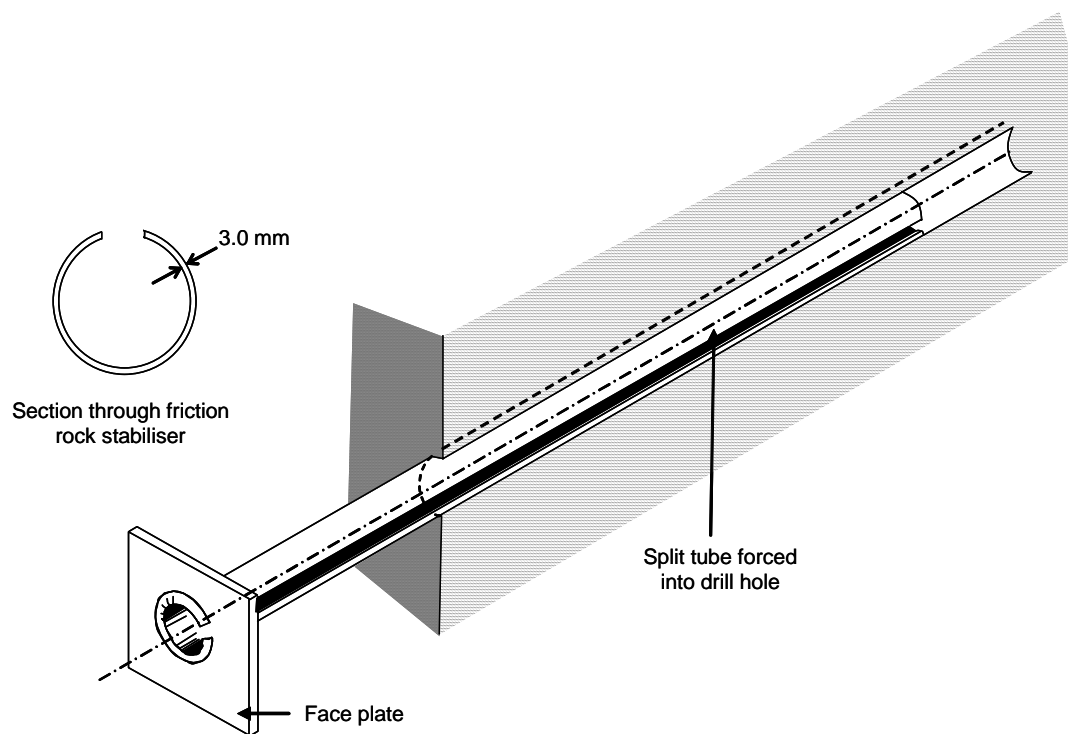


Figure 2.10 The components of a friction rock stabiliser (Hoek, Kaiser & Bawden 1995).

Table 2.1 Chemical composition and mechanical properties of HA350 grade steel for friction rock stabilisers.

Steel Grade	Chemical composition (% Max.)					Minimum upper yield stress (MPa)	Minimum tensile strength (MPa)
	Carbon	Silicon	Manganese	Phosphorus	Sulfur		
HA350	0.20	0.35	1.60	0.040	0.030	350	430

Such, thin tubular devices have a large surface area susceptible to corrosion attack. Despite corrosion remaining one of the prime problems with friction rock stabilisers (Hoek, Kaiser & Bawden 1995) there has been only limited investigations into this issue. The Department of Minerals and Energy of Western Australia initiated a research project focused on the influence corrosion has on the effectiveness of friction rock stabilisers (Ranasooriya, Richardson & Yap 1995). It was found that a 30 percent loss of tensile strength can be attributed a 10 percent localised mass loss or a 20 percent average mass loss. The main forms of corrosion observed were uniform and pitting corrosion and severe corrosion can occur in a relatively short period of time. Laboratory testing found

that transition element metals such as nickel and copper in ore samples resulted in a two to four fold increase in the rate of corrosion (Ranasooriya, Richardson & Yap 1995).

Stimpson (1998) found that corrosion of friction rock stabilisers after 90 days actually increased the frictional capacity by 192 percent. He concluded, however that over longer periods of time the strength capacity will decline as corrosion increases. In an effort to better predict the useful service life of friction rock bolts the US Bureau of Mines initiated electrochemical and weight loss testing in selected underground mine waters (Jolly & Neumeier 1987; Tilman, Jolly & Neumeier 1985). The majority of mine waters precipitated a protective calcium carbonate film lowering the corrosion rate with the exception of waters with high chloride content. It was also observed that there was a tendency towards pitting corrosion of the metals and that particular attention should be given to the pitting of installed bolts. Jolly and Neumeier (1987) concluded that friction rock bolts due to their thin wall construction should not be normally recommended for long-term use.

2.6.2 Swellex bolts

The Swellex bolt (Atlas Copco 2007) consists of a collapsed steel tube that has been sealed at either end. A small expansion hole is located near the collar of the bolt. The element is placed in a borehole and inflated with water at 30 MPa resulting in the collapsed tube expanding to conform to the borehole profile, shown in Figure 2.11. Depending on hole inclination the water used to inflate the bolt is designed to flow out of the expansion hole following installation. The element is coupled to the borehole wall due to frictional forces. Three types of Swellex are available based on steel grade; the standard Swellex, the manganese Swellex with greater tensile strength and elongation and the premium Swellex which has the greatest strength. A rubberised bitumen (Plastisol) coating is available for corrosion protection on the outside surface of the element (CPI Corrosion LTEE 2003).

Research into the corrosion behaviour of Swellex bolts has determined that a Swellex coated in the rubberised bitumen is 1000 times more corrosion resistant than uncoated

Swellex in moderately corrosive waters (CPI Corrosion LTEE 2003). Retrieval and examination of two coated Swellex bolts from the Kvarntorp Mine in Sweden after a service life of nine years in a corrosive environment showed the loss of the coating, but minimal corrosion on the element that did not affect the strength of the bolt (Korrosionsinstitutet 2002a). Empirical calculations concerning the corrosion due to water remaining within the bolt due to expansion and subsequent obstruction of the expansion hole preventing water egress based on groundwater from the Kemi Mine in Finland concluded the internal corrosion will be less than $0.15\text{ }\mu\text{m}$ after 50 years (Korrosionsinstitutet 2002b). However, this groundwater is significantly less saline than groundwaters from Australia.

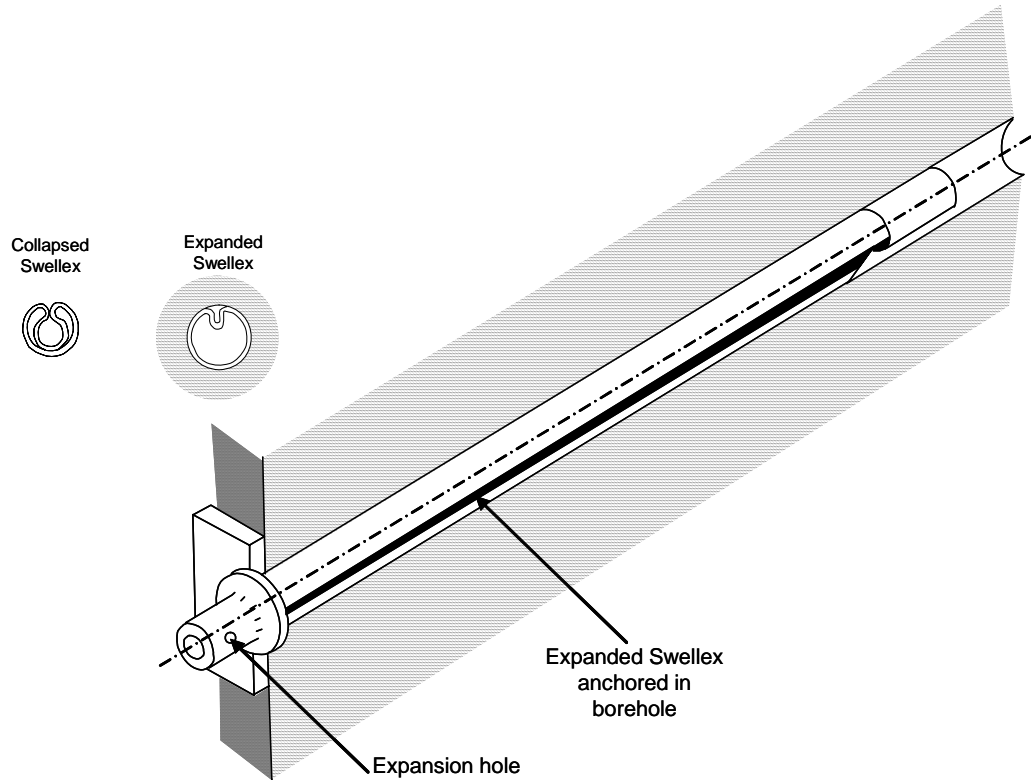


Figure 2.11 The components of the Swellex bolt (Hoek, Kaiser & Bawden 1995).

2.6.3 Cable bolt systems

Cable bolt reinforcement is used to stabilise large single blocks or wedges formed in the backs and walls of excavations. Cable bolts provide effective reinforcement of very large spans where normal rock bolts would prove inadequate geometrically due to their short lengths. Cable strands are able to bend around fairly tight radii, with the installation of long bolts from confined working places possible (Hutchinson & Diederichs 1996). The cable bolt reinforcement system is made up of four components (Windsor 2004) shown schematically in Figure 2.12:

- The rock
- The Element (Strands)
- The Internal Fixture (Grout)
- The External Fixture (Plate and Grips)

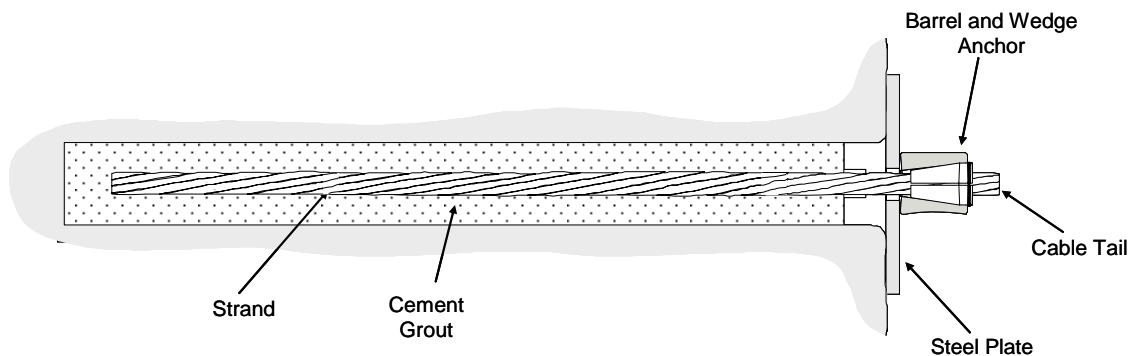


Figure 2.12 A basic cable bolt assembly (Thompson 2004b).

Cable bolts commonly use a 7-wire, stress relieved, high tensile steel strand with plain (round) wires. Six wires are laid helically around a slightly larger diameter central (king) wire. The regular 15.2 mm diameter strand can be produced to provide a number of grades that offer differing yield and ultimate load qualities. The basic cablebolt is the plain strand cable bolt, however, a number of different types of modified cable bolt strand have been developed in response to problems encountered with plain strand (Hutchinson & Diederichs 1996). The modified strand e.g. bulbed strand (Garford Pty Ltd. 1990), generally possess enhanced bond strength and stiffness.

When mining in high stresses, on going time-dependent deformations or unexpected rock failures due to high stress may be experienced. In order for ground support to survive the large displacements and control the rock mass, “yielding” cable bolts have been developed in South Africa e.g. (Wojno & Kuijpers 2001), (Ortlepp et al. 2005) and Australia e.g. (Garford Ground Support Systems 2002). These cable bolts are designed to allow for large displacement of the reinforcement element. This is achieved through having a “sliding” internal anchor mechanism and decoupling of a significant length of the strand from the grout and rock mass. Decoupling of the strand is used to enable tension to be established in the strand and to reduce the cable bolt stiffness in response to rock mass displacements.

The result is a cable bolt system constrained only in the toe and collar regions. In the toe region, there is an initially fixed anchor that is subsequently able to move at a designed force. At the collar, a plate is restrained by a barrel and wedge anchor that is coupled to the strand. A schematic representation of a yielding cable bolt is shown in Figure 2.13. The system is effectively a point anchored system. Consequently, the performance of the plate and barrel and wedge becomes critical for effective reinforcement of the rock.

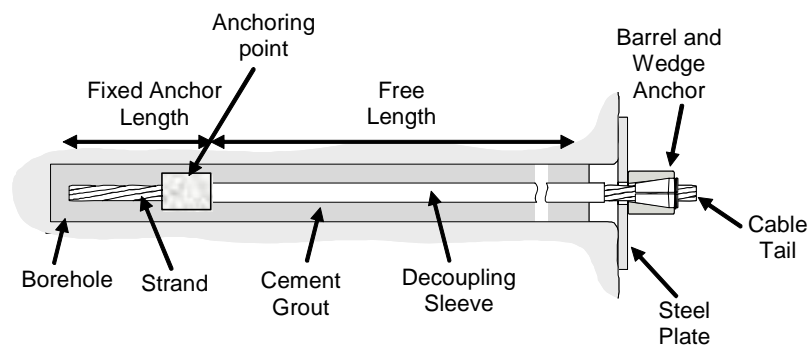


Figure 2.13 Schematic representation of a yielding cable bolt (Thompson 2004b).

A cable bolt element is generally fixed to the rock within the borehole through cementitious grouts comprising of Portland grade cement and water. Various water cement (w/c) ratios and admixtures are used to improve certain chemical or physical properties (Windsor 2004). The external fixture comprises of an assembly of a steel

plate, steel barrel and wedge fittings (or grips) and if necessary, bearing washers and seats. There are two common types of barrels; flat ended to be used with a flat plate and hemispherical ended to be used with a dome plate. These barrels can be used with either two-part or three-part wedges. The barrel and wedge anchors are installed and tensioned to provide a compressive force against the rock mass surface.

With cable bolt systems stabilising large volumes of rock the consequences of premature failure from the effects of corrosion can be significant. Corrosion protection measures such as galvanising, epoxy fused coating, and combination sheathing are all available to the Australian mining industry, but their implementation is limited due to the associated extra cost. Windsor (2004) noted that there are no standards for corrosion protection of cable bolts despite Australia being at the forefront in civil engineering applications. Furthermore, he suggests that some cable bolt installation practices may actually provide conditions that assist corrosion.

Some aspects of reinforcement installation may introduce pre-service faults and defects into the reinforcement system that may initiate and accelerate the process of corrosion. These include the water cement ratio and the degree of encapsulation of the element by the grout. It is recommended that the strand should be clean and free from rust at time of installation and water with a low chloride content should be used with a water cement ratio of 0.30-0.45 (Windsor 2004).

An extensive worldwide study on the corrosion of ground anchors was carried out by the Federation Internationale de la Precontrainte (FIB 1986), which found that corrosion is usually localised within the reinforcement length and that the external fixtures are particularly vulnerable. This has been confirmed by Thompson (2004b) who demonstrated in the laboratory that corrosion of the barrel and wedge fixture causes failure at low loads compared to design.

2.6.4 Rock bolts and dowels

Rock bolts generally consist of a plain steel rod with a mechanical or grouted anchor at one end and a face plate and a nut at the other. They are always tensioned after installation. For short-term applications they are left ungrouted, for permanent ground support the gap between the rock and bolt is filled with grout. Dowels, are not pre-tensioned and consist of a deformed steel bar which is grouted into the rock. As tensioning is not possible the load in dowels is generated by movements in the rock mass (Hoek, Kaiser & Bawden 1995).

UngROUTED rock bolts are coupled to the rock mass through a short anchor, either mechanically or chemically (cementitious or resin), where the anchor strength is limited by the strength of the rock around the borehole. These point anchored bolts are not consistently reliable beyond three to six months due to rock movement and the effect of corrosion (Villaescusa & Wright 1999). Typically, grouting of the element (post installation) is undertaken to ensure long-term protection. Two common rock bolt types are the CT bolt and the Hollow Groutable Bolt (HGB).

The CT bolt shown in Figure 2.14 has a corrugated polyethylene sleeve and a hollow hemispherical washer through which the grout is injected. The grout flows through the inside of the sheath, emerging at the top and then subsequently filling the borehole from the top down. Long-term protection is achieved through the dual protection of the ground and the plastic sheath. The HGB displayed in Figure 2.15 uses a similar concept, with the grout being pumped up through a central hole in the element. While this ensures that the element is grouted from the top down, the reduction of steel from the element make it more susceptible to corrosion damage.

Resin anchored rock bolts and dowels generally have a high speed of installation with the full capacity of the bolt being realised after a few minutes due to the quick set nature of the resin. The resin product is made up of two components; a resin and a catalyst separated within a plastic cartridge. The cartridges are placed in the drill hole ahead of the rock bolt which is spun during installation to break the plastic sheath and mix the

resin and catalyst (see Figure 2.16). Enough resin needs to be placed in the borehole to adequately fill the annulus between the borehole wall and the element.

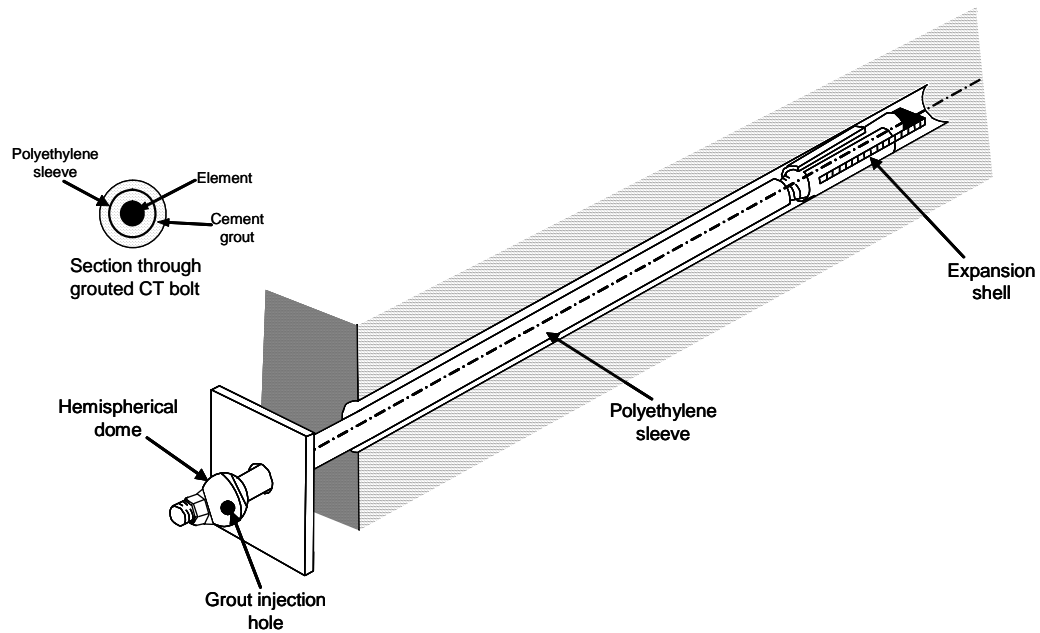


Figure 2.14 The components of a CT bolt.

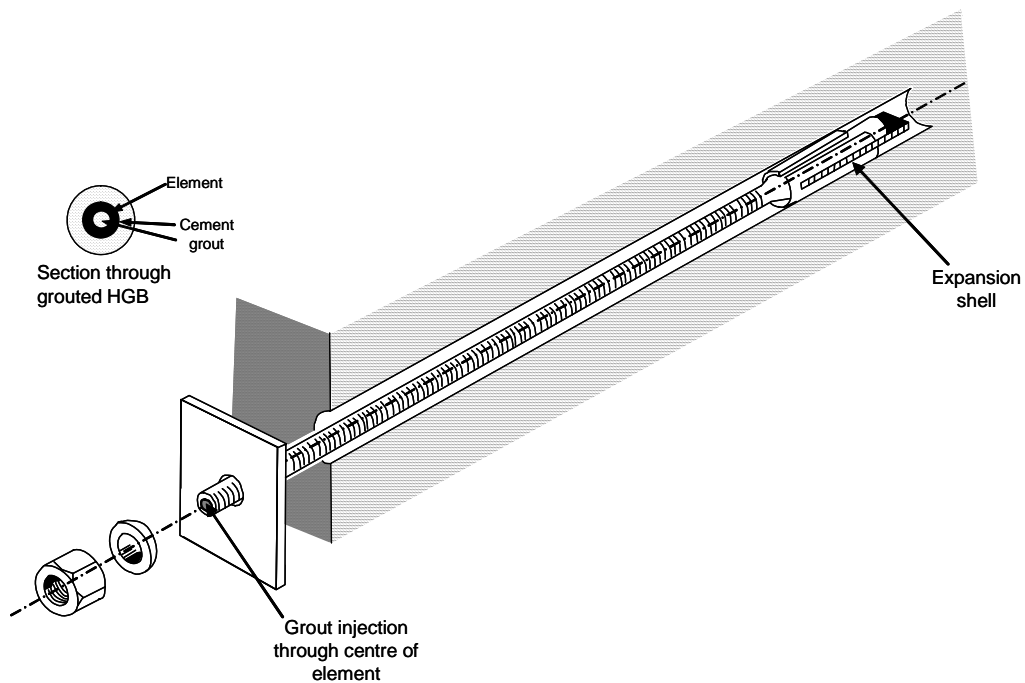


Figure 2.15 The components of the Hollow Groutable Bolt (HGB) (Hoek, Kaiser & Bawden 1995).

Resin grouted elements may be tensioned or non-tensioned. Tensioning fully encapsulated resin rock bolts is achieved by placing a quick set resin at the toe of the borehole with slow setting resin cartridges inserted behind. Tensioning can be completed after a few minutes once the quick set resin has hardened. Resin grout provides a physical barrier protecting the element from the corrosive environment; however, there is some uncertainty about the long-term corrosion protection offered by resin grouts and also about the reaction of some resins with aggressive groundwaters (Hoek, Kaiser & Bawden 1995).

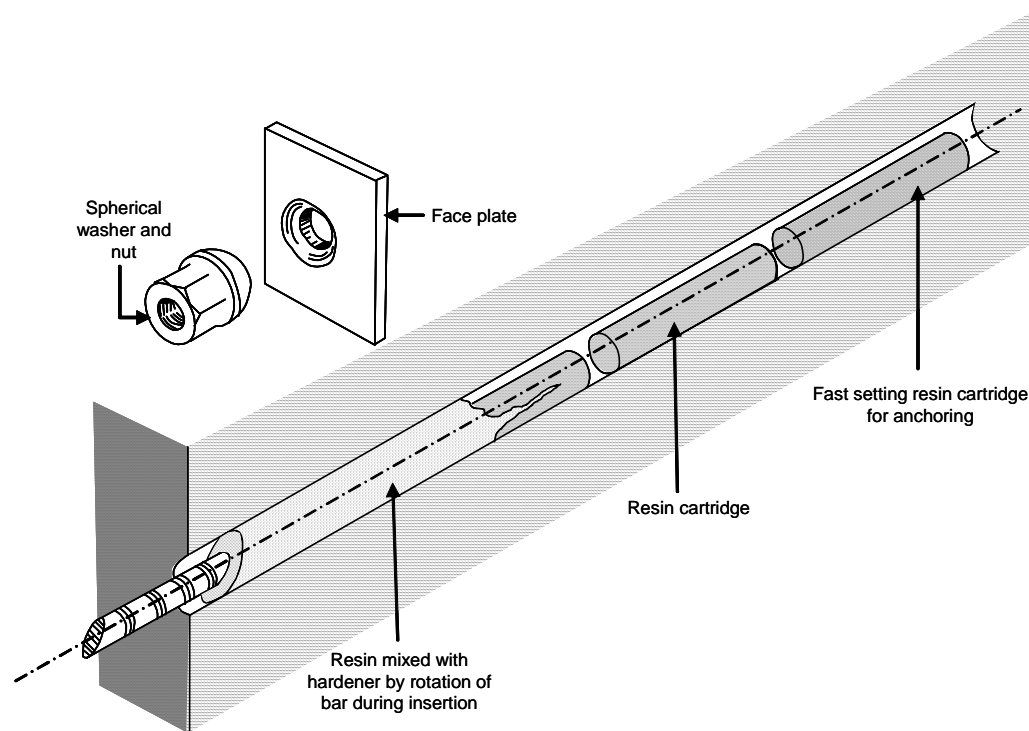


Figure 2.16 The components of a resin grouted rock bolt using threaded bar (Hoek, Kaiser & Bawden 1995).

Cement grouted dowels are easily installed by grouting a borehole with a thick cement grout and pushing the reinforcing bar into the borehole. A simple grouted dowel is shown in Figure 2.17. The non-tensioned reinforcement requires ground movement to activate its reinforcement potential. The benefits of using cement grouts for long-term reinforcement is advocated by Hoek et al. (1995), Brady & Brown (1993) and Satola &

Aromaa (2004) among others. Kendorski (2000) has stated that properly installed resin bolts are just as effective for long-term support as cement grouted reinforcement.

Cement and resin grouts both provide barrier protection to the installed reinforcement. If proper installation standards are maintained, then there should be no uncoated areas of the element through which the environment can access the bolt. This however, is not always the case in underground mining and installation quality does impact on the long-term corrosion resistance of ground support. Additionally ground movement will fracture the grout and expose the bolt to corrosion. Added benefits of using cement grouts is its' corrosion inhibiting properties and the ability to self-heal cracks within the grout column. Carbonation and chloride infiltration of the cement grout may occur after a number of years resulting in a lowering of the pH and a subsequent increase in the rate of corrosion of the reinforcement element. (Satola & Aromaa 2004).

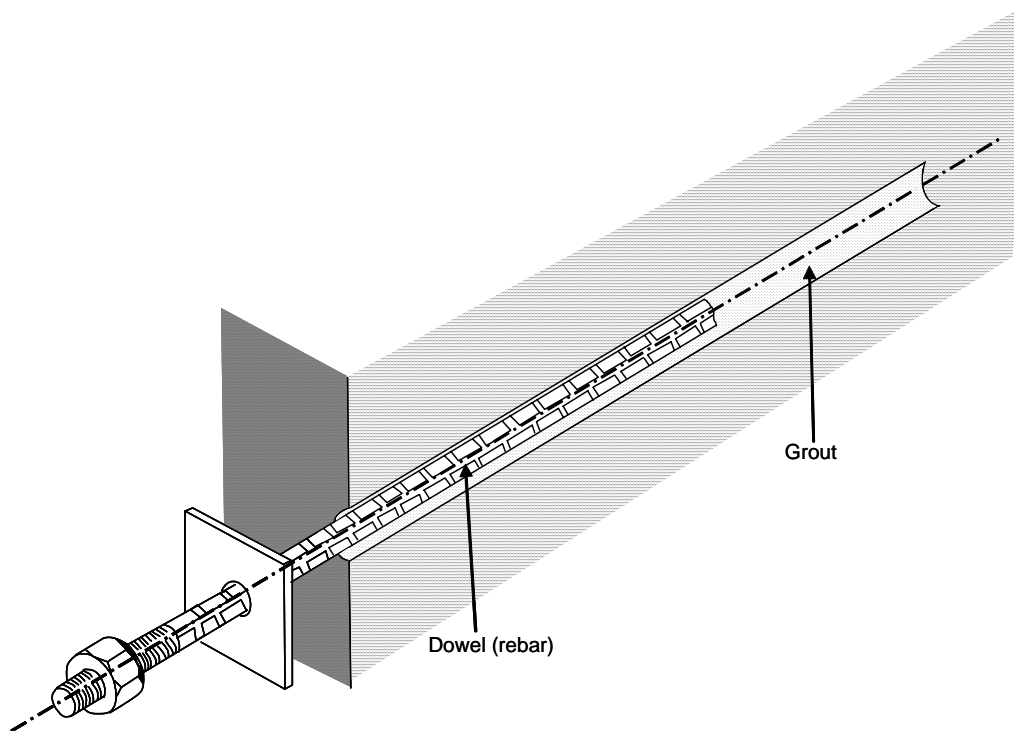


Figure 2.17 Grouted dowel using reinforcement bar inserted into a grout-filled hole (Hoek, Kaiser & Bawden 1995).

2.6.5 Support Systems

Support systems include wire mesh, numerous plate varieties, straps, shotcrete, and membrane liners. They are used as passive support to provide surface restraint at the excavation boundary.

Weld and chain-link mesh is installed to support the small, loose pieces of rock detached from within a bolting pattern, and to reinforce shotcrete. Weld mesh commonly uses 5.6 mm diameter wire spaced at 100 mm centres. Galvanising of the mesh is common, but due to the high surface area per volume of metal associated with the mesh, corrosion can be a concern. In addition, welding is carried out post-galvanising of the wire. Non-galvanised mesh is recommended only for temporary excavations such as stope drive support (Villaescusa 1999b).

There are numerous plate varieties available that are used with corresponding reinforcement. Their steel thicknesses are often considerable, making them somewhat resistant to failure by corrosion. There have been limited studies into the corrosion of plates and straps with most corrosion related failures being due to the failure of the reinforcement element.

Shotcrete is the generic name for cement, sand and fine aggregate concretes, which are applied pneumatically and compacted dynamically under high velocity (Hoek, Kaiser & Bawden 1995). Shotcrete is reinforced with either steel or plastic fibres. Thin membrane liners are either chemically or cementitious based and are applied as a thin coating over the rock surface, however, they have not been widely accepted in the Australian mining industry as an alternative to shotcrete or mesh. Corrosion is not an issue with either product due to their cementitious or chemical composition. Corrosion of the steel fibres in shotcrete is thought to be limited due to the protection afforded by the cement.

2.7 Discussion and Conclusions

Knowledge of the mechanisms of corrosion is well documented and the information presented in this Chapter directly relates to corrosion in the underground mining environment. Similarly, there is a reasonable understanding of rock support and reinforcement principles. There is however, a gap in knowledge regarding how the mechanics of corrosion influences the load transfer, and ultimately the service life of ground support. Current research has only partially achieved this. Corrosion is always related to its environment; it is therefore important to have an adequate understanding of the underground mining environment, in particular the main environmental influences that control the corrosivity of an environment.

CHAPTER 3 ENVIRONMENTAL CONDITIONS IN AUSTRALIAN METALLIFEROUS UNDERGROUND MINES

3.1 Introduction

An understanding of the environmental variables within an underground mine is required to assess an environment's corrosivity and ultimately its effect on the various reinforcement and support systems installed. A comprehensive data collection survey of environmental variables within a number of Australian underground mines was needed due to insufficient information being available at individual mine sites and a lack of published data that adequately describes environmental conditions in Australian underground mines.

Section 3.2 provides an overview of the data collection system and equipment used to conduct the surveys. An assessment of the environmental conditions of the eight surveyed underground mines is presented in Section 3.3. A summary of the information collected from all mine sites and further analysis of the data is presented in Section 3.4 for atmospheric conditions and Section 3.5 for groundwater conditions.

3.2 Corrosion Assessment System for Underground Mines

The Corrosion Assessment System (CAS) was developed to collect systematic data to enable observed corrosion of reinforcement and support systems to be related to the various existing conditions within an underground environment. A wide variety of information was collected at numerous locations within each underground mine providing the full spectrum of possible environmental conditions being experienced by that mine. While only specific locations were examined, they were selected to ensure an accurate representation of the different environments within a mine. However, because environmental conditions in underground mines are never homogenous and are

constantly changing, only approximations can be made for classifying the environment and hence such approximations must be constantly reviewed.

The CAS data sheet, displayed in Appendix A, is designed to collect the important parameters of the rock mass, the groundwater and the atmosphere, as well as the type and condition of the support and reinforcement installed in that area. This information can be used to provide an assessment of the corrosivity of the area and an evaluation of the condition of the installed ground support.

Data collected on the nature of the rock mass includes the rock type, the stresses and the overall structure; massive, layered or blocky. The number of joint sets with their estimated fracture frequency and joint connectivity were recorded along with the condition of the joints (persistence, weathering, profile, roughness, aperture and filling). Any major discontinuities such as shears or faults are also examined for their condition and likely strength. This analysis is not a rock mass classification, but is meant to provide a basic overview of the important parameters pertaining to corrosion. The rock mass structures are primarily important, as they provide a conduit for groundwater and back fill water to flow.

Atmospheric variables were collected at every site. These included the quality of the ventilation; whether it was fresh air or part of the mine exhaust, its flow rate and if there was an observable level of particulates. The wet and dry bulb temperatures were measured using a hygrometer (see Figure 3.1), from which the relative humidity is calculated.

If groundwater was present in sufficient quantities to be collected, it was analysed *in-situ* using a portable TPS 90-FLMV field lab shown in Figure 3.1. This analysis provides measurements of groundwater temperature, pH, dissolved oxygen levels and TDS concentrations. The source of the water; whether a fault, joint, borehole or a combination is noted along with the rate of flow. The flow rate was described qualitatively using nomenclature from the Rock Mass Rating classification (Bieniawski

1989). The conditions can be approximated by calculating the inflow per 10 m tunnel length (l/min) or general conditions can be described as dry (0 l/min), damp (<10 l/min), wet (10-25 l/min), dripping (25-125 l/min) or flowing (>125 l/min). Samples of groundwater are also collected and assayed in an independent laboratory to determine the concentration of dissolved ions. Often the groundwater flow was not sufficient to collect an adequate sample. These regions were classified as wet if some water flow was occurring or damp if water is present but there are no signs of dripping or actual flow.



Figure 3.1 Hygrometer (left) and portable TPS 90-FMLV field lab (right) used to collect environmental information.

The installed surface support was visually examined with a qualitative assessment of the corrosion damage, if any. For hollow reinforcement elements, such as friction rock stabilisers, a borehole camera was used to examine the internal surface of the bolt as shown in Figure 3.2. This provided some indication of the level of corrosion damage. It was concluded early on in the study that assessing the condition of the surface support and extrapolating to include the condition of the reinforcement was not satisfactory. The excavation surface and the internal rock mass are two separate environments with different rates and forms of corrosion. The only way to adequately examine the reinforcement is to overcore the elements.



Figure 3.2 Using a Pearpoint borehole camera to inspect the internal surface of a Friction Rock Stabiliser.

When conducting a corrosion assessment of an underground mine, an emphasis should be placed on areas where groundwater is present. These areas contain only a small percentage of the installed ground support, but the greater corrosiveness of the environment and the irregularity of corrosion attack mean that a higher priority should be placed to inspect such areas. Atmospheric variables by contrast are more homogenous throughout a mine and the projection of results throughout the mine can be achieved with a high level of confidence. In some specific cases, for example, in inadequately ventilated areas, hot, humid conditions can exist that are not observed elsewhere in the mine.

3.2.1 Hard Rock Aquifers

The majority of groundwater encountered by metalliferous underground mining activities in Australia occurs from hard rock aquifers in igneous and metamorphic rocks. The rock itself is generally impermeable but fractures, joints and weathering allow a degree of permeability (water flow). The regolith or weathered zone may increase the porosity from virtually nothing to 10 to 35 percent. Within the Yilgarn Craton the regolith may extend 100 m below surface with major geological structures such as

faults, weathering even deeper. For younger geological terrains in eastern Australia this weathering is much less. Groundwater flow is generally restricted to faults, shears and joints especially when in unweathered rock.

The high salinities of groundwaters in many of the sampled mines are a result of the environmental processes that affect the recharge. In the semi-arid environment over much of inland Australia, the rate of evaporation is much higher than the rate of precipitation. Dissolved salts tend not to evaporate creating groundwaters with concentrated amounts of dissolved salts. These dense saline waters flow downwards under gravity with more saline waters found at depth.

Another major source of hard rock aquifer recharge in inland Australia is from paleochannels. These ancient river systems contain sediments that have a high porosity and permeability and often contain significant quantities of saline and hypersaline groundwaters, due to their much higher capacity than the surrounding weathered rock. Hard rock aquifers that are recharged by this source tend to have large rates of flow for extended time periods.

A simplified profile of a hard rock aquifer, displaying groundwater movements is shown in Figure 3.3. This hypothetical model is representative of groundwater recharge in semi-arid environments in Australia. The igneous/metamorphic rock mass contains a number of large faults which provide storage. Aquifer recharge by different environmental processes creates a number of aquifers with dissimilar groundwater properties.

Hard rock aquifers in areas of higher rainfall tend to have lower salinities as well as higher rates of recharge. Deeper aquifers will also have higher temperatures due to the increased rock mass temperature.

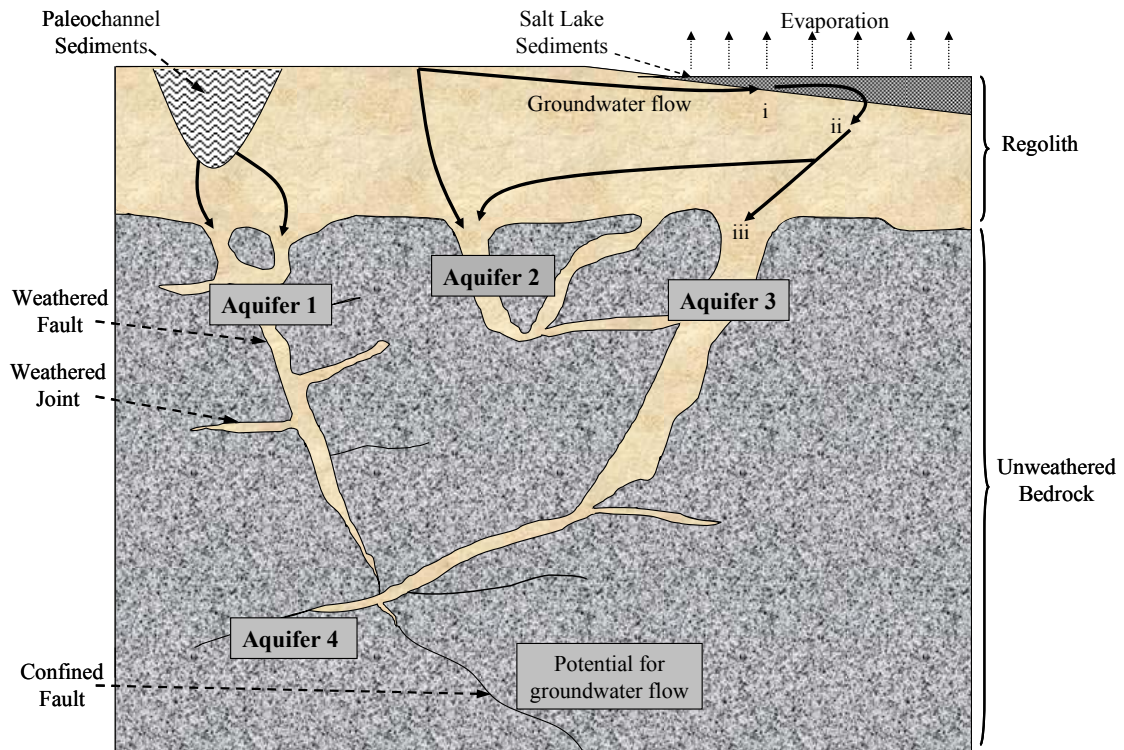


Figure 3.3 Diagrammatic representation of groundwater recharge into hard rock aquifers: (i) Evaporation, leading to saline and dense groundwater; (ii) Downward flow of dense groundwater; (iii) Back-flow of saline groundwaters leading to higher salinity at depth (D J Gray 2001).

The intersection of mine development with water bearing geological structures will create groundwater flow at the excavation boundary. The amount the groundwater will spread away from its original source is related to the discontinuity connectivity. Strongly jointed rock masses will tend to allow the groundwater to flow distant from its source and highly stressed rock masses also crack parallel to the backs and walls. In massive rock masses the groundwater flow will be proximal to the source. This concept is illustrated diagrammatically in Figure 3.4.

The rate and length of time at which flow occurs is related to the permeability, storage capacity and recharge rate of the aquifer. If the recharge rate of the aquifer is large, then water may be able to flow at a consistent rate over many years. Often groundwater flow is seen to occur for limited time durations. This implies that either the rate of recharge is

not sufficient to match the rate of groundwater flow or nearby mining activities, such as stoping, redirect the flow.

At depth groundwater becomes less common as there is no weathering and potentially water bearing structures are confined by the high ground stresses with the distribution of conductive fractures linked to the state of stress (Ingebritsen, Sanford & Neuzil 2006). A depth limit is reached below which groundwater is less common. However, mining activity as it progresses deeper creates a stress change in the rock mass which can lead to unconfining and loosening of the structures allowing groundwater to flow if it is connected to an aquifer closer to surface. The potential for groundwater occurrence will decrease with depth as it becomes more unlikely that unconfining of structures will occur and that they will connect to an aquifer near surface.

An additional mode of groundwater flow at depth occurs in massive excavations such as block caving and sub level caving. This mining method creates a highly fractured rock mass with a large mining foot print, which is considerably more permeable than the surrounding unbroken rock mass. Groundwater will preferentially flow into and down the fractured rock until it encounters less permeable, non-fractured rock, which is generally where the development excavations are located. The depth of mining does not have as significant a control on the groundwater flow as the permeable, broken rock is continuous generally from surface to the current mining level.

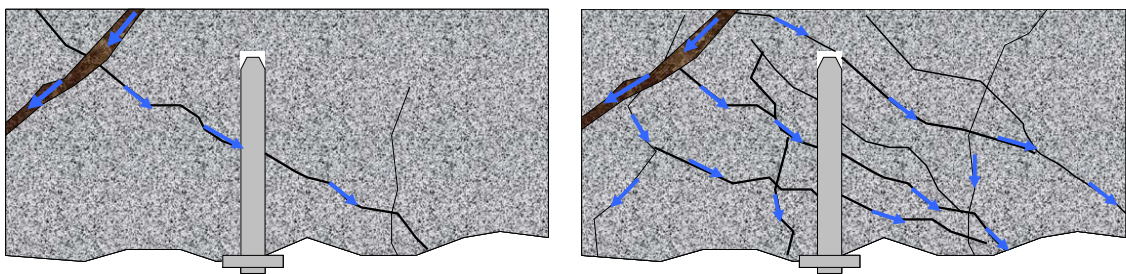


Figure 3.4 Stronger discontinuity connectivity allows the groundwater to interact with more reinforcement and support.

3.3 Environmental Conditions at Selected Australian Mines

An assessment of the environmental conditions utilising the framework of the Corrosion Assessment System was conducted at eight mine sites within Australia, their locations are shown in Figure 3.5. The Argo Mine, the Darlot Mine, the Kanowna Belle Mine, the Kundana Mine and the Leinster Nickel Mine are all located within the Yilgarn Craton of Western Australia. The Cannington Mine and the Enterprise Mine are located in far North Queensland and the Olympic Dam Mine is located in central South Australia.

The following sections provide a summary of the data collected including geological and rock mass information, atmospheric and groundwater conditions and the state of the rock reinforcement and support that relate to the corresponding environment.



Figure 3.5 Location of assessed underground mines.

3.3.1 *Argo Mine, St Ives Gold*

The Argo mine is separated into two distinct ore bodies with the central decline dividing into the North and South. The host geological unit is the Condenser Dolerite, a medium jointed (three joint sets), blocky, very strong rock mass intersected with Blag Flag Greywackes and minor intrusive Felsic Porphyries. A complete geological description is provided by Watchorn (1998). Structurally the area is complex with a number of large geological features that intersect the development. These structures as well as geological contacts provide a conduit for the groundwater flow into the mine.

The primary reinforcement is the Dwyidag Systems International (DSI) 2.4m length, galvanised Friction Rock Stabiliser (FRS) with galvanised dome and butterfly plates. Hot dip galvanising complies with AS 1650 – 1989, with a minimum thickness of 84 microns. Cement grouting of the bolt is conducted for long-term development excavations and groundwater affected areas. Major intersections have 6 m long, bulbed and fully cement grouted cables with barrel and wedge anchors. The surface support consists of plates and galvanised mesh.

Atmospheric environmental conditions at the mine are considered mild in terms of corrosivity. The mine atmosphere is fresh and has a relative humidity in the range of 45 – 82 %, and an average temperature of 20.2°C; the full data is displayed in Table 3.1. A total of twenty eight sample readings were collected throughout the mine. The main areas of possible corrosion problems at Argo is where groundwater is present.

Table 3.1 Atmospheric variables at Argo Mine

Dry Bulb Temperature (°C)		Relative Humidity (%)	
Range	Average	Range	Average
16 - 25	20.2	45-82	62

Groundwater is found at numerous localities within the mine; however, its occurrence decreases with depth. Analysis of the groundwater from sixteen locations revealed similar variables indicating that the groundwater originates from the same aquifer or source. This is most likely related to the large paleochannel present at the surface.

Within the mine four major structures appear to influence groundwater flow. They are the L3 structure, the H1 structure, the mylonite shear as well as an unknown structure that runs from the S3 RAW to the S4 stope Access. These structures allow water to flow from the aquifer into areas of development. Open discontinuities near the development/structure intersection allow the water to spread distally along the opening. The presence of groundwater is generally seen by the accumulation of salt crystals.

Measurements of the *in situ* groundwater analysis are shown in Table 3.2 with level of dissolved ions shown in Table 3.3. The near neutral, hypersaline water is high in chloride and sulphate ions, the presence of which increases the occurrence of pitting corrosion. A controlling factor on the corrosiveness is the low dissolved oxygen concentration of an average 1.89 mg/l. In comparison freshwater has 7-8 mg/l of dissolved oxygen. Oxygen is essential for the electrochemical corrosion process to occur, and the low concentration would limit the rate at which corrosion could take place.

Table 3.2 Groundwater variables tested *in situ* at Argo Mine

TDS (ppm)		pH		Dissolved Oxygen (mg/l)		Temperature (°C)	
Range	Avg.	Range	Avg.	Range	Avg.	Range	Avg.
142,000-274,000	203,416	4.62-7.26	6.2	0.72-2.80	1.89	15.4-21.4	19.2

Table 3.3 Groundwater assay of dissolved ions from Argo Mine

Iron	Calcium	Carbonate	Bicarbonate	Chloride	Sulphate	Nitrate
Fe	Ca	CO ₃ ²⁻	HCO ₃ ⁻	Cl	SO ₄ ²⁻	NO ₃ ²⁻
mg/l	mg/l	mg/l	mg/l	mg/l	mg/l	mg/l
0.5	310	1	50	180,000	24,000	0.2

Examination of the internal surface of six month old Friction Rock Stabiliser (FRS) by borehole camera indicated the presence of corrosion products and precipitation of salts (see Figure 3.6). However, corrosion has not developed significantly on bolts of older age (two years) under similar environmental conditions (see Figure 3.7). The absence of any significant visible corrosion damage is a function of the recent age of the mine and the low corrosivity of the groundwaters, which is related to the very low dissolved oxygen content. It is expected that corrosion will begin to become more developed over

time but the indications are the rate of corrosion is sufficiently low that corrosion related issues should not be expected for some time.



Figure 3.6 External and internal view of FRS from the S/P3 South Decline, approximately 6 months age.



Figure 3.7 External and internal view of FRS of 2 years age, some steel corrosion is evident.

3.3.2 Cannington Mine, BHP Billiton

The Cannington silver-lead-zinc deposit is hosted by a sequence of metamorphosed sedimentary rocks within a quartzo-feldspathic gneiss. Different rock types encountered within the development include Gneiss, Amphibolite, Pegmatite, Quartzite, Muscovite-Sillimanite Schist and Mafic rocks. The ore body itself is separated into the Northern Zone and the higher grade Southern Zone. The main mineralisation assemblage is dominated by galena and sphalerite (Bailey 1998).

The lithology is generally moderately jointed with three to four joint sets creating a blocky rock mass. It is not considered that the rock types encountered within the development and their associated minerals assist corrosion. However, within the ore drives sulphide ore minerals may create localised electrochemical corrosion cells with the rock reinforcement and accelerate corrosion of the ground support.

The Northern and Southern Zones are separated by the large Trepell Fault Zone. Historically this region had significant water flow but has now receded. The Hamilton Fault bounds the southern limit of the deposit. It is a highly sheared zone of 10's of metres that has significant water flow. A number of smaller faults are located between these two major structures and are also associated with ground water flow.

Prior to late 1999 Hollow Groutable Bolts (HGB) were used in conjunction with galvanised mesh and w-plates at Cannington for the primary support. Black, bulbed, unplated cables were installed at intersections. This ground support scheme is installed in most of the decline development and older drive access. Current reinforcement consists of galvanised friction bolts and galvanised, hollow tube (nominal 3 mm thickness), resin anchored jumbolts (Strata Control Systems 2007) used in combination with galvanised mesh, dome and w-plates. Black, bulbed cables with barrel and wedge anchors are installed at intersections.

The mine atmosphere has temperatures and relative humidity in the range of 25 – 32 °C and 66 – 93% respectively (see Table 3.4). This information was collected from fourteen

locations throughout the mine. Generally the atmosphere is considered to be mildly to moderately corrosive, the latter being more prevalent in the lower regions of the mine where the restricted ventilation and higher rock temperatures increase both the temperature and humidity. This is particularly noticeable in drives that intersect the Hamilton Fault, where the combination of long access drives and the intersection of hot flowing water have created a hot, humid atmospheric environment with relative humidity above 90%. This local atmosphere has a significantly longer time of wetness and is regarded as highly corrosive for atmospheric corrosion.

Table 3.4 Atmospheric variables at Cannington Mine

Dry Bulb Temperature (°C)		Relative Humidity (%)	
Range	Average	Range	Average
25.0-32.0	28.4	66-93	81

The occurrence of groundwater is dominated by a number of large structures such as the Trepell and Hamilton fault regions. These strongly sheared areas allow for easy water movement and are characterised by high water flow along a large lateral area of drive. Groundwater or evidence of previous groundwater flow was observed at numerous other localities throughout the mine. The true extent of the flow was often obscured by the application of shotcrete.

Table 3.5 displays the measured *in situ* variables from eight groundwater tests. The controlling factors on the corrosivity of groundwater are the high average temperature of 30 °C and a dissolved oxygen content of 4.02 mg/l. The slightly saline water (see Table 3.6), about a magnitude higher in salinity than common tap water, also assists to create a highly corrosive groundwater.

Table 3.5 Groundwater variables tested *in situ* at Cannington Mine.

TDS (ppm)		pH		Dissolved Oxygen (mg/l)		Temperature (°C)	
Range	Avg.	Range	Avg.	Range	Avg.	Range	Avg.
1,680-3,980	2,610	7.0-8.3	7.8	3.82-4.20	4.02	26.5-37	30

Table 3.6 Groundwater assay of dissolved ions from Cannington Mine.

Iron	Calcium	Carbonate	Bicarbonate	Chloride	Sulphate	Nitrate
Fe	Ca	CO ₃ ²⁻	HCO ₃ ⁻	Cl	SO ₄ ²⁻	NO ₃ ²⁻
mg/l	mg/l	mg/l	mg/l	mg/l	mg/l	mg/l
<0.05	300	<5	48	1,500	800	1

In all areas affected by groundwater there is the potential for high rates of corrosion, if high water flow rates are present then the rates will be even higher. Figure 3.6 displays the internal condition of a galvanised FRS after two and four months, installation in a high water flow (flowing) shear zone. The galvanising has protected the underlying steel for at least two months. However, after four months the galvanising has been stripped with significant steel corrosion occurring. This represents a considerable advancement of damage over a short time period. In similar environmental areas of greater age galvanised weld mesh had been completely corroded. Additionally, steel fibres normally embedded in the shotcrete but exposed due to cracking of shotcrete were also entirely oxidized.

The benefits of using a reinforcement element with a closed cylinder are shown in Figure 3.9. The jumbolts are located in the same ring as the FRS in Figure 3.8, yet they display no internal corrosion. While no observation of the external surface could be made it is expected that if sufficient resin encapsulation was achieved then the resin grout would provide an extra physical barrier to the groundwater.

The earlier ground support scheme involving HGB as the primary reinforcement elements are susceptible to the corrosive groundwaters. The thin-walled elements come into contact with water due to poor grouting practices or cracking of the grout column during rock movement. Previous reports (Laboratory Technical Services Newcastle Steelworks 1995; Pascoe 1995) have documented the failure of HGB due to the loss of cross sectional area by corrosion attack in groundwater affected areas.

The high corrosivity of the groundwaters combined with the use of thin-walled reinforcement, previously HGB and currently FRS and jumbolts, has meant corrosion

related failures of reinforcement have occurred. Galvanising of the elements is beneficial in corrosive atmospheric conditions, but appears largely ineffective for corrosion control in groundwater affected regions, especially those with a high rate of groundwater flow, and requires more efficient corrosion protection techniques.

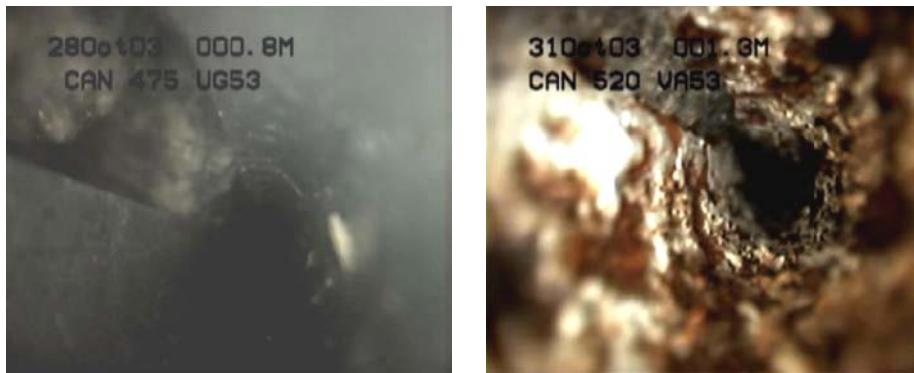


Figure 3.8 Internal pictures of a FRS after two months (left) and four months (right) installation in a shear associated with high groundwater flow.



Figure 3.9 Internal picture a jumbolt after two (left) and four months (right) installation in a shear associated with high groundwater flow.

3.3.3 Darlot Mine, Barrick Gold

The Darlot Gold Mine produces from two distinct ore bodies, the Darlot and Century deposits. The major geological units intersected by mine development are different for each ore body. Development within the Darlot ore body encounters basalt near the surface changing to felsic porphyry at depth. The Century ore body and its associated development are contained within dolerite; alteration closer to the ore produces a magnetic dolerite. Intrusive dykes are found throughout the mine (Krcmarov et al. 2000).

The lithology regardless of rock type is a moderately jointed, strong to very strong rock mass. The Century ore body is bounded by two large reverse faults, the Oval and Lords Faults. These are connected by steeply dipping East-West striking cross faults. Many other major geological structures intersect development at Darlot.

The earlier reinforcement scheme, located in the upper mine development is characterised by HGB. This has been superseded by the use of galvanised FRS in conjunction with cement grouted rebar. Surface support consists of galvanised dome and butterfly plates and galvanised welded mesh. In addition fully grouted, black, bulbed cables with barrel and wedge anchors are used in major intersections.

The mine atmosphere is relatively fresh with low temperatures and relative humidity as displayed in Table 3.7, this information was collected from nineteen locations. The higher relative humidities were observed in areas of the lower decline and return airways. Overall the atmosphere is considered non-corrosive, which combined with the widespread use of galvanised ground support suggests few corrosion related issues in areas that have not been affected by groundwater.

Table 3.7 Atmospheric variables at Darlot Mine.

Dry Bulb Temperature (°C)		Relative Humidity (%)	
Range	Average	Range	Average
15.0-23.0	20.2	60-92	75.6

Measurements of *in situ* groundwater variables at the mine established two distinct groundwater types. The most commonly tested type with eleven samples, denoted as originating from aquifer one is shown in Tables 3.8 and 3.9. The moderately saline water with high dissolved oxygen content averaging 5.55 mg/l was found throughout the mine and is considered highly corrosive. A number of samples collected were slightly acidic in nature; however, the majority were close to neutral.

Three groundwater samples collected near the base of current development showed much higher TDS levels between 49,000 to 86,000 ppm and lower dissolved oxygen content of 3.05 to 3.50 mg/l, less corrosive than groundwater from aquifer one (see Tables 3.10 and 3.11). The different measurements indicate the source is a separate aquifer, denoted as aquifer two, and may be linked to a nearby paleochannel. Deeper resource drilling by the company has intersected a similar water composition signifying that this water type may become more common as mining progresses deeper. All groundwater samples were collected in the presence of large geological structures. It was also noted that many ‘dry’ faults or shears exhibit salt precipitation indicating previous water flow.

Table 3.8 Groundwater variables from aquifer one tested *in situ* at Darlot Mine

TDS (ppm)		pH		Dissolved Oxygen (mg/l)		Temperature (°C)	
Range	Avg.	Range	Avg.	Range	Avg.	Range	Avg.
2,790-6,400	4,540	4.25-8.19	7.39	4.39-7.65	5.55	14.3-23.2	19.7

Table 3.9 Groundwater assay of dissolved ions from aquifer one at Darlot Mine.

Iron	Calcium	Carbonate	Bicarbonate	Chloride	Sulphate	Nitrate
Fe	Ca	CO ₃ ²⁻	HCO ₃ ⁻	Cl	SO ₄ ²⁻	NO ₃ ²⁻
mg/l	mg/l	mg/l	mg/l	mg/l	mg/l	mg/l
<0.05	50	<1	290	380	170	120

Table 3.10 Groundwater variables from aquifer two tested *in situ* at Darlot Mine.

TDS (ppm)	pH	Dissolved Oxygen (mg/l)	Temperature (°C)
Range	Range	Range	Range
47,000-86,000	6.91-7.07	3.05-3.50	20.5-20.8

Table 3.11 Groundwater assay of dissolved ions from aquifer two at Darlot Mine.

Iron	Calcium	Carbonate	Bicarbonate	Chloride	Sulphate	Nitrate
Fe	Ca	CO₃²⁻	HCO₃⁻	Cl	SO₄²⁻	NO₃²⁻
mg/l	mg/l	mg/l	mg/l	mg/l	mg/l	mg/l
<0.5	1,200	<1	80	22,000	3,900	67

Corrosion damage to reinforcement and support is limited to areas where groundwater was or is still present, which is ultimately dictated by the presence of large geological structures. There were numerous localities in the mine that displayed deposition of salt crystals, an indication of previous groundwater flows, but are currently dry, as shown in Figure 3.10. The damage to the installed reinforcement and support ranged from moderate to severe and in most cases the galvanising had been removed. The outcome is that the support is substantially more at risk from future attack by atmospheric corrosion. Numerous examinations of the internal condition of FRS established that the condition of the plate and mesh was not comparable to the condition of the reinforcement. As Figure 3.11 demonstrates the corrosion environment is different on the excavation boundary, which appears dry, as opposed to the inside the rock mass where severe corrosion has taken place. Generally, greater corrosion damage was seen at depths of 0.5–1 m into the rock. A possible explanation is the ventilation is drying out the rock mass to that depth with groundwater still present beyond this zone.

Failure of barrel and wedge anchors at low loads, well below design, has been observed by mine personnel (L Gray 2003) and attributed to excessive corrosion. These areas display dripping groundwater of aquifer one type with samples taken having high dissolved oxygen contents of around 6.0 mg/l.



Figure 3.10 External (left) and internal (right) view of corrosion damage to a galvanised FRS that has been affected by earlier groundwater flow.



Figure 3.11 No corrosion of the plate (left), but strong corrosion of the FRS reinforcement (rights) at 2.1m depth.

The condition of weld mesh in a number of groundwater affected areas was uncertain, which led to the collection and testing of samples as described by Villaescusa (1999b). The typical strength that could be expected from the nominal 5.6 mm diameter wire mesh is 11 to 12 kN. The results are summarised in Table 3.12 and show a moderate level of corrosion (loss of galvanising, uniform steel corrosion) has little impact on the load, however, severe corrosion (uniform steel corrosion, significant pitting corrosion) reduced the load bearing capacity by approximately 40%.

Table 3.12 Results of mesh pull tests at Darlot Mine.

Location of Sample	Failure of Load (kN)	Place of Failure	Corrosion
Marsh 1180 Acc #1	7.63	Heat affected zone	Severe
Marsh 1180 Acc #2	7.16	Weld	Severe
Millennium Dec SP7 #1	11.21	Heat affected zone	Moderate
Millennium Dec SP7 #2	11.56	Heat affected zone	Moderate
Federation Dec #1	12.14	Weld	Moderate
Federation Dec #2	12.70	Heat affected zone	Moderate

The use of thin-walled FRS in groundwater affected areas is not recommended due to the high corrosivity of the water. Wet areas where FRS are installed should be monitored. Borehole camera examinations have shown that excavations that are dry on the surface may have groundwater present deeper into the rock mass. Problems may also arise with fully cement grouted rebar if cracking of the grout column occurs, however this reinforcement type is considered significantly more corrosion resistant. As mining progresses deeper a more saline, less corrosive groundwater is expected to become prevalent but in lower quantities than the upper levels.

3.3.4 Enterprise Mine, Xstrata

The Enterprise Copper Mine is located between 1200 – 1800 m below surface with two distinct ore bodies, the 3000 and 3500 orebodies. Shale and siltstone stratigraphic units occur in the immediate vicinity of the ore bodies. The mineralisation is in the form of chalcopyrite and is mainly present in and along veins. There is also a substantial network of interconnected faults/shears zones throughout the copper ore bodies (T P Davis 2004).

The rock types encountered within permanent development and their associated minerals are not considered to assist corrosion. An exception occurs within ore drives where sulphide minerals may create an electrochemical corrosion cell with the rock reinforcement accelerating corrosion. The presence of groundwater within the mine is minimal, despite the network of large scale geological structures. This is most likely due to the depth of current mining and dewatering of the aquifer by previous mining above the current mine. Some water flow is seen locally near backfilled stopes that are in the process of dewatering.

The primary support installed within the Enterprise deposit is dependent upon the expected life of the excavation. Jumbo installed, 47 mm diameter non-galvanised FRS in conjunction with non-galvanised 5.6 mm diameter weld mesh is used in excavations that have a required opening life of less than 2 years. In longer term development; from 2 to tens of years, black point anchored cement grouted bolts (PAG), 20 mm diameter resin anchored rebar, and black mesh are installed. Black, bulbed, grouted cables with barrel and wedge anchors are installed on intersections. There is little use of galvanised support within the Enterprise mine following cost analysis that recommended the use of galvanised mesh and galvanised FRS only where the FRS are used as long term support (Beck 1999).

The absence of groundwater in the Enterprise mine is attributed to its considerable depth and the effect of previous mining conducted above the deposit, essentially redirecting the groundwater flow. Only two groundwater samples were collected from the rock mass and their variables are shown in Tables 3.13 and 3.14. This near neutral water has comparatively high temperature and dissolved oxygen and a moderate salinity, the combination of which makes this water highly corrosive. Fill water flow from the dewatering of back filled stopes is common. The affected regions can generally be predicted with the fill water flow controlled by the permeability of the rock mass and the hydraulic head pushing the water out. The fill water will have a pH ranging from neutral to basic with a composition that will somewhat reflect the original water added to the paste fill. While the amounts of water flow can be significant the duration is expected to last for only months.

Table 3.13 Groundwater variables tested *in situ* at Enterprise Mine.

TDS (ppm)	pH	Dissolved Oxygen (mg/l)	Temperature (°C)
Range	Range	Range	Range
6,730-8,990	7.27-7.73	3.66-4.60	31.3-34.8

Table 3.14 Groundwater assay of dissolved ion at Enterprise Mine.

Iron	Calcium	Carbonate	Bicarbonate	Chloride	Sulphate	Nitrate
Fe	Ca	CO₃²⁻	HCO₃⁻	Cl	SO₄²⁻	NO₃²⁻
mg/l	mg/l	mg/l	mg/l	mg/l	mg/l	mg/l
<0.05	110	<5	82	970	5,000	0.33

A total of twenty measurements were taken of the atmospheric variables. The mine atmosphere is hot and humid with temperatures in the range of 30 to 45 °C and a relative humidity of 80 to 95% (see Table 3.15). The high temperature and humidity is a function of the depth and extent at which mining has and is taking place, the common use of secondary ventilation, the high ambient rock temperatures, and the high temperatures and humidity of the air already on surface. The high relative humidities contribute to a longer time of wetness and correspondingly elevated rates of corrosion compared to other underground atmospheres.

The rates of atmospheric corrosion are low compared to those expected from groundwater corrosion. However, with the expected life of the mine being several decades, and the extensive use of non-coated black steel for the majority of ground support, corrosion damage may become a significant issue over time.

Table 3.15 Atmospheric variables at Enterprise Mine.

Dry Bulb Temperature (°C)		Relative Humidity (%)	
Range	Average	Range	Average
30.0-45.0	35.0	80.0-95.0	86.1

Where groundwater is present the rates of corrosion are expected to be very high with previous failures of cable bolts documented (O'Hare 1994). Permanent excavations such as decline development, underground workshops and crib rooms that will be open for the life of the mine may develop corrosion related issues with the installed reinforcement and support from the long-term exposure to atmospheric variables. A number of ungrouted point anchored elements have previously failed in these high risk areas due to assumed atmospheric corrosion (see Figure 3.12) but the high estimated corrosion rates of 0.5 mm/year suggest groundwater may be the cause.



Figure 3.12 Failure of a 15 mm diameter point anchored bolt after 15 years of installation due to atmospheric corrosion.

3.3.5 Kanowna Belle Mine, Barrick Gold

The Kanowna Belle gold mine consists of interbedded felsic and conglomerate units. These units are often fault bounded, but exhibit conformable contacts. The hanging wall sequence is dominated by felsic sandstone. A felsic porphyry intruded along the large Fitzroy fault hosts the majority of mineralisation and separates the footwall and hanging wall sequences (Beckett et al. 1998). The felsic/conglomerate contacts are often the conduit for external groundwater flow. The blocky rock mass generally has an average of four joint sets. The mineralogy associated with the different rock types of the Kanowna Belle mine is not expected to influence the corrosive potential of an environment.

Four types of rock reinforcement elements were observed in the areas studied. They included the earlier reinforcement consisting of HGB and the current regime of galvanised FRS, CT bolts, and black plain strand cables. The majority of the FRS were ungrouted with only a minor proportion grouted in selected areas. The CT bolt, HGB and plain strand cable are toe to collar cement grouted bolts and thus theoretically should be fully encapsulated within the grout, which provides good protection from corrosion. However, quality control issues leading to poor grouting practices can leave the elements ungrouted or having only partial encapsulation. Galvanised weld mesh,

galvanised dome plates and galvanised W plates are also used as support within the mine.

The atmospheric conditions at Kanowna Belle, displayed in Table 3.16 show an average temperature of 24.7 °C and a relative humidity of 70%, measured from fifteen locations. Attempts to identify the level of sulphur dioxide in the mine using a portable gas analyser were unsuccessful as the gas levels are below the detection limit of the available equipment.

Table 3.16 Atmospheric variables at Kanowna Belle Mine.

Dry Bulb Temperature (°C)		Relative Humidity (%)	
Range	Average	Range	Average
20.0-29.0	24.7	50.0-91.0	70.0

Mine groundwater is generally encountered near the occurrence of major structures, typically the conglomerate/felsic contact and adjacent to draw points of stopes that have been backfilled. Two distinct groundwater types were observed and are distinguished by their vertical location. Five groundwater samples collected above the 9860 level (490 m below surface) have characteristics shown in Tables 3.17 and 3.18, with four groundwater samples collected below the 9860 level displaying variables shown in Tables 3.19 and 3.20. The two sources of groundwater, named aquifer one and aquifer two respectively, show marked differences in the average TDS, dissolved oxygen and temperature. The deeper aquifer two had a TDS twice that of aquifer one as well as higher water temperatures, but a lower dissolved oxygen content.

The majority of the mine development is not affected by groundwater; however, its occurrence is more common nearer to the surface decreasing with depth. Negligible groundwater was encountered below the 9500 level (850 m below surface). Clamping of the geological structures due to the high stresses is thought to restrict the flow of groundwater at depth. Future stoping of the lower levels will lead to a change in the local stress field, possibly leading to unconfining of structures, which allows

groundwater to flow. Experience has shown the rate and occurrence of groundwater flow generally decreases with depth for all fractured rock aquifers.

Table 3.17 Groundwater variables from aquifer one tested *in situ* at Kanowna Belle Mine

TDS (ppm)		pH		Dissolved Oxygen (mg/l)		Temperature (°C)	
Range	Avg.	Range	Avg.	Range	Avg.	Range	Avg.
30,200-57,800	47,250	6.94-7.62	7.30	3.21-5.58	4.35	20.3-23.1	26.5

Table 3.18 Groundwater assay of dissolved ions from aquifer one at Kanowna Belle Mine.

Iron	Calcium	Carbonate	Bicarbonate	Chloride	Sulphate	Nitrate
Fe	Ca	CO ₃ ²⁻	HCO ₃ ⁻	Cl	SO ₄ ²⁻	NO ₃ ²⁻
mg/l	mg/l	mg/l	mg/l	mg/l	mg/l	mg/l
0.5	1,200	<1	10	27,900	930	36

Table 3.19 Groundwater variables from aquifer two tested *in situ* at Kanowna Belle Mine.

TDS (ppm)		pH		Dissolved Oxygen (mg/l)		Temperature (°C)	
Range	Avg.	Range	Avg.	Range	Avg.	Range	Avg.
89,000-130,700	97,933	7.25-7.46	7.35	2.57-3.20	2.93	25.0-27.8	26.5

Table 3.20 Groundwater assay of dissolved ions from aquifer two at Kanowna Belle Mine.

Iron	Calcium	Carbonate	Bicarbonate	Chloride	Sulphate	Nitrate
Fe	Ca	CO ₃ ²⁻	HCO ₃ ⁻	Cl	SO ₄ ²⁻	NO ₃ ²⁻
mg/l	mg/l	mg/l	mg/l	mg/l	mg/l	mg/l
1.4	2,880	<1	28	64,000	2,640	208

Only minor corrosion of the reinforcement and support was observed in areas not affected by groundwater indicating the corrosivity of the atmosphere is relatively low. The use of galvanised and fully grouted reinforcement is highly beneficial and no corrosion related problems are expected.

In areas affected by groundwater various levels of corrosion on reinforcement and support were observed, with the amount of damage dictated mainly by the rate of water flow and the age of installation. Several cases of unexpected failures of HGB due to severe corrosion have been observed in groundwater affected areas of development age greater than eight years.

Galvanised FRS had ranging levels of corrosion damage that correlated with the age of installation. More corrosion was observed on older reinforcement which was generally installed in the upper levels of the mine. Loss of galvanising and subsequent steel corrosion was observed from borehole camera surveys as early as 3 months following installation.

The corrosion resistant CT bolt is currently used for permanent reinforcement and is designed to last for many years in a corrosive environment. Static loading by Villaescusa and Wright (1999) has shown that even after significant crack opening (50 mm) the corrosion protection capability is still provided by the plastic sheath. A disadvantage with this long-term reinforcement is the need to post-cement grout the point anchored reinforcement to create a fully grouted and corrosion resistant element. Post-grouting does not always take place and failure to grout the element, as shown in Figure 3.13, makes the bolt highly susceptible to corrosion, especially the mechanical anchor. Villaescusa and Wright (1999) state that ungrouted mechanical anchored bolts are not consistently reliable beyond three to six months, due to problems with the expansion shell, which may be related to corrosion.



Figure 3.13 Damage to a CT bolt by mechanised equipment has broken off the plate and nut revealing the element and plastic sheath with no evidence of cement grouting.

The variability of groundwater flow through interconnected joint sets away from the main conduit can make an assessment of ground support difficult. If the reinforcement

happens to intersect water bearing joints, then corrosion is likely to occur. The inconsistency of open jointing is shown in Figure 3.14, which displays two FRS located within a meter of each other with very different levels of corrosion damage.

Corrosion related issues for reinforcement and support at Kanowna Belle are limited to areas where groundwater is present. Commonly, these areas are near backfilled stopes and large geological structures, predominately the conglomerate/felsic rock contact. Water flow from backfilled stopes is expected to occur over a time frame of months, and corrosion related problems are not expected to be significant. Where hollow HGB groutable bolts have been installed at or near a geological contact or some other groundwater source it is considered a high risk area for possible corrosion failure. Another concern is the inadequacy in post-grouting the CT bolts, making them highly susceptible to corrosion damage.

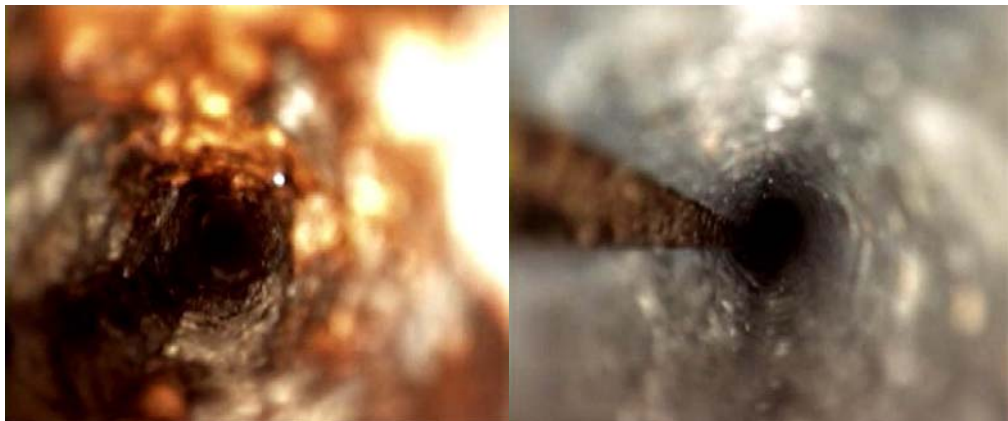


Figure 3.14 Highly corroded FRS (left) and non-corroded FRS (right) of same age (2 years) installed within one meter of each other

3.3.6 Kundana Mine, Barrick Gold

The Kundana Gold Mine consists of deposits of narrow vein auriferous quartz loads ranging from 0.2 m to 3 m in width. The main rock types are basalt, dolerite and intermediate volcanoclastics (Lea 1998). Data collection was focused on the Strzelecki Decline between the 6124 level and the 5760 level which corresponds to a depth below surface of 120 m to 484 m. Decline development was completed at a regular rate over

eight years from the surface thus providing a constant variation of reinforcement age in similar geological and environmental conditions.

The decline was developed in a volcanoclastic, blocky rock mass and with on average three observable joint sets. The joints have a low fracture frequency and a moderate persistence with an undulating profile, rough surfaces with no filling. Generally jointing had a tight aperture, with few open joints in the lower levels. The stress regime ranged from low *in-situ* stresses near the upper level of the decline to high *in-situ* stresses in the lower levels. This is characterised by a change in installed ground support. Galvanised, 47 mm FRS were installed with galvanised mesh in low to moderate stress conditions. Below the 5900 level (344 m below surface) galvanised, 47 mm FRS and yielding, fully grouted rock bolts termed cone bolts are used in conjunction with galvanised mesh and shotcrete. All FRS have galvanised plates and the cone bolts were installed with non-galvanised plates. Black, bulbed cable bolts and plates are installed in decline cross-cut intersections.

The upper Strzelelcki Decline above the 5900 level is the main exhaust outlet for the mine; the atmospheric variables, from nineteen measurements, are shown in Table 3.21. The temperature ranged from 21.0°C to 24.4°C with a corresponding relative humidity of 77% to 92%. The higher temperature and humidity were observed in the deeper levels due to restricted ventilation flow.

Table 3.21 Atmospheric variables at Kundana Mine.

Dry Bulb Temperature (°C)		Relative Humidity (%)	
Range	Average	Range	Average
21.0-24.4	23.0	77.0-92.0	88.0

A total of twenty three water samples were collected from the rock mass, with all, but one sample collected above the 5938 level (306 m). The high *in-situ* stress regime in the lower part of the mine appears to clamp together geological discontinuities restricting groundwater flow. Subsequent ore extraction through stoping relieves the stress on the surrounding rock mass allowing joints to unclamp and water to flow. Experience from

mine personnel (Ross 2003) indicates that groundwater flow increases with nearby stoping.

The results from the groundwater sampling conducted *in-situ*, and shown in Table 3.22, indicate a high level of homogeneity, which suggests the water originates from one aquifer. The groundwater is near neutral in pH and hypersaline with an average TDS of 99,396 mg/l. The temperature and dissolved oxygen average 23.0°C and 3.23 mg/l respectively. Table 3.23 displays the results from assays of the ion content revealing very high concentrations of chloride and sulphate ions.

Table 3.22 Groundwater variables tested *in-situ* at Kundana Mine.

TDS (ppm)		pH		Dissolved Oxygen (mg/l)		Temperature (°C)	
Range	Average	Range	Average	Range	Average	Range	Average
84,500–111,800	99,396	4.52–7.48	7.06	2.67–3.89	3.23	21.0–24.4	23.0

Table 3.23 Groundwater assay of dissolved ions from Kundana Mine

Iron Fe mg/l	Calcium Ca mg/l	Carbonate CO ₃ ²⁻ mg/l	Bicarbonate HCO ₃ ⁻ mg/l	Chloride Cl mg/l	Sulphate SO ₄ ²⁻ mg/l	Nitrate NO ₃ ²⁻ mg/l
0.5	1,600	1	75	69,000	7,800	94

The condition of the rock reinforcement and support was found to be dependent upon the presence of groundwater and the age of the installation. In the upper levels of the decline rehabilitation had occurred in certain areas due to the perceived strong corrosion damage of the original ground support, which had been installed 10 years prior (see Figure 3.15). The basis of this analysis was the condition of the plates which were uniformly corroded but still retained considerable structural integrity. Borehole camera surveys of the reinforcement elements indicated uniform corrosion that increased in severity towards the toe of the bolt. The level of corrosion for bolts of similar age is controlled by the amount of groundwater present. Areas where water was visibly dripping had greater corrosion compared to damp or dry regions.

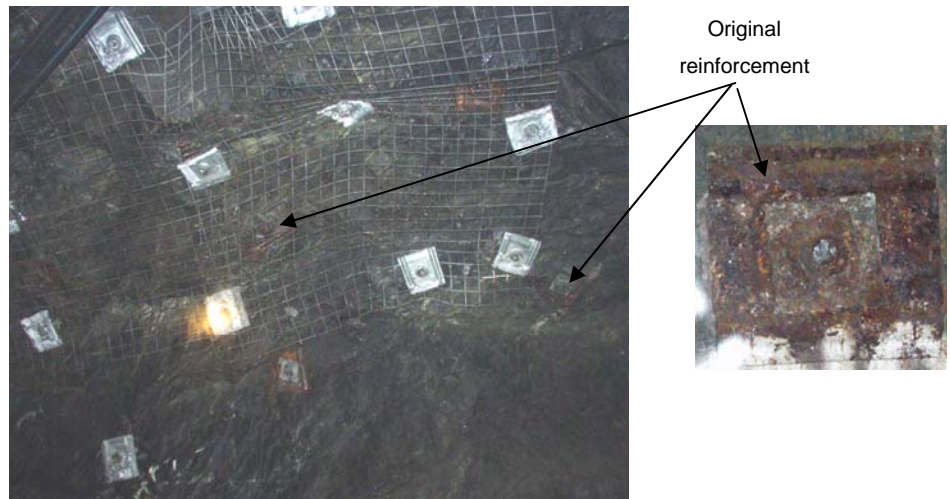


Figure 3.15 Rehabilitation of corroded reinforcement elements. Original reinforcement was installed over 10 years prior.

Corrosion was minimal on areas that were only affected by atmospheric corrosion. This was true even for elements that had been installed for eight or more years as shown in Figure 3.16. The higher humidity in the lower decline had little impact on the galvanised support (see Figure 3.16) but the non-galvanised plates and protruding bolts ends have experienced some uniform corrosion.

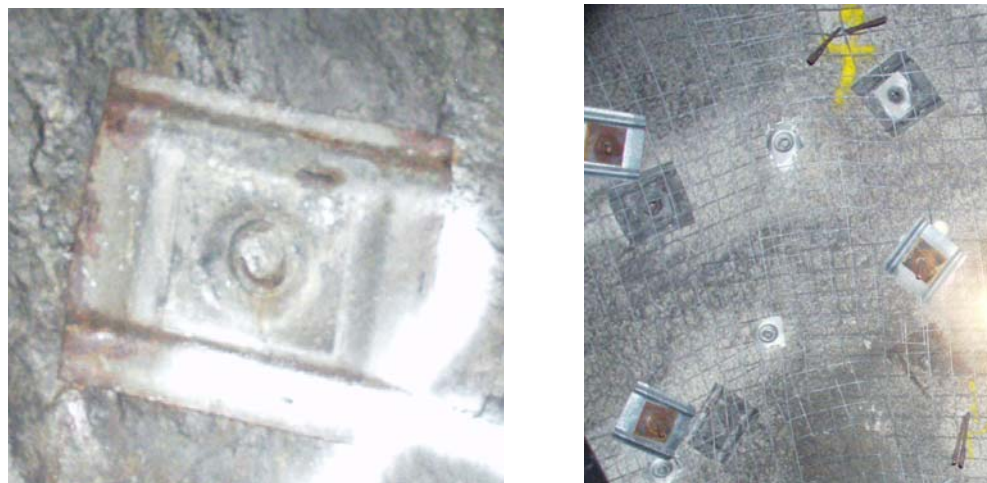


Figure 3.16 Condition of support after undergoing corrosion attack from only atmospheric variables after eight (left) and three (right) years.

Problems arising from corrosion of ground support are limited to areas affected by groundwater, mainly in the upper decline. Groundwater flow is largely controlled by the advancement of open stoping, which creates a local stress change and loosening of water bearing structures. Based on the reinforcement condition in the upper levels that have been installed for up to ten years, the groundwater chemistry is deemed only moderately corrosive. However, the use of thin-walled FRS for long-term openings at even mild corrosion rates will affect the bolts performance and regular monitoring of their condition in wet areas is recommended.

3.3.7 Leinster Nickel Operations, BHP Billiton

The Leinster Nickel mineralisation is hosted in a regionally extensive ultramafic horizon. The ore body is a zone of high-grade massive and disseminated nickel sulphide mineralisation situated within an extensive sheet of weak nickel sulphide mineralisation. The hanging wall consists of a felsic volcanoclastic succession (Libby et al. 1998). The lithology within the hanging wall, which contains the bulk of mine development, is a medium jointed (average 3 joints), strong, competent rock mass. The orebody host ultramafic rock type is comparably soft and ductile, and experiences extensive excavation deformation. The hanging wall rock types and their associated mineralogy do not assist corrosion. Within the actual ore and especially regions of massive sulphide, the sulphide ore minerals may create localised electrochemical corrosion cells with the rock reinforcement and accelerate corrosion of the ground support in addition to creating localised acidic conditions.

Current ground support used at Leinster Nickel Operations is dictated by the rock mass behaviour. Reinforcement and support within the felsic volcanoclastics consist of galvanised 47 mm diameter FRS with galvanised dome and W plates and galvanised mesh is used with occasional cement grouted black rebar. Within the ultramafic unit that hosts the mineralisation significant ground support is installed to counteract the effects of the squeezing rock mass. This involves galvanised FRS with cement/resin debonded grouted rebar, galvanised mesh and shotcrete applied from floor to floor. Grouted cables

are used in major intersections. Rehabilitation of the ore drives is often necessary to repair damage from the large excavation displacements.

Two distinct mine atmospheres, based on their locations within the mine, were encountered during this study. The long-term development such as the decline and shaft platforms were comparatively fresh with lower temperatures and relative humidities compared to the ore drives. The restricted secondary ventilation within the production drives creates higher localised temperatures and humidities and is accordingly more corrosive. Table 3.24 displays the atmospheric variables, measured from eighteen sites. The ventilation return airways also recorded similar readings to the ore drives.

Table 3.24 Atmospheric variables at Leinster Nickel Operations.

	Dry Bulb Temperature (°C)		Relative Humidity (%)	
	Range	Average	Range	Average
Decline	17.0-23.0	21.0	44.0-76.0	67.0
Ore Drives	20.0-26.0	24.8	64.0-90.0	78.0

The occurrence of groundwater is found sparsely in the hanging wall permanent development but is much more common in the ore drives. The sub-level caving mining method appears to have a significant control on the location of groundwater flow. The caving process creates a permeable backfill consisting of caved waste that not only allows largely unrestrained groundwater flow towards the bottom of the cave but acts as a sink for groundwater and could be dewatering the surrounding unbroken rock mass. This could explain the absence of groundwater in the hanging wall development. The occurrence of groundwater in the ore drives can be correlated with the advance of the cave.

Five groundwater samples collected at the ore drives are assumed to originate from the sub level cave with their measurements shown in Tables 3.25 and 3.26. The water is neutral, of moderate salinity with a moderate to high dissolved oxygen content and high temperatures. Two groundwater samples were collected from the return airways which are located a distance from the caving operations. It displayed a much higher salinity and lower dissolved oxygen content with comparable temperatures (see Table 3.25).

Groundwater was also observed at the shaft platforms within 1-2 m of shaft opening, but not in large enough quantities to be studied in detail.

Table 3.25 Groundwater variables measured *in situ* at Leinster Nickel Operations from the sub level cave.

TDS (ppm)		pH		Dissolved Oxygen (mg/l)		Temperature (°C)	
Range	Average	Range	Average	Range	Average	Range	Average
10,374-14,212	12,260	7.50-8.92	8.30	3.27-3.95	3.53	26.4-29.7	28.6

Table 3.26 Groundwater assay of dissolved ions at Leinster Nickel Operations from the sub-level cave.

Iron	Calcium	Carbonate	Bicarbonate	Chloride	Sulphate	Nitrate
Fe	Ca	CO ₃ ²⁻	HCO ₃ ⁻	Cl	SO ₄ ²⁻	NO ₃ ²⁻
mg/l	mg/l	mg/l	mg/l	mg/l	mg/l	mg/l
0.05	430	7	10	7,700	170	7

Table 3.27 Groundwater variables measured *in situ* at Leinster Nickel Operations from the return air way.

TDS (ppm)	pH	Dissolved Oxygen (mg/l)	Temperature (°C)
Range	Range	Range	Range
48,900-50,600	7.03-7.43	2.35-2.61	27.4-31

A corrosion assessment found only isolated areas of damage limited to either older sections of the mine or where groundwater was present. Figure 3.17 displays strongly corroded FRS and weld mesh in an excavation 15 years old. The original support was not galvanised, which has contributed to its present state. Despite the appearance, tests of the weld mesh show it still retains much of its weld strength (see Table 3.28). The result of the low corrosivity of the atmosphere in the hanging wall development and the corresponding low corrosion rates is depicted in Figure 3.18, which displays a borehole camera survey of a non-galvanised FRS of approximately five years' age that has undergone only minor corrosion. The current practice of using galvanised support greatly helps in protecting against atmospheric corrosion.



Figure 3.17 Corrosion damage to 15 year old surface fixtures at Level 1 platform.



Figure 3.18 Minor surface corrosion of black friction bolt at Level 3 access approximately five years age.

Corrosion damage was observed on a number of galvanised FRS that are affected by groundwater in the ore drives and the return airway. Figure 3.19 shows the level of damage which is high, indicating the corrosiveness of both groundwater types. Groundwater originating in the shaft also affects the first few metres of level shaft platforms. Some corrosion of friction bolts was detected, but generally was only mild to moderate. However, the extended life of the shaft access excavations means that problematic corrosion may occur over time.

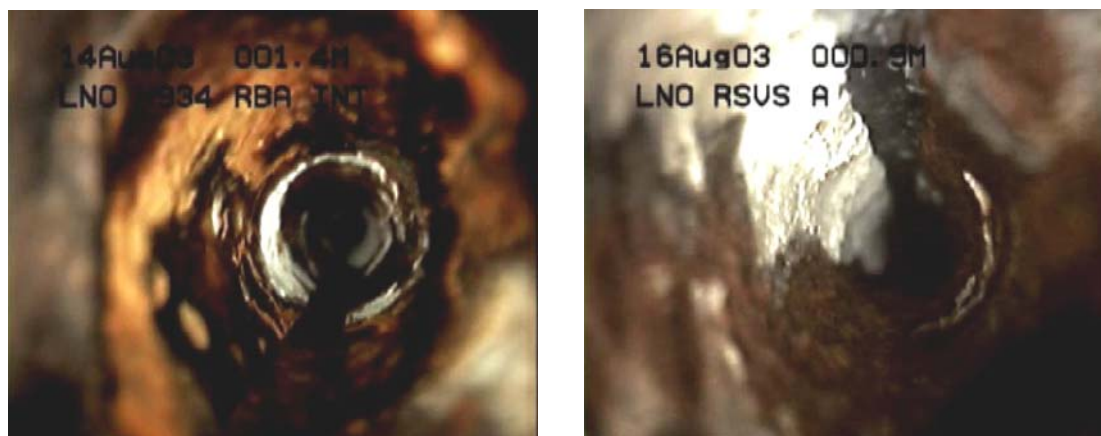


Figure 3.19 Corrosion damage to galvanised FRS in the hanging wall development (left) and ore drive (right).

A number of mesh samples were collected and tested to determine the loss of strength due to corrosion. Their nominal wire diameters are 5.6 mm. The samples taken from the Level 1 platform had what appeared to be severe corrosion damage, as shown in Figure 3.17, with a reduction in strength compared with new mesh samples (11-12 kN) of around 26%. Moderately corroded samples from ore drives displayed similar failure loads to the non-corroded samples.

Table 3.28 Testing of weld mesh samples collected from Leinster Nickel Operations.

Sample Location	Corrosion	Mesh diameter (mm)	Failure Load (kN)	Region of Failure
New mesh sample	None	5.6	12.53	Weld
9740 SHWD (ore drive)	Moderate	5.6	12.39	Heat affected zone
Level 1 platform	Severe	5.0	9.21	Heat affected zone

The majority of reinforcement and support at Leinster Nickel Operations is unaffected by corrosion. This is due to a combination of limited occurrences of groundwater flow and a largely non-corrosive atmosphere. Where groundwater is more prevalent and the atmosphere more corrosive, in the ore drives, the excavations are expected to be open for about two to four years. These same areas also undergo extensive rehabilitation due to the significant squeezing nature of the rock mass and as a consequence new ground support is installed. This combination means it is unlikely corrosion related problems will occur with the ground support. Within the hanging wall development the few areas that contain groundwater should be monitored and rehabilitated when necessary.

3.3.8 Olympic Dam Operations, BHP Billiton

The Olympic Dam copper-uranium-gold-silver deposit is hosted by a network of steeply dipping hematite rich breccia dykes within a fractured granite host (Smith 1993). The competent rock mass is blocky with an average of three joint sets. The immense lateral extension of the deposit has created extensive underground development.

The earlier reinforcement and support scheme consisted of CT bolts; galvanised and non-galvanised 47 mm diameter FRS and galvanised and non-galvanised weld mesh where required. The CT bolt is initially installed as a point anchored system and relies on being post cement grouted to become permanent reinforcement. Failure to cement grout CT bolts has been documented by Simpson (2005) and this renders the bolt susceptible to corrosion. Currently full resin encapsulated bolts are being used as a permanent support, with galvanised FRS and weld mesh.

The mine atmosphere despite the extensive underground development is reasonably fresh with moderate relative humidity (see Table 3.29) for much of the permanent development where the majority (fifteen samples) of measurements were taken. In specific areas such as ore drives (five samples) where secondary ventilation is used, higher temperatures and humidities were detected.

Table 3.29 Atmospheric variables at Olympic Dam Mine.

Dry Bulb Temperature (°C)		Relative Humidity (%)	
Range	Average	Range	Average
21.0-28.0	24.0	55.0-85.0	72.0

Groundwater in sufficient quantities to analyse was not commonly found within the mine and only two samples were able to be collected and analysed, the results are shown in Table 3.30. The wide range of TDS indicates two different aquifer sources. The assay of the groundwater taken from the 44 Cyan 19 stope sample is shown in Table 3.31.

Table 3.30 Groundwater variables tested *in situ* at Olympic Dam Mine.

Location	TDS (ppm)	pH	Dissolved Oxygen (mg/l)	Temperature (°C)
44 Cyan 19	44,000	7.40	3.13	24
32 Jade 2	97,800	7.03	3.09	20.5

Table 3.31 Groundwater assay of dissolved ions from 44 Cyan 19 at Olympic Dam Mine.

Iron	Calcium	Carbonate	Bicarbonate	Chloride	Sulphate	Nitrate
Fe	Ca	CO ₃ ²⁻	HCO ₃ ⁻	Cl	SO ₄ ²⁻	NO ₃ ²⁻
mg/l	mg/l	mg/l	mg/l	mg/l	mg/l	mg/l
0.5	910	1	250	23,000	6,000	64

Generally the corrosion condition of the ground support was minimal, due to the relatively non-corrosive atmosphere. Corrosion of the reinforcement and support is limited to areas that have groundwater or were previously wet; it is distinguished by salt deposition. Severe corrosion of non-galvanised FRS was observed at a number of locations with their condition similar to the FRS displayed in Figure 3.20. This age of installation is approximately six years, suggesting highly corrosive groundwaters. Rehabilitation of corrosion affected areas is carried out by the mine using more corrosion resistant galvanised FRS (see Figure 3.21).



Figure 3.20 Severely corroded FRS at Olympic Dam Mine; the area is damp but groundwater flow is minor.

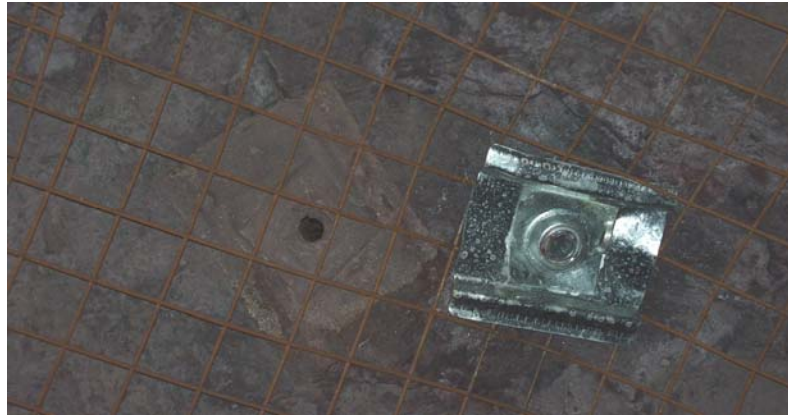


Figure 3.21 Rehabilitation of corroded reinforcement at Olympic Dam Mine.

Similar to the other mines studied, the corrosion related problems at Olympic Dam Mine were constrained by the presence of groundwater. This occurs in isolated areas throughout the mine and affects only a small number of reinforcement elements. Where affected, however, rates of corrosion are high and corrosion resistant ground support is recommended. Of concern are the apparent deficiencies in grouting of the CT bolts which are used for permanent excavations. With the life of the mine being several decades it can be assumed that even the very low rate of corrosion from the mild atmospheric conditions may create some corrosion related issues in the future.

3.3.9 Other mine site groundwater data

Information on groundwater quality was also collected at four other Australian underground mines and is summarised in Table 3.32. The Raleigh mine is located near the Kundana mine with the source of the water being a nearby paleochannel accounting for the hypersaline water. The Waroonga mine is located near Leinster and is only slightly saline with high dissolved oxygen. The Telfer mine is located in northern Western Australia and has saline water.

The Gunpowder mine in northern Queensland is the only mine groundwater tested during this research that was acidic. This is attributed to the previous mining method of *in situ* leaching of the ore by acid solutions that lowered the pH of the local groundwaters. Environmental issues have not arisen as a consequence of the acid

leaching at Gunpowder, but previous documented cases show that aquifers can take up to twenty years to return to baseline conditions (Underhill 1998). This creates a strongly corrosive groundwater that does not require dissolved oxygen for corrosion to occur and dissolves any protective rust layers that may form. Subsequently, significant corrosion of the visible support has occurred over short time durations including complete corrosion of sections of galvanised weld mesh. The groundwater at Gunpowder Mine cannot be considered natural and needs to be examined separately to the other results.

Table 3.32 Groundwater variables measured *in situ* and assayed for other Australian underground mines.

		Raleigh	Waroonga	Telfer	Gunpowder
TDS	(ppm)	185,197	4,140	26,000	7,280
pH	pH units	7.38	7.28	6.5	2.83
Dissolved Oxygen	mg/l	2.98	4.42		4.02
Temperature	°C	14.6	27.3		26.9
Iron, Fe	mg/l	0	<0.1	0.6	
Calcium, Ca	mg/l	971	320	1,600	
Carbonate, CO₃²⁻	mg/l	0	<1	<1	
Bicarbonate, HCO₃⁻	mg/l	42	95	40	
Chloride, Cl	mg/l	82,000	2,100	14,000	
Sulphate, SO₄²⁻	mg/l	14,669	1,120	220	
Nitrate, NO₃²⁻	mg/l		104	<0.2	

3.4 Atmospheric conditions in Australian metalliferous underground mines

Atmospheric conditions within Australian underground mines show variations with temperature and humidity on a local mine wide scale. Higher temperatures and humidities were generally encountered in deeper sections of the mine, areas where the rate of air flow was restricted or secondary ventilation was in use such as ore drives, and return airways. Declines and shafts, often used as the main fresh air intake by contrast had lower values.

In general mine sites within the Yilgarn Craton displayed lower temperatures and lower humidities than those sampled in northern Queensland, as shown in Table 3.33. The

Western Australian mines and Olympic Dam had an average temperature in the low to mid twenties and corresponding humidities of below 80%. The exception to this was the Kundana mine; however, the majority of measurements were taken in the return airway creating a disparity. The mines located in far north-west Queensland (Enterprise and Cannington) have average temperature in the high twenties and mid thirties with humidities above 80%. The differences between the localities are considered to be a combination of higher ambient rock temperatures in Eastern Australia and high surface temperatures in far north-west Queensland. Refrigeration of mine air is required in Enterprise mine during the summer months.

Table 3.33 Atmospheric measurements at selected Australian underground mine sites.

	Dry Bulb Temperature (°C)			Relative Humidity (%)		
	Minimum	Maximum	Average	Minimum	Maximum	Average
Argo	16	25	20.2	45	82	62
Cannington	25	32	28.4	66	93	81
Darlot	15	23	20.2	60	92	75.6
Enterprise	30	45	35	80	95	86.1
Kanowna Belle	20	29	24.7	50	91	70
Kundana	21	24	23	77	92	88
LNO - decline	17	23	21	44	76	67
LNO - ore drives	20	26	24.8	64	90	78
Olympic Dam	21	28	24	55	85	72

Atmospheric contaminants such as sulphur dioxide and nitrous oxides may be present in varying quantities. Sulphur dioxide is commonly formed from the burning of coal or during the processing of some sulphatic ores. In underground mines it may be formed in very small quantities from the slow oxidation of pyritic ores. Significant quantities of nitrogen dioxide are formed due to blasting of explosives. A small amount is found in the exhaust gases of diesel equipment but is generally rapidly diluted by ventilation. Concentrations of the gas can occur in poorly ventilated areas (MINESafe Limited 2006). Current exposure limits for underground mines for sulphur dioxide and nitrogen dioxide are 5.2 mg/m³ and 5.6 mg/m³ respectively. No direct measurements were able to be undertaken of either gas type during the data collection. Available gas monitors were unable to register a reading below 0.1 ppm or 0.26 mg/m³ for sulphur dioxide and 0.19

mg/m³ for nitrogen dioxide implying that the concentrations of these gases were below this threshold.

Atmospheric salinity within Australia diminishes with increasing distance from the ocean, and is also affected by seasonal prevailing winds. The deposition of chloride salts from the airborne chlorides is generally expressed as an annual average to take into account the variation with weather. Higher deposition is observed near the southern coastal areas and reduces significantly further inland. Australia commonly has low rates of salt deposition compared to North America and Europe.

The majority of metalliferous mining is conducted in inland Australia and thus is not greatly affected by salt deposition from atmospheric salinity. The average daily chloride deposition rates for the majority of inland Australia are 4-8 mg/m²day. Near the far north Queensland mines of Enterprise and Cannington they are below 4 mg/m²day (CSIRO & IGC 2002). At these rates, and considering the unique ventilation situation in underground mines chloride deposition is largely insignificant from the point of view of atmospheric corrosion attack. The controlling pollutants are considered to be sulphur dioxide and nitrogen oxides, which are in very low concentrations.

3.5 Groundwater conditions in Australian metalliferous underground mines

Groundwaters in underground mines display a large range in the values of variables such as TDS, pH, dissolved oxygen, temperature and the dissolved ionic species. Table 3.34 displays the average of the variables that were measured *in situ* at all mine sites. Variability with groundwater quality on a local mine scale is seen and also regional trends can be observed.

Table 3.34 Average *in situ* groundwater measurements at Australian underground mines.

	TDS	pH	Dissolved Oxygen	Temperature
	mg/l	pH units	mg/l	°C
Argo	203,416	6.20	1.89	19.2
Cannington	2,610	7.8	4.02	30.0
Darlot Aquifer 1	4,540	7.39	5.55	19.7
Darlot Aquifer 2	66,500	6.99	3.22	20.6
Enterprise	7,860	7.5	4.13	33.0
Kanowna Belle Aquifer 1	47,250	7.3	4.35	26.5
Kanowna Belle Aquifer 2	97,933	7.35	2.93	26.5
Kundana	99,936	7.06	3.23	23.0
Leinster Nickel Aquifer 1	12,260	8.30	3.53	28.6
Leinster Nickel Aquifer 2	49,750	7.23	2.48	29.2
Olympic Dam Aquifer 1	44,000	7.40	3.13	24.0
Olympic Dam Aquifer 2	97,800	7.03	3.09	20.5
Raleigh	185,197	7.38	2.98	14.6
Waroonga	4,140	7.28	4.42	27.3

3.5.1 Total Dissolved Solids

Comparison of the TDS at different mines displays a range of groundwater quality from brackish (<10,000 mg/l), and saline (10,000 to 100,000mg/l) to hypersaline at (>100,000 mg/l). Comparatively seawater is generally considered to be 35,000 mg/l and water having greater than 1000 mg/l is unacceptable for drinking within Australia. Four mines, Argo, Kundana, Kanowna Belle and Raleigh, can be regard as having hypersaline waters and are located in the south of the goldfields of Western Australia. Darlot, Leinster Nickel, Olympic Dam and a separate aquifer at Kanowna Belle have saline waters. Darlot and Leinster Nickel are located in the northern region of the WA goldfields. Brackish waters are found in the eastern Australian mines of Cannington and Enterprise as well as the northern Goldfields mines of Darlot and Waroonga. Mines including Argo, Darlot and Raleigh are thought to have aquifers that are at least partly recharged from neighbouring paleochannels.

A noticeable trend of the groundwaters is the salinity increase from the north to the south of the Yilgarn Craton. Figure 3.22 shows four regions, Northern, Central, Kalgoorlie and Eastern, with the location of the assessed mine site. Gray (2001) suggests the salinity change is partially due to climatic changes from primarily winter rainfall in

the south, to irregular summer cyclonic rainfall, with high run-off, in the north. A difference in the elevations of the regions is large, with the southeast Yilgarn having a change in elevation of only 18 m over more than 300 km. The low piezometric head differences in the south cause very slow groundwater flow resulting in high salinities due to evaporation and concentration of saline waters. Salinities tend to show major increases with depth, and are most likely due to back-flow of denser saline water from salt lakes. The major origin of the salt appears to be from seawater presumably as aerosols, with concentration due to evaporation.

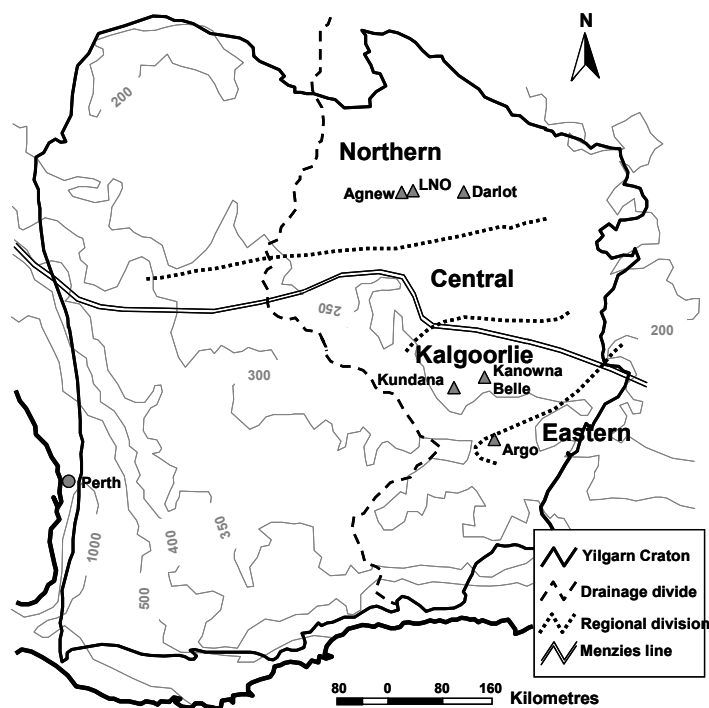


Figure 3.22 Location map of Yilgarn Craton, separated into four regions based on TDS content, with rainfall (mm) in isohyets (D J Gray 2001).

3.5.2 pH

The pH of the natural mine groundwaters sampled had a pH range of 6.20 to 8.30, which varies only slightly from neutral, at pH 7. Acidic waters are considered to have a pH <4 and basic groundwaters pH>10. Only Gunpowder mine had groundwater that could be considered acidic, but this was due to the previous mining technique of *in situ* leaching of the ore using acidic solutions that consequently lowered the pH of the groundwater. Water originating from backfill activities involving cement would be expected to have a more basic pH due to the alkalinity of the cement; however, this was not directly determined in this study.

3.5.3 Temperature

The temperature of the groundwaters in the sampled Australian mines ranged from 14.6°C to 33.0°C. Higher temperatures were seen in mines in eastern Australia, due to the higher ambient rock temperatures, a product of the younger geological age of the region. Generally higher groundwater temperatures were seen with greater depth below surface. Both the Raleigh and Argo mine were comparatively shallower and these exhibited the lowest water temperatures.

3.5.4 Dissolved Oxygen

The dissolved oxygen concentration ranged in values from a low of 1.89 mg/l at Argo mine to a high of 5.55 mg/l within parts of the Darlot mine. The solubility of oxygen in water is a function of temperature and salinity. Both higher temperatures and salinity will reduce the dissolved oxygen content.

An empirical relationship between the solubility of dissolved oxygen in seawater with both temperature and salinity has been developed by Kester (1975) and is calculated:

$$\ln[DO] = A_1 + A_2 \left(\frac{100}{T} \right) + A_3 \ln \left(\frac{T}{100} \right) + A_4 \left(\frac{T}{100} \right) + S \left[B_1 + B_2 \left(\frac{T}{100} \right) + B_3 \left(\frac{T}{100} \right)^2 \right] \quad (3.1)$$

Where:

DO = dissolved oxygen in ml/l

T = temperature in °K

S = salinity in ‰ (parts per thousand)

A₁ = -173.4292

A₂ = 249.6339

A₃ = 143.3483

A₄ = -21.3483

B₁ = -0.033096

B₂ = 0.014259

B₃ = -0.0017000

A comparison between the calculated dissolved oxygen from Equation 3.1; calculated from the temperature and salinity of each *in situ* water sample and the actual measured dissolved oxygen for that sample is shown in Figure 3.23. A good correlation is seen between the theoretical and actual measurements implying the measured dissolved oxygen is a direct product of the water temperature and TDS.

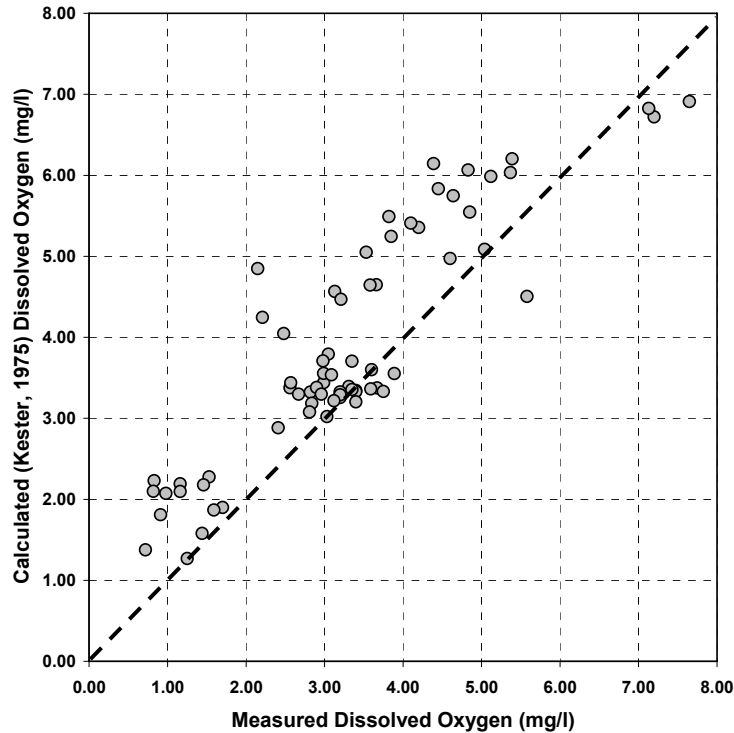


Figure 3.23 The calculated dissolved oxygen concentration compared to the actual measured concentration.

3.5.5 Dissolved Ions

Groundwater assays were undertaken to establish the type and concentrations of the dissolved ionic species for most groundwater aquifers encountered with the exception of Leinster Nickel Aquifer 2 and Olympic Dam Aquifer 2. The combined results in Table 3.35 show high concentrations of the ionic chlorides and sulphates relative to the TDS. Carbonates were not detected in the majority of waters with bicarbonates and nitrates generally having low concentrations. Chloride ions are a significant percentage of the dissolved ions for all waters. A strong quadratic correlation between the TDS and chloride ion concentration is seen in Figure 3.24 suggesting the relationship between TDS and chloride content can be approximated by:

$$Cl^{-} \approx 10^{-6}(TDS)^2 + 0.3697(TDS) \quad (3.2)$$

where:

Cl^{-} = chloride ions in mg/l

TDS = Total Dissolved Solids in mg/l

It appears, however, this association becomes less conclusive once the TDS is greater than 150,000 mg/l. The origins of the chlorides are thought to be due to the deposition of airborne salts accumulating over millions of years (D J Gray 2001).

As Figure 3.25 illustrates a weaker relationship, displayed in Equation 3.3, is seen between the sulphate ion concentration and the TDS. Possible sources for the sulphate ions include sulphatic minerals that are often associated with mineralisation. Some operations, such as Enterprise, Cannington and Olympic Dam, which have massive sulphide or disseminated sulphide deposits, have elevated sulphate to TDS ratios compared to other mines. This however does not hold for all mines containing large concentrations of sulphide minerals with Leinster Nickel comprising very low sulphide concentrations. Groundwaters from Darlot and Waroonga had relatively high concentrations of sulphate ions despite the waters being expected to interact with only minor quantities of sulphide minerals. It is reasonable that regional rock types may be the origin of sulphate ions in the groundwater rather than localised concentrations of sulphide minerals.

$$SO_4^{2-} \approx 4 \times 10^{-7}(TDS)^2 + 0.0087(TDS) \quad (3.3)$$

where:

SO_4^{2-} = sulphate ions in mg/l

TDS = Total Dissolved Solids in mg/l

Table 3.35 Average groundwater analysis assays from Australian underground mines.

	TDS (assay) mg/l	Calcium Ca mg/l	Chloride Cl- mg/l	Carbonate CO ₃ ²⁻ mg/l	Bicarbonate HCO ₃ ⁻ mg/l	Sulphate SO ₄ ²⁻ mg/l	Nitrate NO ₃ ²⁻ mg/l
Argo	230,000	310	180,000	<1	50	24,000	0.2
Cannington	4,000	300	1,500	<1	48	800	0.05
Darlot Aquifer 1	5,400	50	3,570	<1	290	170	120
Darlot Aquifer 2	47,000	1,200	22,000	<1	80	3,900	67
Enterprise	6,200	110	970	<1	82	5,000	0.33
Kanowna Belle Aquifer 1	49,000	1800	27,000	<1	33	1,300	360
Kanowna Belle Aquifer 2	130,000	3,600	80,000	<1	35	3,300	260
Kundana	120,000	1,600	69,000	<1	75	7,800	94
Leinster Nickel Aquifer 1	13,000	430	7,700	7	10	170	7
Olympic Dam Aquifer 1	44,000	910	23,000	<1	250	6,000	64
Raleigh	185,197	971	82,424	<1	42	14,669	
Waroonga	4,460	320	2,100	<1	95	1,120	104

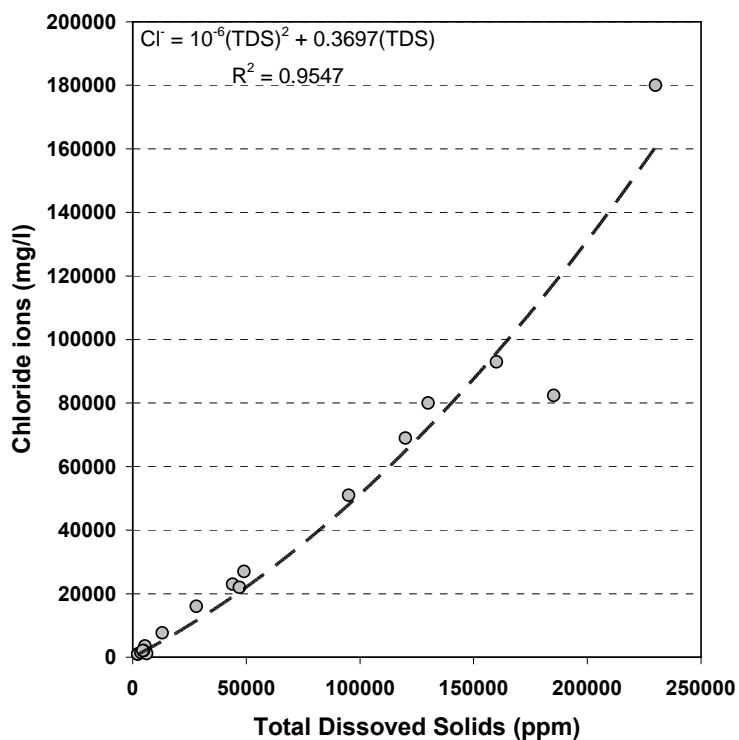


Figure 3.24 Relationship between the TDS and chloride ion concentrations.

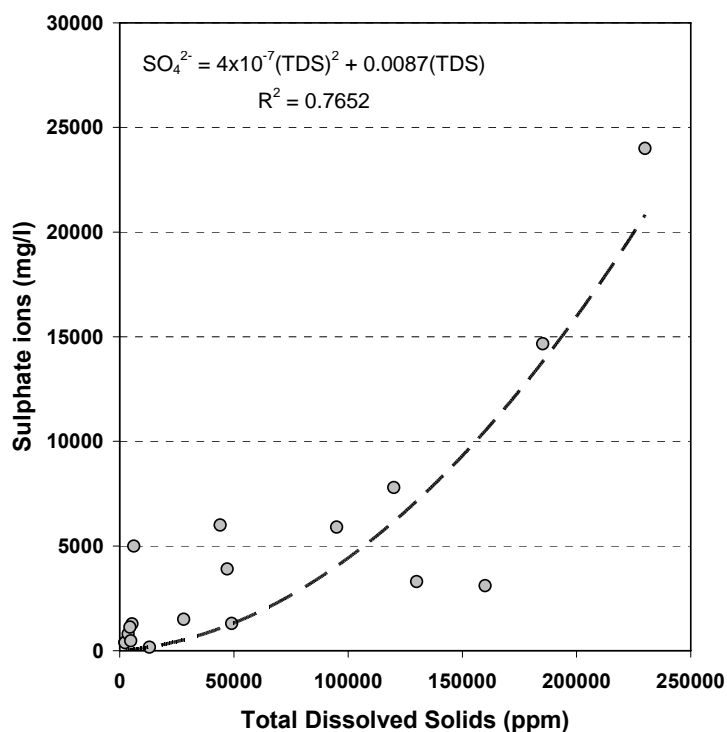


Figure 3.25 A weak correlation between the TDS and sulphate ion concentrations.

The rate of groundwater flow varied from site to site within a mine with the majority classified as either damp or wet with the only flowing water occurring in the Hamilton Fault region at Cannington Mine. Some areas showed evidence through salt deposition of previous groundwater flow. Using the borehole camera it was observed that some of these areas still contain some groundwater away from the excavation boundary and were classed as damp.

3.6 Discussion and Conclusions

A comprehensive and systematic data collection has been completed at eight underground mine sites across Australia utilising the Corrosion Assessment System. This has provided an improved understanding of the environmental conditions in underground hard rock mines with the delineation of two separate environments that control the rate of corrosion.

The atmospheric variables of temperature, humidity and pollutants affect the majority of installed ground support. Variations in the quality of the mine atmospheres were observed with the depth of mining below surface and the ambient rock temperatures. Areas where secondary ventilation is in use and return airways had measurably higher temperatures and humidities. Regardless of the quality of the atmosphere the use of galvanised ground support appears to greatly restrict the rate of corrosion.

The main cause of corrosion in underground mines is groundwater. The groundwater originates in surrounding aquifers, with large geological structures that intersect mine development providing a conduit for water flow. However, only a small percentage of installed ground support is affected. The inter-related groundwater variables that influence corrosion are the total dissolved solids, the pH, the dissolved oxygen concentration and the groundwater temperature. Corrosion of ground support affected by groundwater displayed varying levels of corrosion damage that can be related to the corrosivity of the water, the rate of groundwater flow, the length of time installed and the type of support or reinforcement. Friction Rock Stabilisers appear especially susceptible to corrosion damage.

The data presented in this Chapter provides a summary of environmental conditions that can be considered a suitable cross-section of Australian hard rock underground mines. This provides the initial step in classifying the environment in terms of its corrosivity. An understanding of the environmental variables within an underground mine is needed to assess an environment's corrosivity and ultimately its effect on the various reinforcement and support systems installed.

CHAPTER 4 REINFORCEMENT AND SUPPORT TESTING USING A SIMULATED UNDERGROUND ENVIRONMENT

4.1 Introduction

The environmental conditions that were discussed in Chapter 3 detail the variability and changing nature of the local environmental conditions in a working mine. It is impossible to maintain consistent environmental conditions for the extended periods of time necessary to study the processes and rates of corrosion for different reinforcement materials. To overcome this, a series of corrosion chambers were designed and developed to simulate the corrosive environments of underground mines. This allowed for long-term testing, under controlled experimental conditions to be conducted with a high level of confidence.

The development of the corrosion chambers and the environmental conditions that they were maintained at is detailed in Section 4.2. Sections 4.3 to 4.5 describe the methodology and results from experiments conducted in the corrosion chambers. Section 4.3 examines the load-displacement response and failure modes of cable strand and rebar reinforcement elements to corrosion in various environments. The effect of residual installation water in Swellex bolts is discussed and results presented in Section 4.4. Section 4.5 examines the force-displacement response and the influence corrosion has on the load-bearing capacity of barrel and wedge anchors for cable bolts.

4.2 Development of the simulated underground environment

The testing to be carried out required a large volume of space that could not be provided by commercially available corrosion chambers. Therefore, it was decided to construct a set of purpose built units. Following site works at land located at Curtin University in Kalgoorlie three sea containers were delivered. These were partitioned in half with

remaining gaps sealed with a silicone sealant and polyethylene. An anti-bacterial paint was applied to the walls and roof. Polypropylene rubber lining was secured onto the floor and partly up the walls and a polyethylene sealant applied. Access doors were constructed that sealed when closed. The result was a closed system of six chambers each with dimensions 2 m width, 2.5 m deep and a height of 2 m that simulate the previously described conditions of Argo, Darlot, Enterprise, Kundana, Leinster Nickel and Olympic Dam mines.

The temperature of each chamber was initially controlled by 1000W infrared ceramic heaters. The high maintenance cost of these units necessitated a change to 275W radiation lamps that endured the conditions inside the chamber with better resilience. Humidity is created by two Carel steam humidifiers (see Figure 4.1) that have a maximum capacity of emitting 1.5kg of steam per hour, a rate which is significantly higher than needed. The humidifying units are located on the outside of the chamber with piping connecting them to the distribution unit, which is located inside the chamber a metre above the floor.

To control the temperature and humidity in each chamber a central Power Line Communication (PLC) system with a PC user interface was originally used. This system collected information on the atmosphere of each chamber measured from a dual relative humidity/temperature sensor located within each chamber. A series of switch relays turned the humidifier or heat source on or off maintaining a reasonably constant climate. In addition periodic measurements of the temperature and humidity were automatically recorded to file. This system while being technically sound had a number of maintenance problems and was superseded after 1.5 years of operation to a more robust CLIPSAM multi-port instrumentation unit shown in Figure 4.1.

Each chamber has its own independent instrumentation unit, located on the outside of the chambers and connected directly to the humidifier and heat lamp. The single sensor was replaced by two dedicated humidity and temperature sensors. The required temperature and humidity is displayed on the front of the unit with the measured values

located below it. Variations in the temperature of $\pm 2^{\circ}\text{C}$ and humidity $\pm 5\%$ from the set average causes the processing unit to either turn on or off the heat lamps and humidifier keeping the atmospheric conditions within a set range. Significant variations from the required parameters occurred only when the heat lamps malfunctioned and had to be replaced. Periodic checks of the chambers ensured this was kept to a minimum.



Figure 4.1 CLIPSAM multi-port instrumentation unit (left), heat lamp (top right) and humidifier unit (bottom right).

Groundwater was collected directly from the rock masses and transported to the corrosion chambers. An electric pump was used to propel the water through a purpose built reticulation system. This produced a constant supply of dripping or flowing groundwater being applied to the reinforcement and support being tested. The water flowed back into the rubber lined sump and was recirculated. The groundwater was periodically analysed using a portable water analyser that gave immediate readings of the temperature, pH, dissolved oxygen and TDS. When the conditions departed from the underground situation the water was changed. Some water loss from each chamber was experienced, despite sealing, and water had to be replenished.

4.2.1 Environmental Conditions in the Corrosion Chambers

The required atmospheric conditions for each chamber are shown in Table 4.1. It was decided to maintain the identical temperature and humidity of 30°C and 90% in each chamber with the exception of the Enterprise mine chamber which, was set for 40°C. This was due to the much higher atmospheric and groundwater temperatures observed within the Enterprise Mine. Variations up to $\pm 4^{\circ}\text{C}$ and $\pm 10\%$ are expected from the required values due to the nature of the control system. Some seasonal effects were seen during the months of December to February that resulted in higher temperatures due to the occasional very hot summer day.

Comparisons between the set temperature and humidity and actual measured values was conducted by Henley (2002) with the results shown in Figures 4-2 and 4-3. Variation with temperature was minor, approximately $\pm 2^{\circ}\text{C}$; with the set and measured values being the same for extended time periods. Control of the humidity is more complicated, as it is partly a function of the temperature. The results showed a greater deviation from the set value in the range of $\pm 10\%$.

Table 4.1 Atmospheric conditions in each corrosion chamber.

Chamber	Dry Bulb Temperature (°C)	Relative Humidity (%)
Argo Mine	30	90
Darlot Mine	30	90
Enterprise Mine	40	90
Kundana Mine	30	90
Leinster Nickel Operations	30	90
Olympic Dam Operations	30	90

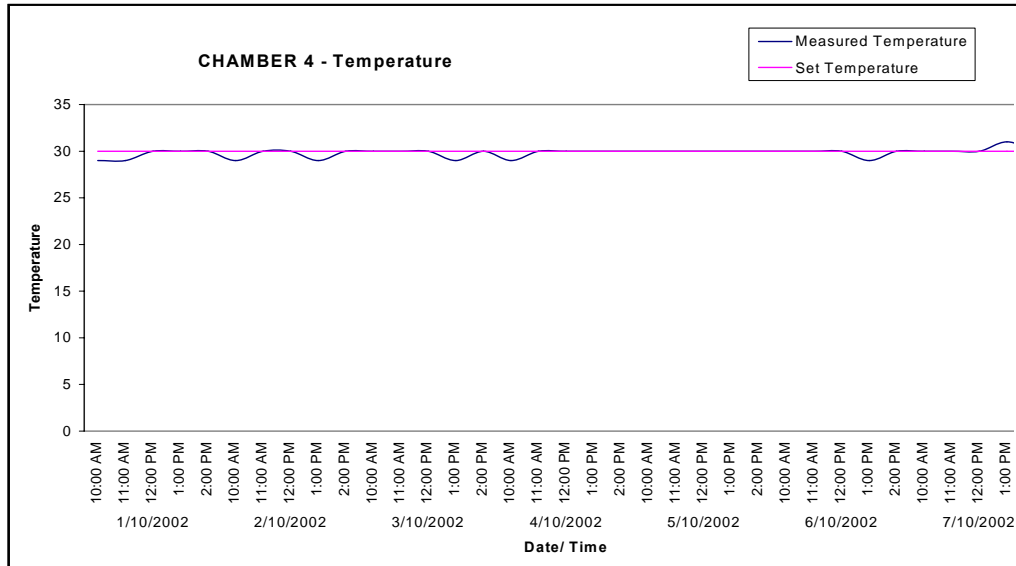


Figure 4.2 Monitoring of temperature in the corrosion chambers.

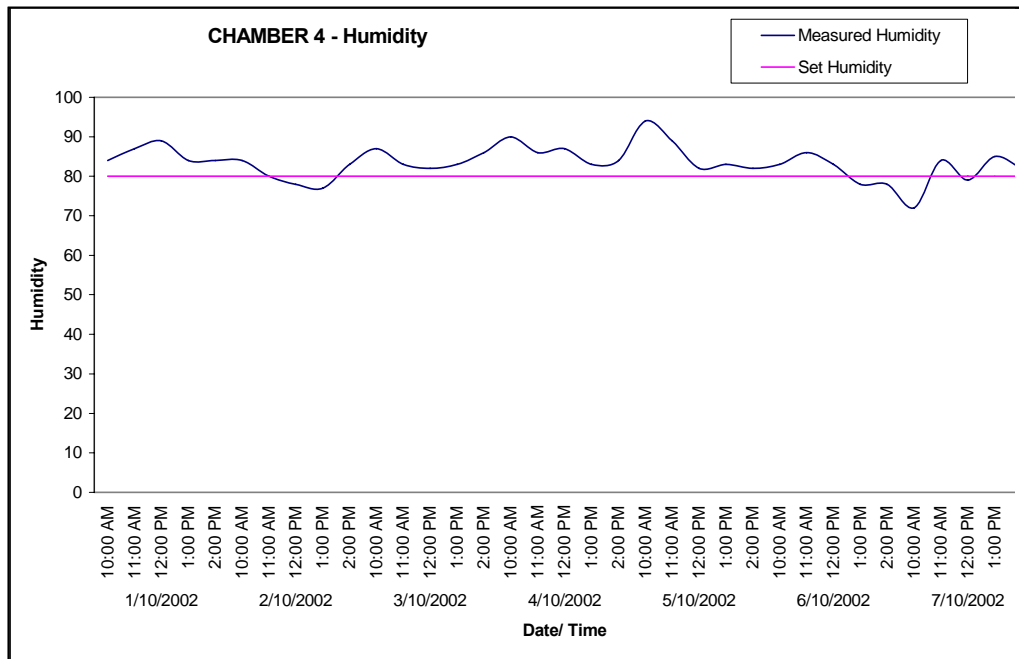


Figure 4.3 Monitoring of humidity in the corrosion chambers.

The groundwater of each chamber was monitored approximately every month using the TPS water analyser for temperature, pH, dissolved oxygen and TDS. The mean values and standard deviations for each constituent over the length of the experiments are shown in Table 4.2. The variations in water properties occur for a number of reasons.

The temperature of the water is controlled by the atmospheric temperatures; any change in it will affect the groundwater, which has a flow on affect to the dissolved oxygen. Rises in salinity were observed over time due to evaporation of the water and concentration of the dissolved ions. This again subsequently affected the dissolved oxygen. Of the measured parameters only the pH had little variation.

Additionally the groundwater collected from the participating mine sites had to be replenished as water was lost from the system. As discussed in Chapter 3 groundwater from the same aquifer displays variations in constituents, therefore it was expected that each batch of supplied groundwater would be marginally different. Before any new groundwater was added to the chambers it was first analysed to make sure it was comparable. At two mines, Enterprise and Olympic Dam, it was not possible to collect groundwater from the same location. At Enterprise Mine a rock fall prevented re-entry and at Olympic Dam the area had been mined out and ventilation was not adequate for entry (uranium mine). At Darlot Mine it was decided to change the groundwater to an aquifer that had recently been intersected in deeper development excavations and was of greater interest to the mine.

Table 4.2 Average groundwater measurements for each corrosion chamber.

Chamber	Temperature °C		Dissolved Oxygen mg/l		pH pH units		TDS mg/l	
	Mean	St Dev	Mean	St Dev	Mean	St Dev	Mean	St Dev
Argo	26.42	3.19	1.72	0.39	7.32	0.22	172,000	8,474
Darlot	26.28	2.01	3.17	0.50	7.69	0.46	37,644	17,046
Enterprise	32.68	4.42	3.44	0.67	7.36	0.78	18,630	9,591
Kundana	26.24	1.92	2.48	0.39	7.27	0.78	79,200	15,651
Leinster	26.29	2.24	3.76	0.40	7.48	0.49	14,782	2,899
Olympic Dam	27.10	4.27	2.78	0.54	7.82	0.26	38,005	7,862

The changes in the groundwater properties for the Darlot, Olympic Dam and Enterprise Mines are shown in Table 4.3. The new Darlot groundwater was about 7.5 times more saline than the previous water, with lower dissolved oxygen content. The new Olympic Dam supplied water was more saline, with lower dissolved oxygen value but could still possibly be considered from the same aquifer source. The new water from the Enterprise Mine was considerably less saline with a much higher dissolved oxygen measurement.

Table 4.3 Variations in groundwater properties.

Chamber	Days	Temperature °C	Dissolved Oxygen mg/l	pH pH units	TDS mg/l
Darlot (previous)	65	24.71	3.72	8.38	5,943
Darlot (new)	993	26.76	3.03	7.52	45,187
Olympic Dam (previous)	562	27.27	2.98	7.89	31,679
Olympic Dam (new)	570	26.90	2.55	7.74	45,519
Enterprise (previous)	602	31.79	3.12	7.28	24,640
Enterprise (new)	235	34.45	4.08	7.53	6,610

4.3 Testing of cement grouted cable strand and rebar reinforcement elements

Cement grouted reinforcement is commonly used in Australian underground mines for its high load transfer capacity and resistance to corrosion damage. This resistance is afforded by the protective alkaline environment of the cement grout and the physical barrier it provides from the surrounding environment. The major factors that cause steel embedded in cementitious systems such as reinforced steel to corrode are the influences of carbonation and chloride infiltration (Slater 1990). However, the time periods over which these processes are expected to affect the underlying steel are considerably longer than the design life of much cement grouted reinforcement. For example, in concrete with a w/c ratio of 0.45 and concrete cover of 25 mm, it will require more than 100 years for carbonation to reach the concrete immediately surrounding the steel (Virmani & Clemena 1998). Chloride infiltration is generally measured in decades not years.

It is therefore concluded that these phenomenon do not have any significant affect on the corrosion damage of installed cables and rebar over short design lives. Instead corrosion begins once the cement grout barrier is removed. This occurs by cracking of the grout column, or in sections where the element is exposed from inadequate installation. This exposes the steel strand or rebar to the surrounding environment. Poor and often inadequate installation of cement grouted reinforcement has been documented by Sundholm (1987), Kendorski (2000) and Windsor (2004) among others. Poor installation practices can include eccentric reinforcement placement in the borehole, insufficient encapsulation, slumping of the grout mixture and the presence of air voids.

Cracking of the grout column can occur during rock mass movement or as a result from the shockwaves of nearby blasting or a combination of both. The rock mass will preferentially move along existing fractures and if a grouted reinforcement element intersects a dilating geological discontinuity cracking of the grout column can occur in this area as the tensile capacity of cement is considerably less than the steel element. This concept is shown diagrammatically in Figure 4.4. For resin grouted elements similar development will occur with Figure 4.5 displaying actual cracking within a resin grouted column.

Cracks within the grout column provide a pathway for gravity assisted water flow to interact with the steel element. Cracking preferentially occurs along geological discontinuities, which are also the conduit for groundwater flow in hard rock aquifers. Without the protection reinforcement elements will undergo corrosion damage. There is currently no commercial non-destructive testing method able to determine if cracking of the grout column has occurred and whether it has resulted in corrosion damage to the element. Overcoring of the element is the only way to ascertain this.

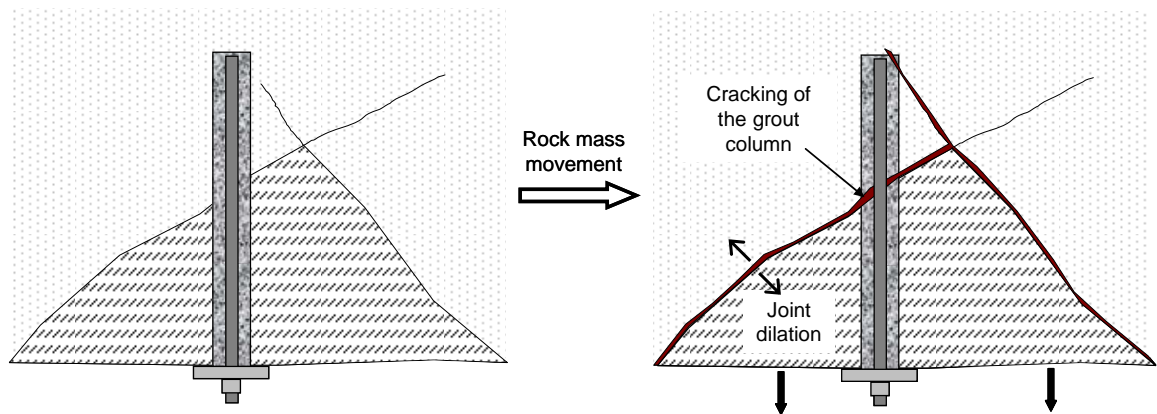


Figure 4.4 Cracking of the grout column due to joint dilation.



Figure 4.5 Cracking within a resin grouted column, these cracks present a path for the surrounding environment to interact with the reinforcement.

In an effort to better understand the response of grouted strand and rebar to corrosion attack following cracking of the grout column and infiltration of groundwater, a variety of strand and thread bar combinations were placed within the six corrosion chambers. These were pull tested at periodic intervals to determine how corrosion affects the reinforcement effectiveness with time for different environments. In addition a migrating corrosion inhibitor (MCI) grout additive was trialled to establish its effect on reducing the corrosion damage.

4.3.1 Reinforcement under investigation

Cable bolts utilised within the Australian mining industry commonly use a 7-wire, stress relieved, high tensile steel strand with plain (round) wires. Six wires are laid helically around a slightly larger diameter central (king) wire. The regular 15.2 mm diameter strand is produced to provide a number of grades that offer differing yield and ultimate load capacities.

Standard strand has a minimum yield force capacity of 213 kN and a minimum breaking force of 250 kN. For comparison compact strand that is deformed following laying results in more steel for the same nominal diameter and results in a minimum yield force capacity of 255 kN and a minimum breaking force of 300 kN (AS 1311 1987). Figure 4.6 shows both grades of cable bolt strand used in Australia. Modifying the geometry of the strand through the introduction of bulbs along the strand length will vary the stiffness of the cable bolt providing greater load transfer capacity.



Figure 4.6 Plain (top) and compact (bottom) cable bolt strands.

A variety of solid bar elements are available to be used with a range of reinforcement systems. Modifications to the bar diameter and thread pattern are used to achieve different load transfer capacities. This investigation examined a standard 20 mm diameter thread bar as shown in Figure 4.7. It has typical yield strength of 170 kN and ultimate tensile strength of 200 kN (AS 1442 1992). The thread is continuous along the bolt axis and provides good load transfer at the element-grout interface. A galvanised version of the thread bar was also tested. Additionally a 20 mm diameter smooth steel bar from the CT bolt was tested.



Figure 4.7 20 mm diameter thread bar.

A migrating corrosion inhibitor (MCI) grout additive was also trialled to observe if it protected the steel element from corrosion damage. The Meyco MCI 2006-1 is based on amino carboxylate chemistry. It is added as a powder admixture to the grout during mixing and upon cement curing the additive diffuses through the concrete migrating to the steel surface. There it forms a thin monomolecular protective layer that prohibits a chemical reaction between chlorides and steel. Numerous studies have proven the ability of MCI to provide corrosion protection for steel in reinforced concrete (Bavarian & Reiner 2001; Bjegovic & Miksic 2001; Miksic 1995). Research by Suess et al. (2001) found that MCI 2006 tripled the time to the onset of corrosion and once corrosion began the corrosion rate was reduced by sixteen fold. Additionally the additive was found to increase the compressive strength of concrete by up to 53.1%. To compare a grout mix that did not contain the MCI was used. It contained the non-corrosion protecting additive Methocel, which improves the workability of the grout mix and accelerates the setting time of the grout (Villaescusa, Sandy & Bywater 1992).

4.3.2 Methodology

The main focus of the testing was on the three reinforcement element types: plain strand cables, bulbed strand cables and thread bar. Each element type was grouted with either methocel or MCI additive added. A galvanised thread bar was also tested. Table 4.4 displays a summary of the reinforcement elements under investigation. Two specimens for each element were required creating fourteen standard test specimens for each chamber.

In addition to the standard tests, two mine sites requested additional elements to be examined. The rebar element for the CT bolt, minus the protective sleeve was tested in the Olympic Dam chamber and the compact strand was tested in the Argo chamber. Both elements were tested with the grout additives.

Table 4.4 Summary of standard reinforcement elements tested.

Reinforcement Element	Coatings	Grout Additive
Plain strand	None	Methocel
Plain strand	None	MCI
Bulbed strand	None	Methocel
Bulbed strand	None	MCI
Thread bar	None	Methocel
Thread bar	None	MCI
Thread bar	Galvanised	Methocel

The methodology used to investigate the load capacity of the reinforcement elements under corrosive conditions is the split pipe testing system (Villaescusa, Sandy & Bywater 1992). The system shown in Figure 4.8 consists of two 500 mm long, galvanised, 68 mm diameter pipes that have been temporarily welded together at the split, which simulates a geological discontinuity. A wooden plug was placed on the end of the pipe, which also centralised the element. Two separate grout mixes made from Portland cement, one that included the Methocel additive (2 g per kg of cement) and the second the MCI additive (2.5 g per kg of cement), were mixed and pumped using a MBT GP2000A grout pump with a water cement ratio of 0.35. The pipes were placed vertically and grouted from the bottom up with the element remaining in a central position and identification tags attached to the specimens.

It is important to know that the cables were not constantly loaded in tension during the experiment as may occur in actual mining practice. The intricate issues relating to loading of the strand, ensuring the strand remains loaded for the duration of the experiment, and continuous measurements of the load added a high level of complexity and cost that could not be realised by any potential benefits. Hence, variables such as stress corrosion cracking were not investigated within this experiment.

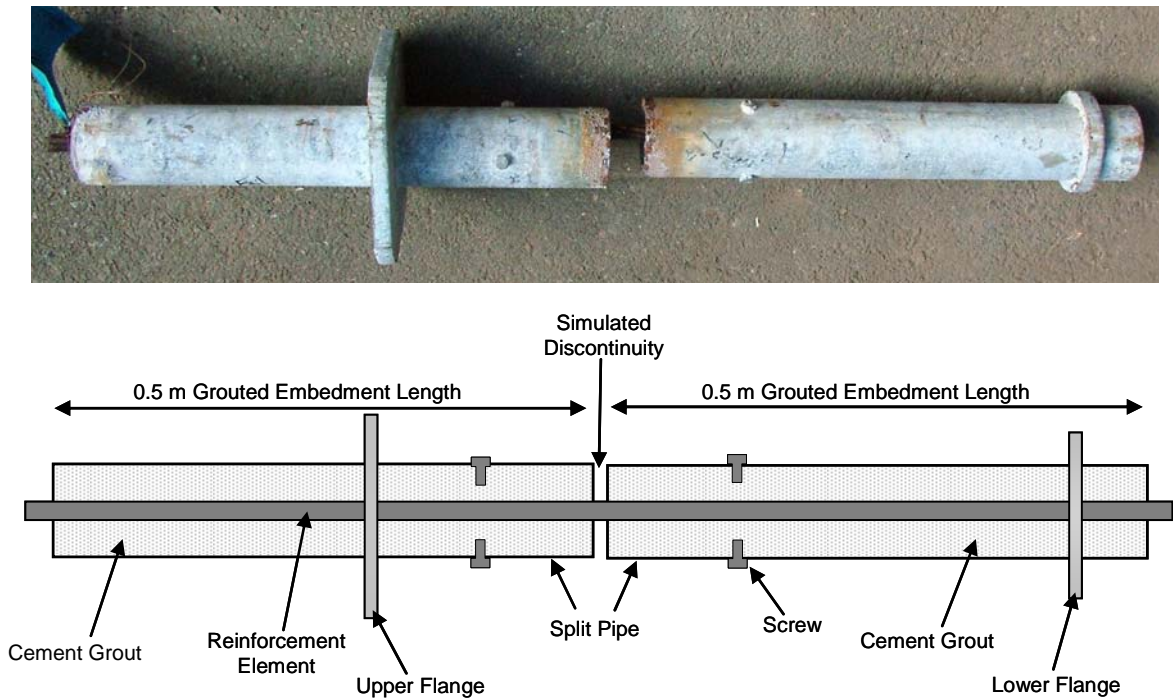


Figure 4.8 The split pipe testing system.

To examine the effect of corrosion over time each specimen was routinely tested using a 50 tonne hydraulic Avery machine type 7110 DCJ. The specimen was placed vertically in the machine with the upper flange resting at the top and a 25 mm thick plate being secured above the lower flange (see Figure 4.9). The hydraulic ram of the testing machine pulls down on the plate and the lower flange, while the upper flange remains stationary resulting in the two pipes pulling apart. The static testing was conducted at a constant increase in load. Transducers located on the machine measured the force being applied and the subsequent displacement. An analogue data collector connected to a PC utilising the Labview software recorded the load-displacement response.

A maximum load of 170-175 kN for the strand elements and 180-185 kN for the rebar elements or a maximum displacement of 10 mm, whichever came first, was applied in all tests. These loads are well below the tensile strength of the elements, thus any failure could be attributed to the corrosion damage. Over an embedment length of 0.5m the plain strand would not be able to utilise its full capacity so a limit was placed on the maximum displacement. This was to ensure that the specimens could be re-tested

following more time under corrosive conditions in the chambers. Similar previous experiments by (Villaescusa, Sandy & Bywater 1992; Villaescusa & Wright 1997) using the split pipe system proved the validity of the testing method and provided a reference for non-corroded tests. In addition to the load-displacement response the open crack width of each bolt was measured with callipers before and after testing. If the element was visible at the crack the severity of the corrosion was noted.



Figure 4.9 The testing set up showing the Avery machine in the background and the PC and analogue data collector to the left. A closer view of the split pipe is shown on the right.

Following a curing time of 7 days the temporary welds attaching the pipe were removed using an angle grinder and an initial slot cut into the grout. The 7 day pull test was conducted in order to open up the split that simulates the geological discontinuity. To increase the frictional resistance at the pipe/grout interface two sets of three screws were installed at equal distances from the split and evenly distributed around the circumference of the pipe. This ensured that all displacement originated at the element/grout interface. Following the 7 day pull tests all specimens were placed horizontally in the corrosion chambers as shown in Figure 4.10.



Figure 4.10 A typical WASM corrosion chamber (left) and water flow through simulated geological discontinuity (right).

Pull testing of the split pipes was undertaken initially after intervals of 6 months in the corrosion chambers. Following the 733 day test due to failure of some elements the interval was reduced to 3 months. Pull testing was therefore conducted at 181 days, 361 days, 546 days, 733 days, 837 days, 922 days, 1034 days and 1132 days. Darlot mine was also tested at 1058 days due to a lack of groundwater to continue the experiment. If failure of the elements occurred the split pipe was cut open along its axis and examined.

4.3.3 Results

Failure of several of the plain and bulbed strand elements occurred at the 733 day test with failure of the final strand elements taking place at the 1132 day test. Failure of the strand was characterised by breaking of one to six of the outside wires. At no stage did the king wire fail and it was always the least corroded of the wires. Typical failure of the strand elements are shown in Figure 4.11. Breakage of the wires always occurred at the simulated discontinuity where the strand is exposed and significant corrosion had taken place.

The evolution of corrosion damage from non-corroded to severe corrosion is shown by Figure 4.12. The non-corroded state occurs when the crack is initially opened and the

grout cover is removed. The application of groundwater to the exposed strand creates increasing levels of corrosion damage culminating in failure, generally when severe corrosion damage has occurred. Severe corrosion damage is characterised by strong pitting corrosion around the circumference of the exposed strand reducing the cross-sectional area of steel and thus the tensile strength of the element.



Figure 4.11 Typical failure of the strand elements with plain strand (left) and bulbed strand (right).







<p>Non-corroded No evidence or only minor evidence of corrosion products</p> 	<p>Light Corrosion Minor surface corrosion of zinc and steel. No evidence of pitting corrosion.</p> 
<p>Moderate Corrosion Surface corrosion covers exposed area of strand. Minor areas of pitting</p> 	<p>High Corrosion Uniform corrosion covers the exposed area of strand. Pitting is irregular around the exposed circumference.</p> 
<p>Severe Corrosion Severe uniform corrosion covers the exposed area of strand. Pitting corrosion is consistent around the entire exposed circumference.</p> <div style="display: flex; justify-content: space-around;">   </div>	

Figure 4.12 Stages of corrosion damage of strand elements.

The results for the plain strand tests are shown in Table 4.5. The first failure occurred at the 733 day test with the last specimen failing at the 1132 day test. The corrosion damage at failure was classed as either high or severe. The peak load at failure ranged from 82.5 kN to 206 kN. There were four cases where the load at failure exceeded 175 kN owing to the bolts being taken to failure due to the completion of the experiment. The crack width, i.e. simulated discontinuity width, at failure ranged from 17 to 75 mm.

Typical load-displacement plots of the testing, for both the methocel and MCI additive are shown in Figures 4.13 and 4.14 respectively. Breakage of the strand is characterised by a sudden drop in load, however as Figure 4.14 displays sudden strand elongation can cause a similar reduction in load as well as an audible cracking noise that is the grout breaking in tension. In these cases the load increases indicating failure has not taken place. The stiffness of the system increases over time and is a product of increased grout strength due to cement curing. The grout with the MCI additive also displayed a higher stiffness compared to the methocel additive grout for each time period before 733 days indicating an earlier higher strength grout.

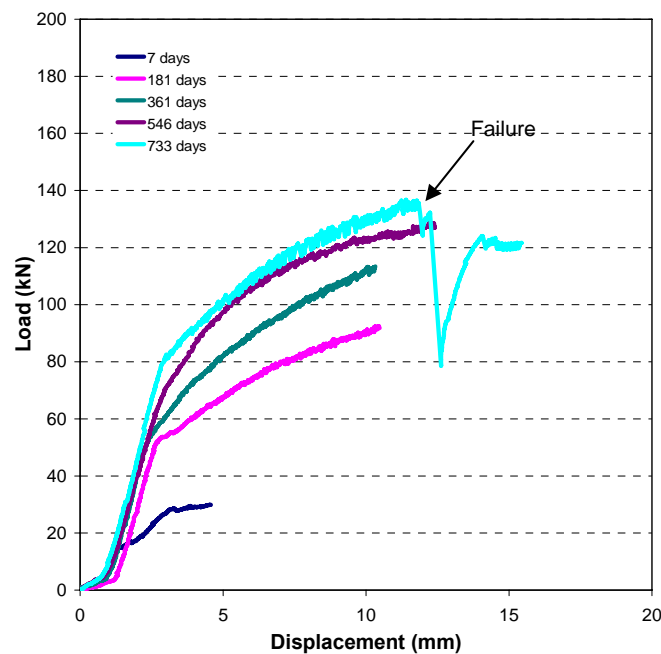


Figure 4.13 Typical load-displacement plot of single plain strand with methocel additive (0.5 m embedment length).

Table 4.5 Laboratory results of corrosion and failure loads for single plain strand elements.

Chamber	Reinforcement type (single strand)	Additive	Service time till failure (days)	Crack width at failure (mm)	Observed corrosion at failure	Peak failure load (kN)
Argo	plain strand	methocel	1132	68.64	severe	140.0
Argo	plain strand	methocel	922	47.31	high/severe	140.8
Argo	plain strand	MCI	1132	58.2	high	206.0
Argo	plain strand	MCI	1132	60.38	severe	158.2
Darlot	plain strand	methocel	1034	46.78	severe	161.9
Darlot	plain strand	methocel	1034	50.12	severe	174.6
Darlot	plain strand	MCI	1058	55.63	high	193.0
Darlot	plain strand	MCI	1034	44.02	severe	177.4
Enterprise	plain strand	methocel	733	23.61	severe	136.7
Enterprise	plain strand	methocel	733	17.12	severe	163.0
Enterprise	plain strand	MCI	733	21.16	severe	135.7
Enterprise	plain strand	MCI	733	18.18	severe	128.4
Kundana	plain strand	methocel	922	75.63	severe	134.4
Kundana	plain strand	methocel	837	61.21	severe	115.5
Kundana	plain strand	MCI	1034	73.74	high	144.8
Kundana	plain strand	MCI	1034	57.13	high	169.7
LNO	plain strand	methocel	922	31.87	severe	126.2
LNO	plain strand	methocel	922	40.52	severe	82.5
LNO	plain strand	MCI	733	24.01	severe	164.0
LNO	plain strand	MCI	837	28.8	high/severe	153.5
Olympic Dam	plain strand	methocel	733	31.06	severe	171.5
Olympic Dam	plain strand	methocel	1132	32.18	severe	183.2
Olympic Dam	plain strand	MCI	1132	30.41	severe	166.2
Olympic Dam	plain strand	MCI	922	30.26	severe	168.7

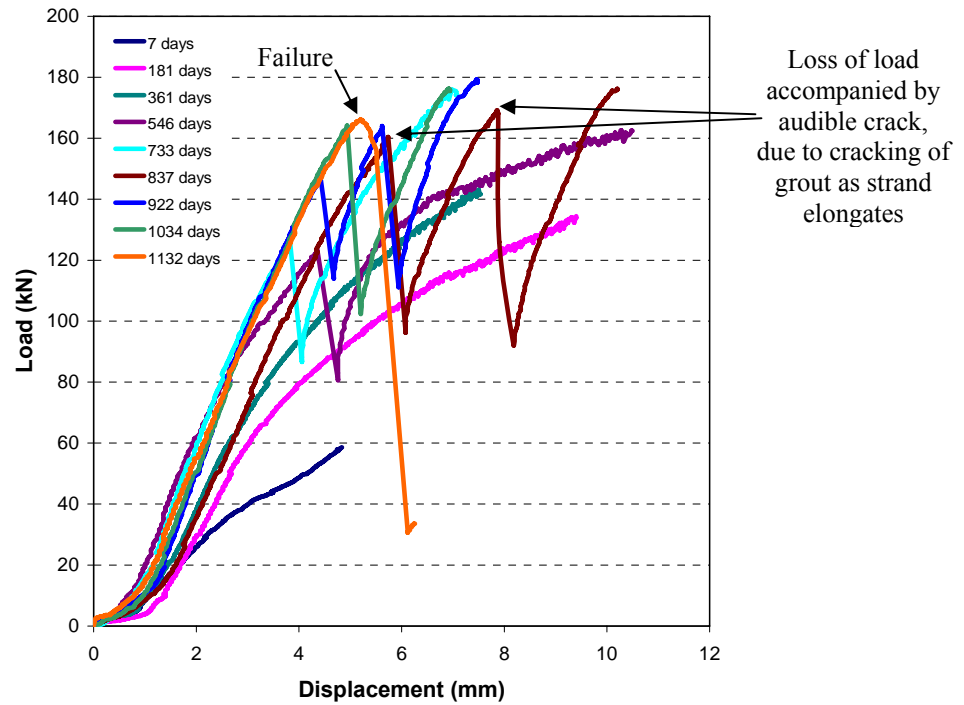


Figure 4.14 Typical load-displacement plot of single plain strand with MCI additive (0.5 m embedment length)

The results for the single bulbed strand, shown in Table 4.6, are similar to the single plain strand with failures contained between 733 and 1132 days. The peak failure load was between 112 kN and 231 kN. Again the few failure loads greater than 175 kN were due to the completion of the experiment. The crack width at failure was generally less than observed for the plain strand due to the bulb restricting strand slippage and elongation. This same process also produces a stiffer element response, which is visible on the load-displacement plots. Typical load-displacement plots for the methocel and MCI additive specimens are displayed in Figures 4.15 and 4.16. Again failure is characterised by a sudden drop in load as the wires break.

Table 4.6 Laboratory results of corrosion and failure loads for single bulbed strand elements.

Chamber	Reinforcement type (single strand)	Additive	Service time till failure (days)	Crack width at failure (mm)	Observed corrosion at failure	Peak failure load (kN)
Argo	bulbed strand	methocel	1132	28.84	high	202.60
Argo	bulbed strand	methocel	1132	24.17	high/severe	184.28
Argo	bulbed strand	MCI	1132	17.06	severe	180.80
Argo	bulbed strand	MCI	1132	27.15	high	203.80
Darlot	bulbed strand	methocel	1058	19.04	severe	181.40
Darlot	bulbed strand	methocel	1058	14.62	high	190.00
Darlot	bulbed strand	MCI	1058	19.12	high	209.60
Darlot	bulbed strand	MCI	922	11.53	severe	168.00
Enterprise	bulbed strand	methocel	837	11.29	severe	169.25
Enterprise	bulbed strand	methocel	733	14.38	severe	147.45
Enterprise	bulbed strand	MCI	733	7.6	severe	168.5
Enterprise	bulbed strand	MCI	837	10.12	high	231.6
Kundana	bulbed strand	methocel	837	47.16	severe	133.35
Kundana	bulbed strand	methocel	837	50.97	severe	172.65
Kundana	bulbed strand	MCI	922	47.6	severe	142.70
Kundana	bulbed strand	MCI	922	57.09	severe	139.45
LNO	bulbed strand	methocel	922	13.65	severe	111.85
LNO	bulbed strand	methocel	837	13.6	severe	167.40
LNO	bulbed strand	MCI	922	15.33	severe	165.10
LNO	bulbed strand	MCI	922	8.82	severe	153.60
Olympic Dam	bulbed strand	methocel	837		severe	173.50
Olympic Dam	bulbed strand	methocel	733	10.67	severe	161.50
Olympic Dam	bulbed strand	MCI	837		severe	166.75
Olympic Dam	bulbed strand	MCI	922	9.95	severe	151.05

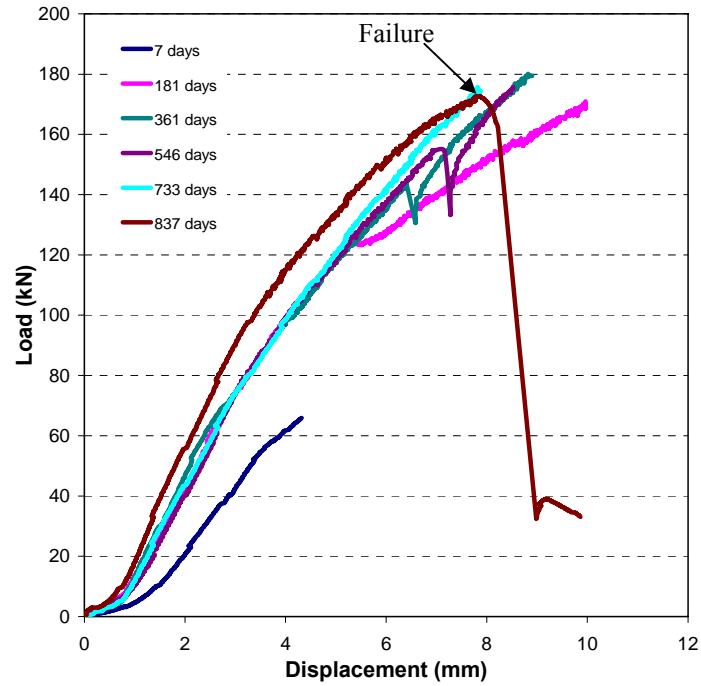


Figure 4.15 Typical load-displacement plot of single bulbed strand with methocel additive (0.5 m embedment length).

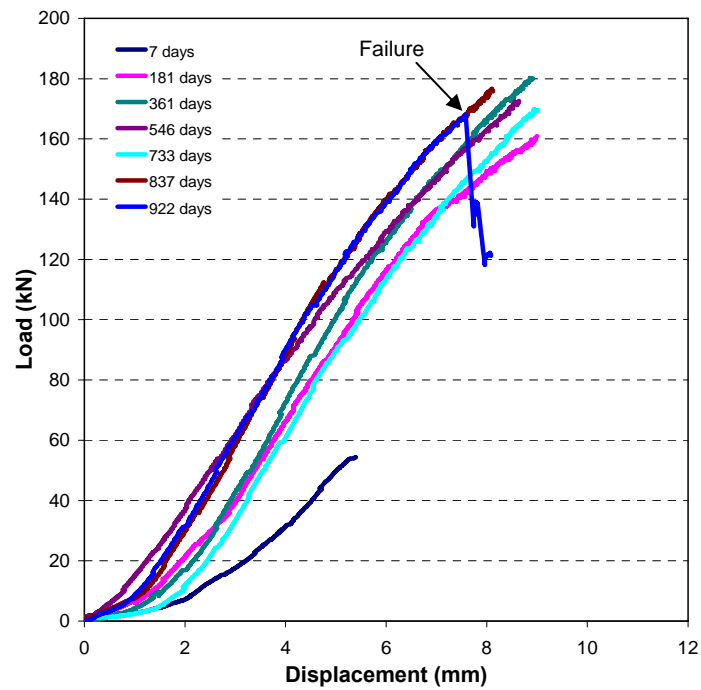


Figure 4.16 Typical load-displacement plot of single bulbed strand with MCI additive (0.5 m embedment length).

The compact strand was only placed in the Argo chamber and failed at the 1132 day test after significant displacement. The results are shown in Table 4.7 and a typical load-displacement plot is displayed in Figure 4.17. Both the tests from the methocel and MCI additive specimens produced similar results. The considerable displacement needed to produce a high enough load for failure is attributed to the geometry of the strand which has less surface area and less capability for grout interlock than plain strand. There is no indication that it differs in corrosion susceptibility compared to the plain strand.

Table 4.7 Laboratory results of corrosion and failure loads for compact strand elements.

Chamber	Reinforcement type	Additive	Service time till failure (days)	Crack width at failure (mm)	Observed corrosion at failure	Peak failure load (kN)
Argo	compact strand	methocel	1132	106.67	severe	164.80
Argo	compact strand	methocel	1132	83.82	severe	156.40
Argo	compact strand	MCI	1132	116.67	severe	154.40
Argo	compact strand	MCI	1132	89.66	severe	146.20

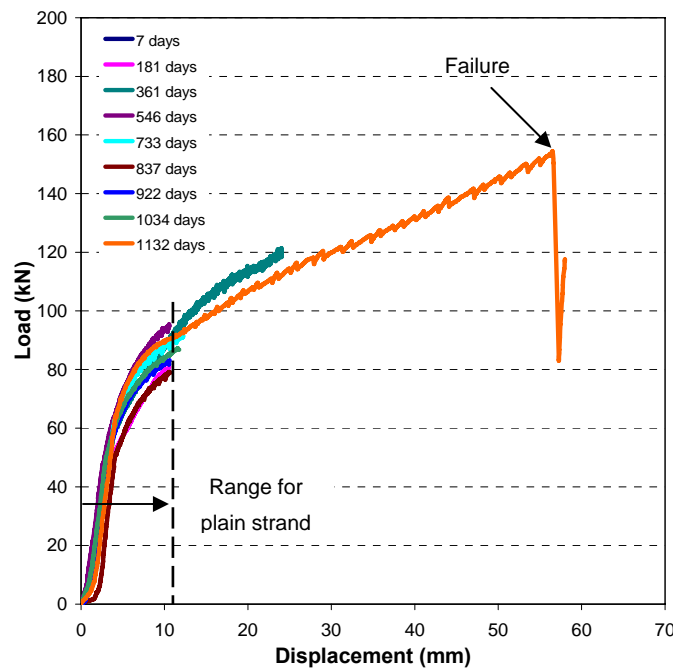


Figure 4.17 Typical load-displacement plot of compact strand with MCI additive (0.5 m embedment length).

The inspection of the samples following the completion of testing indicated that the quality of grouting (see Figure 4.18) was good. There was no evidence for groundwater flow down the king wire; however, the samples were placed in a horizontal position within the chamber which represents the best case scenario. There was only minor migration of corrosion along the bolt axis. As Figure 4.19 displays there is a distinct boundary of corrosion damage where the element is protected by the grout. This was the case for the grout with and without the corrosion inhibitor. These results were for horizontally placed specimens. For vertically placed specimens it is thought that migration of water and subsequently corrosion may occur on the down dip section of the strand.

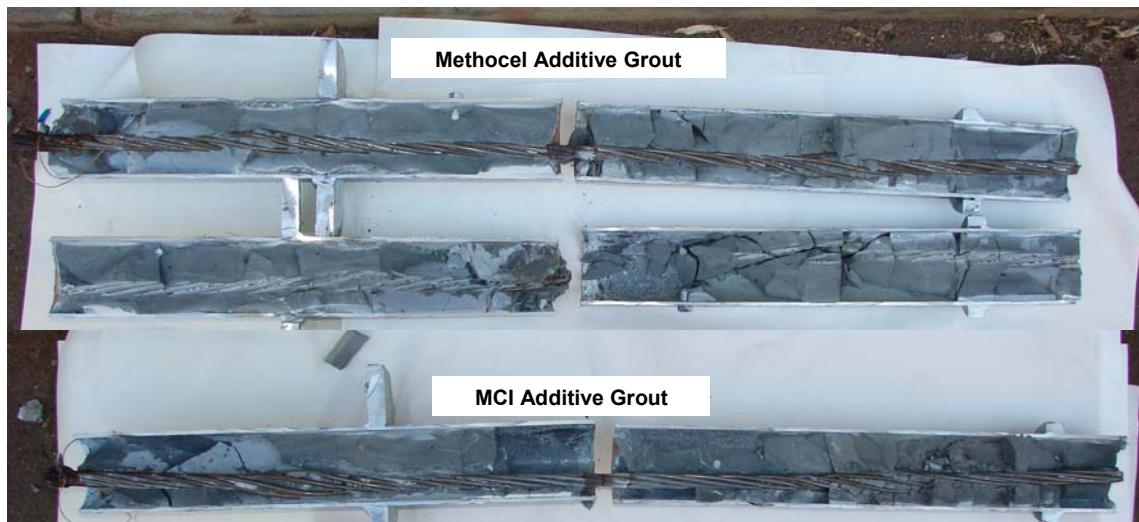


Figure 4.18 Good quality grout was observed for all horizontally placed samples inspected.

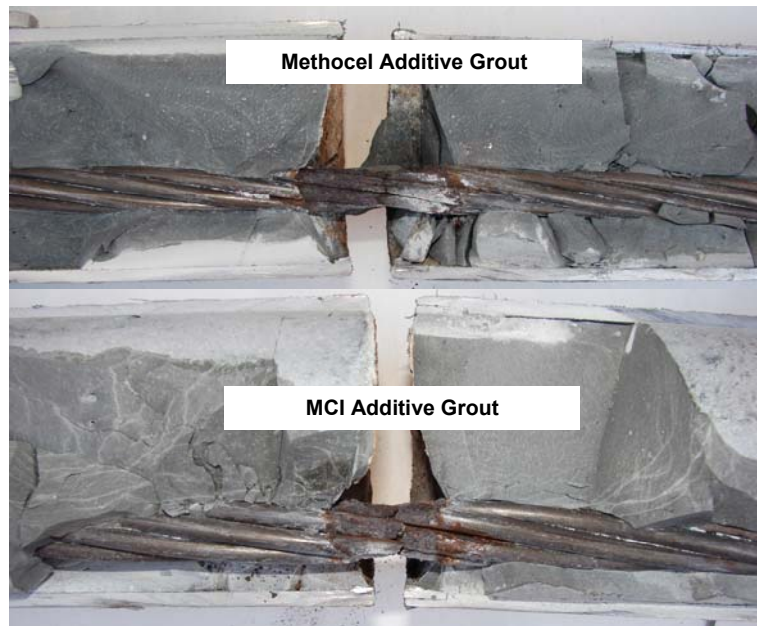


Figure 4.19 Migration of corrosion along the bolt axis was not observed.

No thread bar specimens failed during the course of the experiment; however, three black thread bars with MCI additive had slippage at the element/grout interface at low loads (60-100 kN). The thread bar for each chamber was tested up to the date when the last of the cable bolt strand for that chamber failed. Examination of the thread bar samples indicated that negligible cracking of the grout had occurred due to insufficient elongation of the bar over the 0.5 m embedment length. This greatly restricted the access of groundwater to the steel bar and subsequent corrosion damage was minor, which meant failure at loads less than design was unlikely to occur.

Typical load-displacement plots for the black thread bar with methocel and MCI, galvanised thread bar with methocel and the CT bolt element with methocel are shown in Figures 4.20 to 4.23. They all display increasing stiffness of the system as grout curing creates a higher strength grout, with 180 kN of load being achieved with generally less than 4 mm displacement for the 0.5 m double embedment split-pipe test.

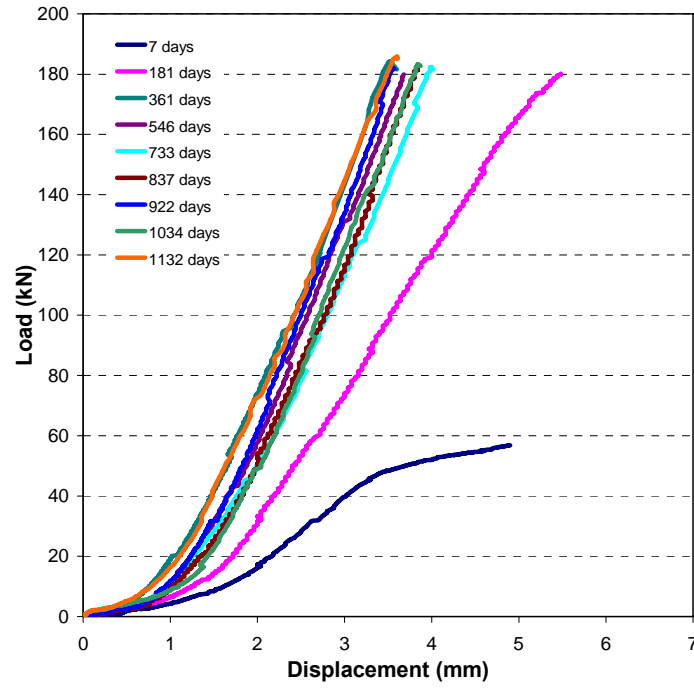


Figure 4.20 Typical load-displacement plot of black thread bar with methocel additive (0.5 m embedment length).

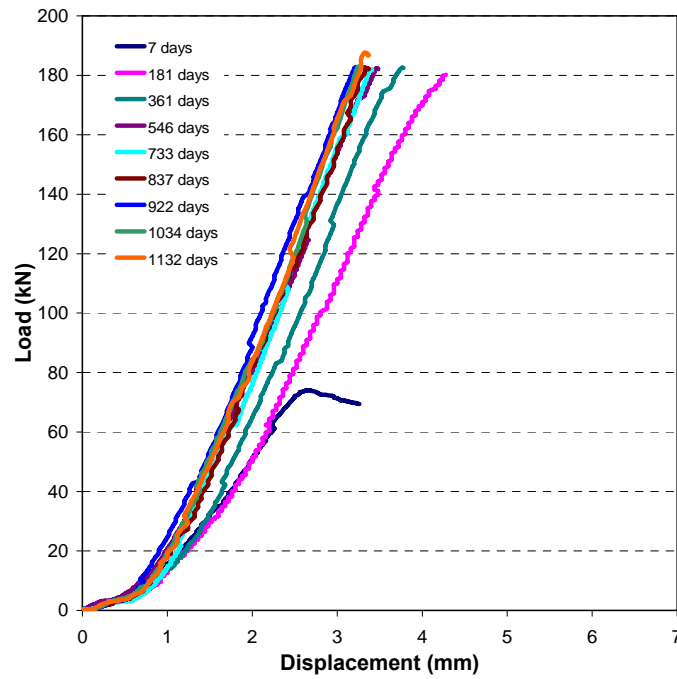


Figure 4.21 Typical load-displacement plot of black thread bar with MCI additive (0.5 m embedment length).

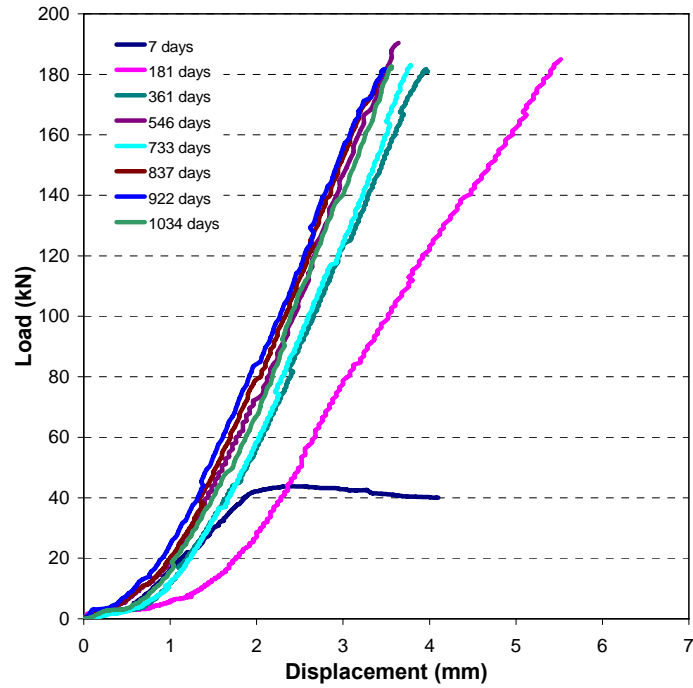


Figure 4.22 Typical load-displacement plot of galvanised thread bar with methocel additive (0.5 m embedment length).

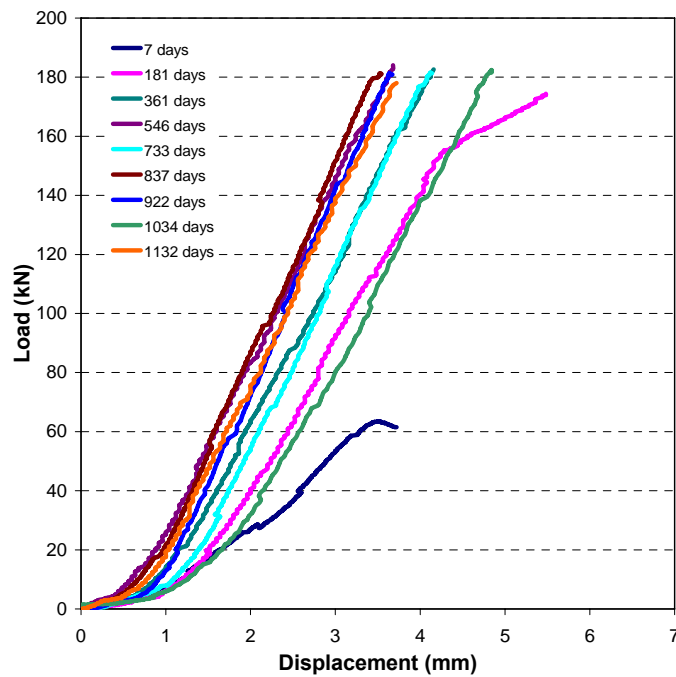


Figure 4.23 Typical load-displacement plot of CT bolt element with methocel additive (0.5 m embedment length).

Despite having only very minor cracking of the grout at the simulated discontinuity the inspection of specimens following the completion of testing showed some corrosion at the fracture. As Figure 4.24 shows the corrosion damage of the black thread bar is minor to moderate with some possible migration of corrosion along the bolt axis having occurred. The zinc coating of the galvanised thread bar is still intact with some zinc corrosion. It is assumed that the groundwater was able to penetrate to the element despite only a very small crack; however, as the amount of groundwater that could access the bolt was small the amount of corrosion damage is in proportion.

There were three black thread bar samples with the MCI additive that had slippage at the element/grout interface at comparably low loads (60-100 kN). A load-displacement plot is shown in Figure 4.25. This occurred in the upper 0.5 m embedment length and only with samples that used the MCI additive. The crack width of these samples was enough to allow direct groundwater contact with the steel. Despite this corrosion damage was moderate. Figure 4.26 displays a cut section of one of the three samples. No evidence of poor grouting that may have led to the low load transfer between the element and the grout is observed. This phenomenon was not experienced with the cable bolts.

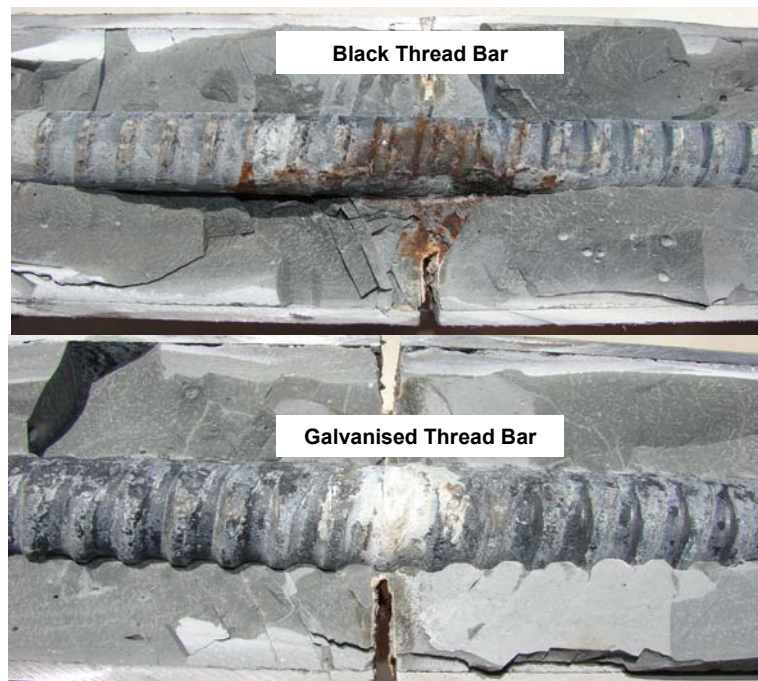


Figure 4.24 Corrosion of the thread bar elements of same age.

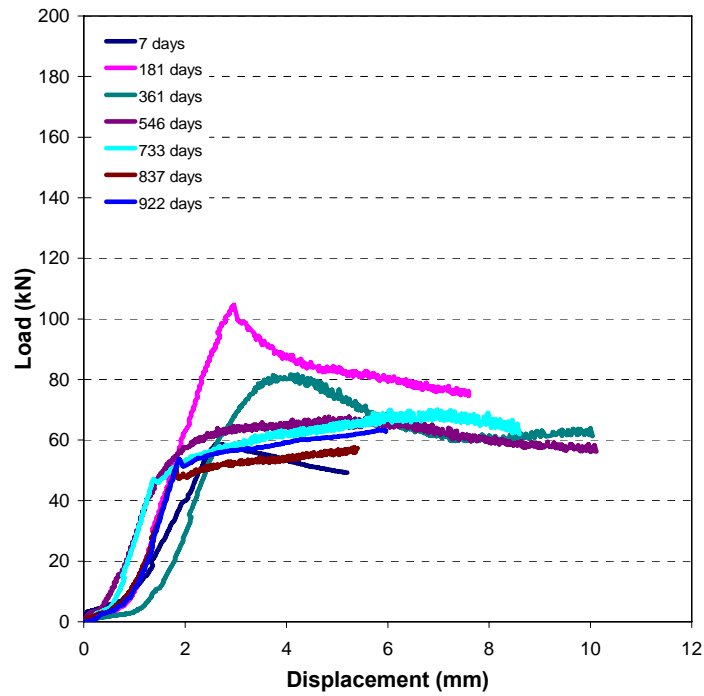


Figure 4.25 Load-displacement plot of black thread bar element with MCI additive that experienced slippage at low loads.



Figure 4.26 A cut section of a black thread bar with MCI additive sample that pulled through the top 0.5 m embedment length.

During the grout installation of the elements, grout samples were collected, placed in the corrosion chambers and tested for their uniaxial compressive strength (UCS) at intervals of 7 days, 181 days, 361 days and 1132 days. The results, displayed in Table 4.8 showed 7 day strength of 51 and 60 kN for methocel and MCI rising to a UCS after 1132 days of 93 and 100 kN respectively. A higher earlier strength for the MCI additive grout is consistent with the stiffness shown by the load displacement plots.

Table 4.8 Uniaxial compressive strength tests of the grout samples.

	Number of samples for each grout type	Methocel Additive Grout UCS (MPa)	MCI Additive Grout UCS (MPa)
7 days	6	51.0	60.0
181 days	6	62.0	66.5
361 days	3	65.0	63.2
1132 days	3	93.1	100.9

4.3.4 Analysis of Results

The focus of the experiment was to establish the effect of corrosion on the cement grouted strand and thread bar. It was noted that prior to the 181 day test significant corrosion had not occurred on the cable strand as demonstrated by Figure 4.27. This was a product of insufficient opening of the crack combined with self healing of the grout preventing water ingress. The research concluded that at least 2 mm crack width is needed before significant corrosion occurs. However, as observed when examining the thread bar some corrosion does occur with crack opening less than 2 mm.

The actual service life due to corrosion of the strand is considered to be from the onset of corrosion to the time of failure. Accordingly, for the cable strand this will be the time of failure minus 181 days. The minimum and maximum service life, that is, the time of the first failure and time of the last failure, for the cable strand in each chamber is shown in Table 4.9 and will be used in the analysis presented in this section.



Figure 4.27 Sufficient opening of crack width to allow for corrosion did not take place until after the 181 day test.

Table 4.9 Actual service life of cable strand in the (accelerated) corrosion chamber environments.

Chamber	Plain Strand		Bulbed Strand	
	Minimum Service Life (days)	Maximum Service Life (days)	Minimum Service Life (days)	Maximum Service Life (days)
Enterprise	552	552	552	656
Leinster Nickel	552	741	656	741
Kundana	656	853	656	741
Olympic Dam	552	951	552	741
Darlot	853	877	741	877
Argo	741	951	951	951

There is a variation between the minimum and maximum service life for each chamber ranging from 104 days in the Enterprise chamber to 399 days in the Olympic Dam chamber. Changes in the groundwater chemistry are not thought to have been a factor; the periodic testing of the water characteristics did not show a change in the conditions that could have explained the discrepancy. Instead it is thought the position of the strand in relation to the water flow direction was the problem. After testing the split pipes they were placed back into the chamber, but they were not always placed in the same position in relation to the downward water flow.

As Figure 4.28 demonstrates those samples that were placed in the same position had corrosion damage over only a few wires as the water flow is concentrated in this region. If a sample is placed in different positions the same amount of corrosion damage is spread over six wires. The strength of the strand in the first scenario is less than scenario two despite the same amount of corrosion damage due to stress concentrations in the thinner strand.

The large majority of corrosion and more importantly the location of failure were located at the simulated discontinuity. As migration of corrosion along the bolt axis or king wire was not observed the simulated discontinuity and the exposed strand are all that is important from a corrosion perspective. Therefore plain and bulbed strand results can be combined as they share exactly the same characteristics at this location. The combined data, including both grout mix types, is presented in Figure 4.29. There is no statistical variation between the plain and bulbed strand information and all further analysis will consider them the same data set. This scenario is for horizontal cables intersecting steeply dipping discontinuities. Vertical cables intersecting shallow dipping structures were not tested during this experiment and are thought to be more vulnerable to corrosion migration along the bolt axis.

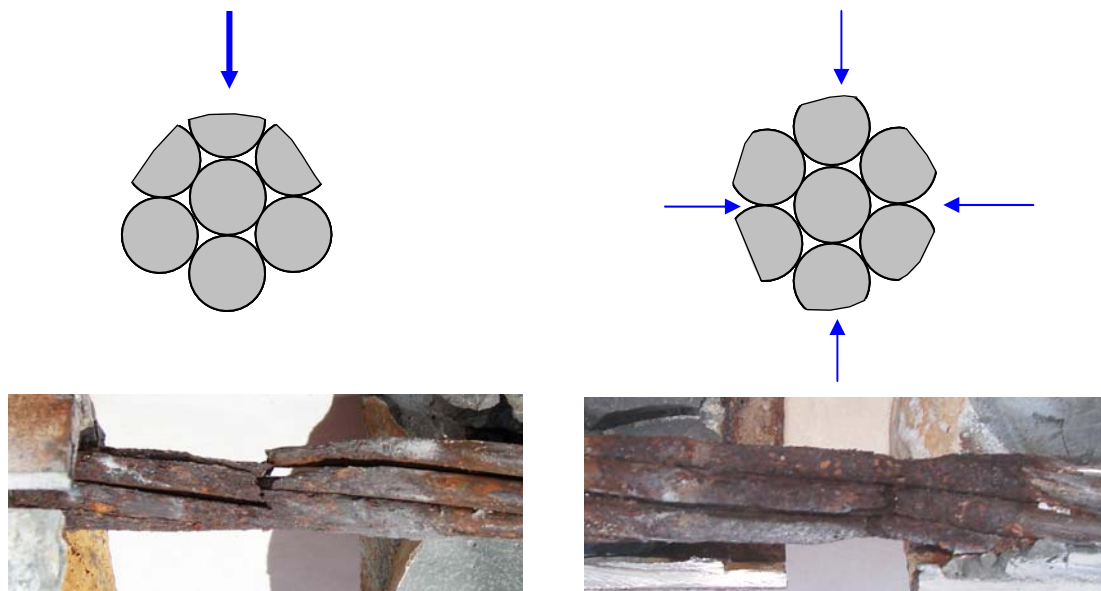


Figure 4.28 Variations in time of failure due to water flow being concentrated in one area (left) or spread around the circumference of strand (right).

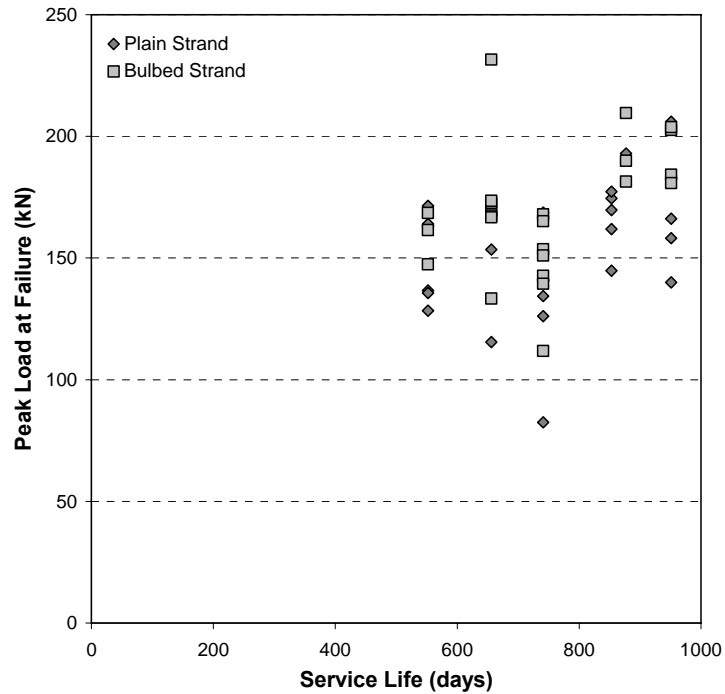


Figure 4.29 Comparison of results between plain and bulbed strand (0.5m embedment length).

The purpose of the MCI additive was to protect the steel from corrosion. Its ability to protect the steel when covered by the grout is inconclusive as migration of corrosion along the bolt axis was not readily observed with both grout mixes. This may not be the case for vertically placed elements where it is more likely for migration of corrosion to occur and the MCI may be of use. For the horizontally placed cable bolt samples the main issue was whether it protected the steel once the grout covering had been removed. As Figure 4.30 displays there was no increased service life for bolts that contained the inhibitor additive over the non-inhibiting additive, with both data sets similar. The thin monomolecular protective layer that forms on the strand once the grout is applied would be quickly washed away once the grout is removed from the strand. Following this no more of the protective layer would be formed.

Additionally it was found that 25% (three samples out of twelve) of the black thread bar tested with the MCI additive had slippage at the element/grout interface during testing. This is compared with none of the black or galvanised thread bar (twenty four samples

in total) experiencing the same problem. While not exhaustive the laboratory evidence from this experiment points towards some problems with the overall strength of the MCI additive grout mix.

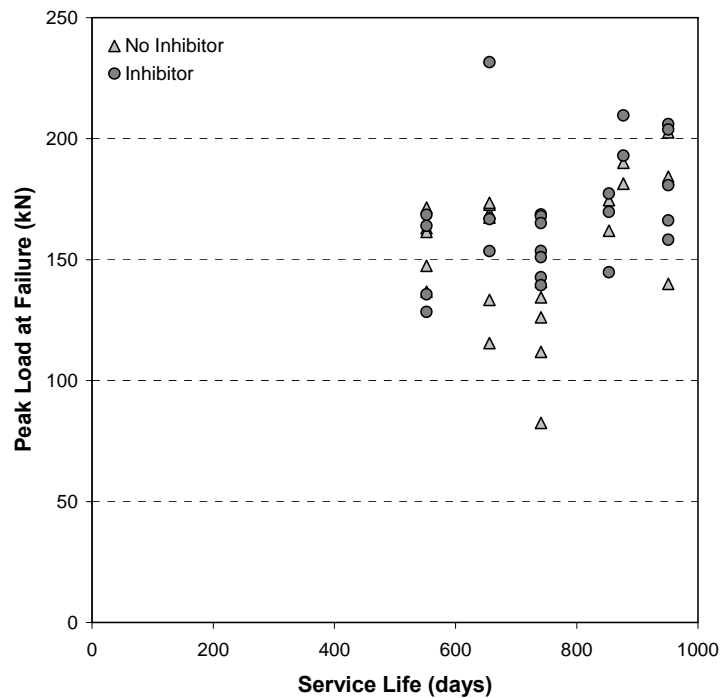


Figure 4.30 Comparison of all strand results between the non-inhibitor and inhibitor grout mixes (0.5m embedment length).

The results have shown that corrosion detrimentally affects the load bearing capacity of the strand; however, the rate at which corrosion damage occurs and hence the timing of failure is a product of the environmental conditions. These conditions, kept as constant as possible and periodically monitored simulate the conditions of the various mines. A summary of all the strand results by corrosion chamber, shown in Figure 4.31, illustrates the tendency for failures to occur during similar time periods for specimens from the same corrosion chamber. This implies that the different environmental conditions in each chamber affect the rate of corrosion differently and therefore failure times.

Comparing the expected service life of the entire cable strand samples in the various chamber environments a trend is observed from the most corrosive to the least corrosive

(see Figure 4.32). The most corrosive environment is from the Enterprise chamber and the least corrosive the Argo chamber. The minimum service life for each chamber is 552 and 741 days respectively. From Figure 4.32 estimates can be made as to the minimum and maximum expected life of cable strand found in similar environments to those described earlier in this chapter in Tables 4.2 and 4.3.

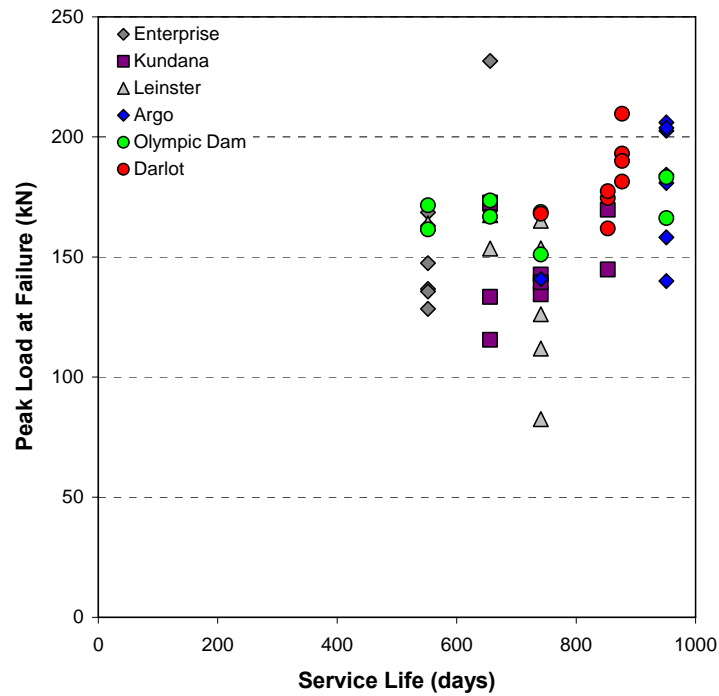


Figure 4.31 Summary of strand results by corrosion chamber (0.5m embedment length).

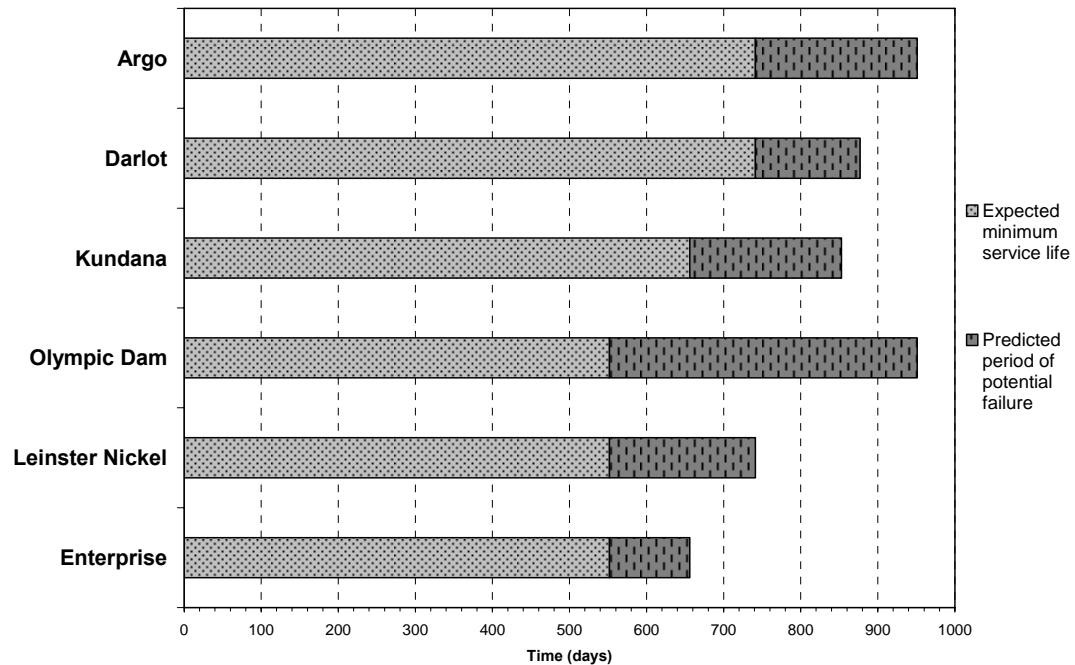


Figure 4.32 The expected service life of cable strand in the corrosion chamber environments.

4.3.5 Discussion of Results

For the results of the cable strand experiment to be applicable to the underground mining environment a number of limitations needs to be placed on the data. Firstly, groundwater needs to be present in the rock mass and there has to be a probability that either cracking of the grout column has occurred or grout encapsulation is poor. As groundwater flows along dilating joints the chances of this are increased. Corrosion will only occur once the groundwater can interact directly with the strand, with significant corrosion only beginning once a greater than 2 mm crack width is achieved. Once significant corrosion damage has commenced the information presented in Figure 4.32 can be used to estimate the expected service life of the cable bolt reinforcement. The expected service life is defined as having a capacity of less than 17.5 tonnes. As this situation essentially leaves the steel itself as the last line of defence the use of a barrier system on the steel, such as a metallic or epoxy coating is required to increase the service life. Inhibitors within the grout are proved to be ineffectual in preventing or slowing the rate of corrosion.

The occurrence and extent of cracking of the grout column for well encapsulated thread bar reinforcement is considerably less than for cable strand. This is due to its lower elongation potential and strong bonding at the element/grout interface. Additionally, the higher volume of steel compared to the surface area make thread bar reinforcement more corrosion resistant than cable strand. Despite only very small cracks occurring in most samples some corrosion of the bar was observed but at a rate that is considerably less than if the crack width is greater than 2 mm. Even when the bar is fully exposed to the environment the corrosion damage is comparably less than for the high tension steel used for the cable strand.

4.4 Testing of the Swellex bolt

Installation of the Swellex bolt requires high pressure water being used for the expansion of the element as shown in Figure 4.33. It is inevitable that some water will remain inside the bolt after inflation. Furthermore, the inflation hole could also be covered by ground support such as shotcrete, trapping water within the bolt. Internal corrosion may be an issue due to this water and has been a matter of investigations. Empirical calculations by Korrosionsinstitutet (2002b) based on the available oxygen in the water and air within the bolt concluded that the total internal uniform corrosion will be less than 15 μm after 50 years. However, no physical trials have been conducted and the empirical calculations do not investigate any possible changes in the water chemistry, primarily the pH. Lowering of the pH would lead to acidic conditions and corrosion may occur regardless of the dissolved oxygen concentration.

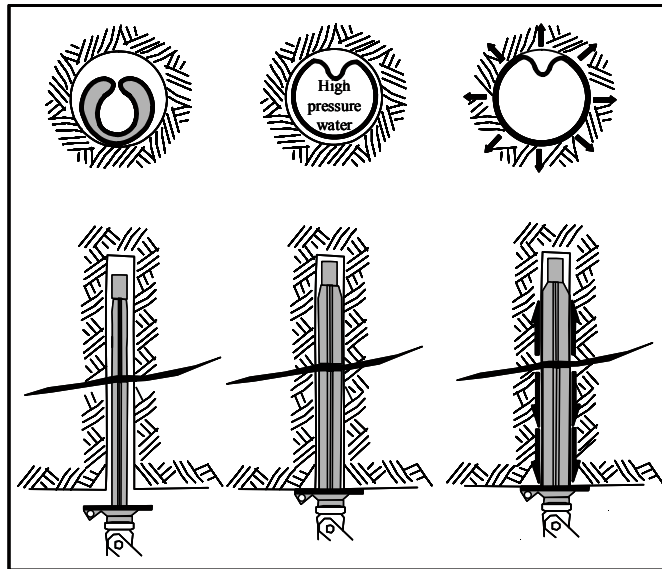


Figure 4.33 Longitudinal and cross sectional view of Swellex bolt during installation (Villaescusa, Thompson & Windsor 2006).

4.4.1 Methodology

A total of eighteen, one metre long standard Swellex bolts, were transported to Leinster Nickel Operations where they were expanded using a pneumatic Swellex pump. The expansion holes of all samples were sealed and the bolts transported to the corrosion chambers in Kalgoorlie. The bolts were placed within the chambers to maintain a constant atmosphere but did not interact with any water other than the residual water inside the bolts. Three different scenarios were examined:

1. Following expansion, the water is allowed to drain freely from the expansion hole.
2. Following bolt inflation the expansion hole is covered preventing any water egress. This is comparable to applying sprayed ground support immediately after reinforcement installation.
3. Following expansion water is allowed to drain freely for a period of two weeks before the expansion hole is covered. This is analogous to the application of sprayed ground support some time after initial reinforcement installation.

The bolts were placed within a corrosion chamber, which maintained a constant temperature and humidity of 30°C and 90% respectively. Three elements for each scenario were examined after 3 and 6 months.

Examination of the elements involved removal of the brushing head and upper brushing head using a drop saw, leaving the 2 mm thick, 0.9 m long element, which was allowed to dry. The residual water for each element was collected and analysed using a portable TPS water analyser for dissolved oxygen, temperature, TDS and pH. An initial visual examination of each bolt was conducted and the level of corrosion recorded. Each bolt was then separated in half using a plasma cutter and cleaned of corrosion products. If uniform or pitting corrosion were present the depth was measured using a pit and crack depth gauge and the rate of corrosion calculated.

4.4.2 Results

Complete drainage of the residual water through the expansion hole did not occur during the first three months despite the elements being placed at favourable angles for water egress. Approximately 10 to 40% of the water drained initially. Complete drainage of the water did not occur until after six months. Analysis of the water chemistry, displayed in Table 4.10, shows a reduction in the dissolved oxygen content of the residual waters. The original measurements of 4.21 mg/l have decreased to between 0.15-0.36 mg/l after three months and 0.0-0.17 mg/l after six months with the lowest readings from the undrained samples. Similar TDS and temperatures are seen with increases in the pH from neutral to moderately basic levels.

Visual assessments of the Swellex bolts revealed only light uniform corrosion with no evidence of pitting for all specimens regardless if undrained or left draining. A typical section of the Swellex bolt is shown in Figure 4.34. No measurements were able to be taken of the uniform corrosion due to its minor occurrence.

Table 4.10 Changes in the chemistry of the residual water.

Time (days)	Scenario	Dissolved Oxygen (mg/l)	TDS (ppm)	pH	Temperature (°C)
Original		4.21	1,202	6.04	23.1
97 days	Free draining	0.36	1,400	9.31	24.5
97 days	Undrained	0.15	1,242	9.09	25.1
97 days	Partially drained	0.31	1,260	8.77	25.1
189 days	Free draining	-	-	-	-
189 days	Undrained	0.00	1126	7.84	27.8
189 days	Partially drained	0.17	1361	8.61	27.1



Figure 4.34 Internal condition of the Swellex bolt after 97 days.

4.4.3 Discussion of Results

Corrosion on the internal surface of Swellex bolts due to the residual water from the installation expansion is limited by the dissolved oxygen. The dissolved oxygen is readily consumed in the corrosion process, thus over time the rate of corrosion will reduce proportionally. After 97 days only minor corrosion has taken place and 96% of dissolved oxygen has been consumed if the element is not allowed to drain with 91% being used if the expansion hole is unobstructed. After 189 days 100% of the oxygen had been consumed in the undrained samples. Some diffusion of oxygen is expected through the expansion hole if it is open replenishing the dissolved oxygen in the residual waters.

As the residual waters show no signs of acidity, it can be concluded that the dissolved oxygen controls the amount of corrosion that will take place inside the bolt. Physical measurements of corrosion were not able to be taken due to the small occurrence;

however, empirical calculations can be computed that provide estimates to the amount of corrosion that has, and will continue to take place. The estimates are shown in Table 4.11 with the full calculations and assumptions in Appendix B.

If the bolt is completely filled with water and the expansion hole blocked, thus not allowing water to egress then the expected depth of uniform corrosion is 0.02 μm . If water is allowed to drain and replaced by approximately 10-40% by air before sealing of the expansion hole the depth of corrosion will be 81 μm . If the expansion is not blocked and the water does not drain due to an unfavourable orientation then oxygen from the atmosphere will diffuse into the residual water and a continuing rate of corrosion of 0.13 $\mu\text{m}/\text{year}$ will take place.

The depths of calculated corrosion damage are extremely low compared to the 2 mm nominal thickness of the Swellex bolt. In the case of the unfavourably angled free draining example following 10 years of installation life there will be an average loss of steel of 1.32 μm (0.00132 mm), which is equivalent to 0.1% mass loss of steel. The empirical calculations are supported by the visual evidence, which observed only very minor surface corrosion. It can be concluded therefore that the presence of residual water in the Swellex bolt from installation expansion produces only minor amounts of corrosion and does not affect the load bearing capacity of the element.

Table 4.11 Calculations of the depth of corrosion for the three scenarios.

Scenario	Calculated depth of uniform corrosion from residual water and air (μm)	Calculated average corrosion rate due to diffusion of oxygen from atmosphere ($\mu\text{m}/\text{year}$)
Unfavourable angle for draining	0.02	0.13
Undrained and sealed	0.02	-
Partially drained and sealed	0.81	-

4.5 Testing of cable bolt barrel and wedge anchors

Corrosion of barrel and wedge anchors and the consequences for the entire cable bolt performance is poorly understood, despite the common use of cable bolts in Australian underground mines since the 1970s. The use of barrel and wedge anchors to restrain plates, straps and mesh in cable bolt reinforcing applications commenced in the early 1980s in Australian mines (Thompson 2004b). Recent developments in cable bolt design have meant an increased reliance on anchors to be serviceable for long periods of time, especially for applications where the strand is decoupled from the cement grout (Garford Ground Support Systems 2002; Ortlepp et al. 2005).

Anchor failures after short time durations and under low loads have been observed in several underground mines in the Eastern Goldfields of Western Australia (e.g. Figure 4.35). Failure is often characterised by the barrel and wedge remaining intact after being found on the floors of drives with no evidence of strand rupture. In an attempt to better understand the behaviour of cable bolt anchors, primarily for yielding cable bolts, various barrel and wedge anchor configurations were placed within the Argo corrosion chamber. Laboratory pull tests were used to determine the force-displacement response and the influence corrosion has on the load bearing capacity of the anchors.

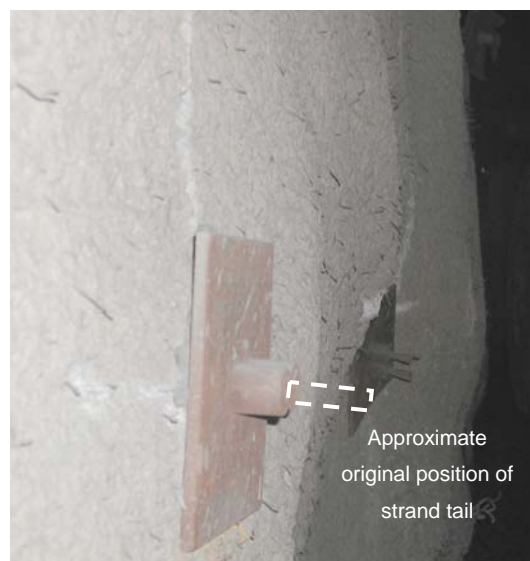


Figure 4.35 Anchors with strand receded compared with original position in a WA mine (Thompson 2004b).

4.5.1 Barrel and wedge anchor systems

Two basic barrel and wedge anchor configurations are presently used in the Australian mining industry. The anchors incorporate either a flat ended barrel to be used with a flat plate or a hemispherical ended barrel to be used with a domed plate. These barrels are used with either two-part or three-part wedges. In the tests described in this investigation, two-part wedges were used with the flat ended barrels and three-part wedges were used with the hemispherical based barrels. These anchors are shown in Figure 4.36. The three-part wedge and hemispherical anchor is currently used with the yielding cable bolt.

Both anchors comprise 45 mm long, 42 mm diameter, hardened steel barrels. The hardened steel wedge has sharp teeth formed at the inner surface that makes contact with the strand. The inner taper angle of the barrel and the outer taper angle of the wedge are approximately equal to 7° (Thompson 2004b).

The three-part wedge is used on strand to ensure a better fit around the circumference of its non-prismatic section, while the two-part wedge was originally designed to be used with single wire. However, if there is compliance with all other design rules for wedges, then a change from the three-part wedge to the two-part wedge is acceptable. Both wedge variants include a rubber 'O' ring or steel circlip that control wedge alignment to prevent 'stepping' of the wedges (Windsor 2004).

The process of anchor installation involves pulling the strand while pushing the wedge along the strand and the barrel against the bearing plate surface. Tension is developed in the decoupled length of strand. After the pulling force is released, the strand pulls the wedge into the conical recess and forces the wedge teeth to bite into, and clamp onto, the strand outer wires (Windsor 2004), (Thompson & Windsor 1995). At the same time, tension in the strand reduces.

There are a range of plates available commercially for use with cable bolts. For this investigation, a 15 mm thick, flat, steel plate with a central hole was selected for the testing, as alignment was not an issue and it would be unlikely to fail during testing.

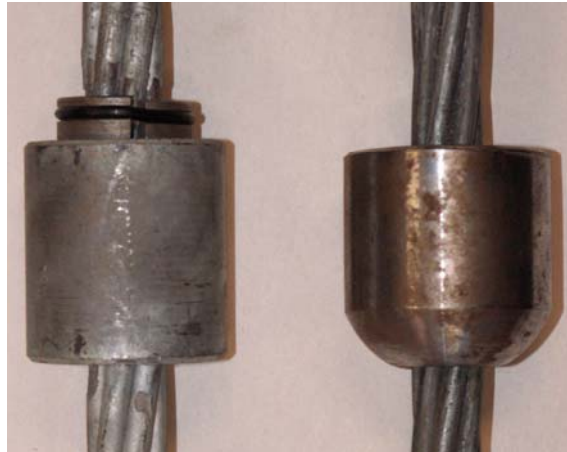


Figure 4.36 Flat end anchor and hemispherical ended anchor.

4.5.2 Methodology

The main component under investigation was the hemispherical barrel and three-part wedge anchor installed in conjunction with compact strand. However, the opportunity was taken to concurrently test a number of other anchors commonly used with either compact or plain strand.

In addition, a number of corrosion protection methods were trialled. The methods included galvanising of the barrel and three simple and commonly found barrier corrosion inhibitors; grease, bitumen and wax. Some tests were conducted with galvanised strand. The major focus of the testing was to determine the effectiveness of the various corrosion protection methods for the hemispherical barrel and three-part wedge used with compact strand. Table 4.12 is a summary of the test combinations.

Table 4.12 Tested combinations of barrel and wedge anchors

Barrel and Wedge Anchor	Strand	Coating
Hemispherical 3-part	compact	none
Hemispherical 3-part	compact	grease
Hemispherical 3-part	compact	bitumen
Hemispherical 3-part	compact	wax
Hemispherical 3-part	plain	none
Hemispherical 3-part	galvanised plain	none
Hemispherical 3-part	plain	galvanised
Flat 2-part	compact	none
Flat 2-part	plain	none

Figure 4.37 is a schematic long-section representation of the testing system used. The split pipe consists of two galvanised, 68 mm internal diameter, 500 mm lengths that have been temporarily welded together at the split to simulate a geological discontinuity (see Page 100). The strand was encapsulated with cement grout within the pipe. In this case, cable bolt “bulbs” were located in the anchoring end. The bulbs were needed to ensure there was no slippage of the strand during testing. A 0.35 water/cement ratio grout was used for encapsulation. One of the 500 mm sections was not grouted and as an extra measure, decoupled to allow for tensioning of the anchor (see Figure 4.37).

Following a curing time of 7 days, the plate and barrel and wedge anchors were installed and the system loaded to 8 tonnes (~80kN) using a hydraulic jack. Note that the actual strand tension is less than this value. Corrosion inhibitors were then applied to the appropriate samples. The majority of samples were placed in the Argo Mine corrosion chamber with the remainder being tested to provide a non-corroded reference test.

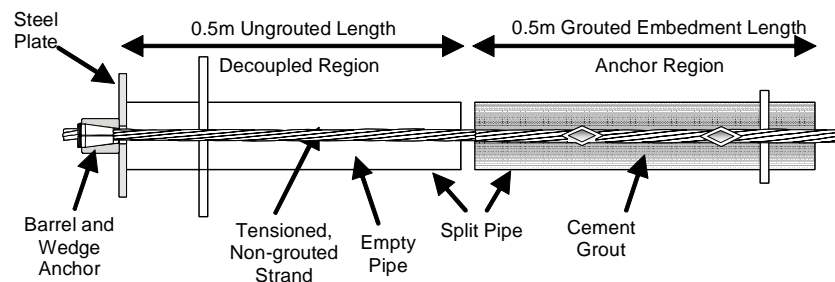


Figure 4.37 Schematic representation of split pipe testing system.

Testing of the various barrel and wedge anchors was conducted immediately after initial anchor installation and at 91 days, 218 days and 297 days of exposure to the conditions in the corrosion chambers. Testing involved subjecting the samples to tension loading provided by the hydraulic Avery machine located in the Rock Mechanics Laboratory at the WA School of Mines (see Figure 4.38). Three tests were conducted for each of the combinations summarised in Table 4.12.



Figure 4.38 Laboratory testing of the barrel and wedge anchors.

The split on the pipe was initially pulled apart. Subsequent load was then applied onto the steel plate and barrel/wedge and wedge/strand interfaces. A maximum force of 200 kN was applied. Load-displacement data were recorded for each test along with the wedge movement. The severity of corrosion on the external anchor was recorded. Following the completion of each test the samples were cut to enable examination of the conditions of the internal sections of the anchors.

4.5.3 Results

The initial testing of the non-corroded specimens was completed with all tests being taken to 200 kN. This provides a basis with which to compare the subsequent tests that had undergone some degree of corrosion. All testing data are summarised in Table 4.13.

Table 4.13 Summary of test results

Barrel and Wedge Anchor Combination			Initial Failure Age (months)	Failure Mode	Failure Load (kN)	
Anchor	Strand	Coating			Min	Max
Hemispherical 3-part	compact	none	7	Wedge/strand slip	22	111
Hemispherical 3-part	compact	grease	10	Wedge/strand slip	27	27
Hemispherical 3-part	compact	bitumen	No failure			
Hemispherical 3-part	compact	wax	No failure			
Hemispherical 3-part	plain	none	No failure			
Hemispherical 3-part	galvanised	none	No failure			
Hemispherical 3-part	plain	galvanised	3	Wedge/strand slip	21	47
Flat 2-part	compact	none	No failure			
Flat 2-part	plain	none	No failure			

The hemispherical barrel and three-part wedge with compact strand shown in Figure 4.39 experienced failure in two of the three samples after 218 days and one sample after 297 days. Failure occurred at the wedge/strand interface with the strand pulling through the anchor and was associated with small wedge movement relative to the barrel. Significantly, failure took place at loads ranging from 22 kN to 111 kN that are significantly lower than the strand force capacity of 250kN. Figure 4.40 shows the load-displacement responses for typical failed and non-failed anchors.



Figure 4.39 Hemispherical barrel and three-part wedge anchor with compact strand before and after placement in corrosion chambers.

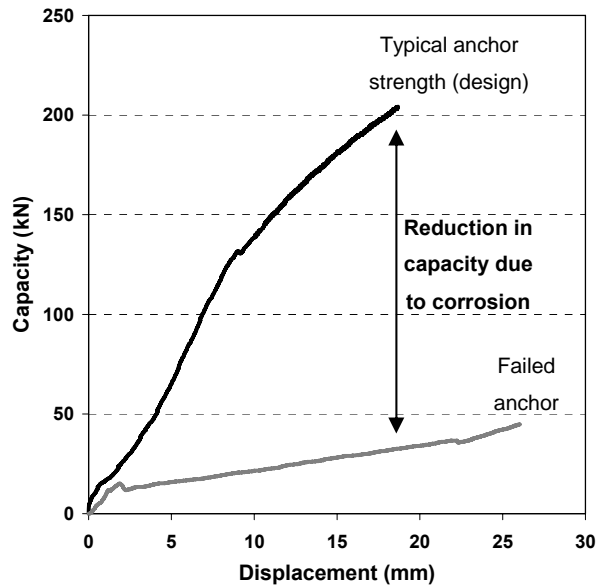


Figure 4.40 Typical load-displacement plot for hemispherical barrel and three part wedge anchor, after 10 months in corrosion chamber.

The internal section of the failed barrel and wedge anchor shown in Figure 4.41 displayed a build up of corrosion products on the internal surface of the barrel together with shearing of the wedge teeth. Anchors that perform properly displayed notably less corrosion accumulation (e.g. Figure 4.42).

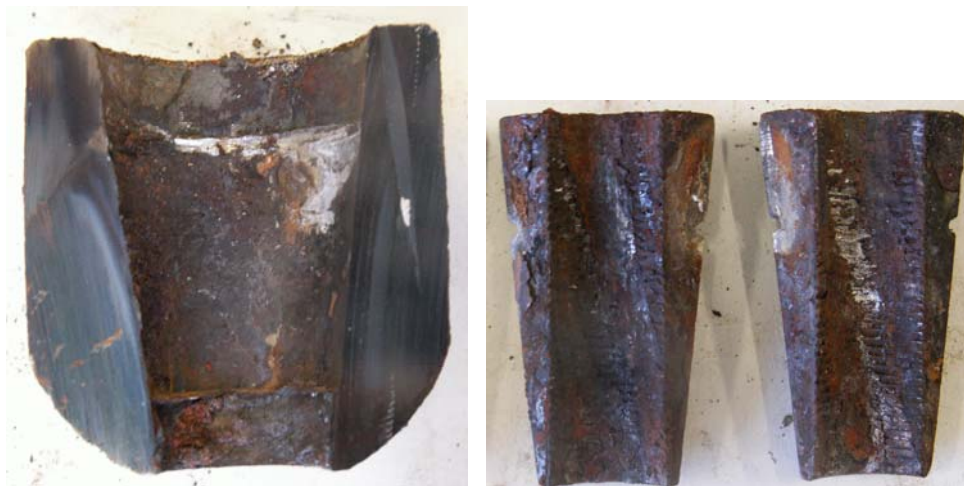


Figure 4.41 Internal condition of failed barrel and three part wedge anchor. Note the corrosion on the barrel surface and the shearing of the wedge teeth.



Figure 4.42 Internal condition of barrel and three-part wedge anchor that did not fail after 297 days in corrosion chamber.

Anchors that were coated with grease, wax or bitumen had significantly fewer instances of failure. Of the three inhibitors used only the grease coated anchor failed once after 297 days. Examination of the sample following testing indicated much higher levels of corrosion on the internal barrel surface than the non-failed counterparts.

The bitumen coating (see Figure 4.43) performed best at preventing corrosion occurring over the entire anchor. Specifically, corrosion on the critical internal barrel/external wedge surface was inhibited. The viscous nature of the coating does not appear to detrimentally influence the load bearing capacity of the anchor.

The absence of corrosion products on the non-failed samples strongly suggests that corrosion is responsible for failure. Corrosion products on the internal surface of the barrel increase the frictional resistance at the barrel/wedge interface and this prevents sliding of the wedge relative to the barrel. This in turn prevents the wedge from gripping the strand. That is, the increase in normal force that results from wedge slip does not occur and this means that load must be transferred by the shear resistance of the wedge teeth. This area loaded in shear is very small and the result is shear failure of the teeth. This allows the strand to slip at loads significantly less than the design capacity associated with the tensile strength of the strand.



Figure 4.43 Hemispherical barrel and three-part wedge with compact strand, bitumen coating, before and after placement in corrosion chamber.

The hemispherical barrel and three-part wedge with black or galvanised plain strand showed no failure of the barrel and wedge anchors with either strand type. Examination of the anchor indicated minimal amounts of internal corrosion for both combinations. The low levels of observed corrosion with the plain strand combinations compared with the compact strand implies that the modified geometry of the compact strand does not allow for a “tight” fit between the wedge and barrel and wedge and strand. This permits higher levels of corrosion to occur on the internal surfaces of the barrel.

The galvanised hemispherical barrel and three-part wedge with plain strand anchor consists of the barrel galvanised to a thickness of 75 μm with the three-part wedge remaining uncoated. The galvanised anchor performed extremely poorly in the testing, with failure of one sample in the 91 day test and failure of all samples in the 218 and 297 day tests at very low loads (less than 50 kN). Figure 4.44 shows a load-displacement response for typical failed and non-failed anchor. Inspection of the anchors revealed that steel corrosion of the anchor was low, but oxidising of the galvanising was noted by the presence of zinc carbonate on the barrel surface (see Figure 4.45).

The effectiveness of zinc galvanising to protect steel from corrosion is well known and documented. However, zinc metal is considerably softer and provides a rougher surface

than the steel it coats. This has the effect of increasing the friction at the barrel/wedge interface due to the steel wedge digging into the galvanising. This prevents wedge movement and subsequently leads to shearing of the wedge teeth and strand slippage. It appears minor levels of zinc corrosion may further increase the problem.

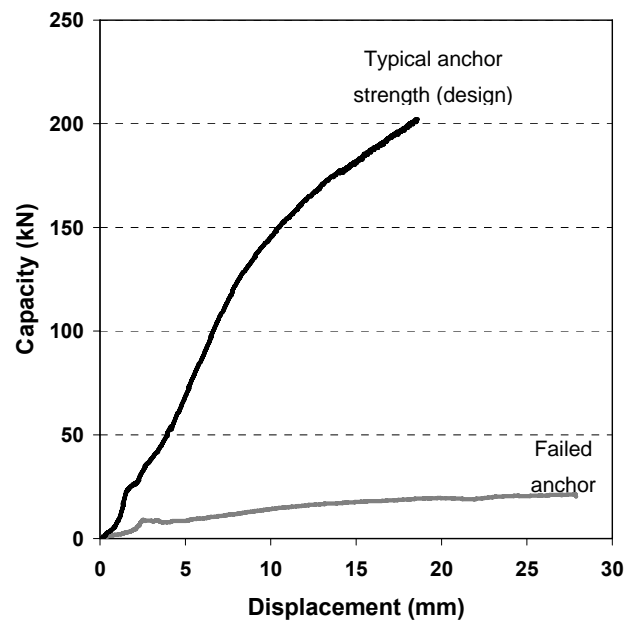


Figure 4.44 Typical load displacement plot for galvanised hemispherical barrel and three-part wedge after 91 days in corrosion chamber.

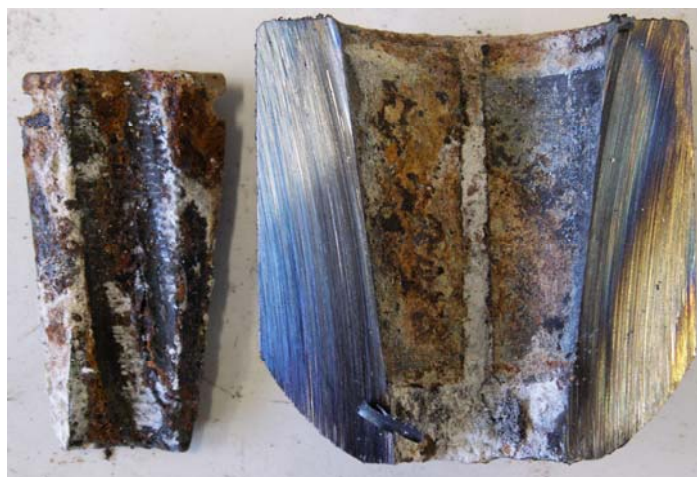


Figure 4.45 Internal condition of galvanised barrel and wedge after testing.

There was no failure of the anchors that used two-part wedges for either the compact or plain strand. This is contrary to previous findings elsewhere. Reported test results by (Thompson 2004b) showed that anchors with two-part wedges failed by slipping relative to the strand after 6 months of exposure to mildly corrosive conditions

Typical load-displacement responses from this investigation after 297 days for the two-part wedges are shown in Figure 4.46. The anchors with two-part wedges produced stiffer responses and less wedge movement than the anchors with three-part wedges. This can be attributed to the conditions that resulted immediately after anchor installation due to the anchor configuration and the equipment used. The influence of the strand on the susceptibility of the anchor to corrosion was again observed with the plain strand combinations displaying less corrosion on the internal surface of the barrel than the compact strand combinations.

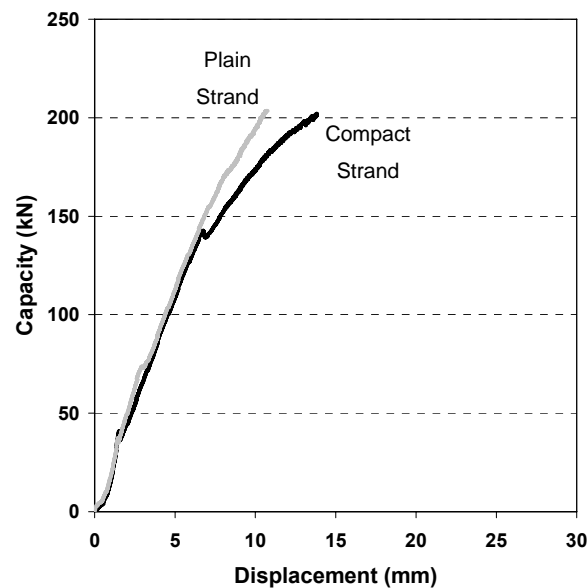


Figure 4.46 Typical load-displacement responses for barrels and two part wedge following 297 days of exposure in a corrosion chamber.

4.5.4 Discussion of results

The long-term performance of a cable bolt anchor in a corrosive environment is controlled by the frictional resistance between the internal surface of the barrel and the outside of the wedge. Corrosion and galvanising of this surface increase the frictional resistance restricting wedge slip and minimising gripping of the strand, which leads ultimately to premature anchor failure, often at low loads.

Another factor that influences the ability of the wedge to slide relative to the barrel is the inherent roughness of the contacting surfaces. The smoothness of the inner surface of the barrel and the outer surface of the wedge may vary between batches from the different suppliers. In some instances, the roughness from machining is clearly visible and easily felt by running one's finger over the surfaces.

Figure 15 summarises the measured wedge movements for each of the 297 day tests. Anchor failure can clearly be seen to correlate with minimal wedge movement. The movement is initially associated with the teeth embedding in the outer wires of the strand and then, secondly, mostly the barrel expanding radially outwards (Thompson 2004b). The lowest amount of wedge slip without anchor failure occurred with the two-part wedges. This is consistent with previous comments made in regard to installation and their stiffer load-displacement responses.

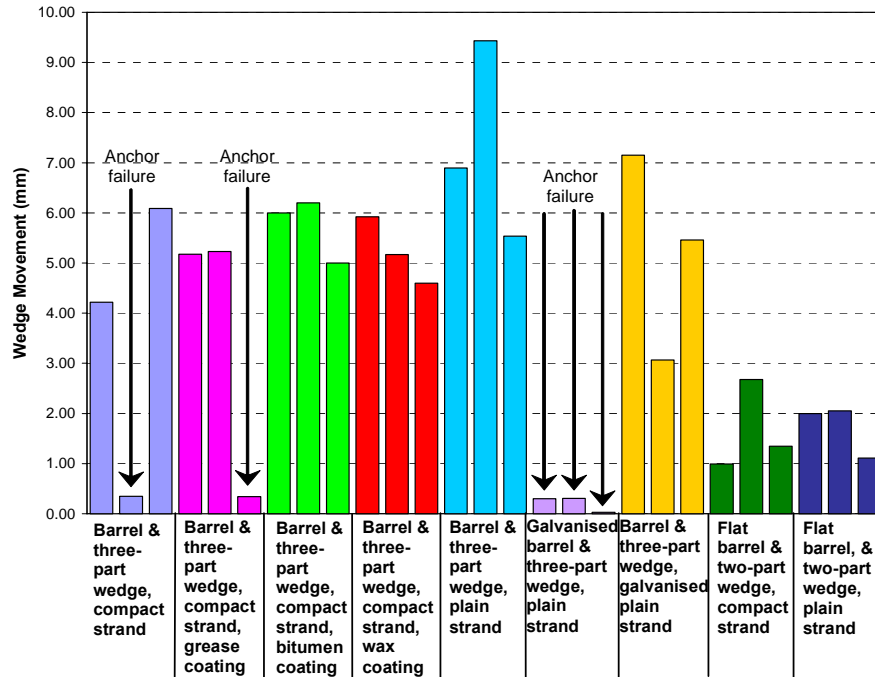


Figure 4.47 Total wedge movement of anchors after 297 days in the corrosion chamber.

The experimental results presented and also in Thompson (2004b) confirm that failure of anchors by sliding relative to the strand can occur when slip at the barrel/wedge interface is inhibited and the wedge teeth shear off. This mechanism is also reported by DSI (2006a). An essential feature of a barrel and wedge anchor is that sliding at the barrel/wedge interface is maintained for the life of the anchor so that the wedge teeth will embed to their full depth into the strand outer wires in response to rock mass movements and the radial force will increase to ensure that the resistance to sliding at the wedge/strand interface remains greater than the strand tension.

The current anchor assembly employed with a commercially available yielding cable bolt has a predicted anchor life of less than 218 days in a hypersaline groundwater affected environment. The service life can be extended to greater than 297 days by the application of simple barrier corrosion inhibitors such as bitumen. The anchors with two-part wedges demonstrate a greater resistance to corrosion than those with three-part wedges. In addition, they also showed a stiffer response when load is applied. The two-part wedges have fewer pathways for the groundwater to infiltrate the internal section of

the barrel, as well as having a closer fit at the barrel/wedge interface. Those anchors tested in combination with plain strand display less corrosion on the internal section of the anchor than the anchors used with compact strand. The modified geometry of the compact strand appears to allow for greater corrosion to occur. This was observed with both the three and two part wedges.

Experience from this testing has also shown that the external condition of the barrel does not give a conclusive indication to the amount of internal corrosion of the anchor. Therefore, a visual assessment system cannot be used to determine the extent in which corrosion is influencing the capacity of an anchor.

Finally, and most importantly, it is critical in service that the ability of the wedge to slide relative to the barrel is maintained so that more tension can develop in the reinforcement to resist rock movement. Galvanising of the anchor is not recommended due to the soft zinc galvanising coating increasing the sliding resistance at the barrel/wedge interface. This prevents the barrel and wedge anchor from being effective. It is therefore strongly recommended that a high quality and long-lived lubricant such as grease is placed at the barrel/wedge interface during installation to provide a low friction interface that also assists in corrosion protection.

4.6 Discussion and Conclusions

The development of the corrosion chambers provided a resource in which long-term, experimentally controlled testing could be conducted on various reinforcement and support in an environment that closely simulates the underground hard rock environment. By conducting the experiments over similar time frames to what occurs in working mines the data collected is directly relevant and no need for interpretation was necessary.

For cement grouted elements, cracking of the grout column provides a pathway for groundwater to reach the exposed steel. Once this occurs corrosion develops and can lead to failure of the element below design requirements. This mechanism is thought to be the most likely cause of failure of cable strand due to corrosion. A minimum and maximum service life has been established for the strand for the six simulated underground environments. Service life ranges from 552 to 951 days depending on the corrosiveness of the environment. Service life is the time taken from the initial origination of a crack greater than 2 mm width in the grout column to failure of the strand at less than 17.5 tonnes. Thread bar was found to be less susceptible to this mechanism of failure due to the experiment's inability to form sufficient cracks in the grout column. Grout additives that inhibit corrosion were found not to work once a crack had been formed. To expand the service life of the elements metallic or epoxy coatings are needed.

Water that remains in the internal section of the Swellex box from expansion during installation does not pose a problem in terms of corrosion. The oxygen that is available inside the bolt is quickly consumed and only minor corrosion damage occurs. Following this the groundwater is largely inert and either no further corrosion occurs.

Barrel and wedge anchors are particularly vulnerable to corrosion at the barrel/wedge interface. Small amounts of corrosion products in this area drastically reduce the ability of the anchor to perform and failure occurs by slippage of the strand through the anchor at loads much less than design and as early as 218 days following installation. A number of basic barrier corrosion protection methods can increase the expected life with a bitumen coating performing best. Galvanising of the anchor is not recommended.

The results presented in this Chapter have been achieved through using a simulated underground environment. To confirm and investigate further the corrosion processes and mechanisms affecting reinforcement in underground mines examination of the reinforcement elements *in-situ* is required. This can only be achieved through overcoring of rock reinforcement.

CHAPTER 5 OVERCORING OF ROCK REINFORCEMENT IN UNDERGROUND MINES

5.1 Introduction

To attain a quality understanding of the corrosion processes and mechanisms affecting rock reinforcement in the underground hard rock environment it is necessary to examine elements *in-situ*. This can only be adequately achieved through recovery of the installed reinforcement and surrounding rock mass by overcoring. This provides an excellent opportunity to not only fully examine the reinforcement but to also conduct laboratory testing to ascertain its load transfer properties and any changes that may have occurred due to corrosion damage.

Overcoring of selected reinforcement was conducted at a number of Australian mine sites. The main focus was on friction rock stabiliser elements, the most commonly used reinforcement in Australia. Also investigated were hollow groutable bolts, cable bolts, cement grouted elements and resin grouted reinforcement. Sections 5.2 and 5.3 in this chapter detail the development of the overcoring rig and the laboratory testing procedures developed to investigate the recovered reinforcement. Laboratory testing included pull and push tests to determine load-displacement responses and measurements of the type and rate of corrosion. Overcoring was completed at the Kundana, Argo, Leviathan, Leinster and Olympic Dam mine sites with the location and environmental conditions where overcoring took place, the observations taken of the overcored elements, and the results from the laboratory testing is described in Sections 5.4 to 5.7.

5.2 Development of the WASM Overcoring Rig

Development of a purpose built drill rig capable of overcoring reinforcement elements within a production mining environment was initiated due to an overwhelming need to examine the bolts *in-situ*. The conventional pull testing programs for quality control (Brown 1981) can only be applied to point anchored reinforcement schemes. In many cases involving older reinforcement the option of pull testing is unavailable and the only method to determine the bolt quality is overcoring.

An initial prototype was designed and developed by Ernesto Villaescusa and Lance Fraser at the W.A. School of Mines. A track mounted drill rig was purchased from a local mining company and its hydraulics and electrics were completely rebuilt. A stationary drill and frame were fitted to the drilling boom and trials were conducted on concrete blocks as shown in Figure 5.1.



Figure 5.1 Overcoring trials of the prototype overcoring rig.

Following the successful development of the prototype AVKO Drilling were approached to develop the prototype to industry standards. The current overcoring drill rig, shown in Figure 5.2, is operated by a diesel track mounted excavator. A 140 mm diameter, triple tube diamond drill bit is mounted onto the excavator boom, which has two hydraulic stabilisers fitted to minimise unwanted movement. The triple tube drill casing ensures that the cored sample does not rotate with the drilling bit and remains stationary. Therefore there is minimal core disturbance. The operating rig requires 1000V of electricity to operate the drill with air and water services.

The WASM drill rig is a versatile overcoring system capable of drilling at any orientation (360 degrees) and lengths up to 3.0 m. Overcoring of *in-situ* bolts can be undertaken in the walls and backs to a collar height of 7.0m. The operation of the drill rig is undertaken by 360 Drilling on behalf of WASM. Safe operating procedures (JSA) have been developed by the 360 Drilling company and drilling operations are very quiet, with average set-up and penetration rates that, in competent rock masses, allow one 2.4 m bolt to be recovered after each 12 hours of drilling.



Figure 5.2 Overcoring drill rig.

Adequate recovery of the overcored elements is dependent on the straightness of the initial borehole, alignment of the barrel to the centre of the element and the ability to minimise movement of the barrel. Extensive time is taken to ensure the latter two factors are controlled; however, the straightness of the bolt is reliant on installation. Elements to be overcored were assessed for their potential recovery; this is relatively simple for ungrouted friction rock stabilisers, but particularly difficult for grouted bolts.

Careful drilling and suitable penetration rates are chosen, so that the recovered 140mm diameter core undergoes minimal disturbance even in very poor rock masses that have been reinforced using friction stabilizers (see Figure 5.3). This not only allows the recovery of the element, but also provides a clear view of the surrounding rock mass and a better understanding of the rock bolt system/rock mass interaction. Bolt overcoring provides a range of information including location and frequency of geological discontinuities, overall rock mass conditions, bolt encapsulation, likely load transfer along the bolt axis and corrosion effects, if any.



Figure 5.3 Full recovery from overcoring friction rock stabiliser collars in very poor rock mass.

5.3 Laboratory Testing of Overcored Samples

As part of the research project, a laboratory procedure was developed to compare the performance of the recovered overcored bolts in terms of encapsulation quality and relative load transfer. Following overcoring the samples were transported to WASM where each overcore sample is geologically mapped to ascertain fracture frequency and the presence of significant structures. The core was then marked and appropriate sections were cut from the sample to test the load-displacement characteristics.

Push tests (Aziz 2004) and pull tests are used to determine encapsulation quality and relative load transfer along a bolt axis. In general, a load-displacement curve provides an indication of stiffness, peak and residual forces as well as the displacement capacity. Push tests are expected to provide a different response to the pull tests. During push testing, the steel bar is compressed into the sample, while in pull testing the bar is tested in tension. An advantage of push testing is that it allows several tests to be carried out along a single bolt axis. A disadvantage is that a push test is likely to over-estimate the stiffness and peak/residual loads. However, provided the push testing is carried out for similar embedment lengths, the results can be used as a relative measure of load transfer along the bolt axis.

The typical embedment length used for push/pull tests is 300 mm. The total sample length required for a push test is 400 mm (see Figure 5.4); thus, for a 2.4 m long bolt it is possible to select up to 5 samples for push testing. This allows the variability of encapsulation and relative load transfer along the bolt axis to be well established. On the other hand, a typical pull test requires a 0.7 metre long sample; a typical sample will have a 300 mm rock-element portion and a 400 mm length of steel exposed (see Figure 5.4). Consequently, for a 2.4 m long bolt only two samples can be selected for testing. This may create a problem if the load transfer variability along the bolt axis needs to be determined.



Push test



Pull test

Figure 5.4 Samples being prepared for testing.

As described earlier, the relative load carrying capacity of the overcored reinforcement elements was mostly determined using short embedment lengths (300 mm) containing the elements and the surrounding rock mass. Some of the rock was removed leaving a section of the element partly exposed. The remaining rock/element section was then confined in a metal jacket to simulate the radial confinement provided by the rock mass *in situ*. The exposed section of the element was then pushed or pulled with a plate used to restrict the movement of the rock (see Figure 5.5). This was done in the rock mechanics laboratory at the WA School of Mines using the hydraulic Avery machine. The load required to push (or pull) the elements through the rock and its displacement were digitally recorded and the elements were then inspected and photographed following testing (see Figure 5.6).



Push test



Pull test

Figure 5.5 Testing of overcored samples to determine relative load transfer.



Figure 5.6 Two reinforcement elements following push (left) and pull (right) testing from 300 mm embedment length.

Following testing the rock was removed from around the samples and the steel elements were examined for corrosion damage. If corrosion was extensive the elements were cleaned of corrosion products using an acidic solution to ASTM Standard G1-90 (1999). This hydrochloric acid solution uses chemical inhibitors to ensure that only the iron oxides are dissolved, leaving non-corroded steel. The removal of the corrosion products it enables a clearer view of the extent of corrosion damage. Measurements of pitting depth and reduction in steel thickness were made using callipers and a pit and crack depth gauge (see Figure 5.7). The elements were analysed in 0.5 m sections along the bolt axis.



Figure 5.7 Measurement of maximum pit depth along bolt axis.

For friction rock stabilisers the maximum tensile strength of the element was tested by welding two short lengths of solid bar on either end of the friction bolt, which are held tight by jaws in the Avery machine and pulled till failure (see Figure 5.8). The load and displacement are recorded for each test. A thorough examination around the locality of the failure is undertaken to assess if corrosion influenced the failure.



Figure 5.8 Friction bolt is prepared for tensile strength testing (left), and tensile testing of friction bolt (right).

5.4 Overcoring at Kundana Mine

Fieldwork conducted at the Kundana Mine and described in Section 3.3.6 identified similar environmental conditions along the Strzelecki Decline. The decline was initially developed in 1995 and has been continuously extended at a constant rate in the following six years. Rock reinforcement consists of 47 mm diameter, galvanised friction rock stabilisers (FRS) installed along its entire length. This provided a unique opportunity to overcore selected FRS from a similar environment with installation ages that varied from four to ten years. This approach gives the ability to determine what environmental factors predominantly affect the rate of corrosion, how the corrosion progresses over time and the impact of corrosion on the load bearing capacity of the bolt.

Overcoring was conducted at or near the decline at four locations shown in Figure 5.9. These were the 6112 level, the 6039 level, the 5926 level and the 5824 level. The environmental conditions at each site were similar to a hypersaline, near neutral groundwater with a low flow rate. Inspection of the visible ground support at each location with a borehole camera showed significant corrosion at 6112, 6339 and 5926 level and lower amounts at the 5824. Two bolts from each location were recovered.

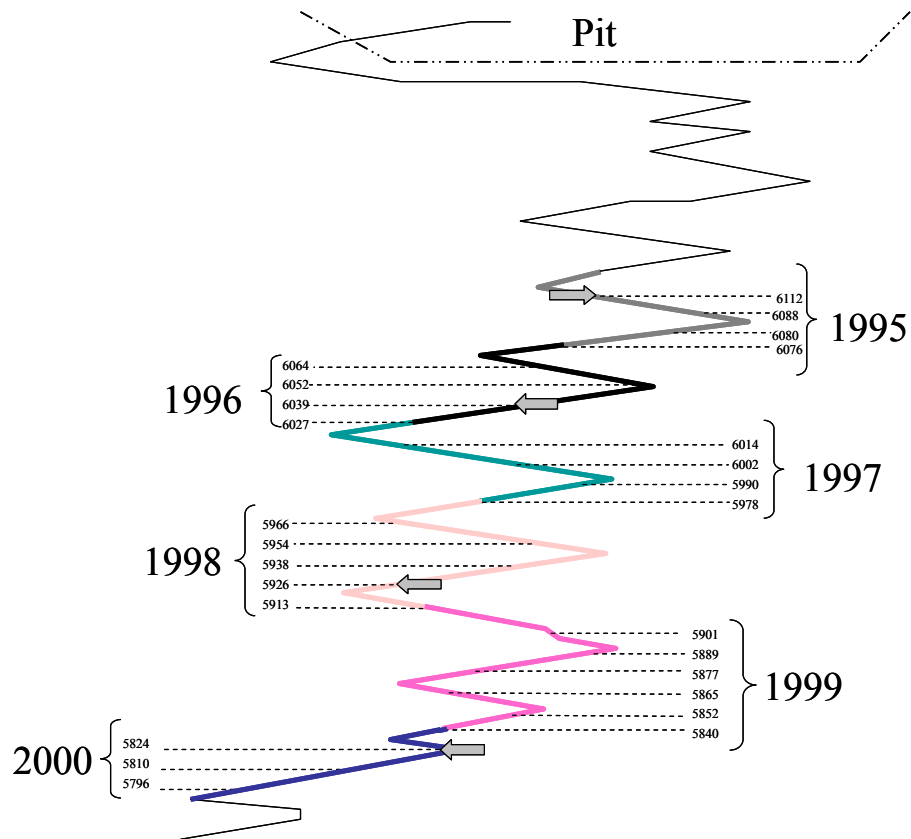


Figure 5.9 Schematic diagram of the Strzelecki Decline with overcore locations marked by grey arrows.

5.4.1 Overcored samples from Kundana Mine

A total of eight elements were recovered all with lengths greater than 1.85 m from the original 2.40 m (see Table 5.1). The host rock in all cases was a highly competent, blocky volcanic sediment with a joint spacing averaged around 250 – 300 mm with the majority of joints mapped open to some extent, although generally no more than 2 mm. The high stress conditions near the excavation boundary would have created a degree of crushing. This combined with unloading, experienced when the rock is overcored, allows the joints to open.

Table 5.1 Recovery of overcored elements from Kundana Mine

Bolt ID	Recovered Length (m)	Location	Joint spacing (mm)
6112 -1	2.03	Wall	250
6112 -2	2.30	Wall	250
6039 -3	2.07	Wall	285
6039-4	2.40	Wall	250
5926-5	2.40	Wall	250
5926-6	1.85	Wall	250
5828-7	2.03	Wall	285
5828-8	2.24	Wall	400

5.4.2 Friction rock stabiliser corrosion damage classification

A corrosion damage classification for galvanised friction bolts was developed to better quantify the amount and severity of corrosion. It has been applied to describe the corrosion of all overcored FRS samples. A summary is provided in Table 5.2 with a more complete description including examples provided in Appendix C.

This classification only describes the level of corrosion experienced by the bolt and does not indicate the corrosivity of the environmental conditions acting on the bolt. Time, which is integral to the corrosion process, must be taken into account to appropriately understand the relationship between the level of corrosion and the corrosivity of the environment. A severely corroded bolt may have been in a moderately corrosive environment for a long time period or conversely in a severe corrosive environment for a short time.

Table 5.2 Corrosion classification for galvanised friction bolts.

Corrosion Classification	Corrosion Description	Average pit depth (mm)
Non-Corroded (NC)	No evidence or only minor evidence of corrosion products	0.0
Light Corrosion (LC)	Minor uniform surface corrosion of zinc and steel. No evidence of pitting	0.0
Moderate Corrosion (MC)	Uniform surface corrosion evident of zinc and steel. Minor areas of severe corrosion and pitting	0.0-1.0
High Corrosion (HC)	Uniform Surface corrosion covers the majority of support/reinforcement. Areas of severe corrosion and pitting common	1.0-2.0
Severe Corrosion (SC)	Severe uniform surface corrosion covers the majority of support/reinforcement. Pitting is very common	>2.0
Extreme Corrosion (EC)	Uniform surface corrosion has greatly reduced the original thickness. Pitting has created large holes in the steel	steel thickness

5.4.3 Load-displacement and tensile strength results

A total of eleven pull tests were conducted with embedment lengths ranging from 285 mm to 506 mm. A summary of results is shown in Table 5.3. The majority of samples were tested from the collar region with only two, the 4B and 5B, being tested near the toe of the bolt. The embedment lengths varied as they were cut in preference to existing geological discontinuities rather than the standard 300 mm described earlier. The peak frictional load achieved varied from 7.0 kN at 366 mm embedment length to 51.9 kN for 498 mm embedment length. In all cases the mode of failure was involved slipping of the element along the element/rock interface as shown in Figure 5.10.

Table 5.3 Summary of test results from the Kundana Mine overcoring.

Bolt ID	Bolt Age (yrs)	Embedment Length (mm)	Peak Load (kN)	Load at 5 mm displacement Residual load (kN)	Tensile Strength (kN)	Corrosion
6112-1A	10	325	49.0	46.5	139.6	Moderate
6112-2A	10	431	24.1	23.1	128.0	High
6039-3A	8	485	12.8	12.2	116.6	High
6039-4A	8	366	7.0	6.7	172.0	High
6039-4B	8	285	11.8	11.3	152.4	High
5926-5A	6	498	51.9	49.4	186.2	Moderate
5926-5B	6	506	44.0	42.0	188.2	Moderate
5926-6A	6	410	18.6	17.6	187.6	Moderate
5828-7A	4	310	24.6	23.7	130.8	High
5828-8B	4	436	19.3	18.7	158.8	Severe



Figure 5.10 Slippage of the FRS at the element/rock interface.

Figures 5.11 and 5.12 display the load-displacement graphs over embedment lengths from 250–300 mm and 400– 500 mm respectively. Figure 5.12 clearly shows a loss of load bearing capacity due to corrosion; the moderately corroded elements generally have twice the load bearing capacity as their highly and severely corroded counterparts.

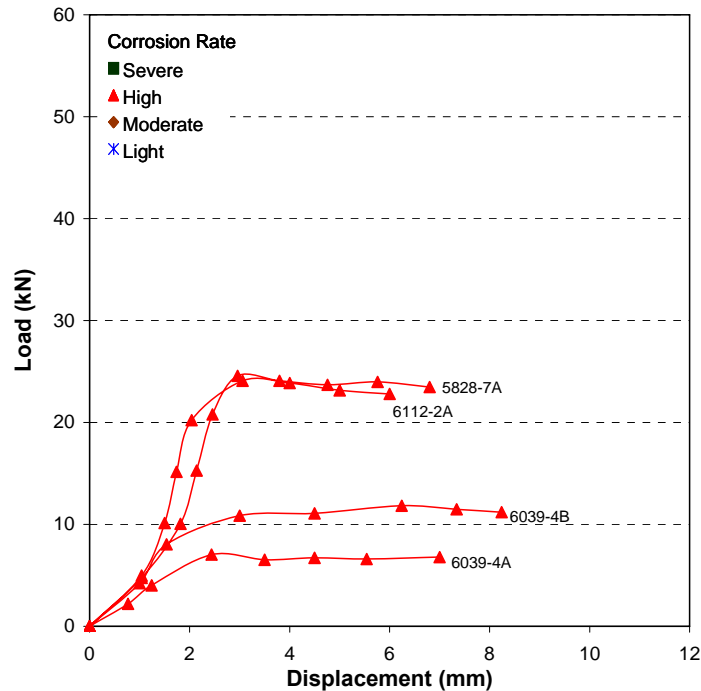


Figure 5.11 Load displacement plot of galvanised 47 mm diameter friction bolts (250-300 mm embedment lengths).

The combined data displaying peak frictional strength over the various embedment lengths are shown in Figure 5.13. The peak frictional strength of the friction bolt for various embedment lengths decreases with increasing levels of corrosion. This is in part due to the corrosion products providing a plane of slip along which the friction bolt slides and in part due to a loss of radial confinement as steel is converted into corrosion products.

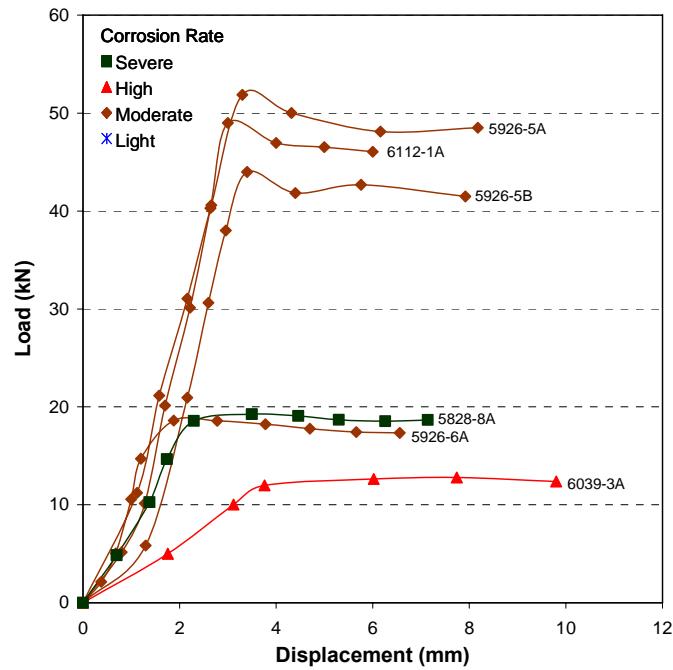


Figure 5.12 Load displacement plot of galvanised 47 mm diameter friction bolts (400-500 mm embedment lengths)

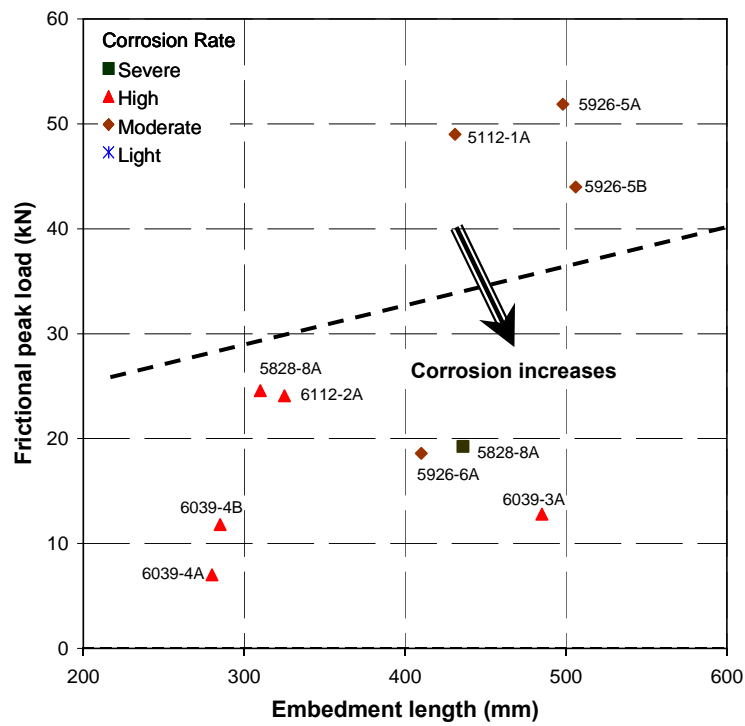


Figure 5.13 Relationship between the peak frictional strength and the embedment length for galvanised 47 mm diameter friction bolts.

Normalising the results to a frictional capacity per metre of embedment length allows for comparison within this data set and with other data. Normalised results for the pull test data is given in Table 5.4. Values ranging from 19.2 to 150.7 kN/m with an average 65.4 kN/m, approximately 6.7 tonnes/meter were determined. This is higher than published results from *in-situ* testing of approximately 4 – 5 tonnes/metre (Villaescusa & Wright 1997) despite quite strong corrosion damage. As Figure 5.14 indicates, there is a decrease in frictional capacity with increasing levels of corrosion damage. However, a level of variability in these results due to the influence of borehole diameter and rock mass quality is evident.

Table 5.4 Normalised results for pull test data from Kundana Mine.

Bolt ID	Bolt Age (yrs)	Embedment Length (mm)	Peak Load (kN)	Force per Length (kN/m)	Force per length at 5 mm displacement (kN/m)	Corrosion
6112-1A	10	325	49.0	150.7	143.2	Moderate
6112-2A	10	431	24.1	55.9	53.7	High
6039-3A	8	485	12.8	26.4	24.15	High
6039-4A	8	366	7.0	19.2	18.3	High
6039-4B	8	285	11.8	41.5	39.8	High
5926-5A	6	498	51.9	104.2	99.2	Moderate
5926-5B	6	506	44.0	86.9	83.0	Moderate
5926-6A	6	410	18.6	45.4	430	Moderate
5828-7A	4	310	24.6	79.3	76.5	High
5828-8B	4	436	19.3	44.2	43.0	Severe

The tensile strength of the elements ranged from 116 kN to 188 kN. Manufacturer's specifications indicate that the typical tensile strength for a 47 mm diameter, galvanised friction bolt is 180 kN (DSI 2006b). When the bolt is only moderately corroded (i.e. it has only undergone minor pitting corrosion) the ultimate tensile strength is relatively unchanged from this value. However, increases in penetration rate result in up to a 30% reduction of the ultimate tensile strength of the steel. Failure of the bolt almost exclusively originated at a pit (see Figure 5.15).

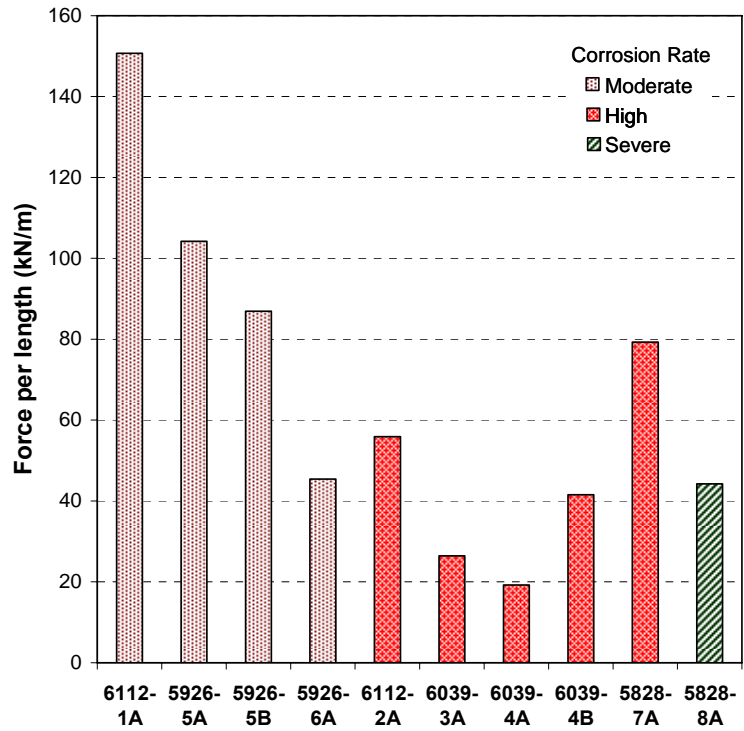


Figure 5.14 Normalised results of pull tests.



Figure 5.15 Failure of friction bolt during tensile testing within pitted region.

5.4.4 Evaluation of damage due to corrosion and analysis of results

Corrosion damage was observed on all overcored samples. The reliability of calculating the uniform corrosion rate is deemed to be poor due to the unknown original thickness of the bolt at the time of installation and the uneven nature of the corrosion. However, relative comparisons in the steel thickness of corroded bolts can be established. High/severely corroded bolts had a reduction in wall thickness of 7-18% compared too moderately and lightly corroded elements. The rates determined for the pitting corrosion are judged to be more precise; however, the reported results do not take into account the loss of the pit depth due to uniform corrosion.

Corrosion is not homogeneous along a bolt axis nor is the rates the same for the internal and external areas of the bolt. In nearly all instances it was found that the pitting rates along the external area of the bolt were higher than for the internal area of the bolt at the corresponding section by about a factor of two. The maximum corrosion penetration rates for each overcored element at 0.5 m intervals are shown in Table 5.5. The pitting rate ranged from 0.04-0.82 mm/yr with an average of 0.21 mm/yr. The variability of corrosion along the bolt axis was profound and is a product of the heterogeneous nature of the environment; primarily controlled by the open discontinuities which provide a conduit for groundwater flow. Bolt 5828-7A is a key example displaying no pitting corrosion at the toe and collar of the bolt, but severe corrosion in the middle section. It was found that the older the age of the bolt, the greater the amount of corrosion. Bolts over eight years of age displayed an average of high to severe corrosion along their entire bolt axis. Bolts of four years age are on average moderately corroded with sections of high to severe corrosion.

It is apparent that there is an increase in both the rate of uniform and pitting corrosion (see Figure 5.16) at the toe of the element to greater than double the rate than near the collar of the bolt. This is thought to be due to drying out the bolt near the collar interrupting the electrochemical corrosion process. The drying out occurs due to a combination of ventilation flow and stress or blast induced fractures allowing the groundwater to dissipate.

Higher rates of corrosion of the element within the toe or stable anchor region affect the element's ability to mobilise the full reinforcing capacity of the system by decreasing the total available frictional resistance of the element in the area where it is most critical. Subsequent loss of frictional resistance in the unstable region is less of a problem due to lower corrosion rates which is also compensated by the presence of the faceplate. This may provide enough resistance to mobilise the element capacity in the unstable region.

Table 5.5 Maximum penetration rates for overcored elements at 0.5m intervals along the bolt axis.

Bolt ID	Bolt Age (yrs)	Average Corrosion Description	Maximum Penetration Rate (mm/yr)			
			Depth Along Bolt Axis (m)			
			(0.0-0.5)	(0.5-1.0)	(1.0-1.5)	(1.5-2.0)
FB 1	10	High	0.09	0.17	0.26	0.20
FB 2	10	High	0.06	0.07	0.20	0.16
FB 3	8	Severe	0.25	0.32	0.44	0.44
FB 4	8	High	0.06	0.13	0.17	0.22
FB 5	6	Moderate	0.06	0.04	0.07	0.11
FB 6	6	Light	0.00	0.07	0.00	NA
FB 7	4.083	Moderate	0.00	0.23	0.82	0.00
FB 8	4.083	High	0.20	0.40	0.33	0.04

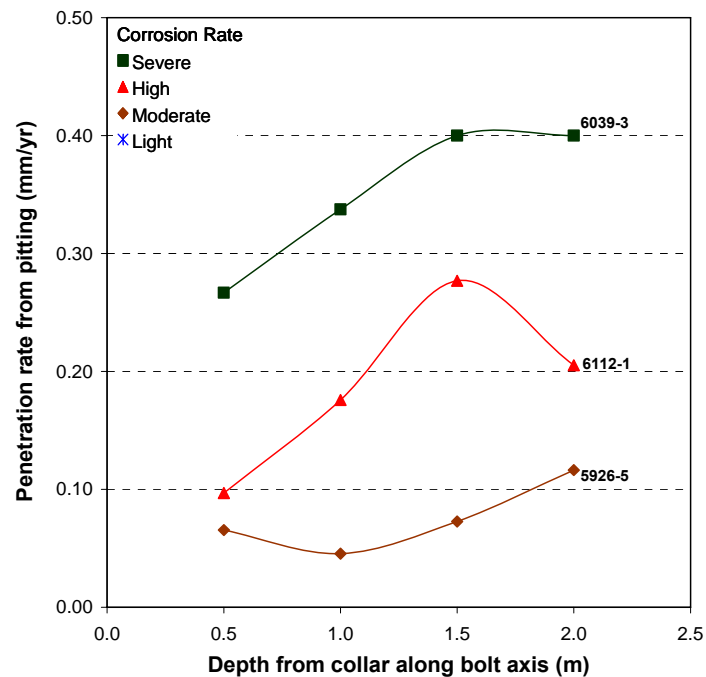


Figure 5.16 Maximum penetration rates due to pitting along bolt axis for severely, highly and moderately corroded bolts.

Evidence of how open jointing results in areas of strong corrosion is provided in Figure 5.17. Severe pitting corrosion has occurred where an open joint along which groundwater flowed contacted the steel element. The level of corrosion is less along the bolt axis distal from the joint due to smaller interaction with groundwater, especially on the ‘up dip’ side of the joint. Where open jointing was not present, high or severe corrosion of the reinforcement did not occur. Therefore, one of the main factors in the corrosion of rock reinforcement is the presence and persistence of open discontinuities in areas where groundwater is present.

A direct correlation between the maximum tensile strength of the corroded friction bolt sections and the maximum pit depth is shown in Figure 5.18. A greater pit depth corresponds to more severe pitting corrosion which lowers the tensile strength of the element. Pitting of FRS can only reach 3 mm depth before it has corroded through the thickness of the steel. Following this the pits expand outwards joining up with proximal pits creating large sections where metal loss is complete, thus continuing the loss of tensile strength. This has further implications as severe pitting generally originates at or near open discontinuities, which often correspond to the boundary between stable and unstable rock regions. Thus the area of the bolt where load transfer occurs from the unstable to stable regions is also the area most prone to pitting corrosion.



Figure 5.17 Open joints (left) have allowed groundwater to flow and interact with the steel element. The same section (right) but with the rock removed displaying severe pitting.

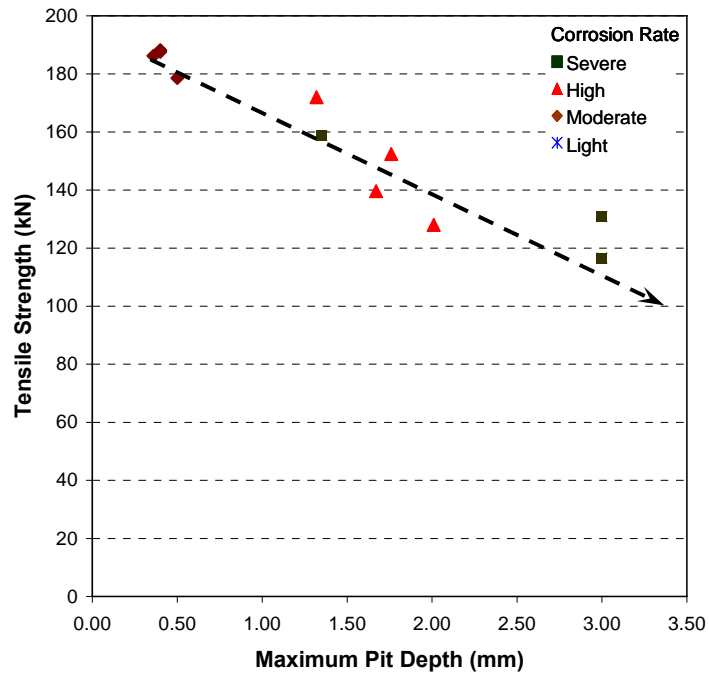


Figure 5.18 Relationship between maximum tensile strength and maximum pit depth.

A basic chemical analysis was undertaken to determine the chemical make up of the corrosion products along the internal and external surfaces of a bolt. Generally steel corrosion products are made up of iron oxides with varying amount of other elements, depending of the steel grade and the environment. The analysis undertaken (see Table 5.6) showed a higher concentration of zinc on the internal surface. This is likely a result of stronger corrosion along the external surface diluting the zinc content, which is thought to have been initially less than the internal surface due to stripping of the galvanising during installation. A study by Tyler (1999) into the damage of galvanising on friction bolts during installation found that there was an average of 33% loss in the external thickness of the hot dip galvanised zinc coating due to the interaction with the rock borehole walls.

Table 5.6 Chemical analysis of corrosion products.

Element	Internal Surface	External Surface
Fe (%)	37.48	41.86
Zn (%)	9.18	2.49
Ca (ppm)	2,335	1,808
Na (ppm)	9,115	9,696

Overcoring at Kundana Mine established that corrosion adversely affects the frictional capacity of friction rock stabilisers with a relationship observed between the extent of damage and peak frictional load. The loss of frictional resistance is due to a loss of radial confinement and corrosion products providing a plane of slip. The tensile strength of the elements was much higher than the frictional strength, with failure occurring at pits and a correlation between the tensile strength and the level of pitting corrosion. Corrosion damage was not homogenous along the bolt axis with greater damage at the external surface and increased corrosion towards the toe of the bolt.

5.5 Overcoring at Argo Mine

Fieldwork conducted at the Argo Mine and detailed in Section 3.3.1 established that corrosion of the main installed reinforcement, the 47 mm diameter galvanised FRS, was occurring as early as 6 months after installation. The aim of the overcoring was to evaluate the level of corrosion on the grouted and ungrouted FRS that were affected by hypersaline groundwater. The impact, if any, on the frictional and tensile load bearing capacity of the bolt was also investigated. In addition, any benefits from the corrosion control methods of galvanising and cement grouting were examined

Overcoring was conducted at three sites, the N1 Access Drive, N3 Access Drive and the N12 Access Drive. These locations had reinforcement ages of 24 months, 12 months and 6 months respectively. Grouted FRS were recovered from the backs and ungrouted FRS from the walls in the N1 and N3. Cement grouting of the elements had not occurred in the N12 at the time of overcoring limiting recovery to ungrouted FRS from the backs.

The environmental conditions at each site were similar with low groundwater flow and strong white salt precipitation at the N1 and N3 sites. The absence of precipitation in the N12 is due to its more recent development. Figure 5.19 shows the environmental conditions at each location. Analysis of the groundwater at each site is consistent with those shown in Tables 2 & 3 in Section 3.3.1. Inspection of the overcoring areas

revealed only minor corrosion of the surface support in the N1 and N3, even when covered with salt crystallisation. The N12 showed no evidence of corrosion.

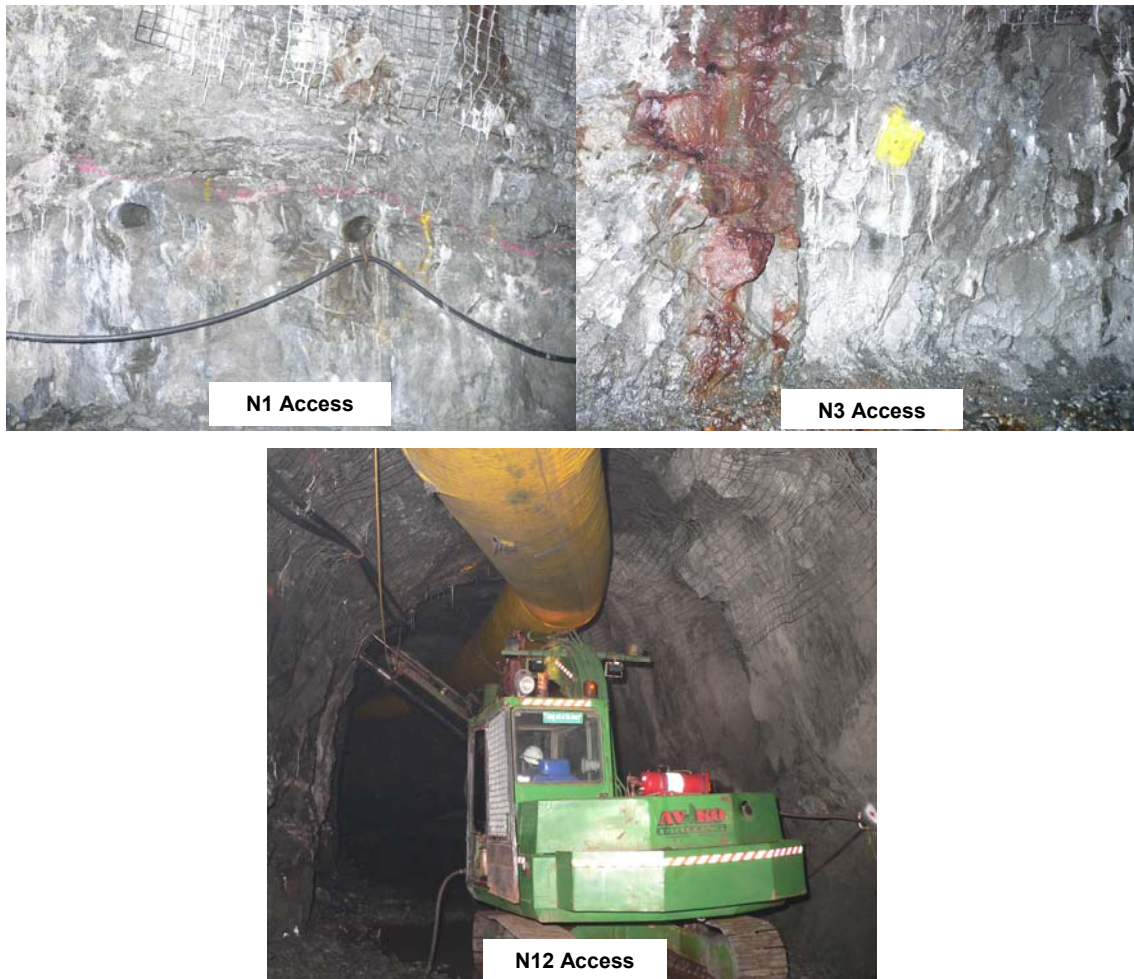


Figure 5.19 Overcoring conditions at the N1 Access Dive (top left), N3 Access Drive (top right) and N12 Access Drive (below centre).

5.5.1 Overcored samples from the Argo Mine

Five bolts were recovered from the N1 Access two of which two were cement grouted, six from the N3 Access of which three were cement grouted, and one from the N12 Access. The total length of recovered bolts is shown in Table 5.7. In all cases the host rock was the Condenser Dolerite.

Table 5.7 Recovery of overcored elements from Argo Mine.

Bolt ID	Recovered Length (m)	Cement Grout	Location	Joint Spacing (mm)
N1-1	2.40	None	Wall	77
N1-2	2.37	None	Wall	82
N1-3	1.57	Grouted	Backs	83
N1-4	1.38	None	Wall	167
N1-5	0.67	Grouted	Backs	143
N3-7	0.53	Grouted	Backs	200
N3-8	2.40	None	Wall	84
N3-9	2.27	Partially grouted	Backs	117
N3-10	2.10	None	Wall	55
N3-11	1.40	None	Wall	56
N3-12	0.60	Grouted	Backs	71
N12-6	2.40	None	Backs	333

Geological mapping of the core illustrated a highly fractured rock mass; the majority of samples had an average discontinuity spacing of less than 200 mm, and the jointing and fracturing was open. A number of highly broken shear zones were also detected. Figure 5.20 displays the discontinuity spacing from the walls and backs. All ungrouted elements were recovered normal to the wall excluding the N12 samples which were recovered normal to the backs along with the grouted samples. The rock mass is more highly fractured normal to the wall than normal to the back. This is possibly due to a sub vertical dominant joint set(s) and/or intact rock fracturing due to stress redistribution or blast related fractures.

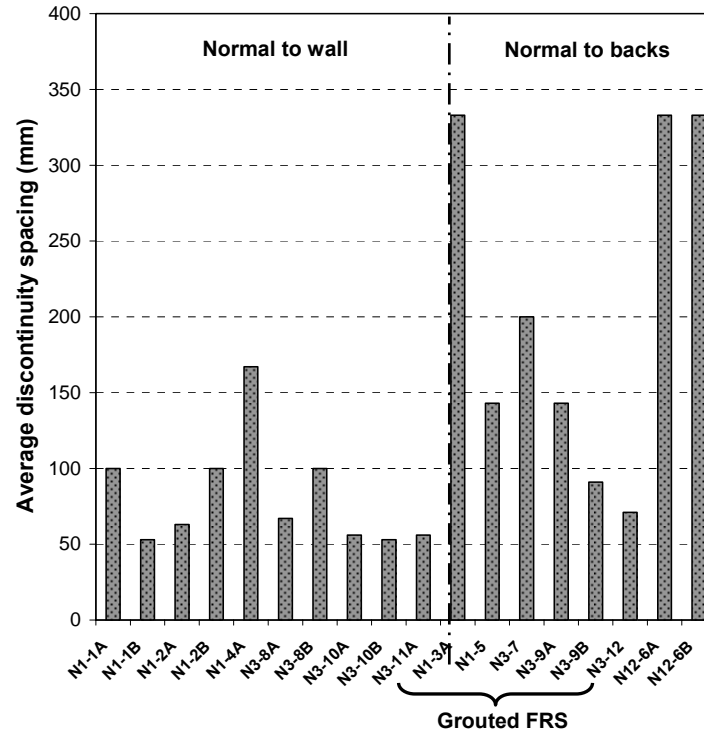


Figure 5.20 Graph of the average discontinuity spacing showing the differences between the rock mass in the walls and the backs.

5.5.2 Load-displacement and tensile strength laboratory results

A total of thirteen laboratory pull tests were completed with the grout quality and a visual assessment of the corrosion along the bolt axis documented. The results are summarised in Table 5.8. Four samples were prevented from being tested by the very broken nature of the surrounding rock mass. The embedment lengths of all tests were 300 mm. In all cases the mode of failure involved slipping of the element along the element/rock interface. Tensile strength tests were conducted on a number of samples following the pull testing.

Table 5.8 Summary of test results from the Argo Mine overcoring.

Bolt ID	Bolt Age (years)	Tested Length (m)	Peak Load (kN)	Load at 5 mm displacement – residual load	Tensile Strength (kN)	Cement Grout	Corrosion
N1-1A	2	0.60-0.90	10.65	8.65	222.20	-	Light
N1-1B	2	1.30-1.60	21.50	20.65	212.80	-	Light
N1-2A	2	0.65-0.95	10.80	10.05	-	-	Light
N1-2B	2	1.35-1.65	13.15	10.15	181.40	-	Light
N1-3A	2	0.50-0.80	44.50	42.75	-	Grouted	Light
N1-4A	2	0.20-0.50	8.40	7.29	-	-	Light
N1-5	2	Not tested	Insufficient recovery		-	Grouted	Light
N3-7	1.5	Not tested	Insufficient recovery		-	Grouted	Light
N3-8A	1.5	0.75-1.05	2.91	2.61	-	-	Light
N3-8B	1.5	0.82-2.13	Pulled out by hand before test		192.80	-	Light
N3-9A	1.5	0.42-0.72	Rock mass broke apart during test		-	Partially	Light
N3-9B	1.5	1.12-1.42	24.54	22.47	-	Partially	Light
N3-10A	1.5	0.69-0.99	8.22	8.13	189.80	-	Light
N3-10B	1.5	1.50-1.80	8.85	7.95	194.40	-	Light
N3-11A	1.5	0.70-1.00	1.86	1.74	-	-	Light
N3-12	1.5	Not tested	Insufficient recovery		-	Grouted	Light
N12-6A	0.5	1.10-1.40	5.45	5.25	-	-	None
N12-6B	0.5	1.50-1.80	3.80	3.10	-	-	None

A summary of the load-displacement results for the N1 Access Drive is shown in Figure 5.21. Load transfer for the ungrouted elements ranged from 8.40 kN to 21.50 kN with the better results occurring in more competent rock masses. The rock mass was generally poor and this had a direct impact on the load transfer. One bolt with a good quality grouting was tested and this achieved the largest peak frictional load capacity of any bolt tested in the mine. Corrosion of the elements was overall light, with uniform corrosion where the galvanising had been breached and isolated areas of pitting corrosion.

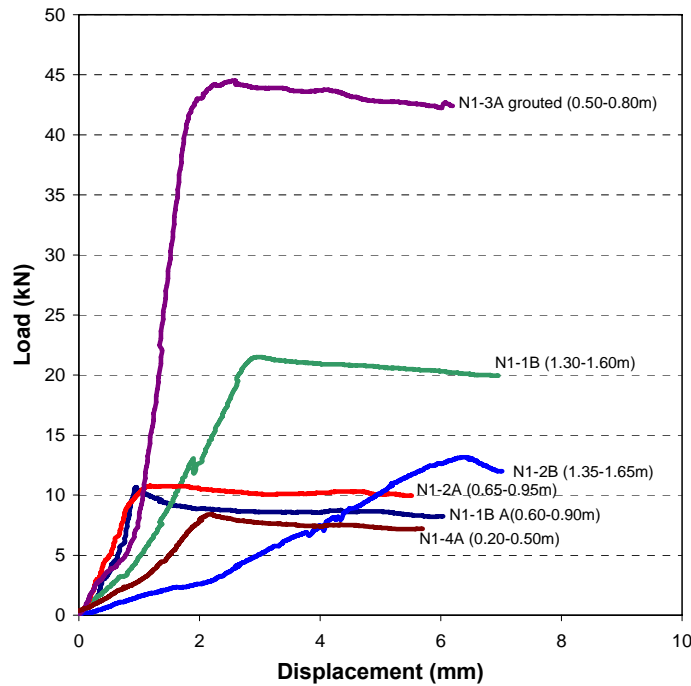


Figure 5.21 Summary of load-displacement results for all pull tests from the N1 Access Drive (300 mm embedment length).

A summary of the load-displacement results for all the N3 Access Drive pull tests is shown in Figure 5.22. The highest load transfer occurred for the only grouted bolt tested. While grout quality was poor the partial grouting was able to provide a higher frictional load by preventing the friction bolt deforming under load. It is clearly seen that grouting of the element (see Figure 5.23), even poorly, will significantly increase the load transfer available (Villaescusa & Wright 1997). The remaining ungrouted tests had less than 50% to only 8% of the frictional capacity of the grouted bolt. The rock mass was generally poor with small discontinuity spacing which contributed to the low load transfer experienced.

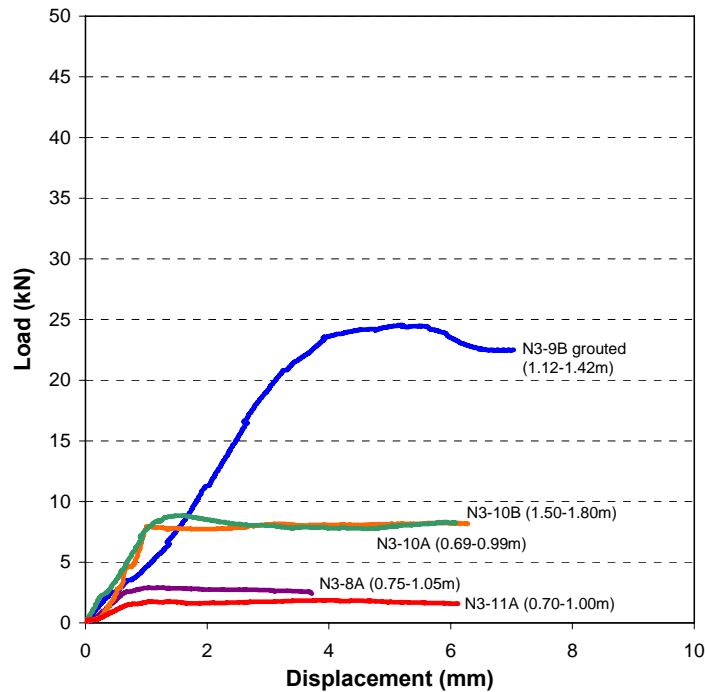


Figure 5.22 Summary of load-displacement results from pull tests for the N3 Access Drive (300 mm embedment length).



Figure 5.23 Good grouting of sample N1-3A (top) and poorer grouting of sample N3-9B (bottom).

The load-displacement results for the element recovered from the N12 are shown in Figure 5.24 with little variation in peak frictional load between sections A and B. The rock mass condition is good with a discontinuity spacing of 333 mm. The element had no corrosion damage with the galvanising intact. With an installation age of 6 months it

can be assumed that galvanising protects the bolt from corrosion for approximately this length of time in this environment.

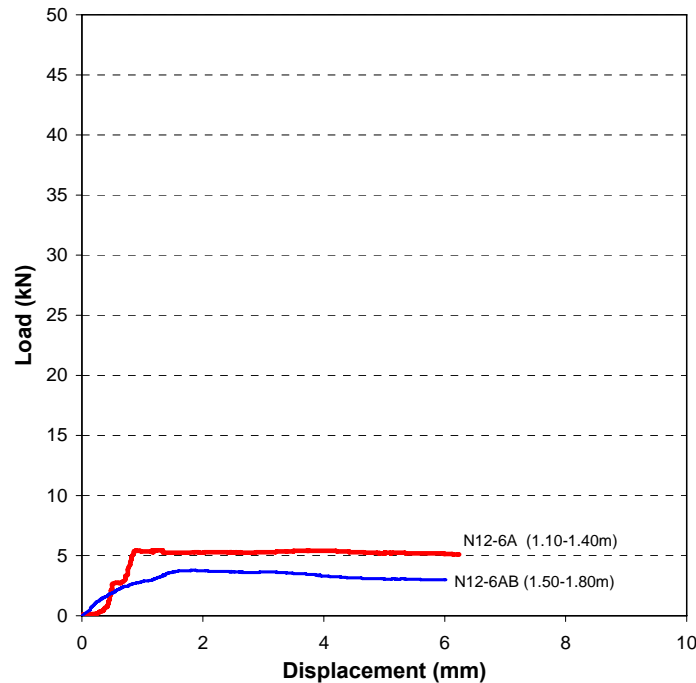


Figure 5.24 Load-displacement results from pull tests of N12 Access Drive 6A and 6B (300 mm embedment length).

The combination of all pull test results is shown in Figure 5.26. The frictional capacity of the ungrouted specimens varied greatly, ranging from 1.86 – 21.50 kN with an average 8.69 kN for 300 mm embedment length. The two grouted elements had much higher peak loads of 44.50 kN and 24.52 kN.

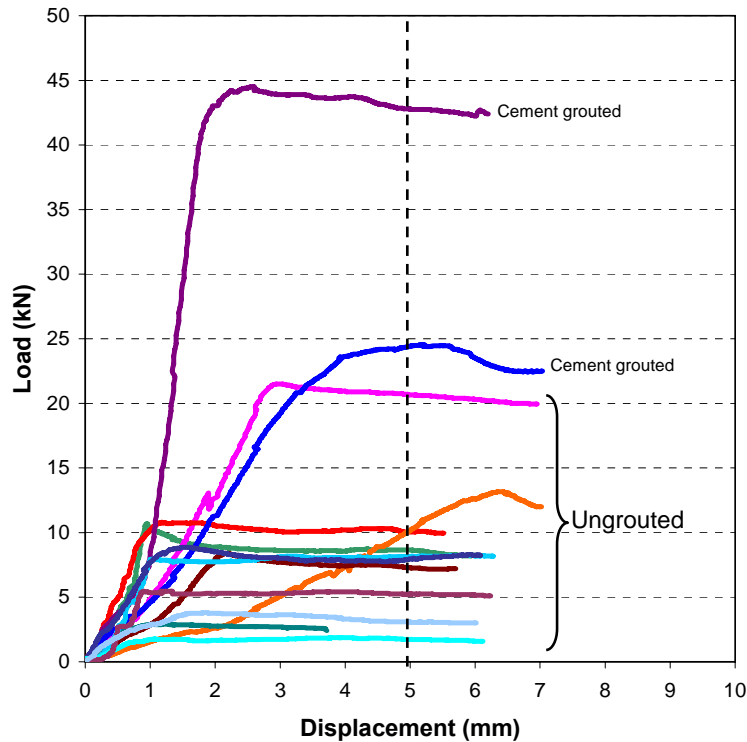


Figure 5.25 Combination of pull test capacities for all FRS tests (300 mm embedment length).

Normalised results from the pull test data are shown in Table 5.9 and plotted for comparison in Figure 5.26. The frictional capacity per meter of embedment length for ungrouped elements ranged from 6.2 to 71.7 kN/m with an average of 30.8 kN/m or approximately 3 tonnes per metre. The benefits of grouting in increasing the load transfer capacity of friction bolts is clearly seen with a maximum capacity of 148.3 kN/m. The poorly grouted sample 9B still had a higher peak frictional load capacity than any of the ungrouped elements.

Examining the samples tested near the collar regions (A samples) and those nearer to the toes region (B samples) it is observed there is a slight increase in load capacity for elements tested near the toe region, which could be a function of a more competent rock mass as it is more distal from the development opening and less prone to blast damage.

Table 5.9 Normalised results for the peak load and residual load.

Bolt ID	Tested Length (m)	Peak Load (kN)	Force per length (kN/m)	Force per length at 5 mm displacement – residual (kN/m)	Grout	Corrosion
N1-1A	0.60-0.90	10.65	35.50	28.83	-	Moderate
N1-1B	1.30-1.60	21.50	71.67	68.83	-	Moderate
N1-2A	0.65-0.95	10.80	36.00	33.50	-	Moderate
N1-2B	1.35-1.65	13.15	43.83	33.83	-	Moderate
N1-3A	0.50-0.80	44.50	148.33	142.5	Grouted	Moderate
N1-4A	0.20-0.50	8.40	28.00	24.30	-	Moderate
N1-5	Not tested	Insufficient recovery			Grouted	Moderate
N3-7	Not tested	Insufficient recovery			Grouted	Light
N3-8A	0.75-1.05	2.91	9.70	8.70	-	Moderate
N3-8B	0.82-2.13	Pulled out by hand before test			-	Moderate
N3-9A	0.42-0.72	Rock mass broke apart during test			Partially	Light
N3-9B	1.12-1.42	24.54	81.80	74.90	Partially	Light
N3-10A	0.69-0.99	8.22	27.40	27.1	-	Moderate
N3-10B	1.50-1.80	8.85	29.50	26.5	-	Moderate
N3-11A	0.70-1.00	1.86	6.20	5.80	-	Light
N3-12	Not tested	Insufficient recovery			Grouted	Light
N12-6A	1.10-1.40	5.45	18.17	17.5	-	None
N12-6B	1.50-1.80	3.80	12.67	10.33	-	None

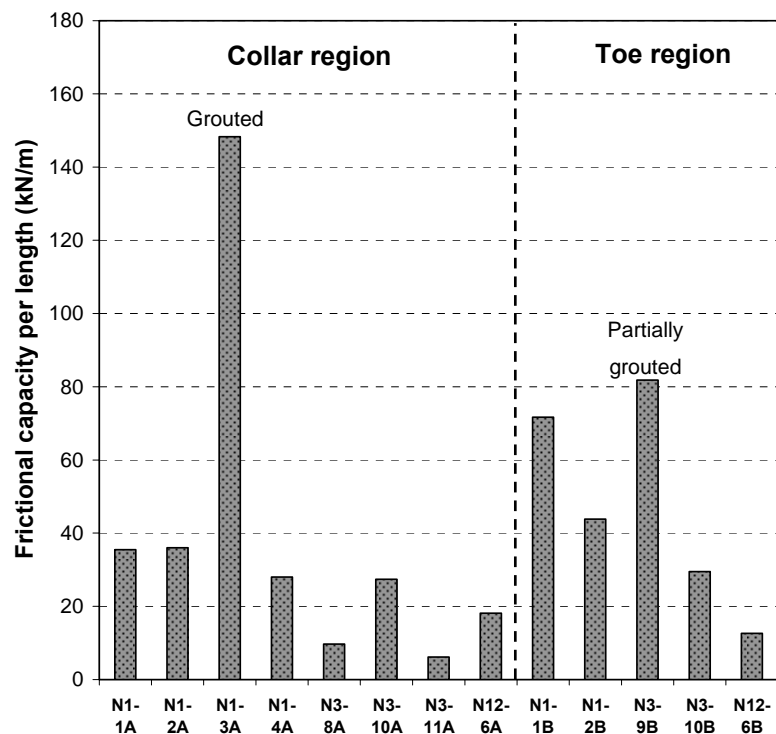


Figure 5.26 Frictional capacity per metre of embedment length of collar (A) and toe (B) samples normalised from pull tests of 300 mm embedment length.

The tensile strength test results ranged from 181 to 222 kN with all tested elements recording a higher strength than manufacturer's specifications (180 kN). Compared with the pull test loads, which are a measure of the frictional capacity, the tensile strength of the element is considerably higher. Hence, a considerable loss of metal would need to occur before tensile failure would occur before slippage.

5.5.3 Evaluation of damage due to corrosion

The corrosion condition of the overcored elements ranged from none, as was observed at the N12 access, to minor amounts of moderately corroded bolt sections in the N1 and N3 access drives. Generally corrosion does not impact on the bolt load transfer abilities till it becomes highly corroded. The maximum measured penetration rate along the bolt axis for each sample is shown in Table 5.10. In all cases the maximum rate was measured from pitting on the external surface. The start of pit development is assumed to be the installation age minus the minimum six months of protection galvanising provides.

The occurrence of pitting is isolated but highly aggressive, a consequence of the high chloride content of the groundwater. Corrosion in the short-term causes little actual damage, which is favourable for the installed reinforcement. Of all the bolts analysed only two recorded any pitting on the internal surface. Corrosion predominately occurs on the external surface of the bolt. The maximum penetration rates measured are aggressive, when compared to a nominal bolt thickness of 3 mm. The average pitting rate for both the N1 and N3 was 0.40 mm/yr indicating that once pitting originates it stabilises and continues at a near constant rate. The range of measured rates equates to a local reduction in wall thickness of about 13% per year up to a maximum of 34% per year.

The ultimate tensile strength of the tube is detrimentally affected by corrosion. As shown in Section 5.4.3 a correlation exists between the maximum tensile strength and pitting corrosion. The relationship for the Argo data, shown in Figure 5.27, fits this trend. However, the data set range is small and pitting has not progressed to have caused large metal loss.

Table 5.10 Pitting rate of overcored elements along bolt axis.

Bolt ID	Bolt Age (years)	Cement Grouting	Average Corrosion Description	Maximum Penetration Rate (mm/yr)				
				Depth Along Bolt Axis (m)				
				0.0-0.5	0.5-1.0	1.0-1.5	1.5-2.0	2.0-2.4
N12-6	0.5		None	-	0	0	0	0
N3-7	1.5	Grouted	Light	0	-	-	-	-
N3-8	1.5		Moderate	0.34	0.52	0.50	0.29	-
N3-9	1.5	Partially grouted	Light	0	0	0.63	-	-
N3-10	1.5		Moderate	0.45	0.20	0.28	0.20	0.20
N3-11	1.5		Light	0	0	-	-	-
N3-12	1.5	Partially grouted	Moderate	0.76	-	-	-	-
N1-1	2		Moderate	0	0	0	0.25	0.37
N1-2	2		Moderate	0.46	0.18	0.43	0.37	0.24
N1-3	2	Grouted	Moderate	0.41	1.03	-	-	-
N1-4	2		Moderate	0	0.25	-	-	-
N1-5	2	Partially grouted	Moderate	0.31	-	-	-	-

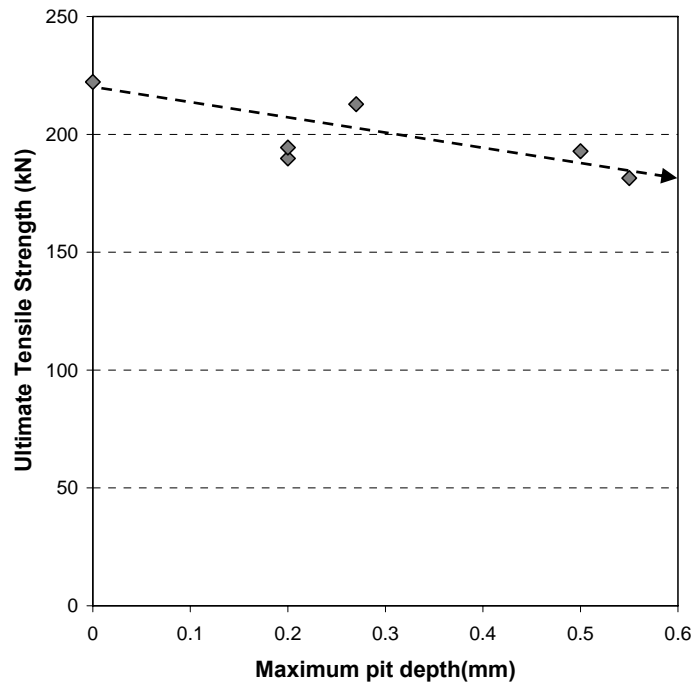


Figure 5.27 Maximum tensile strength and the rate of penetration due to pitting corrosion.

It was not possible to measure the uniform corrosion rate due to its small occurrence; however, another indication of overall corrosivity is seen by examining the loss of galvanising along the bolt axis. Table 5.11 documents the loss of galvanising as a percentage along 0.5 m sections of the bolt axis, with 100% showing total loss of galvanising. Galvanising protects the underlying steel by providing a barrier from the surrounding environment. It will also corrode sacrificially in favour of steel. Over time the galvanising layer is breached and then corrosion of the steel occurs.

Neither corrosion nor loss of galvanising was seen on bolts of 6 months age. However, data from the earlier CAS did show some damage on bolts of just over 6 months age. It can be concluded that galvanising completely protects the element in wet conditions for at least 6 months after installation. Those bolts that had been installed for 2 years still retained some galvanising, mainly near the collar of the bolt.

Table 5.11 Loss of galvanising along bolt axis.

Bolt ID	Bolt Age (years)	Galvanising Loss (%)									
		Depth Along Bolt Axis (m)									
		0.0 - 0.5		0.5 - 1.0		1.0 - 1.5		1.5 - 2.0		2.0 - 2.4	
		Ext.	Int.	Ext.	Int.	Ext.	Int.	Ext.	Int.	Ext.	Int.
N12-6	0.5	-	-	0	0	0	0	0	0	0	0
N3-7	1.5	100	20	-	-	-	-	-	-	-	-
N3-8	1.5	80	80	80	80	100	80	100	80	-	-
N3-9	1.5	75	5	75	10	75	10	-	-	-	-
N3-10	1.5	80	80	80	80	80	90	100	100	100	100
N3-11	1.5	60	40	60	40	-	-	-	-	-	-
N3-12	1.5	80	10	-	-	-	-	-	-	-	-
N1-1	2	60	50	60	50	60	50	80	100	80	100
N1-2	2	50	50	50	50	100	100	100	100	100	100
N1-3	2	100	5	100	5	-	-	-	-	-	-
N1-4	2	60	90	95	95	-	-	-	-	-	-
N1-5	2	100	20	-	-	-	-	-	-	-	-

5.5.4 Cement grouting to prolong reinforcement life

Cement grout not only provides a physical barrier separating the steel from the environment but also is a corrosion inhibitor. Examination of the overcored elements clearly showed that cement grouting of the bolt protects the internal surface. Areas where grout adhered adequately to the bolt surface exhibit no corrosion and still contain galvanising. Loss of galvanising and minor corrosion did occur when voids were left in the grouting due to inadequate grouting (see Figure 5.28).

Cement grouting does not protect the external surface of the element where the majority of corrosion is occurring. The highest penetration rate recorded was for the N1-3 bolt on its external surface despite it being grouted internally. It can be concluded that due to the lesser quantity of corrosion on the internal surface of the bolts the amount of protection offered by cement grouting is limited.



Figure 5.28 Overcored friction bolts with grout removed. Grout protected the element with galvanising still present. Voids in the grout have allowed some corrosion to occur.

5.5.5 Analysis of results

The normalised frictional capacity of the ungrouted specimens varied greatly with an average of 30.8kN/m. Villaescusa and Wright (1997) have stated an average strength for a correctly installed 46 mm diameter FRS to be 4 tonnes per meter, equivalent to 39.2 kN/m. *In-situ* pull tests by (Tomory, Grabinsky & Curran 1998) in a range of different rock masses produced similar results. The average value of the pull tests from overcoring is lower than published data with four tests less than 20 kN/m. Corrosion has

not developed enough to influence the frictional or tensile capacity of the element to a significant degree due to the recent development of the mine and the low corrosivity of the environment. Therefore, it is concluded that the borehole size, the rock mass quality and installation practices such as twisting of the bolt are considered the primary effects on the element capacity in the Argo Mine.

It is known that highly fractured or sheared rock will provide little frictional force on the bolt. Geological mapping of the overcore showed a highly fractured rock mass with large, broken shear zones. Figure 5.29 plots the discontinuity spacing and the peak frictional load. No relationship is indicated from the information.

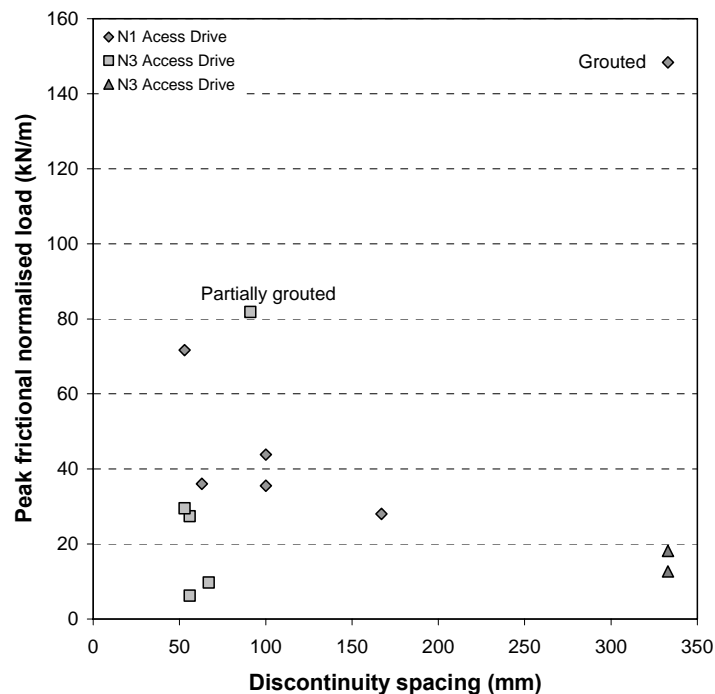


Figure 5.29 Comparison between the discontinuity spacing and the peak frictional load from pull testing.

The borehole diameter of each pull tested sample was calculated through the back analysis of the measured slot width. When a friction bolt is installed into a borehole of a smaller diameter there are resulting changes to the dimensions as shown schematically in Figure 5.30. The hole diameter can be approximated by the following equation:

$$\text{Hole diameter } (2r_2) = 2 \left[r_1 - \left\{ \frac{d_1 - d_2}{2\pi} \right\} \right] \quad (5.1)$$

Where

r_1 – initial radius of friction bolt

r_2 – current radius of friction bolt

d_1 – initial slot width

d_2 – current slot width

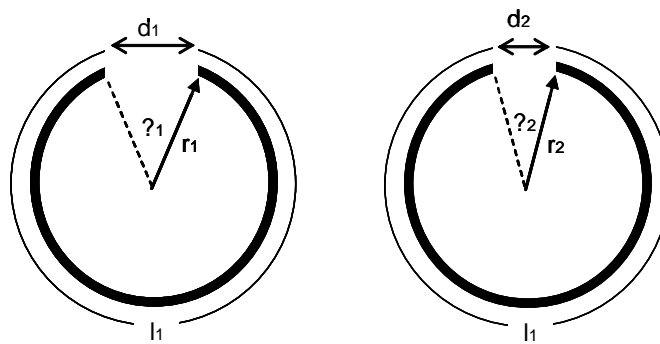


Figure 5.30 Schematic representation of the friction bolt dimensions before (left) and after (right) installation.

Figure 5.31 compares the calculated hole diameter with the frictional capacity. Manufacturer's installation specifications suggest a hole diameter range between 43 mm and 45.5 mm for a 47 mm diameter bolt. Two samples fall outside this range; the N1-1A installed in a smaller than recommended hole and the N3-11A installed in a larger than recommended hole. The N3-11A sample also recorded the lowest frictional capacity of any test with 1.86 kN for a 300 mm embedment length. For those bolts installed within the specified borehole diameter range no trend can be determined

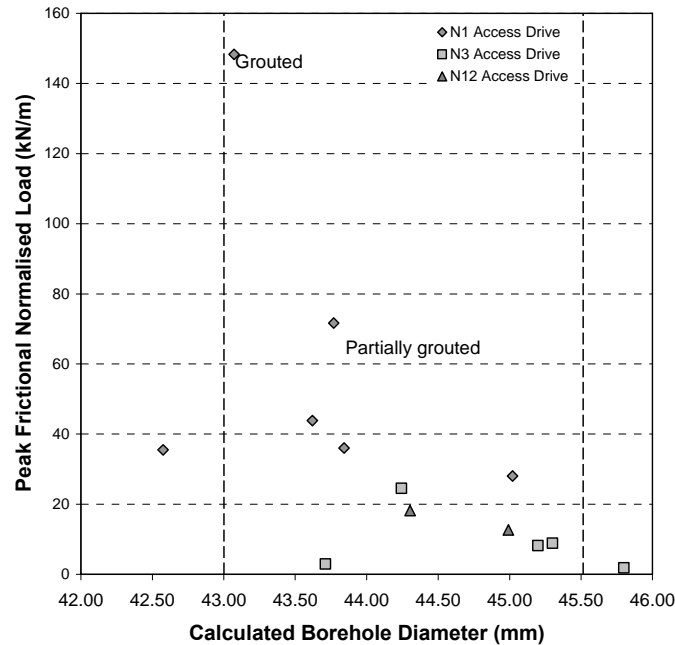


Figure 5.31 Calculated hole diameter compared to the tested peak frictional load.

The quality of the rock mass and the size of the borehole diameter both control the initial bond strength; however, no clear relationships can be determined from this data based on estimates of borehole diameter. What can be seen is the significant increase in load transfer capacity by cement grouting of the bolt. Villaescusa and Wright (1997) presented in-situ pull test results that indicated cement grouting of friction bolts are likely to provide up to three times the initial bond strength per meter of embedment length. The laboratory pull tests conducted provide similar result, as well as additionally showing that even partial grouting of the element provides significant extra load transfer.

While partial grouting does offer some benefits it is strongly recommended that good quality control of grouting be a priority and that full grouting of the bolt axis be achieved. Due to gravity grout will tend to accumulate grout near the collar of the bolt, giving the indication of a fully grouted column. In-situ pull testing of the bolt may not indicate a problem as the design capacity may be reached over the short grouted length. The remaining ungrouted section would have a much lower frictional capacity.

Corrosion occurred on the majority of overcored reinforcement but the level of damage is not sufficient for it to be detrimental at this stage. This implies that the corrosivity of the groundwater affected environments is low. It was found that galvanising provides full protection for a minimum of 6 months in the wet environments investigated. Damage due to corrosion was more prevalent on the external bolt surface, which had more direct contact with the groundwater than the internal surface. The amount of corrosion protection afforded by cement grouting of the FRS is therefore limited.

5.6 Overcoring at Leviathan Mine

The Leviathan underground mine comprising of the Sirius, Victory and Defiance deposits was initially mined by Western Mining Corporation (WMC) until 1999 (Watchorn 1998). Following the abandonment of mining much of the workings flooded due to the close proximity of Lake Lefroy. Dewatering and re-entry of the Leviathan workings by Goldfields St Ives occurred in 2005. Questions were raised about the corrosion condition of the previously installed reinforcement, primarily Hollow Groutable Bolts (Villaescusa, Sandy & Bywater 1992), and if there was a need to rehabilitate. Little research has been conducted previously into the corrosion of rock reinforcement and support in flooded mines.

Two areas of particular interest to the mine are the Conqueror Link and the Jade Decline. Both areas had been submerged for 6 years with rock reinforcement being installed greater than 2 years prior. The main reinforcement element installed is the hollow groutable bolt (HGB), a smooth, hollow tubular bar of 2.4 m length with an outside diameter of 25.5 mm and an internal diameter 18.5 mm leaving a 3.5 mm steel ring (see Figure 5.32). It is installed initially as a mechanical point anchor bolt. As point anchored systems are susceptible to corrosion and rock movement, post cement grouting is conducted to create a permanent reinforcement. Even when grouted the HGB is known to be susceptible to corrosion due to its thin steel wall. Other reinforcement

elements installed include ungrouted point anchored rebar, friction rock stabilisers and cable bolts.



Figure 5.32 Grouted HGB displaying thin steel wall and internal grout.

Environmental conditions at the two sites varied significantly over the life of the reinforcement and can be classified into three stages, pre-flooding, flooding and post flooding. Pre-flooding conditions are assumed to be similar to post-flooding conditions; however there are no records from this time. It is assumed to be a dry rock mass, and with adequate ventilation. This environment produces only minor corrosion. During flooding groundwater from local hard rock aquifers recharged from Lake Lefroy submerged the development with local air pockets; this is evident from crystal growth on the walls and backs. An analysis of groundwater collected from a perched stope, shown in Table 5.12, is thought to reflect the composition of the flood water. It shows neutral, hypersaline water high in sulphide and chloride ions.

Table 5.12 Analysis of groundwater taken from a perched stope.

pH	7.02
Dissolved Oxygen (mg/L)	1.49
Total Dissolved Solids (mg/L)	233,220
Total Suspended Solids (mg/L)	2,761
Sulphate ions SO₄²⁻ (mg/L)	13,608
Carbonate (mg/L)	0
Bicarbonate (mg/L)	54
Chloride ions Cl⁻ (ppm)	25,420
Sodium ions Na (ppm)	44,353

Inspection of the two areas showed high to severe corrosion of the face plates and protruding bolt ends (see Figure 5.33). The corrosion damage was sufficient that in places the original steel had been completely converted to corrosion products. These sections would have been in direct contact with the groundwater. Corrosion attack of the element within the rock mass would only occur if the element had not been properly grouted or along open discontinuities, through which groundwater could move.



Figure 5.33 Severe corrosion of a HGB face plates due to flooding of mine workings.

5.6.1 Overcored samples from the Leviathan Mine

A total of five HGB, two cable bolts, an ungrouted point anchored twisted rebar and a friction rock stabiliser were overcored at the two sites. The rock mass in both areas was good, as seen in Figure 5.34, with the majority of jointing present open to some extent. Joint spacing ranged from 77 mm to 125 mm for the Conqueror Link and 91 mm to 500 mm for the Jade Decline. The total length of the recovered bolts is shown in Table 5.13. The ungrouted point anchor twisted rebar drilled at the Conqueror Link was mistaken for a HGB. The rebar was still in reasonable condition; however, the anchor was not overcored and the plate is severely corroded. Two cable bolts and a friction bolt were overcored from the Jade Decline. The friction rock stabiliser showed extreme corrosion, similar in extent to the surface support.



Figure 5.34 Overcored HGB samples from the Leviathan Mine.

Table 5.13 Recovery of overcored elements from Leviathan Mine.

Bolt type	Overcore location	Recovered length (m)	Joint spacing (mm)
HGB 1	Jade Decline	0.87	91
HGB 2	Jade Decline	0.65	-
HGB 3	Jade Decline	2.40	500
FRS 1	Jade Decline	1.18	167
Plain Cable 1	Jade Decline	1.27	91
Plain Cable 2	Jade Decline	0.84	250
HGB 4	Conqueror Link	1.35	77
HGB 5	Conqueror Link	0.96	125
Point Anchor 1	Conqueror Link	1.14	200

5.6.2 Load-displacement results

From the five recovered overcored HGB samples, two each from the Jade Decline and Conqueror Link were suitable for load-displacement testing. Eleven samples of 300 mm embedment length were prepared for push testing. These samples were taken from along the entire bolt axis. In addition two overcored plain strand samples were pull tested. A summary of the results is displayed in Table 5.14. The results show a range in load transfer of the HGB samples from 21.00 kN (~2.1 tonne) to 142.90 kN (~14.6 tonne) a difference of 85%. Examination of the sample before and after testing indicated that encapsulation quality and not corrosion is the major factor in determining peak load. Poor encapsulation such as shown in Figure 5.35 is typified by longitudinal voids and this combined with the smooth bolt exterior led to low load transfers.

Similar results were observed for the two tests conducted on the plain strand cables. Sample 1-A being poorly encapsulated had a peak load about half that of the well

encapsulated sample 2-A. Figure 5.36 displays the difference in the quality of the grouting prior to testing.

Table 5.14 Summary of pull and push testing results.

Bolt ID	Location from collar (m)	Embedment Length (mm)	Peak Load (kN)	Encapsulation quality	Corrosion
HGB 1-A	0.05-0.35	300	59.85	good	minor
HGB 1-B	0.35-0.65	300	69.95	good	minor
HGB 3-A	0.00-0.30	300	115.35	good	minor
HGB 3-B	0.40-0.70	300	142.90	good	minor
HGB 3-C	0.80-1.10	300	115.35	good	minor
HGB 3-D	1.20-1.50	300	120.10	good	minor
HGB 4-A	0.00-0.30	300	67.85	poor	minor
HGB 4-B	0.30-0.60	300	21.00	poor	minor
HGB 4-C	0.70-1.0	300	25.45	poor	minor
HGB 5-A	0.00-0.30	300	59.60	poor	minor
HGB 5-B	0.30-0.60	300	25.85	poor	minor
Plain Cable 1-A	0.40-0.70	300	36.35	poor	minor
Plain Cable 2-A	0.07-0.37	300	74.15	good	minor



Figure 5.35 Poor grouting leading to low load transfers for sample HGB 4-C.



Figure 5.36 Encapsulation quality for plain cable samples 1-A (left) and 2-A (right).

A composite for all HGB push tests is shown in Figure 5.37. The wide range of values is a function of the grout encapsulation quality and not related to damage due to corrosion. Even elements that had good grout encapsulation still showed varying values due to gravity settling of the grout particles. The load-displacement values are considered relative values, as they were calculated from push testing, which is expected to overestimate the actual pull out strength. A summary of the peak load and residual load (taken at 10 mm displacement) is shown in Table 5.15.

A plot of the peak and residual load for each push test along the bolt axis from the collar region to the anchor region is displayed in Figure 5.38. As a general rule the collar region exhibits higher values compared to sections closer to the toe of the bolt (anchor). However, the varying quality of grout encapsulation makes comparison complicated.

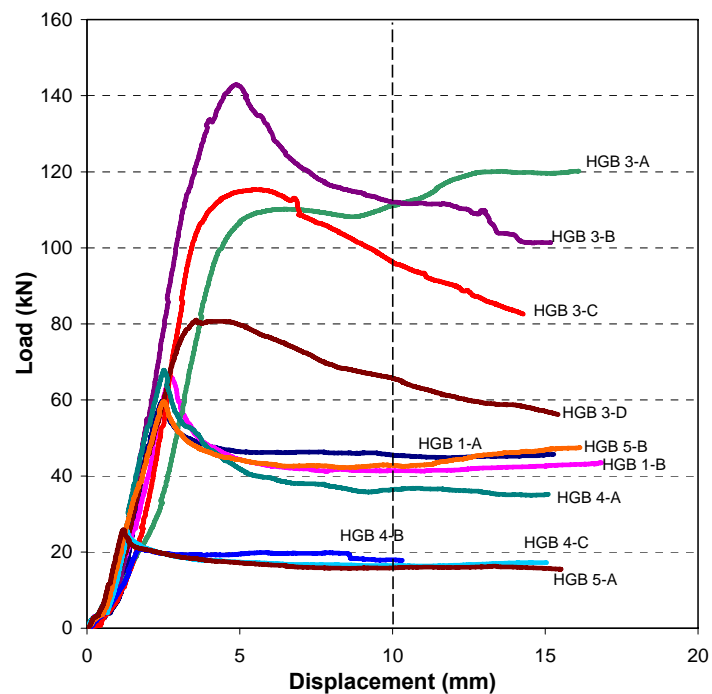


Figure 5.37 Combination of relative push test capacities for all HGB tests (embedment length 300 mm).

Table 5.15 Summary of relative push tests capacities for HGB tests.

Bolt ID	Peak Load (kN)	Displacement at Peak Load (mm)	Load at 10 mm displacement (kN) – residual load	Maximum Displacement (mm)	Load at Maximum Displacement (kN)
HGB 1-A	59.85	2.50	45.55	15.28	45.75
HGB 1-B	65.95	2.76	41.45	16.84	43.50
HGB 3-A	120.20	16.10	111.10	16.10	120.20
HGB 3-B	142.90	4.86	112.00	15.18	101.35
HGB 3-C	115.35	5.48	96.25	14.28	82.55
HGB 3-D	81.00	3.58	65.70	15.42	56.20
HGB 4-A	67.85	2.50	36.45	15.10	35.20
HGB 4-B	21.00	1.70	17.95	10.32	17.80
HGB 4-C	25.45	1.30	16.45	15.04	17.20
HGB 5-A	59.45	2.52	42.80	16.14	47.50
HGB 5-B	25.85	1.18	15.85	15.52	15.50

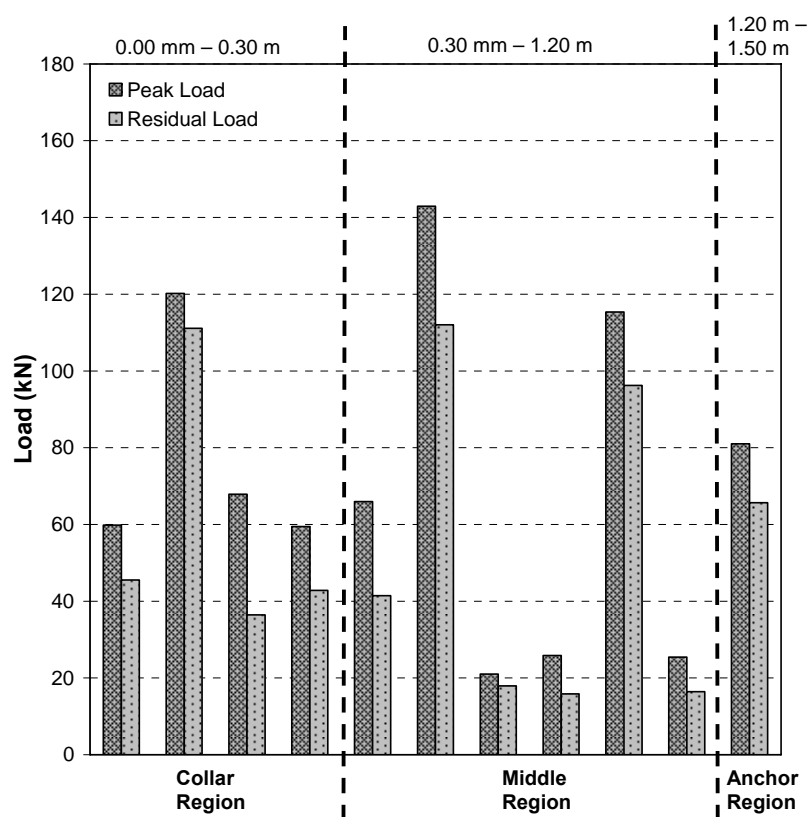


Figure 5.38 Peak and residual load for relative push test of HGB along bolt axis.

5.6.3 Evaluation of damage due to corrosion and analysis of results

Corrosion damage to the HGB reinforcement consisted of light uniform surface corrosion in areas where it was fully grouted, most likely occurring before grouting of the element, ranging to isolated areas of stronger uniform corrosion in less well encapsulated regions (see Figure 5.39). This level of corrosion did not affect the reinforcements' load transfer capabilities nor was it sufficient to reduce the tensile strength despite the thin-walled nature of the element.

Despite the common occurrence of longitudinal voids in the grout column these areas did not undergo any significant corrosion, even when intersected by an open joint, as illustrated in Figure 5.40. The bolt in this example would have been highly susceptible to corrosion attack by groundwater but a build-up of solids at the void/joint boundary and in the joint itself occurred effectively prevented any groundwater flow. The deposition of suspended solids and precipitation of dissolved solids would have occurred relatively quickly after flooding as there is little corrosion damage to the element. This process originates as the groundwater was effectively stagnant, compared to the usual scenario of gravity assisted water flow. This allowed for deposition and precipitation of solids to occur.



Figure 5.39 Light surface corrosion in fully grouted areas (top) with isolated areas of stronger surface corrosion where grout encapsulation was not as good (bottom).



Figure 5.40 Minor corrosion of bolt even when open joint intersect exposed element.

An additional benefit of cement grouting is its migration along open discontinuities into the rock mass. As shown in Figure 5.41 a large crack had formed before bolt installation, during which cement grout migrated into, not only providing a larger barrier to potential groundwater flow but also assisting in interlocking of the rock mass.

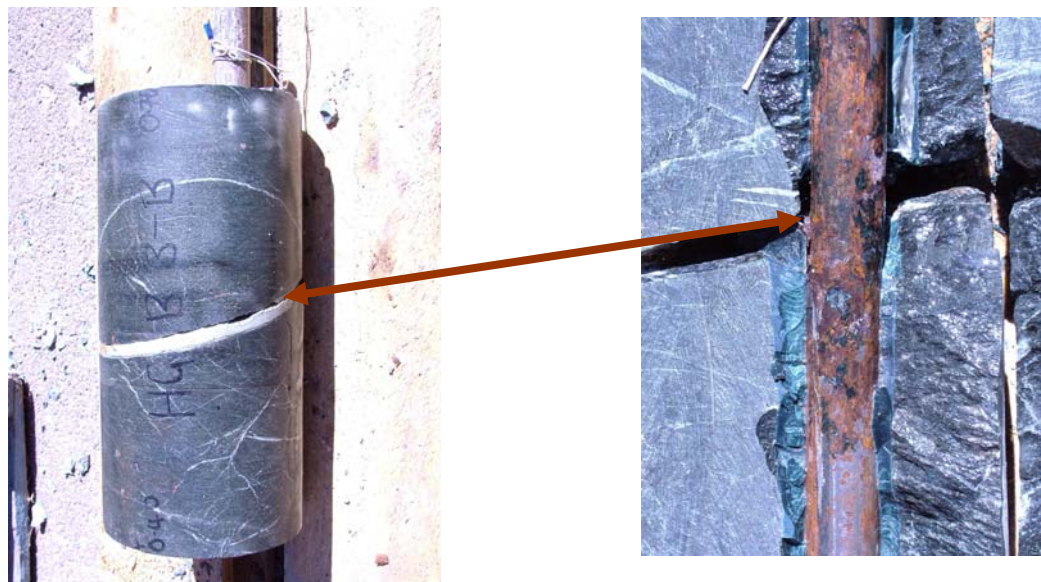


Figure 5.41 Corrosion protection due to migration of grout preventing groundwater interaction with bolt.

An initial assessment of the visible support noted uniform high to severe corrosion of all plates and exposed bolt ends as is expected for steel exposed underwater for extended periods. While direct testing was not conducted on the support it is assumed that their load bearing capacity would be greatly diminished. An evaluation of the overcored FRS, seen in Figure 5.42, observed extreme corrosion along its entire axis including total loss of metal due to extensive pitting in some areas. There was also a build-up of compact mud along the first 0.5m of the bolt due to the deposition and precipitation of suspended and dissolved solids. Pull testing of the bolt proved problematic due to the extensive corrosion and results were not obtainable. However, it can be concluded that all surface support and ungrouted reinforcement that had direct contact with the groundwater has significant corrosion damage that renders it ineffective and rehabilitation is necessary.



Figure 5.42 Severe corrosion of friction bolt and deposition of solids.

5.7 Overcoring at Other Mines

Overcoring was also conducted at the Leinster Nickel Mine and the Olympic Dam Mine. These overcoring projects were focused on the performance of grouted reinforcement in terms of installation and encapsulation quality rather than the evaluation of corrosion damage to the reinforcement. Despite this, useful data was collected about the implications of grouted elements to corrosion attack. Additionally a number of corroded friction rock stabilisers were selected and overcored from each site to provide supplementary data for the previous overcoring campaigns.

5.7.1 Overcoring at Leinster Nickel Mine

Overcoring at the Leinster Nickel Mine was limited to one location, the 9965 level cross cut 27. Located in the felsic volcanoclastic hanging wall near the geological boundary with the ultramafic the area had groundwater with environmental characteristics as described in Section 3.3.7. The age of the reinforcement was approximately three years. The rock mass was highly fractured near the excavation boundary which made recovery of the whole element and rock section difficult.

Two 47 mm galvanised friction rock stabilisers were recovered, however due to the broken rock conditions only one was able to be tested for its load-displacement response. In addition a resin anchored rebar and two cement grouted thread bar were recovered.

Load-displacement results of the tested friction rock stabiliser, shown before testing in Figure 5.43, provided a peak load of 40.2 kN. The load-displacement plot is shown in Figure 5.44. The corrosion damage of the element was moderate to high with a maximum tensile strength of 142 kN. The other recovered friction bolt had a tensile strength of 180 kN. Both elements failed in tension in areas of strong pitting corrosion. Measurements of pitting rate were between 0.22 – 1 mm/year.



Figure 5.43 Recovered 47 mm galvanised friction rock stabiliser.

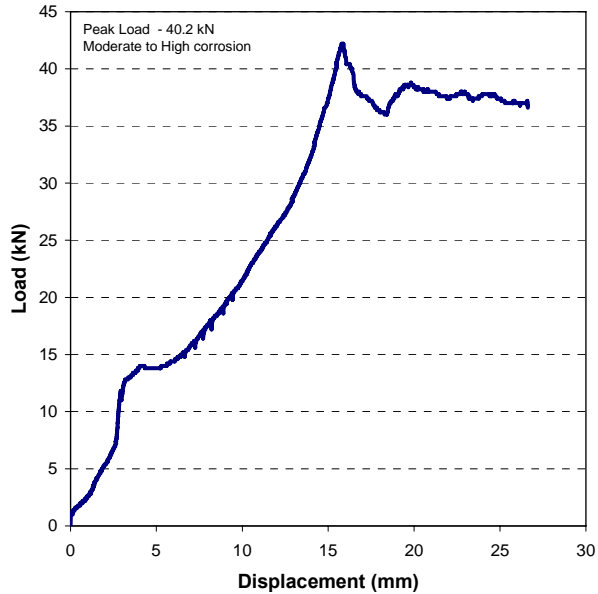


Figure 5.44 Load-displacement plot of a galvanised 47 mm diameter friction rock stabiliser (300 mm embedment length).

The cement grouted solid bars had significant migration of the cement into the broken rock mass as shown in Figure 5.45. This not only allowed a degree of rock mass interlocking, it also provided a greater level of protection of the element from the surrounding environment. An assessment of the corrosion on the elements indicated little corrosion damage.



Figure 5.45 Cement grout migration interlocking a broken rock mass.

5.7.2 Overcoring at Olympic Dam Operations

Overcoring of resin encapsulated bolts at Olympic Dam was done at a wide variety of locations. Galvanised, 47 mm diameter FRS were recovered from two areas the 31 Scarlet 1 and the 32 Jade 2. Both areas were located in the hematite rich breccia and appeared damp with only minor groundwater flow. The installation age at the 31 Scarlet was approximately four years and the 32 Jade six years. The rock mass was highly competent with few fractures. Additionally a CT bolt was recovered.

The recovered friction rock stabilisers had extreme corrosion damage with significant loss of steel as can be seen in Figure 5.46. This level of damage would impact on the ability of the element to perform as intended to such as extent that the reinforcement would be rendered ineffective. Only one sample was able to be pull tested, with the load-displacement plot shown in Figure 5.47. It reached a peak load of 16.5 kN after which the element broke into two pieces in an area of very extreme corrosion damage characterised by a significant loss of steel.

The level of corrosion damage indicates a highly corrosive environment. At the time of overcoring there was only minor water flow; this may not have always been the case, however, previous environmental information is not available. It appears that areas of strong pitting corrosion grow until it consumes the thickness of the bolt, then spreads outwards, joining up with other pits creating large localised areas with no steel remaining. These areas have a very low tensile strength and fail at very low loads, as seen with the tested sample.



Figure 5.46 Extremely corroded friction rock stabilisers recovered from Olympic Dam Mine.

The recovered CT bolt was found to be fully cement grouted inside of the polyethylene tube but had little or no grout on the outside of the tube (see Figure 5.48). This meant any load transfer would involve just the mechanical anchor at the toe of the bolt, making it a point anchored system rather than a fully mechanically coupled, corrosion resistant system as per design. The implications are that the expected design life would be considerably less than originally planned.

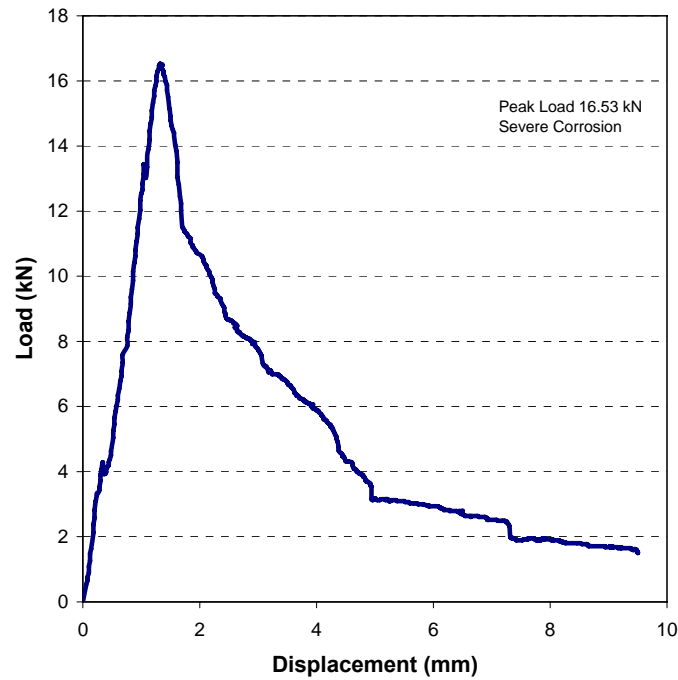


Figure 5.47 Load-displacement plot of galvanised friction rock stabiliser from Olympic Dam operations (300 mm embedment length).



Figure 5.48 Overcored CT bolt with cement grout on the inside of the tube (top) but not outside (bottom).

A number of resin encapsulated elements were overcored and Villaescusa et al. (2006) have documented their quality and performance. It was found that there were significant lengths along the bolt axis where resin was not present or poorly mixed as shown in

Figure 5.49. There was no resin encapsulation in 80% of lengths in the collar region, 31% in the middle region and 30% in the toe region. These areas along the bolt are at a greater risk from corrosion damage as they are not protected from the surrounding environment. It was also observed that resin grout did not migrate into open joints and shears as seen with cement grout. No significant corrosion was seen on the exposed sections but overcoring was not conducted in high corrosion risk areas and the bolt age was less than 1.5 years. With highly corrosive environments already observed at Olympic Dam corrosion related issues may arise in the future.



Figure 5.49 Poor encapsulation of a resin bolt from Olympic Dam Mine.

5.8 Discussion and Conclusions

The ability to examine reinforcement *in-situ* through overcoring provides unparalleled detail in the mechanics relating among the rock mass, the element and the influence of corrosion. For FRS increasing levels of corrosion damage were found to reduce the frictional capacity, thus lowering the load transfer. This is thought to be mainly due to the removal of steel lowering the radial stress the bolt provides against the rock mass. Additionally, corrosion products may provide a plane of slip reducing frictional resistance. The frictional capacity is still well below the tensile strength of the element except in the cases of extreme corrosion. Failure by loss of tensile load appears controlled by the prevalence and severity of pitting corrosion and the interaction of those pits. Generally, corrosion does not appear to impact significantly on the bolt load transfer capacity till it becomes highly corroded.

The extent of corrosion damage was found to be greater on the external surface of the element and more evident near the toe of the bolt. This has implications with the transfer

of load from the unstable section of the rock to the stable section in which the more corroded section of the element is located. Observation from the excavation boundary may fail to detect significant corrosion damage. Additionally the collar (unstable) region has the extra benefit of a plate. Cement grouting of the element protects only the internal surface with the majority of corrosion damage still occurring on the exterior.

Grouted reinforcement provides the best protection of the reinforcement types investigated by providing a barrier to the outside environment. In particular cement grout appears to provide the best encapsulation quality and the grout also migrates into open discontinuities and broken rock masses creating a thicker barrier to any potential groundwater flow. Resin grouted reinforcement assemblies were found to have problems with encapsulation of the element, with significant lengths of the bolt ungrouted. Aside from the issues associated with reduced load transfer in these areas they are also at much greater risk of corrosion damage than the encapsulated regions.

Fully cement grouted reinforcement in mines that have been previously submerged did not exhibit major corrosion damage for sections located within the rock mass. This is opposed to the bolt ends that protrude from the rock, unenclosed reinforcement such as friction rock stabilisers, and surface support which were severely to extremely corroded.

CHAPTER 6 CALCULATION OF CORROSION RATES BY DIRECT TESTING OF COUPONS

6.1 Introduction

A large variety of methods exist to determine the corrosion susceptibility of a given material under specific environmental conditions. These include an array of electrochemical and accelerated corrosion tests; however, the most widely used and simplest method of corrosion monitoring involves the exposure and evaluation of the corrosion in actual test coupons (Dean & Sprowls 1987). This method is cost effective and easy to replicate, and provides the opportunity to test in the environmental conditions under consideration over real time periods. In this study test coupons were placed in the corrosion chambers and underground mining environments, allowing for comparison of the corrosivity of each environment as well as providing practical and relevant corrosion rates.

A benefit of having representative corrosion rates for various environments is the ability to compare between the properties of each environment, helping to define the main influences on the corrosivity. By providing the rates of damage, service lives of reinforcement and support can be estimated. An overview of the aim of the testing, detailing the advantages and limitations, is provided in Section 6.2. The methodology used to prepare, place, clean and evaluate the coupon specimens is described in Section 6.3. The results, including corrosion rates calculated for the specimens placed in the corrosion chambers, are given in Section 6.4, and similarly Section 6.5 provides the results for the coupons placed in the underground environment.

6.2 Aim of testing

The purpose of direct testing of coupons is to establish the corrosivity of various environments and to establish a corrosion rate for a given material. The results from the testing not only allow the comparison of various atmospheric environments or those affected by groundwater but they also provide applicable rates of corrosion. Two types of testing were carried out; the first can be classified as long-term laboratory testing and involves using the test materials in simulated conditions, utilising the corrosion chambers, so that the tests can be closely controlled and unintentional disturbances can be avoided. The second, service tests, places the test materials in the actual service environment, the underground mine.

A limitation with coupon testing is that it is unable to detect rapid changes in corrosivity. This is not thought to be a problem as the environmental properties under investigation are generally slow changing. However, the long exposure times, hundreds of days, can be a disadvantage due to the constantly changing nature of underground mines that may alter the surrounding environment, restrict access to previous development and in some cases destroying the samples. The main advantage is that actual corrosion rates are established and are not estimated as in the case of laboratory accelerated tests. The longer the time of exposure the closer the rates of corrosion are to the actual long-term rates.

The material used for the coupons is a HA300 grade steel and is not the same as the HA350 grade used in the manufacture of friction rock stabilisers, although its properties are similar. It was chosen as it was the closest available grade in sheet form. Coupons were placed in all corrosion chambers for up to 282 days. The placements of samples in underground mines were tailored to suit each individual site, and differed in terms of environments investigated and time of exposure. As already discussed some samples placed at the mine sites were damaged or were unable to be collected.

6.3 Methodology

The preparation, placement, cleaning and evaluation of the corrosion coupon specimens was conducted to ASTM standard G4 that was designed to provide guidance for this type of testing (ASTM G1-90 1999). The coupons were obtained from a hot-rolled sheet of carbon steel grade HA300, with a chemical composition shown in Table 6.1. The 1000x2000x0.6 mm sheet was guillotined into rectangular test specimens of 120x30x0.6 mm dimensions. Two 2 mm diameter holes were drilled in the upper left and right corners for the identification tags to be attached following measuring and weighing. To ensure an exact and reproducible finish, each coupon was sand blasted using silica grit (see Figure 6.1). The coupons were then rinsed with distilled water, followed by acetate, cleaned with tissue paper and allowed to dry on paper towels.

Following the drying process each coupon was measured to the third significant figure and weighed to the fifth significant figure. The identification tags, which were uniquely designed to survive the corrosive conditions, were attached to the coupon with cable ties. The tags consisted of a plastic key ring which had an identification code melted into it by a soldering iron. Each code described the proposed location of the coupon and an identification number. The corrosion coupons were then placed in an airtight sealed plastic bag ready to be placed.

Table 6.1 Chemical composition and mechanical properties of HA300 grade steel.

Steel Grade	Chemical composition (% Max.)					Minimum upper yield stress (MPa)	Minimum tensile strength (MPa)
	Carbon	Silicon	Manganese	Phosphorus	Sulfur		
HA300	0.20	0.35	1.60	0.040	0.030	300	400

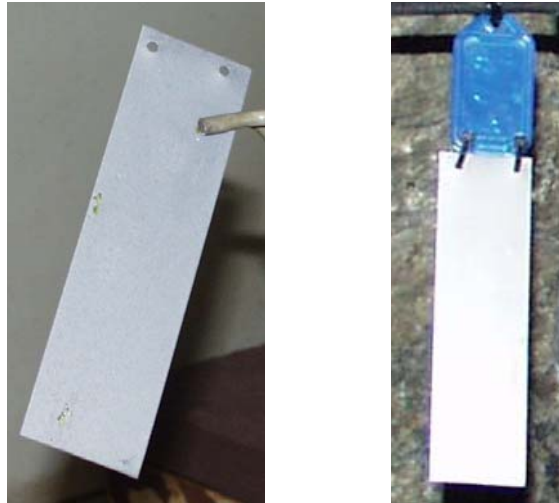


Figure 6.1 Coupon following sand blasting (left) and fitted with identification tag (right).

Placement of the coupons occurred as soon after preparation as possible; in the case of the WASM corrosion chambers it was immediately after. For some mine sites a time lapse of 2-4 weeks was experienced before placement, however, as the bags were airtight no corrosion occurred. In the corrosion chambers the coupons were attached to the dripping reticulation by a cable tie. At the mines, locations were selected based on the environmental conditions with areas that were more concealed preferred to prevent interference with the experiment. The coupons were placed by cable ties to available surface support such as weld mesh as shown in Figure 6.2. As the coupons were placed at the excavation boundary and not inside the rock mass they may underestimate the actual corrosion rate.



Figure 6.2 Placement of corrosion coupons in an underground environment.

Three coupon specimens were collected from each location for each time period. The cleaning and evaluating were conducted as soon as possible but as some specimens were mailed from the mine sites some delay was inevitable. In these cases the mine personnel were instructed to ensure the coupons were completely dry before sending. Collected corrosion coupons from two different mining environments are shown in Figure 6.3. To clean the coupons they were firstly mechanically cleaned of any loose corrosion or salt products and the identification tag removed. They were then placed in an acidic solution treated with antimony trioxide and stannous chloride that removed any corrosion products and left intact the remaining non-corroded steel. The cleaned specimens were then washed with distilled water and acetate, wiped clean and allowed to dry. The coupons were then re-weighed to determine the mass loss.



Figure 6.3 Corrosion coupons collected from Enterprise Mine after 213 days in an atmospheric environment (left) and from Cannington Mine after 354 days in a groundwater affected environment (right).

To calculate the corrosion rate the initial total surface area of the specimen and the mass loss during the tests are determined. The average corrosion rate may then be obtained as follows:

$$\text{Corrosion Rate (mm/yr)} = (K \times W) / (A \times T \times D) \quad (6.1)$$

Where:

K = constant to derive appropriate units, for millimetres per year use 8.76×10^4 ,

W = mass loss of coupon in grams,

A = area of original coupon in cm^2 ,

T = time of exposure in hours, and

D = density of the steel in g/cm^3 (7.86 g/cm^3).

6.4 Results from the Corrosion Chambers

The coupons placed in the corrosion chambers provide a very good assessment of the corrosivity of the respective groundwaters. As each chamber maintained relatively consistent environmental conditions, including flowing water the only significant difference was in the groundwater conditions that were being measured. These conditions, shown in Table 6.2, differ slightly from those in Section 4.2.1 as they were averaged from measurements taken only during the duration of the coupon testing. Strong water flow is considered the worst case scenario for corrosive conditions. The coupons were completely covered by the flowing water for the entire duration of the test and are more indicative of worst case conditions inside the rock mass with strongly flowing water than the coupons tested in the field on the excavation boundary. The coupons were tested for mass loss at 94 days, 180 days and 282 days. The corresponding rates of corrosion are shown in Table 6.3. Due to the high rates of corrosion experienced by some chambers the coupons were completely oxidised by the 180 or 282 day test and no results could be obtained.

The reduction in the rate of corrosion over time for each chamber is seen to be reasonably constant. On average a reduction in the corrosion rate from the 94 day to the 180 day test by a factor of 1.34 and from the 94 day to the 282 day test a reduction of 2.26 is seen. These reduction factors are used to extrapolate data from the Enterprise, Leinster and Darlot chambers to provide estimates of corrosion rates for the 282 day test and from the Enterprise and Leinster chambers for the 180 day test. These estimated results are shown in italics in Table 6.3 and denoted by dashed lines in Figure 6.4.

The most corrosive environment was for the Enterprise chamber. This was followed in descending order of corrosivity by the Leinster, Darlot, Kundana, Olympic Dam and Argo chambers. This order of corrosivity was observed, where results were obtainable, for the 180 and 282 day test. Also observed is a reduction in the corrosion rate for the later tests. It can be assumed that the 282 day corrosion rate calculation is close to the long-term corrosion rate.

Table 6.2 Groundwater conditions in the corrosion chambers for the duration of the coupon testing.

Chamber	Dissolved Oxygen (mg/l)	TDS (ppm)	pH pH units	Temperature (°C)
Enterprise	4.10	6,720	7.50	35.2
Leinster	3.74	13,200	7.32	27.4
Darlot	3.20	43,837	7.50	26.7
Kundana	2.44	86,612	7.40	26.9
Olympic Dam	2.45	46,044	7.90	27.0
Argo	1.73	171,000	7.22	27.4

Table 6.3 Rates of corrosion for coupons in the corrosion chambers.

Chamber	Corrosion Rate (mm/yr)			Groundwater flow
	94 days	180 days	282 days	
Enterprise	1.32	<i>0.99</i>	<i>0.58</i>	strongly flowing
Leinster	1.19	<i>0.90</i>	<i>0.53</i>	strongly flowing
Darlot	0.85	0.67	0.38	strongly flowing
Kundana	0.41	0.31	0.20	strongly flowing
Olympic Dam	0.33	0.24	0.12	strongly flowing
Argo	0.08	0.05	0.04	strongly flowing

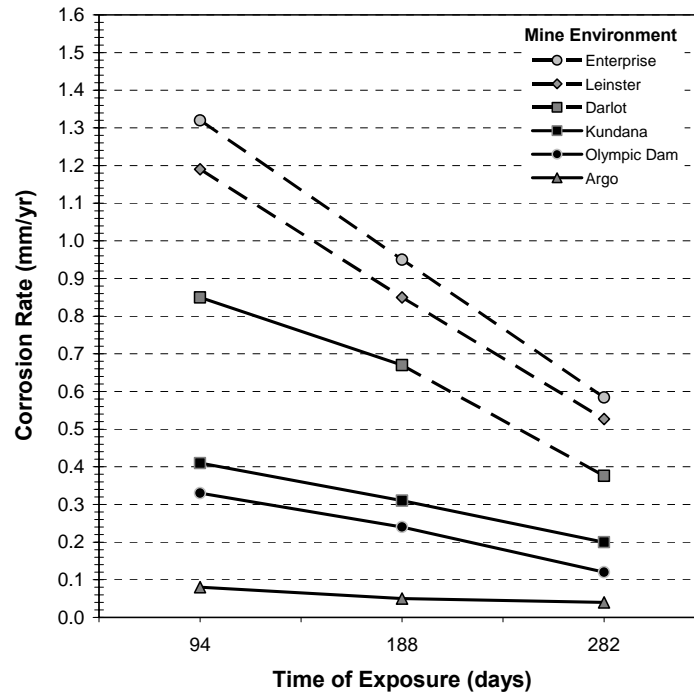


Figure 6.4 Corrosion rates for each WASM chamber over time.

6.5 Results from Testing in Underground Mines

The calculation of corrosion rates by the coupon method does not exactly replicate the conditions of rock reinforcement as the coupons are not located within the rock mass. However, these are the closest results to actual rates of corrosion in such environments that were studied. A brief description of the actual environmental conditions where the coupons were placed is provided in this Section. A more detailed discussion on the environmental conditions, including the groundwater and atmospheric quality has already been summarised in Chapter 3. A number of issues also arose when conducting the experiments in a working mine that meant some or no coupons were recovered or recovered intermittently. Mining activities are such that access is limited and in some cases it can be lost during the experiment.

6.5.1 Argo Mine

Five sites were selected on or near the South decline. The results are presented in Table 6.4 and Figure 6.5. The three sites with groundwater were wet and the remaining two were located in dry ventilation with low temperatures and humidities. The groundwater affected regions had rates of corrosion between 0.015-0.034 mm/yr after 445 days, which is taken to be the long-term corrosion rate. Over the same time period the determined atmospheric corrosion rate ranged between 0.003-0.004 mm/yr. Generally the rates of corrosion stayed relatively constant.

Table 6.4 Rates of corrosion in selected environments at Argo Mine.

Location	Environment	Corrosion Rate (mm/yr)				Groundwater flow
		97 days	253 days	349 days	445 days	
South decline #1	Damp, wet area, salt deposition	0.022	0.021	0.030	0.034	wet
South decline #2	Damp, wet area, salt deposition, coupon bent 90°	0.070	0.017	0.024	0.027	wet
Sump 2	Damp/wet area	0.004	0.014	0.011	0.015	wet
South S/P 3	Dry atmosphere no groundwater	0.012	0.008	0.004	0.004	dry
Sump 3	Dry, relatively fresh atmosphere	0.004	0.004	0.006	0.003	dry

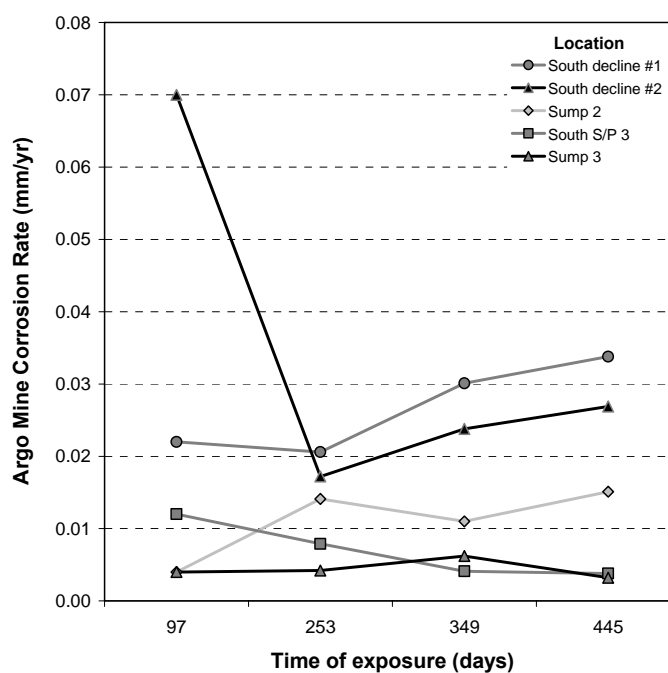


Figure 6.5 Corrosion rates from coupons for each location at the Argo Mine.

6.5.2 Cannington Mine

Three locations were chosen that had groundwater flow, with two, the 550 51XC and the 520 Va 53 located on the surface of the Hamilton Fault, with large volumes of flowing water. The 296 sf66 monitoring site had a lower rate of flow and can be termed dripping. The long-term rate of corrosion is calculated to be 0.151 mm/yr for the Hamilton fault region and 0.133 mm/yr for the 296 sf66. Corrosion rates for two different atmospheres were calculated. The hot and humid atmosphere had rate of 0.17 mm/yr, more than double that of the fresher atmosphere (0.008 mm/yr). The full results are shown in Table 6.5 and Figure 6.6.

Table 6.5 Rates of corrosion in selected environment at Cannington Mine.

Location	Environment	Corrosion Rate (mm/yr)				Groundwater flow
		116 days	223 days	354 days	620 days	
550 51XC	Hot, humid & high groundwater flow	-	0.283	0.125	0.151	flowing
520 Va 53	Hot, humid & high groundwater flow	0.184	-	-	-	flowing
295 sf66	Hot, humid with groundwater	-	-	-	0.133	dripping
295 sf66	Hot and humid atmosphere	0.044	0.040	0.023	0.017	dry
475 Ug 53	Fresh, moderately dry atmosphere	0.002	0.002	0.008	-	dry

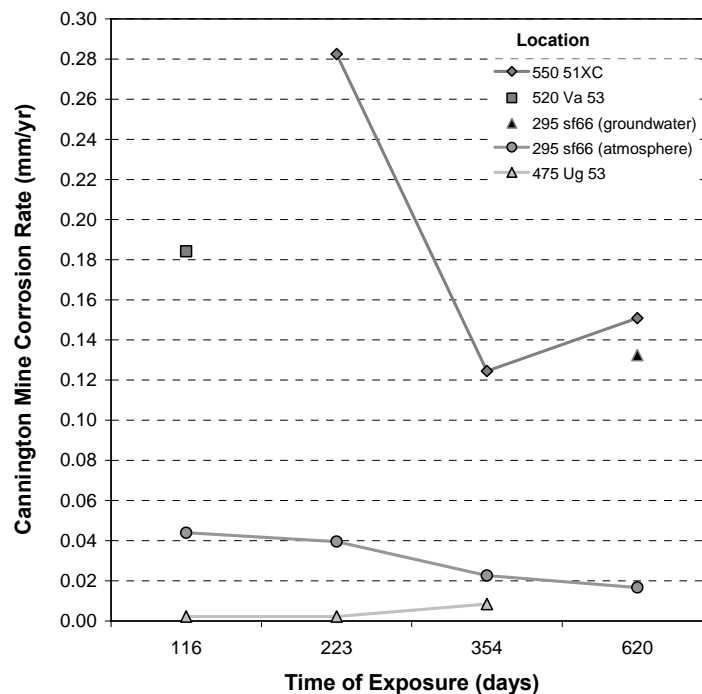


Figure 6.6 Corrosion rates from coupons at each location at Cannington Mine.

6.5.3 Enterprise Mine

Due to an absence of groundwater and the long expected mine life the testing at the Enterprise Mine concentrated on a range of atmospheric environments ranging from very hot ($>35^{\circ}\text{C}$) and humid (90%), fresh ventilation and return airways. The results presented in Table 6.6 and Figure 6.7 show a variation in long term atmospheric corrosion rates from 0.0035 to 0.0175 mm/yr. The greater corrosion as expected occurred in the hot, humid atmospheres located in secondary ventilation. Surprisingly, the lowest rate took place in the area of assumed highest pollutants, the return air way. This area has high air flow velocities and subsequent low air temperatures and more importantly low humidity.

Table 6.6 Rates of corrosion in selected environments at Enterprise Mine.

Location	Environment	Corrosion Rate (mm/yr)		
		111 days	213 days	371 days
30A	Hot and humid atmosphere	0.0524	0.0253	0.0175
26B	Very hot (35°C) and humid (90%) atmosphere	0.0254	0.0165	-
29E S705	Hot and humid atmosphere	0.0015	0.0034	0.0075
28D	Hot and humid atmosphere	0.0126	0.0094	0.0066
21C WS	Fresh ventilation, low pollutants	0.0009	0.0034	0.0059
31C	Return Air Way, high pollutant content	0.0069	0.004	0.0035

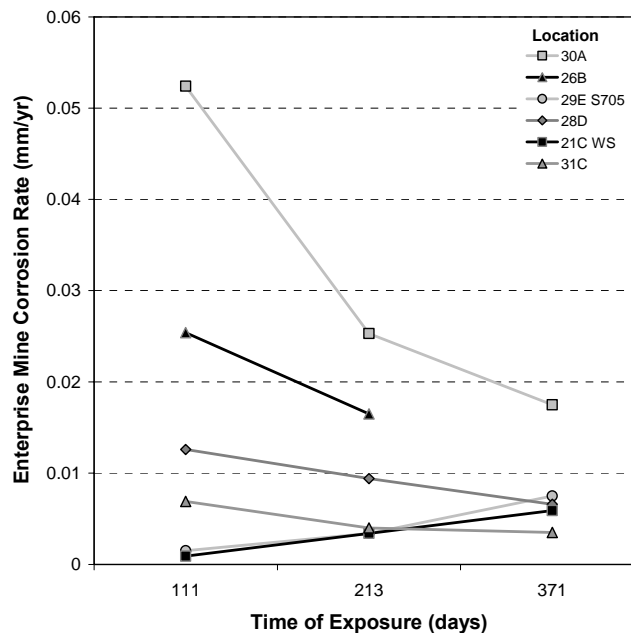


Figure 6.7 Corrosion rates from coupons for each location at Enterprise Mine.

6.5.4 Olympic Dam Mine

Only one time period was tested at the Olympic Dam mine due to problems with access to the sites. The results of the 357 day test, shown in Table 6.7, can be considered the long-term corrosion rate. Rates between 0.026 to 0.048 mm/yr were calculated for the groundwater affected environments, with the higher rates in the wet areas. A rate of 0.003 mm/yr was measured for coupons placed in a well ventilated, low humidity and moderate temperature drive.

Table 6.7 Rates of corrosion in selected environments at Olympic Dam Mine.

Location	Environment	Corrosion Rate (mm/yr)	Groundwater flow
		357 days	
31 Yellow 10	Dripping groundwater	0.048	wet
34 Cyan 19	Dripping groundwater	0.040	wet
26 Jade 302	Damp/dripping groundwater	0.026	damp
41 Amber 137	Fresh ventilation	0.003	dry

6.6 Discussion and Conclusions

Rates of corrosion have been calculated for a range of atmospheric and groundwater affected environments. This is thought to be the first time this has been achieved for Australian underground hard rock mines. In general there is a reduction in the rates over time as the products of corrosion, the iron oxides, protect to some extent the underlying steel from further corrosion. This reduction becomes less pronounced with increasing exposure times and long-term corrosion rates can be established. The length of time needed to establish the long-term rate is dependent on the environment, but approximately 200-300 days are required.

For atmospheric environments the corrosion rates ranged from 0.003 mm/yr for low temperature and humidity ventilation (fresh atmospheres), through to a peak of 0.0175 mm/yr for hot and humid conditions. Similar rates were observed in different mines with comparable temperatures and humidities. Rates measured in return air ways, expected to contain the highest levels of pollution, were comparable to the fresh atmospheres. It is

concluded that air temperature and humidity influence the corrosivity of an atmosphere significantly more than the level of pollutants.

For the field testing conducted in groundwater affected areas the rates ranged from 0.015 mm/yr to 0.151 mm/yr. It is likely that the field tests conducted on the excavation boundary underestimated the actual corrosion rates, as they were not located inside the rock and would have had less interaction with any water available. This is more pronounced for the flowing rock masses as the volumes of water are much greater. Despite being a simulated environment it is considered the corrosion chamber results are representative of a flowing rock mass as they were continually immersed in flowing water for the entire test duration.

The irregularity of the groundwater properties and flow rate observed during the underground *in-situ* tests provided a range of results but difficulty in ascertaining which variables influence the corrosivity. Fortunately, the controlled environments in the corrosion chambers with the periodic analyses of the water properties has meant that the results from the chamber tests can be used to establish the links between the measured water properties and the corrosivity.

CHAPTER 7 CORROSIVITY CLASSIFICATIONS FOR AUSTRALIAN UNDERGROUND MINES

7.1 Introduction

The completion of a systemic field study of environmental conditions combined with the direct measurements of corrosion rates has provided the information with which to classify the underground mining environment corrosivity in terms of its environmental properties. Two environments are of interest, those that are influenced by groundwater and those that are affected only by atmospheric variables. A major aim of this study is to classify an underground environment in terms of its properties and establish an approximate corrosion rate.

This chapter describes the analyses of the data collected in this project to establish a corrosivity classification for both groundwater-affected and atmospheric environments. Current published classifications are reviewed to ascertain their relevance. Relationships between the main environmental properties and the measured corrosion rates are determined and new classifications for both groundwater- affected and atmospheric environments are proposed.

7.2 Groundwater corrosivity classification

The main cause of corrosion in underground mines has been established by this study to be due to the influence of groundwater. The inter-related groundwater properties, primarily pH, TDS, dissolved oxygen and temperature, control the corrosivity of the water. Large variations in their concentrations occur across the investigated underground mines. For environments with groundwater the influence of atmospheric variables is negligible and they are not considered. Additionally, the amount of corrosion damage

sustained by support and reinforcement is further influenced by the rate of groundwater flow and the period of time it is installed in the environment.

A variety of published corrosivity classifications are available. The main classifications have been reviewed and the relevance of each to the underground mining environment is determined from the data collected by the coupon tests. By inputting the environmental conditions of the corrosion chambers into the classifications and comparing their proposed corrosivity with the actual measured 94 day corrosion chamber corrosion rates from Chapter 6, the practicability of each classification is established. To provide a clear understanding of the principles at work relationships between the groundwater properties and the measured corrosion rates from the corrosion chambers are also investigated to develop an appropriate corrosion classification for groundwater affected hard rock mining environments in Australian underground mines.

7.2.1 Soil corrosion classifications

The probability of corrosion of metals in soil has been widely researched with numerous classifications (AWWA C105 1998; DIN 50929-3 1985). Parameters that are usually examined include groundwater, degree of aeration, pH, redox potential, resistivity, soluble ionic species, the horizontal and vertical homogeneity (i.e. the difference in soil structure), and microbiological activity. Despite some similarities in the controlling parameters the different material and chemical properties of soil means soil corrosivity classifications are not practical to be used in hard rock environments.

7.2.2 Saturation indices

Water saturation indices relate the solubility of dissolved ions to their tendency to precipitate. One of the most notable is the Langelier Saturation Index (LSI), which is an indicator of the degree of saturation of water with respect to calcium carbonate. The LSI is defined as the difference between the measured pH, and the calculated pH at saturation of calcite or calcium carbonate (see Appendix D). If LSI is negative, then there is no potential to scale, as the water will dissolve the calcium carbonate. If the LSI

is positive, then scale can form and calcium carbonate precipitation may occur protecting the metal from corrosion attack.

LSI values for the sampled mine groundwaters shown in Table 7.1 indicates that only three mines show the potential for scale to form, thus the potential to protect the metal. An example of the calculation of the LSI values is shown in Appendix D. When compared with the measured corrosion chamber corrosion rates, shown in Figure 7.1, no relationship between the LSI and the measured corrosion rate could be established for the hard rock environmental data studied here. The LSI parameter is related to the stability of scale formation, not an indicator of corrosivity. It omits all other factors associated with water corrosivity including dissolved oxygen, temperature, dissolved ions and rate of flow. The potential for carbonate scale is also ineffective above a critical value of chloride concentration, approximately 25 ppm (Sastri, Hoey & Revie 1994). It must be noted that all mine groundwaters analysed had chloride contents well above this low value. Protective carbonate scaling will not form in Australian underground mine groundwaters regardless of the LSI and should not be included in any classification scheme.

Table 7.1 LSI ratings for studied Australian underground mine groundwaters.

Chamber	LSI rating	Potential to Scale
Enterprise	-0.42	No potential to scale
Leinster	-0.87	No potential to scale
Darlot	0.36	Scale can form
Kundana	0.33	Scale can form
Olympic Dam	1.14	Scale can form
Argo	-0.76	No potential to scale

7.2.3 Groundwater corrosion classification – DIN 50929-3

The German originated DIN 50929 classification (DIN 50929-3 1985) assesses the corrosive potential of water based on the water type, its location relative to the water/air interface, the chloride and sulphate content, acidity, calcium ion content, and pH (see Appendix D). Each parameter is given a positive or negative numerical rating based on the effect it has on the corrosivity. The ratings are then summed to obtain the probability

of corrosion for either unalloyed iron (W_I) or galvanised steel (W_L). The more negative the number, the more corrosive the water. The classification is separated into four corrosivity levels with the most corrosive group having a W_I less than -8 with a qualitative corrosion description and assessment on the coating quality.

The calculated ratings for the groundwaters, shown in Table 7.2, depict W_I values that all fall in the same maximum corrosion category, described as medium corrosion, despite the input parameters having a wide range of values. Many of the ratings are much lower, by a factor of two to three, than the -8 boundary. This classification does not distinguish between the different mine groundwaters and groups all environments in the same category. Additionally, when comparing the ratings with the corrosion chamber corrosion rates (see Figure 7.2) no correlation is observed. Appendix D provides an example of the calculation of the W_I and W_L values.

As well as being unable to distinguish between the corrosivity of the mine groundwaters the classification also takes into account parameters that are not relevant to the waters under investigation. Protective scaling due to calcium carbonate formation is not expected to influence the corrosivity of the waters. In addition the classification does not account for the effect of temperature or dissolved oxygen, both of which appear to control to some extent the corrosion potential of mine groundwaters in Australia. On a positive side, the classification does consider if the water is flowing, but not the rate at which it flows.

Table 7.2 DIN 50929 corrosion classification ratings for Australian underground mine groundwaters.

Chamber	W_I	General corrosion	W_L	Quality of coatings
Enterprise	-12	Medium	-6	Satisfactory
Leinster	-18	Medium	-8	Satisfactory
Darlot	-16	Medium	-8	Satisfactory
Kundana	-16	Medium	-8	Satisfactory
Olympic Dam	-12	Medium	-7	Satisfactory
Argo	-22	Medium	-10	Not adequate

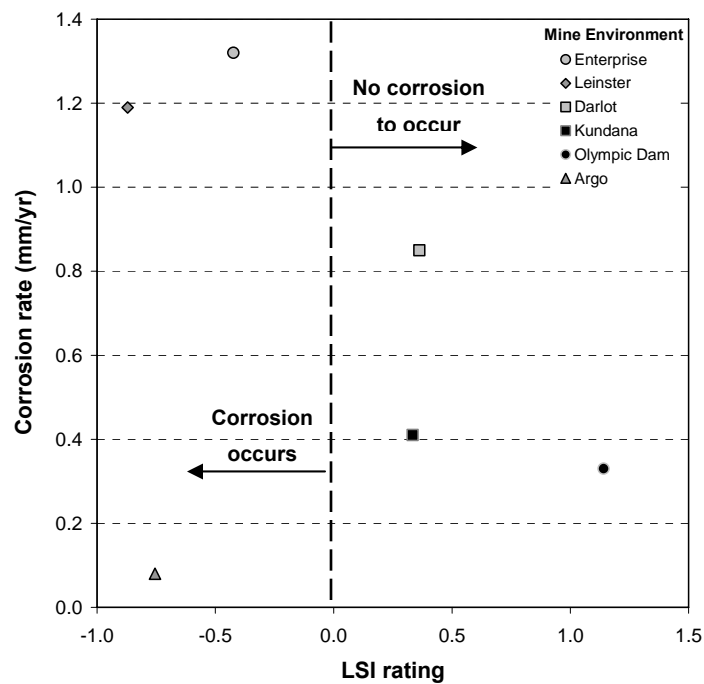


Figure 7.1 Comparison between the calculated LSI rating and the corrosion chamber corrosion rates.

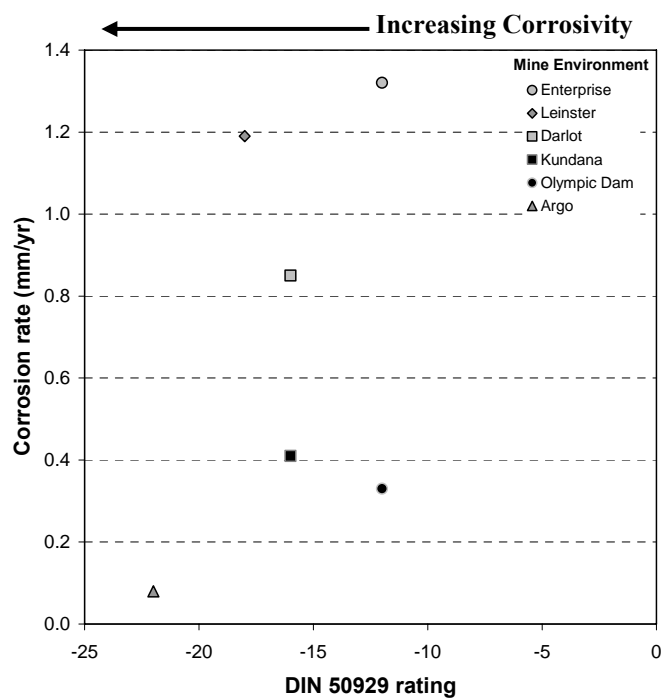


Figure 7.2 Comparison between the calculated DIN rating and the corrosion chamber corrosion rates.

7.2.4 Wet underground rock corrosion classification – Li and Lindblad (1999)

Li & Lindblad (1999) have proposed a corrosivity classification for the underground environment with relation to the corrosion of steel rock bolts in wet conditions. The main corrosion-related parameters used are pH, dissolved oxygen and resistivity. The ambient temperature, rock mass quality and precipitation of calcium carbonate are termed influencing parameters and have less effect on the final rating which is expressed as W_{wet} . The value is graded into four classes ranging from 2 to 10, with values greater than 10 being placed in the very severe corrosion category (see Appendix D).

The ratings for the classification when applied to the corrosion chamber data are shown in Table 7.3. All groundwaters fall in the very severe corrosion category. When comparing the ratings with the corrosion chamber corrosion rates, as displayed in Figure 7.3, no association is observed. The temperature of the water, despite being described as an influencing factor, has a strong weighting on the final rating. The groundwater with the highest rating, Enterprise, also had the highest temperatures. The remaining waters had similar temperatures and subsequently similar ratings.

The Li & Lindblad (1999) corrosion classification was developed for Northern European conditions where the average water temperature is much less than the conditions experienced in Australia. Thus it tends to substantially overestimate the influence of temperature on the corrosivity of the groundwater. Despite the shortcomings of the classification it does take into account the rock mass quality through the use of the rock mass classification, Rock Mass Rating (RMR).

Table 7.3 Li and Lindblad (1999) corrosion classification ratings for Australian underground mine groundwaters.

Chamber	W_{wet}	Corrosion Description	Corrosion Rate (mm/yr)
Enterprise	28.7	Very severe corrosion	>0.30
Leinster	14.6	Very severe corrosion	>0.30
Darlot	13.9	Very severe corrosion	>0.30
Kundana	14.1	Very severe corrosion	>0.30
Olympic Dam	14.2	Very severe corrosion	>0.30
Argo	12.5	Very severe corrosion	>0.30

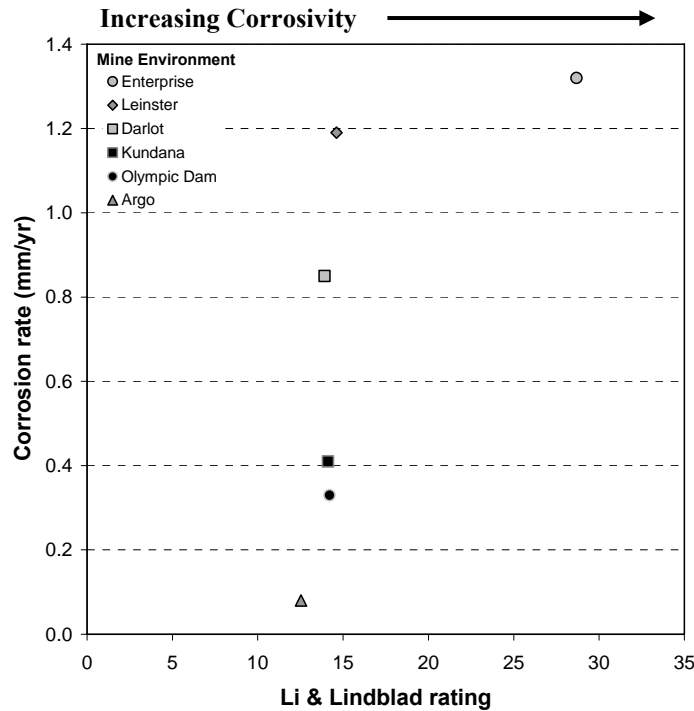


Figure 7.3 Comparison between the calculated Li & Lindblad (1999) rating and the corrosion chamber corrosion rates.

7.2.5 The main groundwater properties and the measured corrosion rate

A review of the existing corrosion classifications revealed that none adequately fit the experimental data and could not be readily used to predict the corrosivity of groundwater affected environments examined in this study. It was therefore necessary to examine each of the main groundwater properties individually to ascertain their influence. As previously stated in Chapter 2 corrosion of steel is independent of pH values between 4 and 10. All the natural groundwaters sampled had a pH in the range of 6.2 to 8.3. Therefore it can be assumed that pH has limited effect within this study. The remaining properties; temperature, TDS and dissolved oxygen, were examined using the same data used with the previously described classifications.

No relationship between the corrosion chamber 94 day corrosion rate and the average temperature, shown in Figure 7.4, was observed. A good exponential relationship exists between the TDS of the water and the corrosion rate (see Figure 7.5). The higher TDS

waters result in a lower corrosion rate presumably as the higher TDS waters reflect a lowering dissolved oxygen concentration. This is confirmed when observing the very good direct linear relationship that exists between the dissolved oxygen and the measured corrosion rates displayed in Figure 7.6. The higher dissolved oxygen content results in increased rates of corrosion as oxygen is essential for the electrochemical reaction to take place.

There is a clear indication shown by the correlation with the experimental values from the corrosion chamber coupon testing that the corrosivity of the groundwaters can be directly estimated from the dissolved oxygen concentration of the water. This theorem is further reinforced when it is considered that the dissolved oxygen content has already been shown in Chapter 3 to be directly related to the temperature and salinity of the water. Thus with one parameter all three are taken into account. The good correlation with the TDS and the corrosion rates is partly due to the temperature values being similar and having a comparable effect on the corrosion rate.

The measurement of the dissolved oxygen content can be used to establish the corrosive potential of groundwater in Australian underground mines. However, by itself it cannot be used to determine a rate of corrosion. Two other factors need to be considered; the influence of time and the rate of groundwater flow.

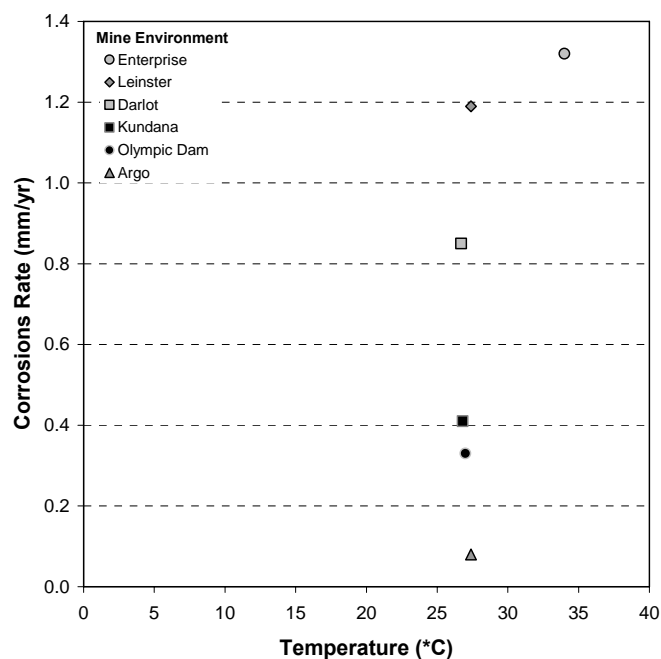


Figure 7.4 Relationship between the corrosion chamber corrosion rates and the temperature of the groundwater.

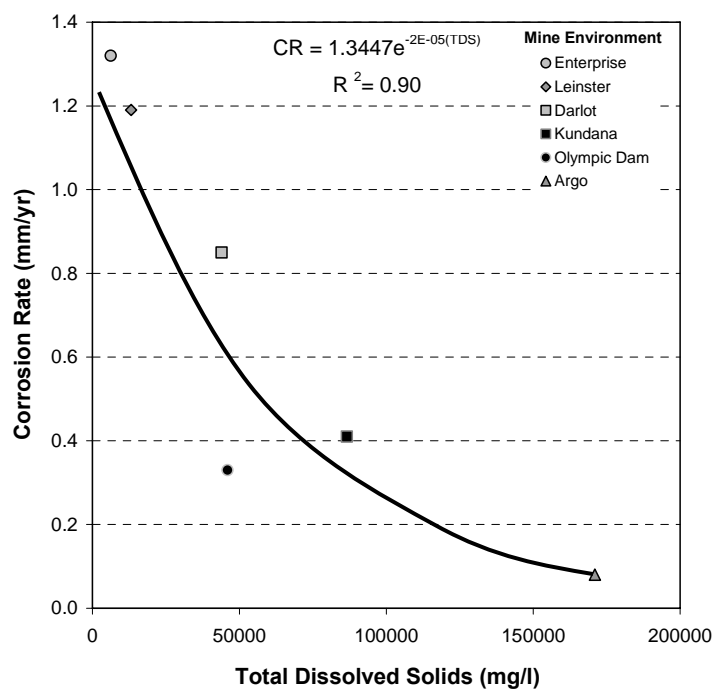


Figure 7.5 Relationship between the corrosion chamber corrosion rates and the TDS of the groundwater.

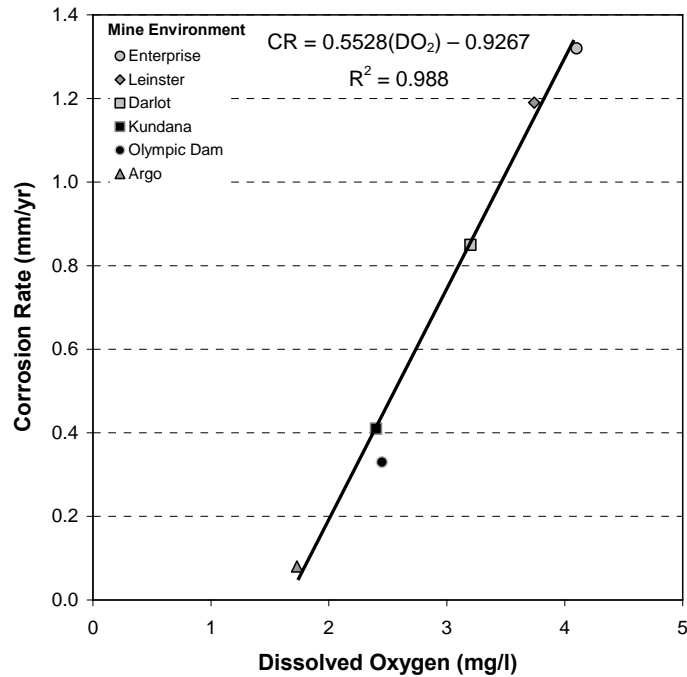


Figure 7.6 Relationship between the corrosion chamber corrosion rates and the dissolved oxygen content of the groundwater.

7.2.6 The influence of time

In general there is a reduction in the rate of corrosion over time as corrosion products partly inhibit further corrosion. This rate becomes constant after a certain period of time, dependent upon the environmental conditions. The information presented in Figure 7.7 is of the coupon test data from the corrosion chambers against the dissolved oxygen content, which remained more or less constant for the duration of the test. The Argo chamber had a decrease of 50% in the rate of corrosion from the 94 day test to the 282 day test with the Kundana chamber showing a 51% decrease and Olympic Dam chamber a 64% decrease over the same time period. This represents a relatively constant reduction for the different groundwater types. Coupon results that were not obtainable from these tests due to high corrosion rates fully consuming the steel have been estimated in Chapter 6. The 282 day rate is more representative of the long-term corrosion rate than any calculated for previous time periods.

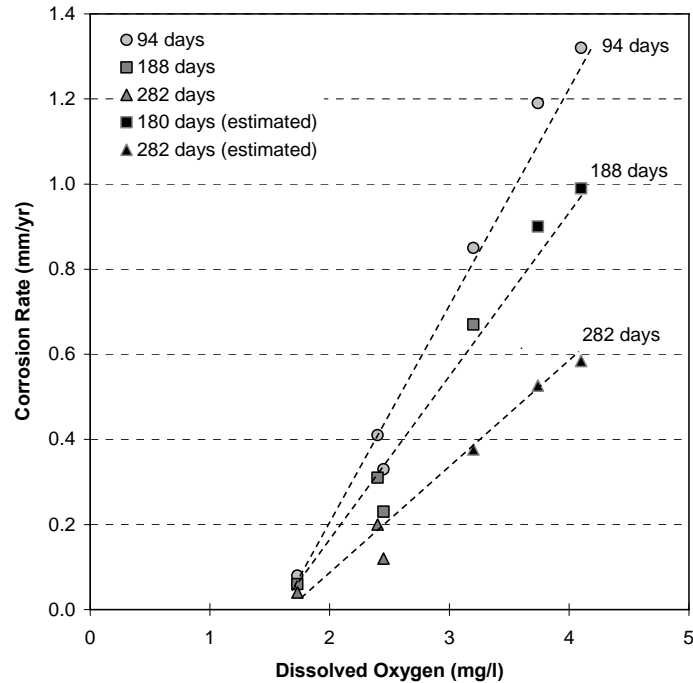


Figure 7.7 Comparison of the coupon tests results for the corrosion chambers over time.

The data collected from the coupon tests on mine sites, previously discussed in Chapter 6, showed a greater variability in time taken for corrosion rates to become constant. However, after approximately 300 days the rate of corrosion becomes reasonably regular. It is therefore concluded that the long-term corrosion rate can be taken from coupon tests results of a minimum of 250-300 days. Any corrosion rate used in design should only be the long-term corrosion rate.

7.2.7 The influence of the groundwater flow rate

The rate of groundwater flow affects the corrosion rate by two processes. Increases in the flow rate simultaneously increase the rate at which dissolved oxygen is brought in contact with the steel surface. This provides more available oxygen for the electrochemical process and thus higher rates of corrosion occur. Higher flow rates also increase the level of physical erosion of the corrosion products and reduce the thickness of the partially protective cover increasing the corrosion rate.

To investigate the effect of flow rate the coupon test results conducted at the mine sites, which had various rates of flow, are compared with those of the chambers. The water properties are comparable and a similar time of exposure periods is examined. Coupons from the Argo chamber (flowing) had a higher corrosion rate by a factor of 3.5-4 times that of the mine site results (wet). Similarly the Olympic Dam chamber results (flowing) had a higher corrosion rate by a factor of 2.5-3 compared with the field results for a wet rock mass and 4.5 time increase compared to a damp rock mass.

The expected increase in corrosion rates with increasing water flow is observed in the experimental data. If all the long-term corrosion rates, for both the chamber and field tests are plotted against dissolved oxygen they can be grouped based on their respective groundwater flow conditions as shown in Figure 7.8. Despite the small data set, changes in the corrosion rate can be seen for dissimilar groundwater conditions.

The evaluation of groundwater flow conditions is qualitative, thus a range of variability with the results is expected. This is seen by comparing the flowing conditions in the chambers with the flowing conditions in the field. Those coupons in the chambers had much higher rates of corrosion. This is attributed to not only the qualitative measure of groundwater flow but also the positioning of the coupons in the field on the excavation boundary where the actual flow over the coupons is less than in the rock mass. This issue affects all field test results but is believed more pronounced for flowing conditions due to the greater volumes of water.

Therefore, the coupon results from the mine sites will tend to underestimate the actual corrosion rates and this is required to be taken into account. By contrast the results from the corrosion chambers were in ideal conditions and are considered to be from the upper end of corrosion rates for a flowing rock mass while those from the field are considered to be from the lower end of expected rates. Following the evaluation of the coupon data and re-evaluating the groundwater flow conditions at the mine sites it is considered necessary to divide the flowing groundwater section into strongly flowing and flowing.

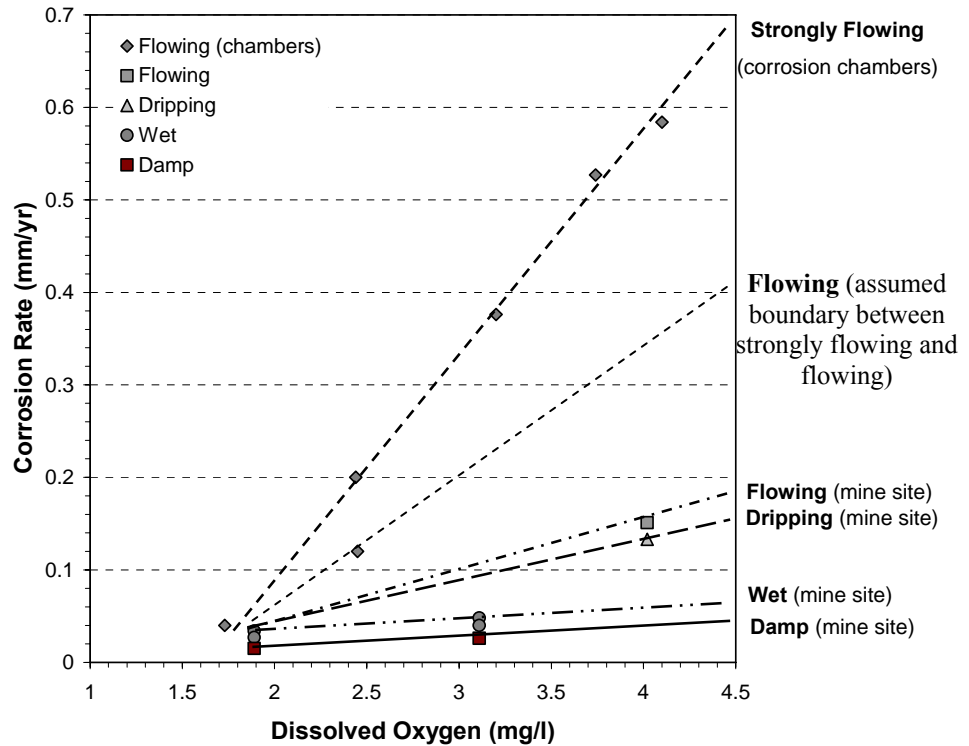


Figure 7.8 Corrosion coupon test data from the field and chambers grouped by water velocity.

7.2.8 Corrosivity Classification for Underground Hard Rock Environments

Currently available classifications have been shown to be inadequate for the groundwater affected, hard rock conditions found in Australian underground mines. A new classification is proposed based on the comprehensive data collection survey and the calculation of corrosion rates by coupon testing undertaken as part of this study. The corrosivity classification for groundwater affected, hard rock environments is shown in Figure 7.9, with Table 7.4 presenting the information in tabulated form. The classification considers two factors in determining the corrosivity; the groundwater dissolved oxygen content as measured *in-situ* from a dissolved oxygen probe and the groundwater flow conditions as described in Table 7.5. Uniform corrosion rates for HA300 grade steel can then be estimated for different environments.

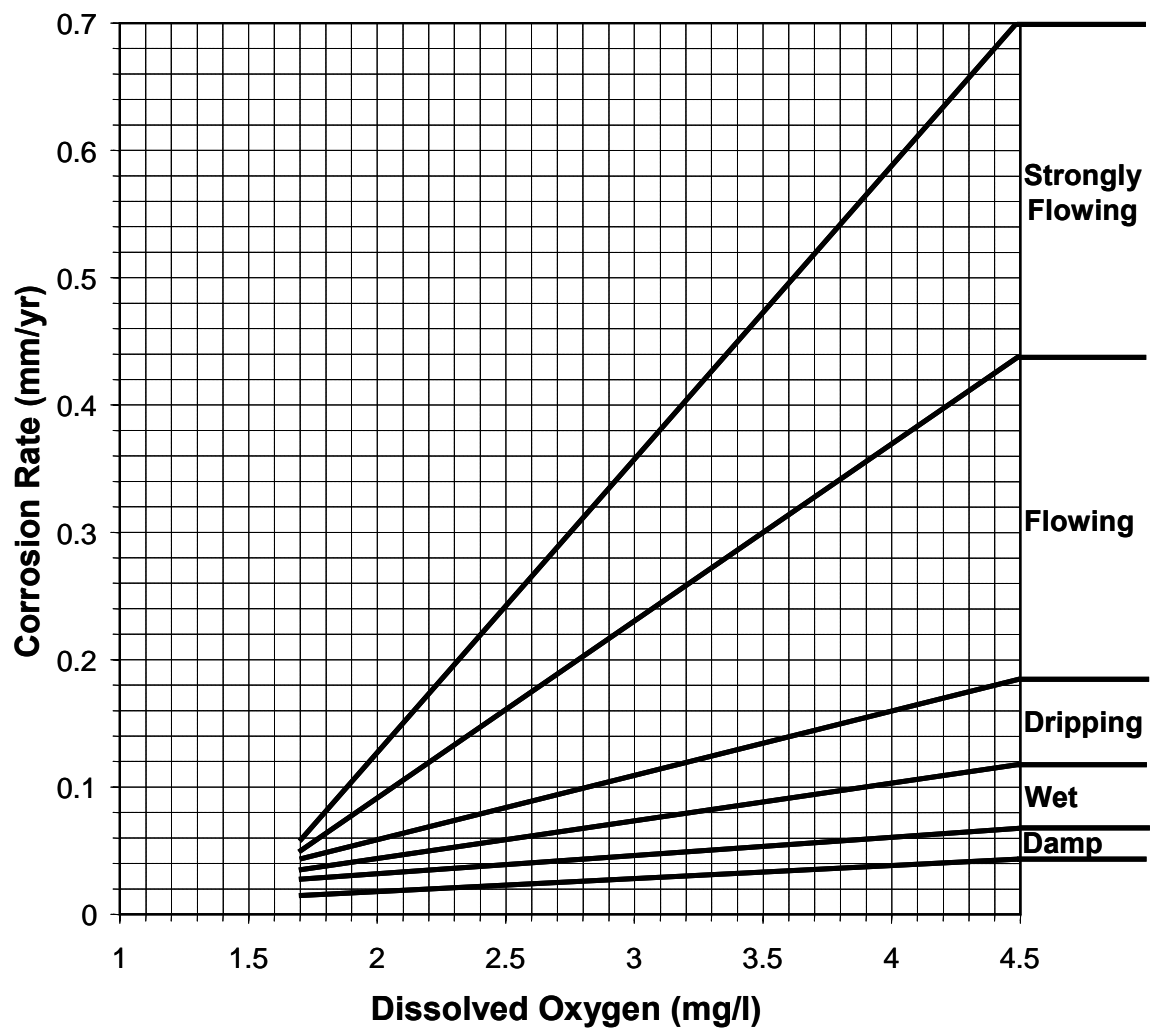


Figure 7.9 Corrosivity classification for groundwater affected, Australian hard rock environments.

Table 7.4 Range of maximum expected corrosion rates for HA300 grade steel in groundwater affected, Australian hard rock environments.

Strongly Flowing				
Dissolved Oxygen (mg/l)	1-2	2-3	3-4	4-5
Corrosion Rate (mm/yr)	<0.120	0.120-0.360	0.360-0.580	0.580-0.80
Flowing				
Dissolved Oxygen (mg/l)	1-2	2-3	3-4	4-5
Corrosion Rate (mm/yr)	<0.090	0.090-0.225	0.225-0.365	0.365-0.500
Dripping				
Dissolved Oxygen (mg/l)	1-2	2-3	3-4	4-5
Corrosion Rate (mm/yr)	<0.060	0.060-0.105	0.105-0.160	0.160-0.200
Wet				
Dissolved Oxygen (mg/l)	1-2	2-3	3-4	4-5
Corrosion Rate (mm/yr)	<0.040	0.040-0.075	0.075-0.100	0.100-0.120
Damp				
Dissolved Oxygen (mg/l)	1-2	2-3	3-4	4-5
Corrosion Rate (mm/yr)	<0.020	0.020-0.030	0.030-0.040	0.040-0.050

Table 7.5 Descriptions of groundwater flow conditions (Bieniawski 1989)

Groundwater conditions	Description
Damp	Rock mass is discoloured from dry rock mass. Very minor drips.
Wet	Rock mass discoloured. Dripping from fractures moderately common.
Dripping	Numerous drips and trickling of water from fractures.
Flowing	Water flows from fractures.
Strongly Flowing	Large continuous water flow from many fractures.

The classification provides a range of possible corrosion rates for a specific dissolved oxygen content and groundwater flow. As the groundwater condition is from qualitative observation rather than quantitative assessment this variation in values is necessary. Projection of the corrosion rates for measurements of dissolved oxygen less than 1.5 and greater than 4.5 is uncertain due to insufficient data. The given corrosion rates are for uniform corrosion only; it is however appropriate to assume that pitting corrosion will increase with higher rates of uniform corrosion. The classification does not take into account the rock mass quality. It is assumed that if the classification is to be applicable, the reinforcement will intersect water bearing discontinuities. In addition, the rock mass damage from the stress re-distribution is expected to increase the permeability within the zones where reinforcement is utilised.

7.3 Atmospheric Corrosivity Classification

The majority of reinforcement and support in underground mines is affected by atmospheric variables; the temperature, the humidity and the level of pollutants. Variations in the atmospheric properties are due to the depth of mining below surface, the ambient rock temperatures and the interaction of primary and secondary ventilation. The main pollutants, sulphur dioxide and nitrogen oxides are thought to occur in very small concentrations and do not impact significantly on the corrosivity of the atmosphere. By investigating published classifications and examining the relationship between the atmospheric properties using the field results from the coupon testing, an atmospheric classification for Australian underground mines can be developed.

7.3.1 *Atmospheric corrosion classification – ISO 9223*

The ISO 9223:1992 (ISO 9223 1992) standard, located in Appendix E, classifies the corrosivity of an atmosphere based on measurements of time of wetness (TOW), and pollution categories, sulphur dioxide (P) and airborne chlorides (S). The corrosivity of the atmosphere is divided into five categories ranging from very low (C1) to very high (C5) with corresponding rates of corrosion for carbon steel and zinc. This standard is widely used throughout the world to classify the atmospheric corrosion potential in many different environments; however, it often needs to be modified and calibrated to that specific environment.

The TOW is estimated as the length of time when the relative humidity is greater than 80% at a temperature greater than 0 °C. The classification states that the calculated time does not necessarily correspond with the actual time of exposure to wetness, because wetness is influenced by: the type of metal, the shape, mass and orientation of the object, the quantity of corrosion product, the nature of pollutants on the surface and other factors which the standard does not take into account. However, this criterion is usually sufficiently accurate for the characterisation of most atmospheres. There are five broad categories of TOW which range from less than 0.1% of the year (i.e. indoors climate controlled) up to greater than 60% of the years (i.e. outdoors in damp climates).

The calculation to determine the TOW of a climate uses the annual mean low and high temperatures, in addition to the highest temperature with a relative humidity greater than 95%. This data is generally sourced using continuous measurements which were beyond the scope of the project. The assessment of the atmospheres within the mines took place over only a few days which represent about 1% of the total year. The underground environment also has no wetting of surfaces due to dew or rainfall. All condensation is due to the humidity.

Based on the data collected the majority of mining environments can be placed into the τ_3 category, which has a TOW of between 250 to 2,500 hours per annum, which equates from 3 to 30% of the year. The deposition of pollution, airborne salinity and sulphur dioxide, is minor and the lowest category was chosen for both. The resulting corrosivity category is C2 which has a corresponding corrosion rate between 0.0013 to 0.025 mm/yr and is regarded as low corrosivity. Comparing this with the result from the coupon testing, which ranged from 0.004 to 0.017 mm/yr, it is seen that the wide variety of corrosion rates calculated for the underground atmospheric environments fit well into the C2 corrosion category.

7.3.2 Dry underground rock corrosion classification – Li & Lindblad (1999)

Li and Lindblad (1999) proposed a second classification for dry rock conditions in underground mines (see Appendix E). The parameters included are deposition rate of sulphur, nitrogen oxides and chloride, as well as the relative humidity and ambient temperature. The final rating, W_{dry} , is classed into three sections ranging from no or little corrosion (W_{dry} 0-6) to severe corrosion ($W_{\text{dry}} > 10$), all with corresponding corrosion rates. This classification differs from the ISO 9223 by introducing nitrogen dioxides, a by-product of blast gases, and using a separate temperature and relative humidity factor in place of the time of wetness.

The classification ratings shown in Table 7.6 all fall into the same category predicting little or no corrosion with an estimated corrosion rate of less than 0.05 mm/yr. When the ratings are compared with atmospheric corrosion rates measured from the coupons

placed at mine sites (see Figure 7.10) a reasonable correlation is observed. However, the corrosion rates predicted from this classification are not sensitive to changes observed in practice being more than double the highest measured rate.

Table 7.6 Li and Lindblad (1999) dry rock ratings for various underground environments.

Location	Temperature (°C)	Humidity (%)	Air Flow rate	W _{dry} rating	Classification corrosion rate (mm/yr)
Cannington 475 Ug53	30	74	medium	2.00	<0.05
Cannington 295 sf66	32	93	medium	4.59	<0.05
Enterprise 30A	35	90	medium	5.66	<0.05
Enterprise 29E	31	80	medium	4.29	<0.05
Enterprise 28D	30	80	medium	4.00	<0.05
Enterprise 31C	25	70	medium	1.41	<0.05
Argo sump 2	21	76	high	1.07	<0.05
Argo stockpile 3	20	66	high	1.00	<0.05

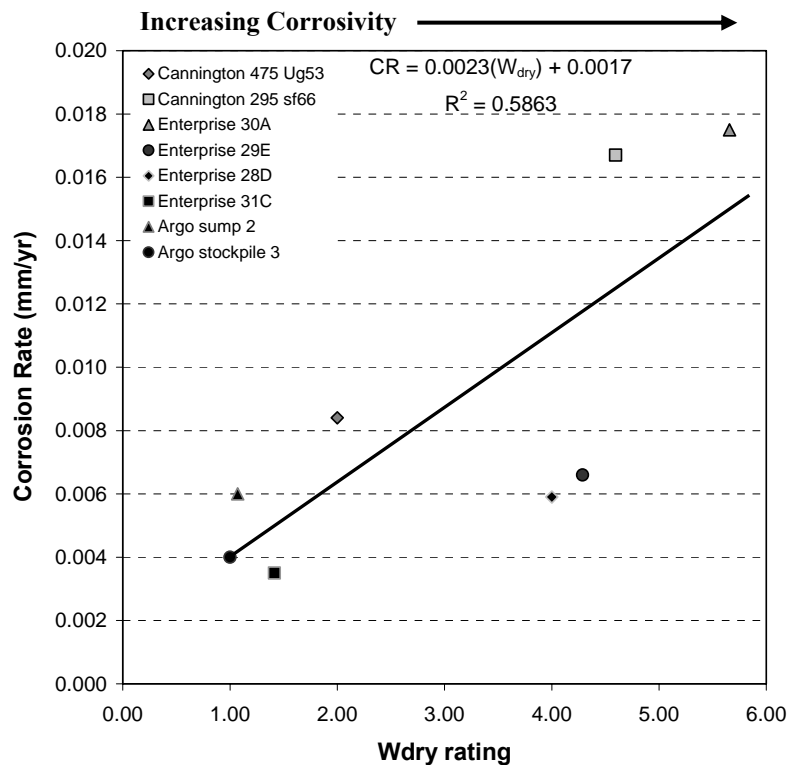


Figure 7.10 Relationship between corrosion rates and W_{dry} rating.

7.3.3 The main atmospheric properties and the measured rates of corrosion

The two reviewed classifications for atmospheric corrosion classed all atmospheres tested in Australian underground mines into a singular category. This is despite the coupons being placed in a variety of environments that was representative of the range of atmospheres surveyed. It is concluded that compared to other atmospheric environments such as urban and industrial, those found in underground metalliferous mines in Australia are similar in properties that cause corrosion and have a low corrosivity. The low corrosivity is a product of the enclosed nature and strong air flow of the underground environment. With no rain or dew, low level of pollutants and strong ventilation flows, even in the hotter, humid areas the effective time of wetness is low. Without water the electrochemical corrosion process cannot proceed. These statements are true for the significant majority of atmospheres surveyed; however some locations were observed that do not have adequate ventilation and are assumed to have a much higher TOW and subsequently higher rates of corrosion. These environments were isolated cases and were not covered in this study.

To further refine the corrosivity of the atmospheres the measured corrosion rates are compared with the atmospheric properties of dry bulb temperature and relative humidity. These plots shown in Figures 7.11 and 7.12 both compare against already known responses to atmospheres with low pollutants from Roberge (2000). Similarities are observed for both the dry bulb temperature and humidity plots. A good linear correlation is seen between the measured relative humidity and the measured corrosion rates. There is only a minor difference when compared to the expected relationship as predicted by Roberge (2000). Thus a simpler humidity rating would be appropriate when classifying the underground atmospheric environment.

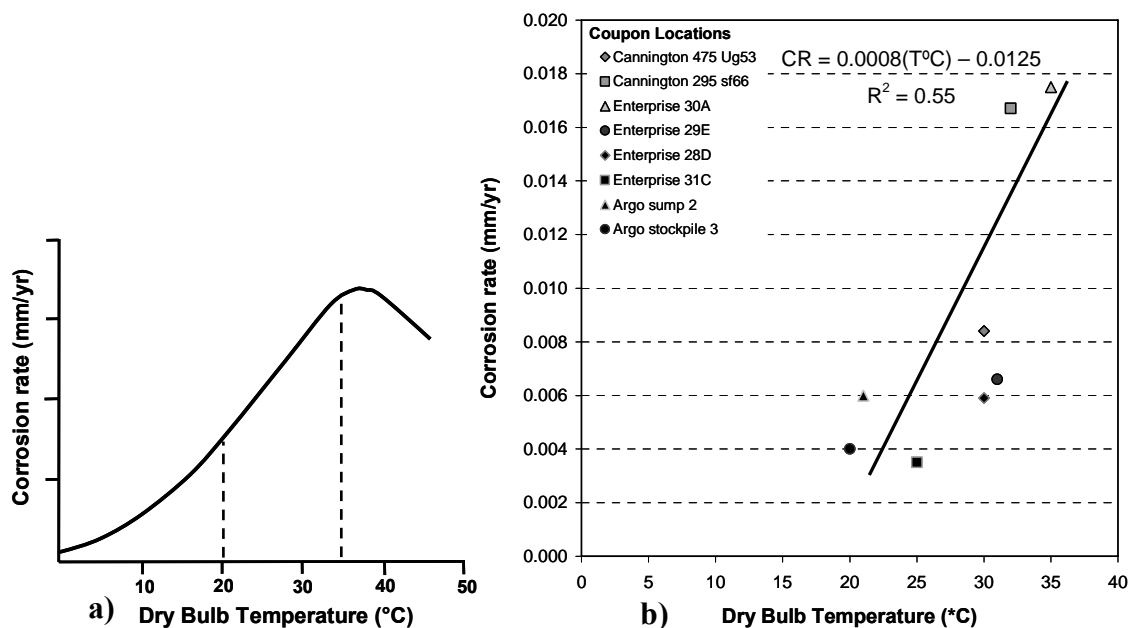


Figure 7.11 Relationship between the corrosion rate and temperature from a) Roberge (2000) and b) from the site coupon rates and measured temperature.

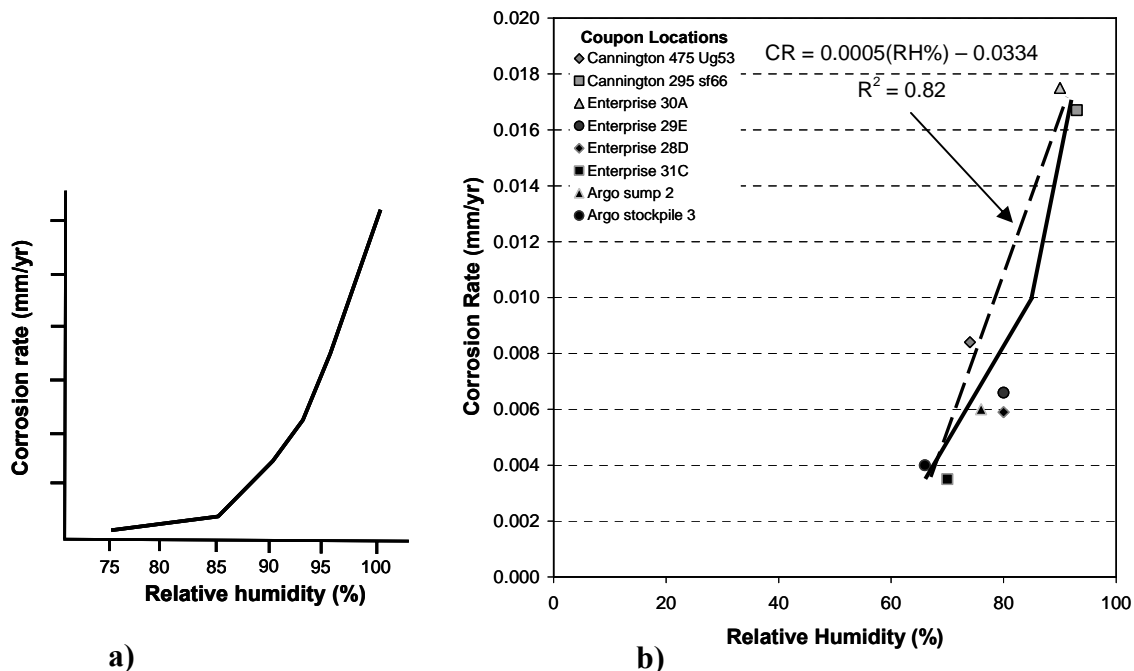


Figure 7.12 Relationship between coupon corrosion rates and relative humidity from a) Roberge (2000) and b) from the site coupon rates and measured humidity.

7.3.4 Corrosivity classification for atmospheric environment in hard rock underground mines

The narrow range of atmospheric environments in Australian underground hard rock mines has eliminated the need to use multipart classifications. Instead a basic classification is proposed that employs only the relative humidity, which is partially a product of the temperature, to predict a range of corrosion rates for HA300 grade steel. This classification is based on the information collected from the comprehensive survey of Australian underground mines and the results of the coupon testing. It assumes there is adequate ventilation flow for the majority of the excavation life. The classification shown in Table 7.7 has three categories of relative humidity and associated rates of steel corrosion. Approximate corrosion rates for zinc galvanising are included that were derived from the ISO 9223 standard (ISO 9223 1992) for similar environments. This classification is suggested for use in all Australian underground hard rock mines.

Table 7.7 Corrosivity classification for underground, hard rock, metalliferous atmospheric environments.

Relative Humidity (%)	<60	60-90	90-100
Corrosion Rate for steel (mm/yr)	<0.002	0.002-0.010	0.010-0.020
Corrosion rate for zinc (µm/yr)	<0.100	0.100-0.350	0.350-0.700

CHAPTER 8 CORROSION OF ROCK SUPPORT AND REINFORCEMENT

8.1 Introduction

The information collected in this research project: the observations from the field study, the measurements and results of the corrosion chamber experiments, the descriptions of corrosion damage and laboratory results from the overcored elements provide a comprehensive study of the effect of corrosion on reinforcement elements. This chapter applies this knowledge in conjunction with the newly developed corrosion classifications to make available guidelines for the design of friction rock stabilisers (FRS), cable bolts and grouted solid bar elements in underground hard rock mines. Additionally corrosion protection methods are discussed. While not a major focus of this study a summary of support systems are provided.

8.2 Corrosion Protection Methods

There are two widely utilised corrosion protection methods for rock support and reinforcement in underground hard rock mines. The first one consists of cement grouting of reinforcement elements so that a barrier between the steel and the outside environment is created and the second consists of zinc galvanising of the steel.

When the grout column stays intact it should protect the underlying steel for many years, even in flooded mines. The length of time needed for corrosion to occur through the cement grout by the processes of carbonation and chloride infiltration is longer than the operational life of most mines. This is especially true if cement grout migrates into open joints and fractures in the rock mass. No information was found for similar effects with resinous grouts. Corrosion of fully encapsulated strand/bar is unlikely to occur unless the steel is exposed directly to the surrounding environment. This is thought to take place

when cracks in the low tensile strength grout column occur due to rock movement and/or blast vibrations. Groundwater is then able to interact directly with the steel. Due to the self-healing properties of cement grout a minimum of 2 mm width cracks is required for unimpeded corrosion attack.

This project did not directly investigate the effect of poor installation practices, particularly the effects of inadequate grout encapsulation on the service life of the reinforcement, but it is considered that it would greatly increase the likelihood of failure due to corrosion damage as the steel is immediately exposed to the surrounding environment. Cement grout provides greater protection than resinous grouts as it is a corrosion inhibitor and also has some degree of crack self healing. Evidence of poor encapsulation was observed for both grout types. Corrosion inhibitors can be added as an admixture to cement grouts. They are ineffectual in preventing corrosion once a crack has formed.

Zinc galvanising is commonly applied to many support and reinforcement systems to increase the service life. No direct measurements were taken to establish its effectiveness in various environments; however, qualitative observations were made. In atmospheric environments deterioration of hot dipped zinc coatings were not seen, even for elements of many years age, unless the coating was damaged during installation. Therefore, it can be concluded that hot dip galvanising will provide corrosion protection for many years, even the life of the mine, in atmospheric conditions if undamaged. In groundwater affected environments the zinc coating lasted a minimum of two months for groundwater with a high dissolved oxygen and high flow rate. In less corrosive conditions; low dissolved oxygen and low flow rate, the galvanising fully protected the element for over 6 months with some protection for up to two years.

8.3 Rock Reinforcement Systems

The relative corrosion resistance of various reinforcement systems in similar corrosive environments is displayed in Table 8.1. Fully cement encapsulated bar elements are the most corrosive-resistant, with additional protection of a plastic sheath providing the highest longevity. Failure to grout considerably increases susceptibility to corrosion attack. Resin encapsulated elements are not as corrosion resistant as the resin grout has no inherent corrosion protection qualities and provides only barrier protection to the environment. Cable strand is less corrosion resistant again due to it comprising of small diameter strands entwined to create the element. Corrosion damage to a single strand can seriously weaken the entire cable bolt system. By comparison similar damage to a bar element will not create the same loss in load bearing capacity.

Swellex are more corrosion resistant than FRS as they are full enclosed. Corrosion from the residual inflation water is not an issue. FRS are the least corrosion resistant of any reinforcement investigated. The thin-walled elements have a large surface area susceptible to corrosion attack. Grouting of the internal bolt section provides only limited protection. Zinc galvanising increases the expected service life of all reinforcement elements.

Table 8.1 Relative longevity of reinforcement systems subjected to similar corrosive environments.

Cement Grouted Sheathed Bar	<div></div> <div>More Corrosion Resistant</div> <div></div> <div></div> <div></div> <div></div> <div></div> <div></div> <div></div> <div></div> <div></div> <div></div> <div>Less Corrosion Resistant</div>
Cement Grouted Galvanised Bar	
Cement Grouted Black Bar	
Resin Grouted Black Bar	
Cement Grouted Galvanised Strand	
Cement Grouted Black Strand	
Ungouted Sheathed Bar	
Cement Grouted Galvanised Friction Rock Stabiliser	
Galvanised Friction Rock Stabiliser	
Black Swellex Bolt	
Cement Grouted Black Friction Rock Stabiliser	
Black Friction Rock Stabiliser	

8.3.1 Friction Rock Stabilisers

Friction rock stabilisers (FRS) are the most widely used form of reinforcement in Australian underground mines. Overcoring and subsequent laboratory testing of FRS has

provided an excellent insight into the effect of corrosion damage on the load transfer capacity of the element. Two modes of failure have been observed to occur.

As corrosion progresses the original thickness of the FRS is reduced as the steel is converted to corrosion products. This rust provides no structural integrity and the frictional capacity is reduced. The frictional resistance against the borehole wall is a function of the springiness of the element. By reducing the steel thickness the springiness and thus radial stresses acting on the rock mass surface are lowered. This reduces the pull out strength of the bolt. Additionally corrosion products may reduce the friction between the two surfaces by providing a plane of slip.

The normalised pull tests results discussed in Chapter 5 indicated a loss of frictional resistance with increasing levels of corrosion. Those elements with moderate corrosion damage displayed frictional capacities of 45-150 kN/m; this is compared to 19-79 kN/m for elements with high or severe corrosion damage, a decline in capacity of 45-50%. Estimates of the reduction of wall thickness between the moderately corroded and the high/severe corroded bolts range from 0.20-0.35 mm, approximately a 7-18% reduction. The small reduction in thickness is thought responsible for the large decrease in frictional capacity. The borehole diameter was not measured for these tests; however, the slot width was large indicating larger boreholes.

It is apparent that a small loss in steel thickness results in a relatively large decrease in the pull out strength. This is explained by examining the section modulus of the FRS. The section modulus is the ratio of the moment of inertia of the cross section of the element undergoing flexure to the greatest distance of an element of the beam from the neutral axis. It has a cubic relationship with the wall thickness, thus small changes in the thickness are amplified (Thompson 2007). An approximate 20% reduction in the steel thickness will result in an estimated 50% decrease in pull out strength.

The time taken for a 20% reduction of the FRS wall thickness under various corrosive conditions can be estimated. As has been stated previously the internal rate of corrosion

is approximately half of the external rate. Using an external rate of corrosion based on the environmental conditions calculated using the corrosion classification provided in Chapter 7 with an internal corrosion rate of half of that rate, the time taken for the FRS frictional capacity to be reduced by 50% can be calculated and is shown in Figure 8.1 and Table 8.2. This estimate assumes constant uniform corrosion over the FRS section and does not take into account variations in the borehole profile and the influence pits will have on the stiffness and springiness of the bolt.

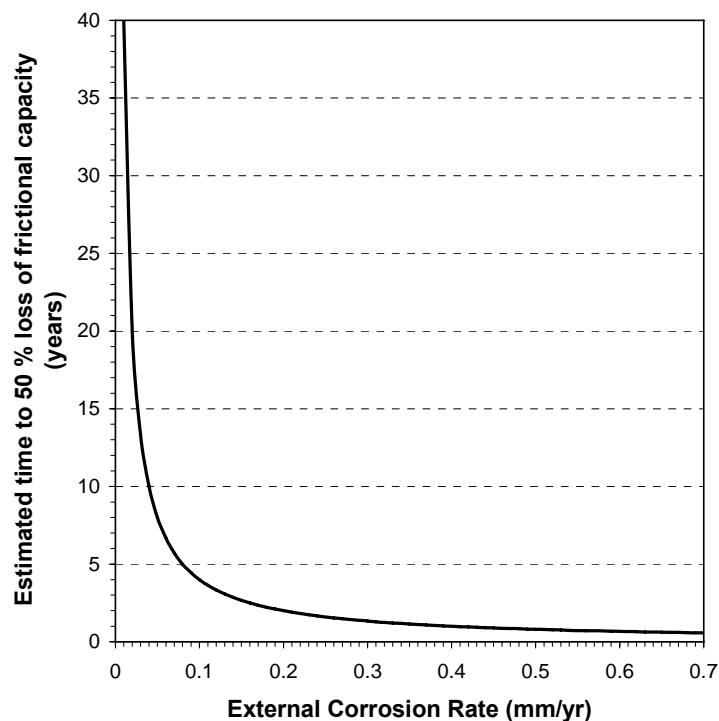


Figure 8.1 The estimated time taken for a 20% reduction in steel thickness of a 47 mm diameter, nominal 3 mm thickness FRS corresponding to a 50% decrease in pull out strength.

Table 8.2 Estimated time taken for a 20% reduction in steel thickness of a 47mm diameter, 3mm thickness FRS corresponding to a 50% decrease in pull out strength.

Corrosion Rate (mm/yr)	0.05	0.1	0.2	0.3	0.4	0.5	0.6	0.7
Time till 50% loss of frictional capacity (years)	8.0	4.0	2.0	1.33	1.0	0.8	0.7	0.6

The tensile strength of the FRS is also detrimentally affected by corrosion as steel is consumed. In this failure mode pitting corrosion has been shown to play a major role with initial failure originating in the structural weakness of the pits. A relationship between the maximum pit depth and tensile strength was observed with strong pitting generally confined to localised areas often in the vicinity of open joints. Once the pit has oxidised through the FRS wall it continues to grow and spreads outwards joining up with nearby pits.

In all but one test the tensile strength of the element was much higher than the frictional strength. At some point however, related to the spread of pitting corrosion, the tensile capacity becomes less than the frictional capacity. If corrosion is occurring all over the element then the frictional capacity will be reducing along with the tensile capacity and it is expected that the loss of frictional resistance is the most likely mode of failure. However, due to the heterogeneous nature of corrosion it will differ along the bolt axis with higher levels of corrosion found towards the toe of the bolt. This has implications for load transfer from the unstable section to the stable section, with the latter located in the area of greater corrosion and not having the added benefit of a plate. If corrosion occurs only at a discrete point then the frictional capacity of the element will be largely unaffected but the tensile strength will be reduced at that point and tensile failure is more likely to occur. The prediction of pit evolution and subsequently the time taken till tensile failure was not achieved in this study.

8.3.2 Cable bolts

Cable bolt systems are used to reinforce large blocks or wedges often in long life excavations. Premature failure of these reinforcement systems due to corrosion can cause significant safety and operational issues. It is strongly recommended that best practice installation requirements such as those detailed by (Windsor 2004) are followed to minimise the potential for corrosion damage to occur.

Approximate minimum and maximum service lives have been measured from the corrosion chamber experiments described in Chapter 4. The service life is estimated as

the material loss required to cause failure of the strand loaded to 175 kN or approximately 17.5 tonnes, a 30% decrease in the original capacity of 250 kN. Groundwater is assumed to be present and it is assumed that either cracking of the grout column has occurred or grout encapsulation is poor. Comparing the measured service lives to the corresponding corrosion rates of the simulated environment calculated using the corrosion classification, estimates can be made to the expected minimum and maximum service lives (<17.5 kN) of 15.2 mm diameter black strand across a range of corrosion rates, shown in Figure 8.2 and in Table 8.3. This provides estimates for horizontally placed elements; for vertical cables migration of corrosion down the bolt axis may occur.

It is estimated that even in the most corrosive conditions observed in underground mines (corrosion rate 0.15 mm/yr) cable strand will last at least one year once cracks have formed. This figure is much higher than the expected life of uncoated barrel and wedge anchors, found to be approximately 7 months at comparatively corrosive conditions (corrosion rate 0.06 mm/yr). It is recommended that barrel and wedge corrosion protection systems such as a long life lubricant at the barrel/wedge interface and barrier coatings are applied following installation.

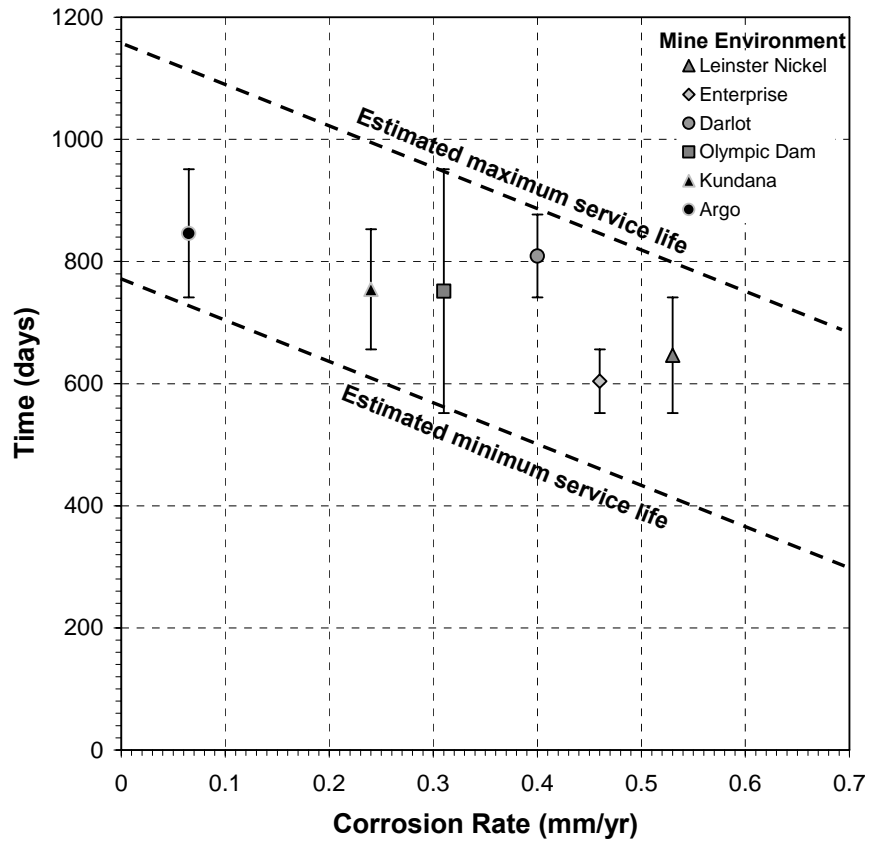


Figure 8.2 Service life estimates for cable strand in strong groundwater flow environments.

Table 8.3 Service life estimates for cable strand in strong groundwater flow environments.

Corrosion Rate (mm/yr)	Estimated Minimum Service Life (days)	Estimated Maximum Service Life (days)
0.05	740	1125
0.10	705	1090
0.15	670	1055
0.20	635	1020
0.25	600	985
0.30	565	950
0.35	530	515
0.40	495	880
0.45	460	845
0.50	425	810
0.55	390	775

8.3.3 Cement and resin grouted rock bolts

Cement and resin grouted elements are commonly used as reinforcement for long life excavations. Their capacity to resist corrosion damage is therefore extremely important. The results from the corrosion chamber experiments proved inconclusive in determining service life, however, analytical calculations can be used to estimate service lives of solid circular bar elements following the exposure of the steel to the surrounding environment. The material loss required to cause failure of a reinforcement element loaded to a specified stress level is calculated by the following equations (Thompson 2004a). If a solid circular bar with area A_0 and radius r_0 is stressed to a working stress σ_w and the material has a yield strength σ_y and ultimate strength σ_u then:

$$r_{ycr} = r_0 \sqrt{\frac{\sigma_w}{\sigma_y}} \quad (8.1)$$

$$r_{ucr} = r_0 \sqrt{\frac{\sigma_w}{\sigma_u}} \quad (8.2)$$

Where:

r_{ycr} is the critical radius for yield strength, and

r_{ucr} is the critical radius for ultimate strength.

The service life (t) can be estimated by calculating the required material loss from equations 8.1 and 8.2 and dividing it by the expected rate of corrosion:

$$t = \frac{r_0 \left(1 - \sqrt{\frac{\sigma_w}{\sigma_y}} \right)}{ICorr} \quad (8.3)$$

$$t = \frac{r_0 \left(1 - \sqrt{\frac{\sigma_w}{\sigma_u}} \right)}{ICorr} \quad (8.4)$$

Where:

t is the estimated service life in years, and

$ICorr$ is the corrosion rate calculated from the corrosion classification in Chapter 7.

Service lives till yield and ultimate failure of 20 mm and 25 mm diameter thread bar have been calculated for a range of working stresses and are shown in Figures 8-3 to 8-6. The working stresses are 50%, 66%, 75% or 90% of the yield strength of the bolt as taken from manufacturer's specifications. For a 20 mm diameter thread bar the yield and ultimate strength are typically 170 and 200 kN (DSI 2007a). For a 25 mm diameter thread bar the strengths are 260 and 305 kN (DSI 2007b). The service lives estimated are for black steel reinforcement that is in direct contact with the environment. Corrosion rates are established by using the appropriate corrosion classifications provided in Chapter 7.

Based on the most corrosive conditions observed in the corrosion chambers with a corrosion rate of 0.58 mm/yr the estimated service lives till ultimate failure for a 20 mm diameter bar range from 2.1 years with a working stress of 90% to 6.0 years with a 50% working stress. For a 25 mm diameter bar the corresponding service lives range from 2.6 to 7.5 years. There is a significant increase in service life by a factor of two to three that can be achieved by reducing the effective working stress of the element. The expected service lives are also higher than those seen for cable strand in the same environment.

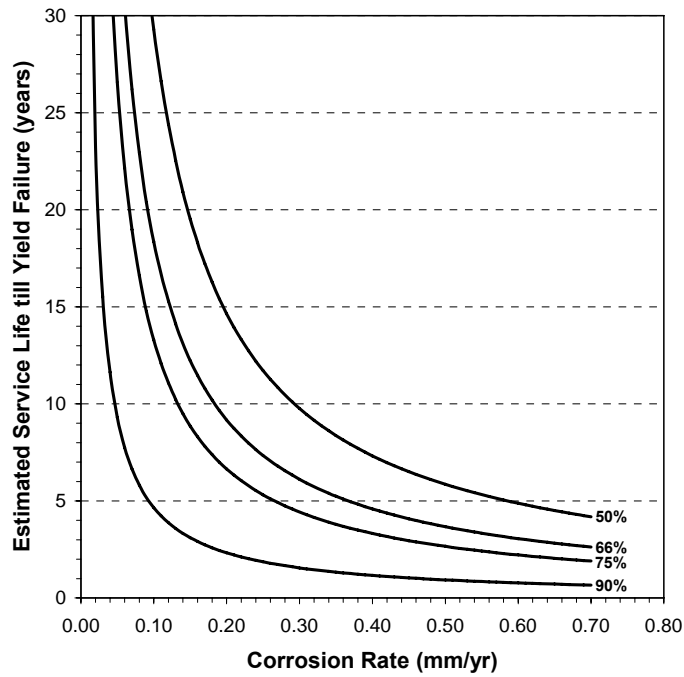


Figure 8.3 Estimated service life to yield failure for 20 mm thread bar due to corrosion at various working stresses (percentage of yield strength).

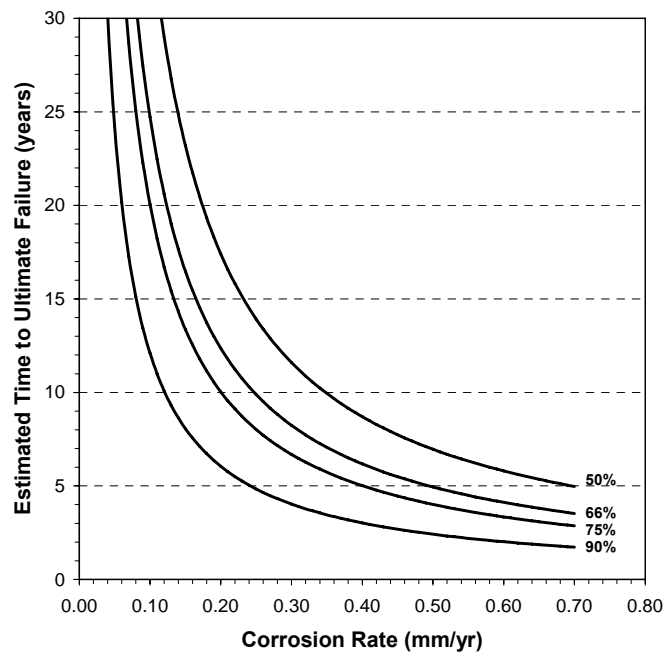


Figure 8.4 Estimated service life to ultimate failure for 20 mm thread bar due to corrosion at various working stresses (percentage of yield strength).

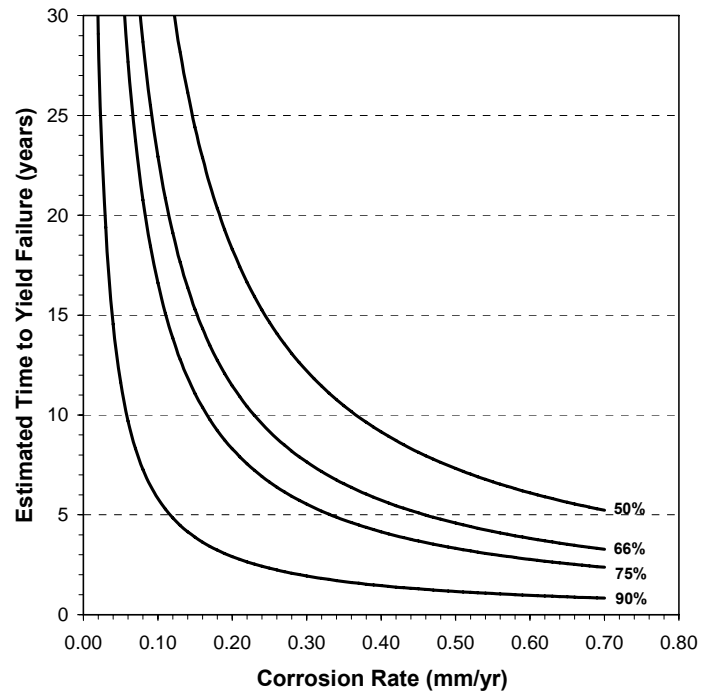


Figure 8.5 Estimated service life to yield failure for 25 mm thread bar due to corrosion at various working stresses (percentage of yield strength).

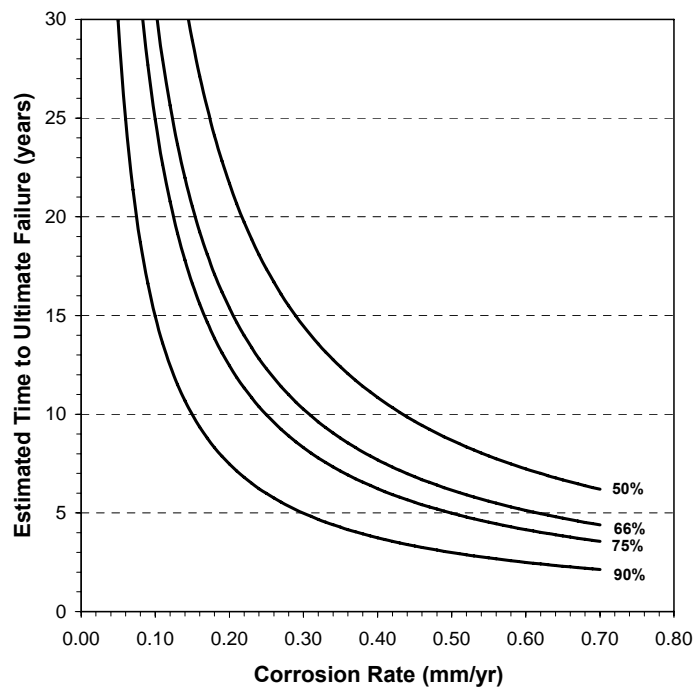


Figure 8.6 Estimated service life to ultimate failure for 25 mm thread bar due to corrosion at various working stresses (percentage of yield strength).

8.4 Rock Support Systems

The relative corrosion resistance of support systems are shown in Table 8.4. Shotcrete and mesh combinations provide the greatest impediment to corrosion damage. Shotcrete is a cement based product and thus provides corrosion protection for steel fibres or mesh it is used in conjunction with. For support that is not coated by shotcrete the steel thickness and galvanising controls the susceptibility to corrosion. Straps and plates are more corrosion resistant than mesh.

Table 8.4 Relative longevity of support systems subjected to similar corrosive environments.

Shotcrete and Synthetic Fibres		More Corrosion Resistant
Shotcrete and Galvanised Mesh		
Steel Fibrecrete		
Shotcrete and Black Mesh		
Galvanised Strap		
Black Strap		
Galvanised Plate		
Black Plate		
Galvanised Weld Mesh		
Galvanised Mesh Strap		
Black Weld Mesh		
Black Mesh Strap		Less Corrosion Resistant

8.4.1 Plates

It was generally observed that steel plates were more corrosion resistant than FRS elements in most environments. This may not be the case for fully encapsulated bolts, especially in mines that have been previously flooded. It is thought that drying out of groundwater affecting the plate, especially at low groundwater flow rates, takes place due to the ventilation flow in the drive. This reduces the effective corrosion rate acting on the plates. Table 8.5 displays a qualitative assessment for the longevity of black plates assuming corrosion attack from both plate surfaces. For atmospheric environments, the expected plate life extends for decades, however this may decrease to years and months in highly corrosive environments. Thicker plates are notably more corrosion resistant.

Table 8.5 Qualitative assessment for longevity of black plates in a range of corrosive environments.

Corrosion Rate (mm/yr)	Plate Thickness (mm)			
	1.9	4.0	7.0	10.0
Atmospheric	decades	decades	decades	decades
0.1-0.2	years	years	decades	decades
0.2-0.3	years & months	years	years	decades
0.3-0.4	years & months	years	years	years
0.4-0.5	months	years & months	years	years
0.5-0.6	months	years & months	years	years

8.4.2 Weld Mesh

Severe corrosion damage to weld mesh occurred in high water flow environments. However, for most other environments weld mesh appeared to perform well in terms of corrosion resistance compared to its nominal 5.6 mm diameter. Testing the tensile strength of corroded weld samples collected from underground locations showed a reduction of strength between 26% and 40% for highly corroded samples with failure occurring in the weld and heat affected zones. Only at two mine sites, Cannington and Gunpowder, was weld mesh observed to be completely corroded. The limited data collected by this study has not allowed conclusions or predictions on mesh corrosion.

8.4.3 Shotcrete

Corrosion of the reinforcing steel fibres in shotcrete can occur when cracks form in the shotcrete groundwater interacts with the fibres. Due to their small thickness they are quickly consumed. Synthetic fibres do not have this problem. It is not known how the loss of the steel fibres affects the strength of the shotcrete as they are localised in an area that has already failed.

CHAPTER 9 CONCLUSIONS

The purpose of this thesis is to investigate corrosion and relate how the environmental conditions in Australian underground hard rock mines impact on the service life of rock support and primarily rock reinforcement. The investigations have resulted in the development of corrosion classifications for the Australian underground hard rock mining environments and guidelines have been provided for the design of reinforcement; principally friction rock stabilisers, cable bolts and solid bar elements. This has been achieved through the completion of environmental characterisation of a number of underground mines, laboratory testing using a simulated underground environment, examination of reinforcement elements *in-situ* and the exposure and evaluation of test coupons to obtain corrosion rates for the underground mining environment.

The improved understanding of environmental conditions in underground hard rock mines led to the delineation of two separate environments; namely, atmospheric and groundwater affected. Uniform corrosion rates have been established for a range of atmospheric and groundwater affected environments with atmospheric corrosion rates being found to be much less than groundwater affected. Atmospheric corrosion is controlled by the relative humidity of the atmosphere. Corrosion by groundwater is controlled by the dissolved oxygen content of the water; this was found to be a function of the total dissolved solids, the water temperature and the flow rate of the groundwater. Two corrosion classifications have been proposed for Australian underground hard rock mines; one for atmospheric environments and another for groundwater affected environments.

The relative corrosion resistance of rock reinforcement systems from the most resistant to the least resistant is: fully cement grouted solid bars, fully resin grouted solid bars, cable bolts, galvanised friction rock stabilisers, black Swellex bolts and black friction rock stabilisers. Galvanising protects the reinforcement for decades in atmospheric conditions. In groundwater affected environments, galvanising protects reinforcement for a minimum of 2 months in highly corrosive conditions to greater than 6 months in

low corrosive conditions. Full encapsulation by cement grout protects the underlying steel elements for many years, even in completely flooded mines, unless the steel is exposed directly to the surrounding environment. This results either from poor encapsulation during installation or after installation from cracks forming in the grout column due to ground movement and/or blast vibrations.

Friction rock stabilisers suffer from two modes of failure; the loss of frictional resistance and the loss of tensile strength. A large loss of frictional resistance due to a relatively small reduction in wall thickness was measured. An estimated 50% decrease in pull out strength results from an approximate 20% reduction in the steel thickness. The loss of tensile strength is related to the level of pitting corrosion. Corrosion damage is not homogeneous along the bolt axis with greater damage on the external element surface and towards the toe of the borehole. If corrosion occurs all over the internal and/or external element surfaces, failure of the bolt is expected due to loss of frictional resistance and sliding. If corrosion occurs at a discrete location, tensile failure is expected. Cement grouting provides corrosion protection that is mainly restricted to the internal surface of the steel element.

Cable bolts and solid bar elements suffer corrosion damage when the element is exposed to the surrounding environment. Service lives for solid bar elements have been estimated using analytical solutions. Cable bolt steel strand was tested in six simulated groundwater affected underground environments. Service life for cable bolts was defined as a 30% reduction in strand capacity to approximately 17.5 tonnes. With this criterion, the service life for horizontally placed single cables is estimated to be between 552 and 951 days. Service lives for cable bolt strand in different underground environmental conditions can be estimated using the information provided in this study project. The long-term effective performance of barrel and wedge cable bolt anchors is controlled by the frictional resistance between the internal surface of the barrel and the outside surface of the wedge. Corrosion increases the frictional resistance at the interface between these two surfaces. Testing showed that anchor failure by sliding relative to the strand at low loads resulted after 218 days in groundwater affected environments.

Corrosion protection methods can be used to increase the service life of barrel and wedge anchors.

The relative corrosion resistance of rock support systems from the most resistant to the least resistant is: shotcrete, shotcrete and mesh combinations, strap, plate and mesh. Plates were observed to be more corrosion resistant than the accompanying friction rock stabilisers. Galvanised weld mesh was seen to be relatively corrosion resistant in most underground environments.

9.1 Limitations and recommendations for future work

The complex interaction between the hard rock environment and corrosion processes and the methodology used to obtain data has meant that there are certain limitations with the findings of this study.

There is a high level of confidence that common underground environmental conditions have been quantified in this study; however, there may be specific underground environmental conditions that were not examined. The period of time over which the environmental assessments were conducted is small compared with the life of mines. Atmospheric conditions are expected to have some seasonal variation and groundwater properties may also vary during the life of a mine.

The simulated environments and the experiments conducted were designed to be as close as possible to observed conditions. However, as they were only simulated the results may not directly reflect actual underground hard rock environmental conditions. The cable bolt strand experiments were conducted for strongly flowing water conditions and the barrel and wedge anchor experiments were conducted for flowing ground water conditions. Other groundwater conditions were not examined. The cable bolt experiments were performed on horizontal strand that was not tensioned. In practice, strand will be installed in near vertical boreholes and will be expected to be loaded. The possible influence of stress related corrosion was not investigated.

Overcoring of rock reinforcement was conducted for a statistically small number of bolts compared with the number that are installed. Information was not available for the environmental conditions since bolt installation at the overcoring locations. It was therefore necessary to assume that the conditions at the time of overcoring were representative of the conditions since the time of installation. The original conditions of the bolt elements were also unknown.

The long term rates of corrosion calculated from the coupon testing for the corrosion chambers and used in the corrosivity classification were not available for every time period as the coupons become completely oxidised before the completion of the experiment and corrosion rates could only be estimated. For coupons placed at mine sites they were located on the outside rock surface and not inside the rock mass where environmental conditions can be expected to be slightly different. The environmental conditions were assumed to remain reasonably constant for the duration of these tests. The creation of the groundwater affected corrosivity classification was completed on the basis of a small number of data points, especially for the flowing, dripping, wet and damp conditions. The groundwater flow conditions could only be described qualitatively.

The findings of this thesis have contributed significantly to an improved understanding of corrosion mechanisms that affect the serviceability of rock reinforcement in underground hard rock mines. However, a number of opportunities for future investigation have been identified. The areas for future study include:

- Refinement of the current corrosivity classifications. This would involve continued investigations of the corrosion rates of groundwater affected environments, the placement of coupons within boreholes in the rock mass and a quantitative characterisation of the ground water flow rate.
- Corrosion resistance of resin encapsulated steel reinforcement elements.
- Corrosion of surface support components such as mesh, plates and shotcrete steel fibres.

REFERENCES

- AS 1311 1987, 'Steel tendons for prestressed concrete-7-wire stress-relieved steel strands for tendons in prestressed concrete'. Standards Australia, p. 18.
- AS 1442 1992, 'Carbon steels and carbon-manganese steels - Hot-rolled bars and semifinished products'. Standards Australia, p. 22.
- AS 1594 2002, 'Hot-rolled steel flat products'. Standards Australia, p. 25.
- AS 4534 2006, 'Zinc and zinc/aluminium-alloy coatings on steel wire'. Standards Australia, p. 36.
- AS 4680 1999, 'Hot-dip galvanised (zinc) coatings on fabricated ferrous articles'. Standards Australia, p. 23.
- ASTM G1-90 1999, 'Standard Practice for Preparing, Cleaning, and Evaluating Corrosion Tests Specimens'. ASTM International.
- Atlas Copco 2007, *Swellex product range*. Retrieved 8/9/07, from www.sg01.atlascopco.com/SGSite/default_prod.asp?redirpage=products/product_group.asp&redirid=Rock%20bolts
- AWWA C105 1998, 'Standard for Polyethylene Encasement for Ductile-Iron Piping for Water and other Liquids'. American Water Works Association.
- Aziz, N 2004, 'Bolt surface profiles - an important parameter in load transfer capacity appraisal', *Ground Support in Mining and Underground Construction*, eds. E Villaescusa & Y Potvin, Balkema, Perth, pp. 221-30.
- Bailey, A 1998, 'Cannington silver-lead-zinc deposit', in DA Berkman & DH Mackenzie (eds), *Geology of Australian and Papua New Guinean Mineral Deposits*, The Australasian Institute of Mining and Metallurgy, Melbourne, pp. 783-92.
- Bardel, E 2004, *Corrosion and Protection*, Springer, London.
- Bavarian, B & Reiner, L 2001, 'Corrosion Protection of Steel Rebar in Concrete Using MCI Inhibitors', *EUROCORR*, Italy.
- Beck, D 1999, *Use of galvanised bolting and meshing products in Enterprise Mine*, Mount Isa Mines Limited (unpublished).
- Beckett, TS, Fahey, GJ, Sage, PW & Wilson, GM 1998, 'Kanowna Belle gold deposit', in DA Berkman & DH Mackenzie (eds), *Geology of Australian and Papua New Guinean Mineral Deposits*, The Australasian Institute of Mining and Metallurgy, Melbourne, pp. 201-6.

- Bieniawski, ZT 1989, *Engineering Rock Mass Classifications*, Wiley, New York.
- Bjegovic, D & Miksic, B 2001, 'MCI Protection of Concrete', in *Cortec Corp. Supplement to Material Performance*, pp. 10-3, January 2001.
- Brady, BHG & Brown, ET 1993, *Rock Mechanics for Underground Mining*, 2nd edn, University Press, Cambridge.
- Brown, ET 1981, 'Suggested Methods for Rockbolt Testing', in *Rock Characterisation Testing and Monitoring*, Pergamon Press.
- Bryson, JH 1990, 'Corrosion of Carbon Steels', in *Metals Handbook Ninth Edition - Corrosion*, vol. 13, ASM International, Ohio, pp. 510-30.
- CISA 1994, *Corrosion Control in Southern Africa*, Mintek, South Africa.
- Collins, D 2002, 'Failure Investigation: Rock Anchor Bolts for Big Bell Gold Operations'. Materials Insight Pty Ltd, p. 19.
- Corrosion Doctors 2006, *Corrosion of reinforced concrete*. Retrieved 20/11/2006, from <http://www.corrosion-doctors.org/Concrete/Nature.htm>
- CPI Corrosion LTEE 2003, *Corrosion Behaviour of Swellex - Project No: 2103-012-C Swellex*, Internal Atlas Copco Report.
- CSIRO & IGC 2002, *Estimated average daily salt deposition map of Australia*, Industrial Galvanizers Corporation. Retrieved 9/8/2006, from <http://www.corp.indgalv.com.au/mapping/frameset.htm>
- Davis, RL 1979, 'Split-set rock bolt analysis', *Int. J. Rock. Mech. Min. Sci. & Geomech.*, vol. 16, pp. 1-10.
- Davis, TP 2004, 'Mine-scale structural controls on the Mount Isa Zn-Pb-Ag and Cu orebodies', *Economic Geology*, vol. 99, no. 3, pp. 543-59.
- Dean, SW & Sprowls, DO 1987, 'In-Service Monitoring', in JR Davis (ed.), *Metals Handbook Ninth Edition: Corrosion*, vol. 13, ASM International, USA.
- Department of Industry and Resources 1997, 'Geotechnical Considerations in Underground Mines - Guideline', p. 32.
- Department of Industry and Resources 2002, 'Mines Safety and Inspection Regulations 1995', vol. 10.28 (2) (e). Western Australian Government, p. 217.

- DIN 50929-3 1985, 'Corrosion of metals; probability of corrosion of metallic materials when subject to corrosion from the outside; buried and underwater pipelines and structural components'. Deutsches Institut für Normung.
- DSI 2006a, from www.dywidag-systems.com
- DSI 2006b, *Friction bolt*, 17/5/2006, from http://www.dsiminingproducts.com/au/products/Rock_Roof_Bolts_Overview.html
- DSI 2007a, *20 mm Thread Bar Bolt*. Retrieved 21/3/07, from http://www.dsiminingproducts.com/au/products/Rock_Roof_Bolts_20mm_Threadbar.html
- DSI 2007b, *25 mm Thread Bar Bolt*. Retrieved 21/3/07, from http://www.dsiminingproducts.com/au/products/Rock_Roof_Bolts_25mm_Threadbar.html
- FIB 1986, 'Corrosion and corrosion protection of prestressed ground anchorages - State of the Art Report'. Thomas Telford, p. 34.
- Garford Ground Support Systems 2002, *Dynamic cable bolt for seismic loading resistant ground control*, Garford Engineering.
- Garford Pty Ltd. 1990, 'An improved economical method for rock stabilisation'. Perth, p. 4.
- Gray, DJ 2001, 'Hydrogeochemistry in the Yilgarn Craton', *Geochemistry: Exploration, Environment, Analysis*, vol. 1, pp. 253-68.
- Gray, L 2003, 'Personal communication'.
- Harvey, SM 1999, 'Elimination of fatalities taskforce - Underground rockfalls project', *Proceedings of the International Symposium on Rock Support and Reinforcement Practice in Mining*, eds. E Villaescusa, CR Windsor & A Thompson, Balkema, Kalgoorlie, pp. 387-93.
- Hebblewhite, BK, Fabjanczyk, M, Gray, P & Crosky, A 2004, 'Premature bolt failure in Australian coal mines due to stress corrosion cracking', *Proceedings for the International Symposium on Ground Support in Mining and Underground Construction*, eds. E Villaescusa & Y Potvin, Balkema, Perth.
- Heidersbach, RH 1990, 'Marine Corrosion', in *Metals Handbook Ninth Edition - Corrosion*, vol. 13, ASM International, OHIO, pp. 893-926.
- Henley, S 2002, *Construction of Chambers for Rock Reinforcement Corrosion Research*, Bachelor of Engineering thesis, Western Australian School of Mines.

- Higginson, A & White, RT 1983, 'A preliminary survey of the corrosivity of water in South African gold mines', *Journal of the South African Institute of Mining and Metallurgy*, vol. 6, no. 83, pp. 133-41.
- Hoek, K, Kaiser, PK & Bawden, WF 1995, 'Support of Underground Excavations in Hard Rock', in, Balkema, p. 160.
- Hutchinson, DJ & Diederichs, MS 1996, *Cablebolting in Underground Mines*, BiTech Publishers Ltd, Canada.
- Ingebritsen, S, Sanford, W & Neuzil, C 2006, *Groundwater in Geologic Processes*, Cambridge University Press, Cambridge.
- ISO 9223 1992, 'Corrosion of metals and alloys; corrosivity of atmospheres; classification', vol. 9223. ISO.
- Jolly, AF & Neumeier, LA 1987, *Corrosion of friction rock stabilizer steels in underground coal mine waters*, US Bureau of Mines, Information Circular No 9159.
- Jones & Ricker, RE 1990, 'Stress Corrosion Cracking', in *ASM Metals Handbook*, vol. 13, ASM, USA, pp. 145-63.
- Jones, DA 1996, *Principles and Prevention of Corrosion*, Prentice-Hall, Upper Saddle Rive, USA.
- Kaesche, H 1985, *Metallic Corrosion*, National Association of Corrosion Engineers.
- Kendorski, FS 2000, 'Rock reinforcement longevity', *19th Conference on Ground Control in Mining*, Balkema: Rotterdam, Morgantown.
- Kester, DR 1975, 'Dissolved Gases Other Than CO₂', in JP Riley & G Skirrow (eds), *Chemical Oceanography*, 2nd edn, vol. 1, Academic Press.
- Korrosionsinstitutet 2002a, *Evaluation of two Swellex Bolts having been exposed at Kvarntorp Mine for 9 years*, Internal Atlas Copco report.
- Korrosionsinstitutet 2002b, *Evaluation of internal corrosion for Swellex Bolts due to water trapped inside the bolt - Kemi Mine, Finland*, Internal Atlas Copco report.
- Krcmarov, RL, Beardsmore, TJ, King, J, Kellet, R & Hay, R 2000, 'Geology, regolith, mineralisation and mining of the Darlot-Centenary gold deposit, Yandal Belt', in RR Anand (ed.), *Yandal greenstone belt; regolith, geology and mineralisation*, Australian Institute of Geoscientists, Sydney, pp. 351-72.

- Laboratory Technical Services Newcastle Steelworks 1995, *Examination of corroded rockbolt - BHP Minerals CGM/1/95*, BHP Steel Rod and Bar Products Division (unpublished).
- Lea, JR 1998, 'Kundana gold deposits', in DA Berkman & DH Mackenzie (eds), *Geology of Australian and Papua New Guinean Mineral Deposits*, The Australasian Institute of Mining and Metallurgy, Melbourne.
- Li, C & Lindblad, K 1999, 'Corrosivity classification of the underground environment', *International Symposium on Rock Support and Reinforcement Practice in Mining*, eds. Villaescusa, Windsor & Thompson, Balkema, Kalgoorlie, pp. 69-75.
- Libby, JW, Stockman, PR, Cervo, KM, Muir, MRK, Whittle, M & Langworthy, PJ 1998, 'Perseverance nickel deposit', in DA Berkman & DH Mackenzie (eds), *Geology of Australian and Papua New Guinean Mineral Deposits*, The Australasian Institute of Mining and Metallurgy, Melbourne, pp. 321-8.
- Miksic, B 1995, 'Migrating Corrosion Inhibitors for Reinforced Concrete', *Proceedings of the 8th European Symposium on Corrosion Inhibitors*, Ferrara, Italy, p. 569.
- MINESafe Limited 2006, *Mine Gases*. Retrieved 8/8/2006, from <http://www.minesafe.org/underground/gases.html>
- O'Hare, S 1994, *Corrosion of cablebolts laboratory pull tests*, Mount Isa Mines Limited (unpublished).
- Ortlepp, WD, Human, L, Erasmus, PN & Dawe, S 2005, 'Static and dynamic load-displacement characteristics of a yielding cable anchor-determined in a novel testing device', *Rock Burst and Seismicity in Mines (RaSiM6)*, Australian Centre for Geomechanics, Perth, pp. 529-34.
- Pascoe, M 1995, *HGB Corrosion Tests and Wax Paint Trials*, BHP Minerals (unpublished).
- Potvin, Y, Nedin, P, Sandy, M, Rosengren, K & Rosengren, MD 2001, *Towards the Elimination of Rockfall Fatalities in Australian Mines*, MERIWA Project No. M341.
- Ranasooriya, J, Richardson, GW & Yap, LC 1995, 'Corrosion behaviour of friction rock stabilisers used in underground mines', *Proc. Underground Operators Conference*, The Australian Institute of Mining and Metallurgy, Kalgoorlie, pp. 9-16.
- Rawat, NS 1976, 'Corrosivity of underground mine atmospheres and mine waters: A review and preliminary study', *Journal of British Corrosion*, vol. 11, no. 2, pp. 86-91.

- Roberge, PR 2000, *Handbook of Corrosion Engineering*, McGraw-Hill, New York.
- Robinson, J & Tyler, DB 1999, 'A study of corrosion in underground reinforcement at Mount Isa Mines, Australia', *Proceedings of the International Rock Support and Reinforcement Practice in Mining*, eds. Villaescusa, Windsor & Thompson, Balkema, Kalgoorlie, pp. 69-75.
- Ross, A 2003, 'Personal communication'.
- Sastri, VS, Hoey, GR & Revie, RW 1994, 'Corrosion in the mining industry', *CIM Bulletin*, vol. 87, no. 976, pp. 87-99.
- Satola, I & Aromaa, J 2004, 'The corrosion of rock bolts and cable bolts'.
- Simpson, SJ 2005, *Evaluation and implementation of resin bolts at Olympic Dam Mine*, Bachelor of Engineering Thesis, WA School of Mines.
- Slater, JE 1990, 'Corrosion in Structures', in JR Davis (ed.), *Metals Handbook*, vol. 13 Corrosion, ASM International, Ohio, pp. 1299-310.
- Smith, RN 1993, 'Olympic Dam: some developments in geological understanding over nearly two decades', *Proc. Australasian Institute of Mining and Metallurgy conference*, AusIMM, Adelaide.
- Stimpson, B 1998, 'Split set friction stabilisers: an experimental study of strength distribution and the effect of corrosion', *Canadian Geotechnical Journal*, no. 35, pp. 678-83.
- Strata Control Systems 2006, *Strata bolt*, 17/5/2006, from <http://www.stratacontrol.com.au/catalogue/section.php?id=5§ion=1>
- Strata Control Systems 2007, *Jumbolt*. Retrieved 8/9/07, from www.stratacontrol.com.au/catalogue/product.php?id=56&product=Jumbolt
- Suess, T, Prom, K & Stehly, RD 2001, *Report on Corrosion Inhibitor Testing*, American Engineering Testing Inc, St Paul, Minnesota.
- Sundholm, S 1987, 'The quality control of rock bolts', *Proc. Int. Congress on Rock Mechanics*, eds. Herget & Vongpaisal, ISRM, Montreal, pp. 1255-64.
- Thompson, AG 2004a, *Corrosion Report No 4 (unpublished)*, MERIWA project 333 report.
- Thompson, AG 2004b, 'Performance of cable bolt anchors - An Update', *MassMin2004*, eds. A Karzulovic & MA Alfaro, Instituto de Ingenieros de Chile, Santiago, pp. 317-23.

- Thompson, AG 2007, 'Personal Communication'.
- Thompson, AG & Windsor, CR 1995, 'Tensioned cable bolt reinforcement - an integrated case study', *Proc. 8th Int. Cong. on Rock Mechanics*, Balkema, Tokyo, pp. 679-83.
- Tilman, MM, Jolly, AF & Neumeier, LA 1985, 'Corrosion of roof bolt steels in Missouri Lead and Iron Mine Waters', vol. Information Circular No. 9055, ed. UBo Mines, p. 16.
- Tomory, PB, Grabinsky, MW & Curran, JH 1998, 'Factors influencing the effectiveness of Split Set friction stabilizer bolts', *CIM Bulletin*, vol. 91, no. 100, pp. 205-14.
- Tyler, DB 1999, 'Hot dip galvanised split sets: installation damage report'. MIM Ltd, internal memo.
- Uhlig, HH & Revie, RW 1985, *Corrosion and Corrosion Control*, 3rd edn, Wiley-Interscience.
- Underhill, D 1998, 'In situ leach uranium mining - current practice, potential and environmental aspects', *ABARE Outlook 98 Conference*, Canberra.
- Villaescusa, E 1999a, 'Keynote lecture: The reinforcement process in underground mining', *Proc. Int. Rock Support and Reinforcement Practice in Mining.*, eds. Villaescusa, Windsor & Thompson, Balkema, Kalgoorlie, pp. 245-57.
- Villaescusa, E 1999b, 'Laboratory testing of weld mesh for rock support', *Rock Support and Reinforcement Practice in Mining*, eds. Villaescusa, Windsor & Thompson, Balkema: Rotterdam, Kalgoorlie, pp. 155-9.
- Villaescusa, E, Sandy, MP & Bywater, S 1992, 'Ground support investigations and practices at Mount Isa', *Rock Support in Mining and Underground Construction*, eds. PK Kaiser & DR McCreath, Balkema, Sudbury, Canada, pp. 185-93.
- Villaescusa, E, Thompson, A & Windsor, C 2006, 'Some support considerations in rapid excavations for mining development', *2006 Australian Mining Technology Conference*, eds. H Gurgenci, M Hood, P Lever & P Knights, Australasian Institute of Mining and Metallurgy, NSW, pp. 151-71.
- Villaescusa, E, Varden, R & Hassell, R 2006, 'Quantifying the performance of resin anchored rock bolts in the Australian underground hard rock mining industry', *41st U.S. Symposium on Rock Mechanics*, eds. D Yale & J Tinucci, USRM, Golden, Colorado.

- Villaescusa, E & Wright, J 1997, 'Permanent excavation support using cement grouted Spit Set bolts', *Proc. Int. Symp. Rock Support*, Norwegian Society of Chartered Engineers, Lillehammer, pp. 660-70.
- Villaescusa, E & Wright, J 1999, 'Reinforcement of underground excavations using the CT Bolt', *Rock Support and Reinforcement in Mining*, eds. Villaescusa, Windsor & Thompson, Balkema: Rotterdam, Kalgoorlie, pp. 109-15.
- Virmani, YP & Clemena, GG 1998, *Corrosion Protection: Concrete Bridges*. Retrieved 21/11/2006, from <http://www.tfhr.gov/structur/corros/introset.htm>
- Watchorn, RB 1998, 'Kambalda-St Ives gold deposits', in DA Berkman & DH Mackenzie (eds), *Geology of Australian and Papua New Guinean Mineral Deposits*, The Australasian Institute of Mining and Metallurgy, Melbourne, pp. 243-54.
- Windsor, CR 2004, 'A review of long, high capacity reinforcing systems used in rock engineering.' *Proc. Int. 5th Ground Support in Mining & Underground Construction*, eds. E Villaescusa & Y Potvin, Balkema, Perth, pp. 17-41.
- Windsor, CR & Thompson, A 1993, 'Rock Reinforcement - Technology, Testing, Design and Evaluation', in J Hudson (ed.), *Comprehensive Rock Engineering*, Pergamon Press, Oxford, pp. 451-84.
- Wojno, LZ & Kuijpers, JS 2001, 'Cone cable - New generation yieldable tendon for large deformations under quasi-static and dynamic loading', *Proceedings of the 4th International Symposium on Roofbolting in Mining*, AUT, pp. 173-82.

Every reasonable effort has been made to acknowledge the owners of copyright material. I would be pleased to hear from any copyright owner who has been omitted or incorrectly acknowledged.

Appendix A
Corrosion Assessment Data Sheet

SITE SPECIFICATION							
Mine Site	Location	Inspected By	Date of Inspection	Date of Excavation	Current Age	Excavation Type	Expected Life

ROCK MASS			
NATURE OF THE ROCK MASS			
Massive	Layered		Blocky
	Thin/Medium/Slabby	Cross Joint Spacing	Small/Medium/Large
	<0.2/ />0.5 m	<1/ />2 m	<0.5/ />1.5 m

INTACT ROCK					
Type	Minerals	Density	Compressive Strength	Stiffness Ratio	Failure Mode
		L/M/H	L/M/H	L/M/H	Brittle/Ductile
		<2.5/ />3 t/m ³	<50/ />100 MPa	<200/ />500	

MAJOR DISCONTINUITIES					
Condition					
Weathering	Profile	Roughness	Aperture	Filling	Seepage
L/M/H	S/U/P	V S/S/R	Width (m)	None/Type	None/Drip/Flow

JOINTS								
Geometry			Condition					
Number of Sets	FF	Joint Connectivity	Persistence	Weathering	Profile	Roughness	Aperture	Filling
	L/M/H	L/M/H	L/M/H	F/S/M/H	S/U/P	VS/S/R	Tight/Open	None/Type
	0-4/4-7/>7		<5/5-10/>10					

ENVIRONMENTAL CONDITIONS						
GROUND WATER						
Location	Dry	Damp	Wet	Dripping	Flowing	Comments
Matrix						
Discontinuities						

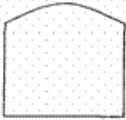

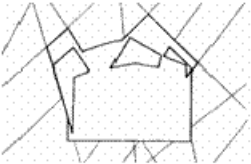
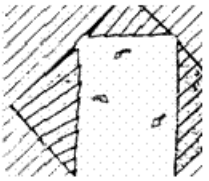
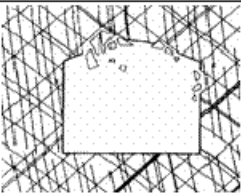
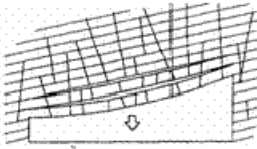
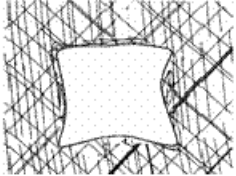
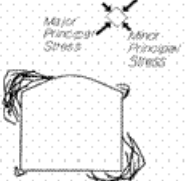
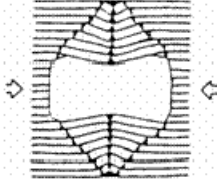
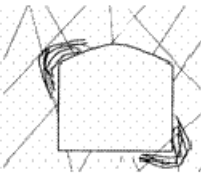

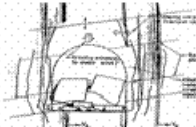
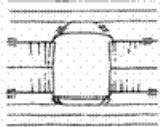
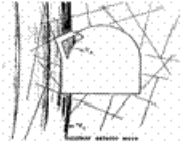
Source	Properties						
	Temperature	pH	Electrical Conductivity	Redox Potential	Dissolved Oxygen	TDS	Salinity
	°C		µS/cm or mS/cm	mV	mg/l	ppm	ppm

ATMOSPHERE							
Ventilation Type	Flow Rate	Particulates	Gases	Temperature		Relative Humidity	Dew Point
Fresh/Exhaust	L/M/H	L/M/H		Dry Bulb	Wet Bulb		
				°C	°C	%	°C

STRESSES

Stresses	Global			Local			Seismic Potential		
	Low	Moderate	High	Low	Moderate	High	Low	Moderate	High

OVERALL ROCKMASS CONDITION

Stress	Rock Mass		
	Massive	Layered	Jointed
Low Stress			
	Stable	Arch Formation	Discrete Large Blocks
			
		Flexural Toppling and Sliding	Unravelling of Small Blocks
Moderate Stress			
			Sliding, crushing and squeezing
High Stress			
	Crushing and spalling	Buckling perpendicular to layers	Crushing and spalling
			
			Strain Burst
			
	Violent Rock Burst	Tensile Splitting shearing and sliding	Rock Burst

SITE SPECIFICATION

Mine Site	Location	Excavation Type	Date of Excavation	Date of Inspection	Inspected By

REINFORCEMENT

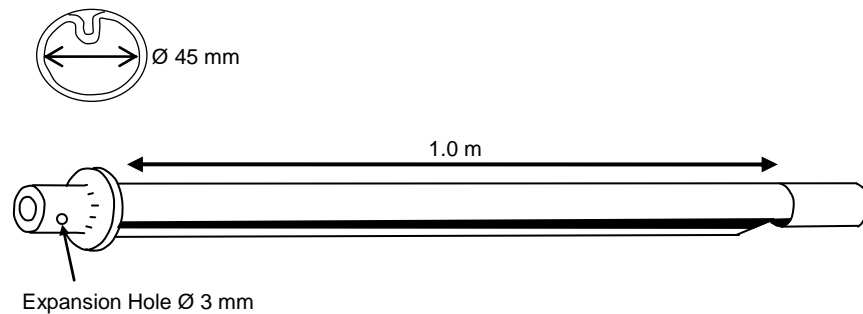
System Number	Date of Installation	Component	Type	Dimensions	Material	Coating	Condition/Comments
R1		Element					
		Internal Fixture					
		External Fixture					
		Plate					
R2		Element					
		Internal Fixture					
		External Fixture					
		Plate					
R3		Element					
		Internal Fixture					
		External Fixture					
		Plate					
R4		Element					
		Internal Fixture					
		External Fixture					
		Plate					

SUPPORT

System Number	Date of Installation	Component	Type	Dimensions	Material	Coating	Condition
S1		Plate					
S2		Strap					
S3		Mesh					

Appendix B

Empirical calculations to determine internal Swellex corrosion



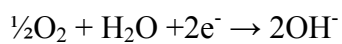
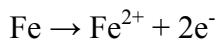
Dimensions of the Swellex bolt under investigation.

Known:

Inner surface area:	0.141 m ²
Inner volume:	0.00159 m ³
Molecular weight oxygen, Mo	16.0
Molecular weight iron, MFe	55.85
Density of Iron, ρFe	7.9x106 g/m ³
Original dissolved oxygen content of water	4.21 g/m ³

Scenario 1 – Undrained then sealed

The bolt is assumed to be completely filled with residual water and sealed from the outside environment. The water contains 4.21 g/m³ dissolved oxygen, which equates to 0.00669g O₂ for the full volume of the bolt. The corrosion half equations are:



Thus

1 mol O₂ corresponds to 2 mol Fe²⁺

0.00669g O₂ equals 2.09×10^{-4} mol O₂.

The oxygen in the trapped water can reduce:

$$= 2 \times 2.09 \times 10^{-4} \times 55.85$$

$$= 0.023 \text{ g Fe}$$

The depth of corrosion associated with this mass loss:

= weight of reduced iron/inner surface volume/density of iron

$$= 0.023 / 0.141 / 7.9 \times 10^6$$

$$= 2.09 \times 10^{-8} \text{ m}$$

$$= 0.02 \text{ } \mu\text{m}$$

The average corrosion will be 0.02 μm due to oxygen in the residual water.

Scenario 2 – Partially drained then sealed

The water inside the bolt is allowed to drain for approximately 14 days before being sealed from the outside environment. The approximate loss of water during this time is 0.59 l, which is replaced by 0.00059 m³ of air leaving the percentage of water at 63%. This equates to an inner surface area affected by the residual water of 0.089 m³. Air contains 8.52 mol O₂/m³.

The moles of oxygen in the trapped air

$$= 0.00059 \times 8.52$$

$$= 5.03 \times 10^{-3} \text{ mol O}_2$$

The oxygen in the trapped air can reduce:

$$= 2 \times 5.03 \times 10^{-3} \times 55.85$$

$$= 0.56 \text{ g Fe}$$

The depth of corrosion associated with this mass loss:

= weight of reduced iron/inner surface volume (affected by water)/density of iron

$$= 0.56/0.089/7.9 \times 10^6$$

$$= 8.0 \times 10^{-7} \text{ m}$$

$$= 0.80 \text{ } \mu\text{m}$$

Total depth of corrosion (air and residual water)

$$= 0.80 + (0.63\% \times 0.02)$$

$$= 0.81 \text{ } \mu\text{m}$$

The average corrosion will be 0.81 μm .

Scenario 3 - Free draining but placed at unfavourable angle

The Swellex element has been installed at an angle that is unfavourable for water to drain. The expansion hole is open and air can diffuse through the expansion hole into the residual water. We assume the bolt is completely filled with water. The diffusion constant for water at 20 °C is $1.97 \times 10^{-9} \text{ m}^2/\text{s}$. The expansion hole diameter and depth is 0.003m and its surface area is $7.07 \times 10^{-6} \text{ m}^2$.

If we assume the dissolved oxygen content of the water to be zero (the oxygen having already been used up) the rate of oxygen diffusion is:

$$= 7.07 \times 10^{-6} \times 1.97 \times 10^{-9} \times (8.52/0.003)$$

$$= 3.96 \times 10^{-11} \text{ mol/s O}_2$$

Equivalent per year

$$= 1.25 \times 10^{-3} \text{ mol/year O}_2$$

Corrosion due to diffused oxygen

$$= 1.25 \times 10^{-3} \times 2 \times 55.85$$

$$= 0.14 \text{ g/year Fe}$$

The depth of corrosion associated with this mass loss:

= weight of reduced iron/inner surface volume/density of iron

$$= 0.14/0.141/7.9 \times 10^6$$

$$= 1.26 \times 10^{-7} \text{ m/year}$$

$$= 0.13 \text{ } \mu\text{m/year}$$

The average corrosion due to residual water is 0.02 μm ; this will increase by 0.13 $\mu\text{m/year}$ due to oxygen diffusion from the atmosphere into the residual water.

After 10 years

$$= 0.02 + (0.13 \times 10)$$

$$= 1.32 \text{ } \mu\text{m}$$

The average corrosion after 10 years will be 1.32 μm or 0.00132 mm.

Appendix C

Galvanised Friction Rock Stabiliser corrosion damage classification

Non-corroded (NC)

No evidence or only minor evidence of corrosion products

Average pit depth: 0.0 mm



Light Corrosion (LC)

Minor uniform surface corrosion of zinc and steel. No evidence of pitting

Average pit depth: 0.0 mm



Moderate Corrosion (MC)

Uniform surface corrosion evident of zinc and steel. Localised areas of severe corrosion and pitting.

Average pit depth: 0.0 – 1.0 mm



High Corrosion (HC)

Uniform surface corrosion covers the majority of the support/reinforcement. Areas of severe corrosion and pitting common.

Average pit depth: 1.0 – 2.0 mm



Severe Corrosion (SC)

Strong uniform surface corrosion covers all the support/reinforcement. Pitting is very common

Average pit depth: >2.0 mm



Extreme Corrosion (EC)

Uniform surface corrosion has greatly reduced the original thickness of the support/reinforcement. Pitting has consumed the steel thickness creating large holes in the support/reinforcement.

Average pit depth: steel thickness



Appendix D
Groundwater Corrosivity Classifications
Langelier Saturation Index (LSI)

$$LSI = pH - pH_s$$

Where:

pH is the measured water pH, and

pH_s is the pH at saturation in calcite or calcium carbonate and is defined as:

$$pH_s = (9.3 + A + B) - (C + D)$$

Where:

$$A = (\text{Log}_{10} [\text{TDS}] - 1)/10,$$

$$B = -13.12 \times \text{Log}_{10} (^\circ\text{C} + 273) + 34.55,$$

$$C = \text{Log}_{10} [\text{Ca}^{2+} \text{ as CaCO}_3] - 0.4, \text{ and}$$

$$D = \text{Log}_{10} [\text{alkalinity as CaCO}_3].$$

Langelier Index Calculation for Enterprise Mine

pH = 7.5, TDS = 6,720, Water Temperature = 35.2 °C, Calcium = 110 mg/l,
Alkalinity = 82 mg/l

$$A = (\text{Log}_{10} [6,720] - 1)/10 = 0.28$$

$$B = -13.12 \times \text{Log}_{10} (35.2 + 273) + 34.55 = 1.90$$

$$C = \text{Log}_{10} 110 - 0.4 = 1.64$$

$$D = \text{Log}_{10} 82 = 1.91$$

$$pH_s = (9.3 + 0.28 + 1.90) - (1.64 + 1.91) = 7.92$$

$$LSI = 7.5 - 7.93 = -0.42$$

No tendency to scale

DIN 50929-3 classification

Free corrosion under water is estimated by:

$$W_0 = N_1 + N_3 + N_4 + N_5 + N_6 + \left(\frac{N_3}{N_4} \right)$$

Corrosion at the water/air interface is estimated by:

$$W_1 = W_0 - N_1 + N_2 \times N_3$$

Quality assessment of hot dip galvanised steel at the water/air interface is estimated by:

$$W_L = M_1 + M_3 + M_4 + M_5 + M_6 + M_2$$

No.	Parameters investigated/measured	Unit	Rating for	
			unalloyed iron	galvanized steel
1	Type of water		N_1	M_1
	Flowing water		0	-2
	Standing water		-1	+1
	Water near the shore of lakes		-3	-3
	Anaerobic fen water, coastal waters		-5	-5
2	Location of structure		N_2	M_2
	Under water		0	0
	Water/air interface		1	-6
	Splash zone		0,3	-2
3	c (Cl^-) and $2c$ (SO_4^{2-})	mol/m ³	N_3	M_3
	<1		0	0
	>1 to 5		-2	0
	>5 to 25		-4	-1
	>25 to 100		-6	-2
	>100 to 300		-7	-3
	>300		-8	-4
4	Acidity up to pH 4,3 (alkalinity $K_{S4,3}$)	mol/m ³	N_4	M_4
	<1		1	-1
	1 to 2		2	+1
	>2 to 4		3	+1
	>4 to 6		4	0
	>6		5	-1
5	c (Ca^{2+})	mol/m ³	N_5	M_5
	<0,5		-1	0
	0,5 to 2		0	+2
	>2 to 8		+1	+3
	>8		+2	+4
6	pH value		N_6	M_6
	<5,5		-3	-6
	5,5 to 6,5		-2	-4
	>6,5 to 7,0		-1	-1
	>7,0 to 7,5		0	+1
	>7,5		+1	+1
7	Structure/water potential, U_H , (for detecting impressed current cathodes)	V	N_7	
	> -0,2 to -0,1		-2	
	> -0,1 to 0,0		-5	
	> -0,0		-8	
Sampling and analyses as specified in DIN 50930 Part 1.				

Information relating to the assessment of water for the DIN 50929 classification.

W_0 or W_1 value	Deep and wide pitting corrosion	General corrosion	B_D, W_D, W_L values	Quality of coatings
≥ 0 - 1 to - 4 < - 4 to - 8 < - 8	Very low Small Medium High	Very low Very low Small Medium	≥ 0 - 1 to - 4 - 5 to - 8 < - 8	Very good Good Satisfactory Not adequate

Estimating the probability of corrosion of steel and zinc in water for the DIN 50929 classification.

DIN 50929 calculations for Enterprise Mine

Type of water	Flowing	$N_1 = 0$	$M_1 = -2$
Location of structure	Water/air interface	$N_2 = 1$	$M_2 = -6$
$c(\text{Cl}^-)$	27.4 mol/m^3		
$2c(\text{SO}_4^{2-})$	4.2 mol/m^3	$N_3 = -6$	$M_3 = -2$
Acidity	$\text{CO}_3^{2-} = 0.02 \text{ mol/m}^3$		
	$\text{HCO}_3^- = 1.34 \text{ mol/m}^3$	$N_4 = 2$	$M_4 = 1$
$c(\text{Ca}^{2+})$	$\text{Ca}^{2+} = 2.74 \text{ mol/m}^3$	$N_5 = 1$	$M_5 = 3$
pH value	pH = 7.5	$N_6 = 0$	$M_6 = 0$

$$W_1 = \left(0 - 6 + 2 + 1 + 0 + \frac{-6}{2} \right) - 0 + (1 \times -6) = -12$$

High pitting corrosion, medium general corrosion

$$W_L = -2 - 2 + 1 + 3 + 0 - 6 = -6$$

Satisfactory quality of coating

Li and Lindblad (1999) Corrosivity classification for wet underground rock conditions

The corrosion in wet underground rock conditions is estimated by:

$$W_{wet} = (N_{pH} + N_{O_2} + N_R) K_I K_R$$

Parameter		Ranges of the Value				
Basic parameters						
1	pH value: Rating, N_{pH} :	>11 0	11-9 1	9-7 2	7-5 3	<5 4
2	Oxygen (ppm): Rating, N_{O_2} :	<1 1	1-2 2	2-4 3	4-7 4	>7 5
3	Resistivity (Ω -cm): Rating, N_R :	>10 000 0	10 000-2 000 0.25	2 000-1 000 0.5	1 000-500 1	<500 2
Influencing parameters						
4	Temperature Factor, K_t :	$K_t = 2^{\left(\frac{T-20}{10}\right)}$, (T= 0-60°C)				
5	RMR:	I	II	III	IV	V
	Rock mass quality:	Very good	Good	Fair	Poor	Very poor
	RQD	100-95	95-75	75-50	50-25	<25
	Spacing of rock joints	>2 m	2-0.6	0.6-0.2	0.2-0.06	<0.06
	Water inflow/10 m tunnel length, (l/min):	<1	1-10	10-25	25-125	>125
	Factor, K_R :	1	1.25	1.5	1.75	2
The Redox potential is considered an appropriate parameter to replace the parameters of the pH value and oxygen. It has the following descriptive relation with the corrosivity of soils:						
Redox potential (mV):		>400	400-200	200-100	<100	
Description:		No corrosion	Little	Moderate	Severe	

Table 2. System I: total rating (W_{wet}) and the corresponding class number of corrosivity.

Total Rating, W_{wet} :	2	2-4	4-7	7-10	>10
Class Number:	I	II	III	IV	V
* Adjustment of Class Number for precipitation: Class Number drops one when precipitation occurs.					
In descriptive terms:	No or very little corrosion	Little corrosion	Moderate corrosion	Severe corrosion	Very severe corrosion
Reference corrosion rate of carbon steel, (mm/y):	<0.05	0.05-0.10	0.10-0.15	0.15-0.30	>0.30

Rating system for the parameters for Li & Lindblad's (1999) corrosivity classification for wet underground rock conditions.

Li & Lindblad's (1999) calculations for Enterprise Mine

pH	7.5	$N_{\text{pH}} = 2$
Dissolved Oxygen	4.1 ppm	$N_{\text{O}_2} = 4$
Resistivity	$\Omega\text{-cm}$	$N_R = 2$
Temperature	35.2°C	$K_t = 2.87$
Rock mass quality	good	$K_R = 1.25$

$$W_{\text{wet}} = (2 + 4 + 2) \times 2.87 \times 1.25 = 28.7$$

Very severe corrosion predicted, >0.30 mm/yr.

Appendix E

Atmospheric Corrosion Classifications ISO 9223 Atmospheric corrosivity classification

Corrosivity category	Corrosion rate		Time of wetness ¹⁾ expressed in hours where RH > 80 %, θ > 0 °C (h/a)															
	r_{corr} (1st year) ²⁾ g/(m ² ·a)	r_{lin} (steady state) ³⁾ μm/a	$\tau \leq 10$ (class τ_1) Indoors, climatic control	$10 < \tau \leq 250$ (class τ_2) Indoors, no climatic control except in damp climates	$250 < \tau \leq 2\,500$ (class τ_3) Outdoors in dry, cold climates, ventilated sheds in temperate climates	$2\,500 < \tau \leq 5\,500$ (class τ_4) Outdoors in temperate climates, unventilated sheds in temperate climates, ventilated sheds in damp climates	$\tau > 5\,500$ (class τ_5) Outdoors in damp climates; humid, unventilated sheds											
C 1	$r_{corr} \leq 10$	$r_{lin} \leq 0,1$																
C 2	$10 < r_{corr} \leq 200$	$0,1 < r_{lin} \leq 1,5$																
C 3	$200 < r_{corr} \leq 400$	$1,5 < r_{lin} \leq 6$																
C 4	$400 < r_{corr} \leq 650$	$6 < r_{lin} \leq 20$																
C 5	$650 < r_{corr} \leq 1\,500$	$20 < r_{lin} \leq 90$																
Airborne salinity ⁴⁾ Chloride deposition rate [mg/(m ² ·d)]																		
Industrial pollution ⁵⁾ by sulfur dioxide (SO ₂)			S ₀	S ₁	S ₂	S ₃	S ₀	S ₁	S ₂	S ₃	S ₀	S ₁	S ₂	S ₃	S ₀	S ₁	S ₂	S ₃
Concentration μg/m ³	Category	Deposition rate mg/(m ² ·d)	$S_0 \leq 3$	$3 < S_0 \leq 60$	$60 < S_0 \leq 300$	$300 < S_0 \leq 1\,500$	$S_0 \leq 3$	$3 < S_0 \leq 60$	$60 < S_0 \leq 300$	$300 < S_0 \leq 1\,500$	$S_0 \leq 3$	$3 < S_0 \leq 60$	$60 < S_0 \leq 300$	$300 < S_0 \leq 1\,500$	$S_0 \leq 3$	$3 < S_0 \leq 60$	$60 < S_0 \leq 300$	$300 < S_0 \leq 1\,500$
$P_c \leq 12$	P ₃	$P_d \leq 10$																
$12 < P_c \leq 40$	P ₁	$10 < P_d \leq 35$	1	1	1 or 2	1	2	3 or 4	2 or 3	3 or 4	4	3	4	5	3 or 4	5	5	
$40 < P_c \leq 90$	P ₂	$35 < P_d \leq 80$	1	1	1 or 2	2 or 3	3 or 4	3 or 4	3 or 4	4 or 5	4	4	4	5	4 or 5	5	5	
$90 < P_c \leq 250$	P ₃	$80 < P_d \leq 200$	1 or 2	1 or 2	2	2	3	4	4	4 or 5	5	5	5	5	5	5	5	

Derivation of corrosivity of atmospheres for carbon steel from ISO 9223 standard.

Corrosivity category	Corrosion rates (r_{corr}) of metals				
	Units	Carbon steel	Zinc	Copper	Aluminium
C 1	g/(m ² ·a) μm/a	$r_{\text{corr}} \leq 10$ $r_{\text{corr}} \leq 1,3$	$r_{\text{corr}} \leq 0,7$ $r_{\text{corr}} \leq 0,1$	$r_{\text{corr}} \leq 0,9$ $r_{\text{corr}} \leq 0,1$	Negligible —
C 2	g/(m ² ·a) μm/a	$10 < r_{\text{corr}} \leq 200$ $1,3 < r_{\text{corr}} \leq 25$	$0,7 < r_{\text{corr}} \leq 5$ $0,1 < r_{\text{corr}} \leq 0,7$	$0,9 < r_{\text{corr}} \leq 5$ $0,1 < r_{\text{corr}} \leq 0,6$	$r_{\text{corr}} \leq 0,6$ —
C 3	g/(m ² ·a) μm/a	$200 < r_{\text{corr}} \leq 400$ $25 < r_{\text{corr}} \leq 50$	$5 < r_{\text{corr}} \leq 15$ $0,7 < r_{\text{corr}} \leq 2,1$	$5 < r_{\text{corr}} \leq 12$ $0,6 < r_{\text{corr}} \leq 1,3$	$0,6 < r_{\text{corr}} \leq 2$ —
C 4	g/(m ² ·a) μm/a	$400 < r_{\text{corr}} \leq 650$ $50 < r_{\text{corr}} \leq 80$	$15 < r_{\text{corr}} \leq 30$ $2,1 < r_{\text{corr}} \leq 4,2$	$12 < r_{\text{corr}} \leq 25$ $1,3 < r_{\text{corr}} \leq 2,8$	$2 < r_{\text{corr}} \leq 5$ —
C 5	g/(m ² ·a) μm/a	$650 < r_{\text{corr}} \leq 1\,500$ $80 < r_{\text{corr}} \leq 200$	$30 < r_{\text{corr}} \leq 60$ $4,2 < r_{\text{corr}} \leq 8,4$	$25 < r_{\text{corr}} \leq 50$ $2,8 < r_{\text{corr}} \leq 5,6$	$5 < r_{\text{corr}} \leq 10$ —

Atmospheric corrosion rates of metals for different corrosivity categories

Li & Lindblad (1999) Corrosivity classification for dry underground conditions

The corrosion in dry underground rock conditions is estimated by:

$$W_{dry} = N_{ox} N_{rh} K_t$$

Parameters		Ranges of the Value			
1	SO ₂ + NO _x + NaCl :	rural atm.	urban atm.	industrial and marine atm.	
	Concentration, (g/m ³):	<100	100-200	200-350	>350
	Deposition rate, (mg/m ² /day):	<20	20-100	100-200	>200
	Rating, N _{ox} :	1	2	3	4
2	Relative humidity (%):	<60	60-75	75-100	dew
	Rating, N _{rh} :	0	1	2	3
3	Temperature Factor, K _t :	$K_t = 2^{\left(\frac{T-20}{10}\right)}$, (T= 0 - 40°C)			

Table 5. System II: total rating (W_{dry}) and the corresponding class number of corrosivity.

Total Rating, W_{dry} :	0-6	6-10	>10
Class number:	I	II	III
In descriptive terms:	No or very little corrosion	Little corrosion	Moderate to severe corrosion
Reference corrosion rate of carbon steel, (mm/y):	<0.05	0.05-0.10	>0.10

Ratings system for the parameters for Li & Lindblad's (1999) corrosivity classification for dry underground rock conditions.

Li & Lindblad's (1999) calculations for Cannington 475 Ug53

$$SO_2 + NO_x + NaCl \quad \text{low} \quad N_{ox} = 1$$

$$\text{Relative Humidity} \quad 74\% \quad N_{rh} = 1$$

$$\text{Temperature} \quad 30^\circ\text{C} \quad K_t = 30$$

$$W_{dry} = 1 \times 1 \times 2 = 2$$

No or very little corrosion, <0.05 mm/yr.